

Investigation of Meteorological Events Preserved in High Resolution Snow Pit and Firn Core Records

by

Alison McMorrow

Bachelor of Arts (Geography) / Bachelor of Economics

Bachelor of Antarctic Studies (Honours)

Submitted in fulfillment of the requirements

for the Degree of

Doctor of Philosophy

University of Tasmania

June, 2006

Declaration

This thesis contains no material which has been accepted for a degree or diploma by the University or any other institution. To the best of my knowledge and belief this thesis contains no material previously published or written by another person except where due acknowledgement is made in the text.

ALISON MCMCMORROW

Authority of access

This thesis may be made available for loan and limited copying in accordance with the *Copyright Act 1968*.

ALISON MCMORROW

University of Tasmania

June, 2006

Acknowledgements

Many thanks are required here. First, I would like to thank my supervisors, Mark Curran, Tas van Ommen, Vin Morgan and Bill Budd. Thanks also to Rob Massom for taking over from Bill as a supervisor late in my candidature. A special thanks also to Anne Palmer for her incredible depth of chemistry knowledge and patience with my incredibly basic chemistry questions. Thanks also to the many faces of Glaciology, especially Barbara Smith for helping me dig and Linda van Ommen for conducting the hydrogen peroxide analysis that didn't quite make it into this thesis. Thanks also to Ian Allison for providing information on the AWS animal.

Big thanks to all the crew who transported me to Antarctica, up to Law Dome and helped dig all those pits, particularly Woll, Squizzy, Pete, Flea, Trev and Buzz! You guys provided many a laugh on those cold days and worked your butts off in the name of science (and a couple of glasses of red).

Thanks also to Ian Simmonds and his crew from the Uni of Melbourne for providing the back trajectory analysis, and to Neal Young from ACE CRC for providing the AVHRR images. Thanks also to the members of the ACE CRC, IASOS and the AAD for providing support and knowledge throughout my PhD. A fantastic bunch of people devoted to a special place.

I would also like to acknowledge the Antarctic CRC (now the ACE CRC) and the Trans-Antarctic Association for providing financial support for me to attend and present these results to the international scientific community.

A huge thanks goes to my family, my mum Brenda, my dad Jim, and my sisters Frances and Christine. You all helped me out over the years and I will never forget that. Also thanks to my friends, particularly Susan for her amazing desserts, Ruth for the horsey chats, Tash for her endless laughter and Grant for his beautiful music. A big woof-thanks to my puppies, Rama, Tilda and Zoe, who provided inspiration for snow pit names and many tail wags and nuzzles on the tough days.

Finally, to my fiancé Jimmy, and my son Liam. Your smiling faces provided the best encouragement and your cuddles the best comfort and support. Thank you.

List of abbreviations

$\delta^{18}\text{O}$	oxygen isotope ratio
AAD	Australian Antarctic Division
ANARE	Australian National Antarctic Research Expeditions
AVHRR	advanced very high resolution radiometer
AWS	automatic weather station
CRC	Cooperative Research Centre
ENSO	El Niño Southern Oscillation
DMS	dimethyl sulphide
DMSP	dimethyl sulphoniopropionate
DON	dissolved organic nitrogen
DoY	Day of Year
DSS	Dome Summit South
H_2O_2	hydrogen peroxide
HCL	hydrochloric acid
IC	ion chromatography
MSA	methane sulphonate
N_2O	nitric acid
NOAA	National Oceanic and Atmospheric Administration
nss SO_4	non-sea salt sulphate
OH	hydroxide
PSC	polar stratospheric cloud
SMOW	Standard Mean Ocean Water
SO_2	sulphur dioxide

List of publications

Type of Publication	Number	Reference
Papers in refereed journals	6	1 – 6
Conference and seminar presentations	7	7 – 13

1. McMorrow, A. J., van Ommen, T. D., Morgan, V. and Curran, M. A. J. 2003. Ultra high seasonality of trace ion species and oxygen isotope ratios over 4 annual cycles. *Annals of Glaciology*. **39**. 34-40.
2. Curran, M., van Ommen, T., Palmer, A., Morgan V. and McMorrow, A. Non-sea-salt sulphate in ice cores, correction for sulphate depletion. (in preparation).
3. Pedro, J., Curran, M., van Ommen, T., Smith, B., Morgan, V., McMorrow, A. and Smith, A. High resolution snow pit study of ^{10}Be at Law Dome, Antarctica. (in preparation).
4. McMorrow, A. J., Curran, M. A. J., van Ommen, T. D., Morgan, V. and Allison, I. 2002. Features of meteorological events preserved in a high resolution Law Dome snow pit. *Annals of Glaciology*. **35**. 463-470.
5. Curran, M. A. J., Palmer, A. S., van Ommen, T. D., Morgan, V., Phillips, K. L., McMorrow, A. J. and Mayewski, P. 2002. Post-depositional methansulphonic acid movement on Law Dome and the effect of accumulation rate. *Annals of Glaciology*. **35**. 333-339.
6. McMorrow, A. J., Curran, M. A. J., van Ommen, T. D., Morgan, V., Pook, M. J. and Allison, I. 2001. Intercomparison of firn core and meteorological data. *Antarctic Science*. **13**(3), 329-337.
7. Talk presented at the International Glaciological Society, International Symposium on Antarctic Glaciology. Milan, Italy. 25th to 29th August 2003. Ultra high seasonality of trace ion species and oxygen isotope ratios over 4 annual cycles. McMorrow, A. J., van Ommen, T. D., Morgan, V. and Curran, M. A. J.
8. Talk presented in the Institute of Antarctic and Southern Ocean Studies seminar series. August 2003. Ultra high seasonality of trace ion species and oxygen isotope ratios over 4 annual cycles.
9. Talk presented by Andrew Smith at the 18th International Radiocarbon Conference. Wellington, New Zealand. 1st to 5th September 2003. Snow pit study of the deposition of cosmogenic beryllium at Law Dome, Antarctica. Smith, A. M., Pedro, J. B., Curran, M. and McMorrow, A. J.

10. Poster presented at the International Glaciological Society, International Symposium on Ice Cores and Climate. Kangerlussuaq, Greenland. 19th to 23rd August 2001. Features of meteorological events preserved in a high resolution Law Dome snow pit. McMorrow, A. J., Curran, M. A. J., van Ommen, T. D., Morgan, V. and Allison, I.
11. Talks given at Palaeoclimate Day at the Antarctic CRC (February 2002) and the Australian Ice Cores Conference at the Antarctic CRC (April 2002).
12. Talk presented by Andrew Smith at the 9th International Conference on Accelerator Mass Spectrometry, AMS – 9, Nayoga, Japan, September 9-13 2002. High resolution study of the deposition of cosmogenic ¹⁰Be and ⁷Be in Antarctic Snow. Smith, A. M., Curran, M., Pedro, J. B., McMorrow, A. J., Smith, B. T. and Morgan, V. I.
13. Poster presented by Mark Curran at the 22nd General Assembly of the International Union of Geodesy and Geophysics. University of Birmingham, UK. 18-30th July 1999. McMorrow, A. J., Curran, M. A. J., van Ommen, T. D., Morgan, V., Pook, M. J. and Allison, I. 2001. Intercomparison of firn core and meteorological data.

Abstract

A key problem in ice core palaeoclimate studies is the interpretation of the various measurable parameters in ice in terms of climate and environmental conditions. This study is aimed at developing a closer understanding of the connection between high resolution snow/firn measurements and meteorological conditions. Ultra high resolution snow pit and shallow firn core records of oxygen isotope ratios ($\delta^{18}\text{O}$) and a suite of trace chemical species including marine biogenic sulphur compounds (methane sulphonate (MSA), non-sea salt sulphate), nitrate and major sea salt ions (sodium, chloride, magnesium), were generated at a high accumulation site on Law Dome, East Antarctica. Concordance between accumulation events identified in the records up to 7.7 km apart confirms that the observed chemical and isotopic variations are the result of regional rather than local surface effects. This allows calibration of the snow pit and firn core records with measured meteorological parameters.

Event scale dating of the records was established using hourly snow accumulation measurements from a co-located automatic weather station (AWS). The ultra high resolution nature of this study and independent dating scale provide an opportunity to examine exact timings in the seasonality of each chemical species. The traditional summer-maximum species of $\delta^{18}\text{O}$ and MSA show consistent relative phasing during mid-summer over four annual cycles. Nitrate shows an erratic seasonal cycle with a general trend characterised by narrow peaks during spring and early summer, preceding the mid-summer peaks in $\delta^{18}\text{O}$ and MSA. Non-sea salt sulphate cycles indicate similar characteristics to MSA signals during summer, but are more comparable to nitrate signals during spring, autumn and winter. This suggests the summer non-sea salt sulphate signal is driven by biological activity, yet appears to be linked with nitrate signals outside the summer season. Finally, the sea salt species indicate a seasonal cycle characterised by maximum concentrations during autumn, winter and spring.

Event scale dating of the snow pit and firn core records allows direct comparisons between the chemical and isotopic signals and observed meteorological conditions. Local meteorological conditions recorded by the AWS are combined with synoptic scale meteorology derived from Advanced Very High Resolution Radiometer satellite imagery and back trajectory analysis to identify potential source regions and transport mechanisms influencing the chemical and isotopic signals. Potential source regions and transport mechanisms are examined for the marine biogenic indicators (MSA, non-sea salt sulphate). Results indicate that the seasonal variation in marine biogenic activity is reflected in the Law Dome records, and the sea ice zone provides an important source region. However, results also indicate that lower latitudes, and the Heard Island region (50°S, 70°E) in particular, may provide an important additional source region for MSA and non-sea salt sulphate outside the summer season. High sea salt signals are generally associated with intense cyclonic systems, yet variations in atmospheric circulation and transport mechanisms also impact on the sea salt record. Comparisons between $\delta^{18}\text{O}$ signals and local air temperatures reveal the $\delta^{18}\text{O}$ record is an excellent proxy for temperature at Law Dome, although high (warm) $\delta^{18}\text{O}$ events are found to be influenced by atmospheric circulation and associated with rapid advection of air from low latitudes. Finally, results suggest that spring nitrate signals at Law Dome may be linked to the intrusion of stratospheric air through the breakdown in the polar vortex during spring.

Table of Contents

Declaration	ii
Acknowledgements	iii
List of Abbreviations	v
Abstract	vii
List of Publications	v
Table of Contents	viii
List of Tables	xiv
List of Figures	xiv
 Chapter 1 Introduction and Review of Relevant Literature	 1
1.1 Overview	1
1.2 Oxygen Isotopes in the Antarctic	2
1.2.1 The Isotopic Composition of Precipitation	2
1.2.2 The Ice Core Palaeothermometer	4
1.3 Trace Ion Chemicals in the Antarctic	6
1.3.1 Sea Salt Ions	6
<i>Sea Salt Particle Production</i>	6
<i>Sea Salt Ions as Climate Indicators</i>	7
1.3.2 Marine Biogenic Sulphur Compounds	9
<i>The Natural Sulphur Cycle</i>	9
<i>Marine Biogenic Compounds as Climate Indicators</i>	10
1.3.3 Nitrate	12
<i>Sources of Nitrate in Polar Snow</i>	12
<i>Nitrate as a Climate Indicator</i>	14
1.4 Deposition of Atmospheric Contaminants to Polar Snow	15
1.4.1 Dry Deposition	15
1.4.2 Wet Deposition	16
1.4.3 Fog Deposition	17
1.4.4 Drifting and Blowing Snow	18
1.4.5 Post Depositional Modification of Chemical Species	19
1.5 Chapter Summary and Thesis Outline	21

Chapter 2	Site Characteristics, Sample Retrieval, Preparation and Analysis	22
2.1	Overview	22
2.2	Physical and Climatological Conditions of Dome Summit South (DSS), Law Dome	22
2.3	Snow Pit Sample Retrieval	26
2.4	Firn Core Retrieval and Sample Preparation	28
2.5	Sample Analysis	31
2.5.1	Oxygen Isotope Ratios ($\delta^{18}\text{O}$)	31
2.5.2	Hydrogen Peroxide	31
2.5.3	Trace Ion Chemical Species	32
	<i>Methods</i>	32
	<i>Standards and Sample Calibration</i>	34
2.6	Concluding Remarks	37
Chapter 3	High Resolution Spatial and Temporal Comparison Across Law Dome	38
3.1	Overview	38
3.2	Intra-Pit Spatial Variability (30 cm to 2 m)	39
3.2.1	The <i>Rama</i> Snow Pit	39
	<i>Statistical Analysis of the Spatial Reproducibility</i>	41
	<i>Summary</i>	45
3.3	Inter-Pit Spatial Variability (50 m to 100 m)	46
3.3.1	The <i>Rama</i> , <i>Karioke</i> and <i>Paddy</i> Snow Pits	46
3.4	Inter-Core Spatial Variability (100 m to 11.7 km)	48
3.5	Concluding Remarks	60
Chapter 4	Local Meteorology at DSS, Law Dome	62
4.1	Overview	62
4.2	Antarctic Meteorology	62
4.3	Automatic Weather Stations in the Antarctic and at Law Dome	63
4.4	Features of Local Meteorology at DSS	65
4.4.1	Air Temperature	65
4.4.2	Wind Speed and Direction	70
4.4.3	Atmospheric Pressure	76
4.5	Meteorological Bias in Ice Core Records	81
4.5.1	Snow Accumulation	81
4.5.2	Local Meteorology of Accumulation Events at Law Dome	83

4.6	Concluding Remarks	86
Chapter 5	High Resolution Dating of the Snow Pit Records	88
5.1	Overview	88
5.2	Identification of Net Accumulation Events	89
5.2.1	Defining Events in the <i>Rama</i> and <i>Matilda</i> Snow Pits	90
5.2.2	Accumulation Events	93
	<i>Matilda Events</i>	93
	<i>Extending Matilda – DSS0102 Events</i>	95
	<i>Rama Events</i>	98
	<i>Extending Rama – S0k Events</i>	99
	<i>Summary</i>	102
5.3	Densification of the Snowpack	102
5.3.1	Density Profiles	102
5.3.2	Density Effects on the Extended Firn Core Records	104
	<i>Season 1 – S0k</i>	105
	<i>Season 2 – DSS0102</i>	106
	<i>Correcting for Densification – DSS0102</i>	107
5.4	Concluding Remarks	109
Chapter 6	Seasonal Characteristics of High Resolution Firn Core Signals	111
6.1	Overview.....	111
6.2	Summarised Literature Review for Seasonality Studies of $\delta^{18}\text{O}$ and Trace Chemical Species in Antarctic Ice Cores	112
6.2.1	$\delta^{18}\text{O}$	112
6.2.2	Marine Biogenic Sulphur Compounds	112
6.2.3	Nitrate	113
6.2.4	Sea Salts	114
6.3	Seasonality of $\delta^{18}\text{O}$ and Trace Ion Species over Four Annual Cycles at Law Dome	115
6.3.1	$\delta^{18}\text{O}$	116
	<i>Seasonal Cycle</i>	116
	<i>Temperature and $\delta^{18}\text{O}$</i>	117
	<i>Cyclonic Precipitation and $\delta^{18}\text{O}$</i>	122
6.3.2	MSA	123
	<i>Seasonal Cycle</i>	123

	<i>Temperature and MSA</i>	124
6.3.3	Nitrate	126
	<i>Seasonal Cycle</i>	126
	<i>Temperature and Nitrate</i>	126
6.3.4	Non-sea Salt Sulphate	128
	<i>Seasonal Cycle</i>	128
	<i>Temperature and Non-sea Salt Sulphate</i>	128
6.3.5	Sea Salts	130
	<i>Seasonal Cycle</i>	130
	<i>Wind Speed, Direction and Sea Salts</i>	130
6.4	Sources Regions for Seasonal Signals Preserved in Law Dome Ice Cores	133
	6.4.1 Seasonality in Atmospheric Circulation for Net Accumulation Events	135
6.5	Concluding Remarks	136
 Chapter 7 Pilot Study: Examination of Three Accumulation Periods in the Rama Snow Pit		
7.1	Overview	139
7.2	Chemical and Isotopic Signals	140
7.3	Local Meteorological Conditions	143
7.4	Synoptic Scale Meteorological Conditions	144
7.5	Source Regions and Transport Mechanisms for the Snow Pit Signals	147
7.6	Concluding Remarks	149
 Chapter 8 Investigation of Specific Meteorological Events Preserved in High Resolution Snow Pit Records		
		150
8.1	Overview	150
8.2	Current Seasonal Studies from Law Dome Ice Cores	151
8.3	Glaciological and Meteorological Tools	152
	8.3.1 Glaciological Tools	152
	<i>Dating the Chemical and $\delta^{18}\text{O}$ Records</i>	153
	<i>Differentiation in Dating between Pilot Study and Chapter 8</i>	154
	8.3.2 Meteorological Tools	154
	8.3.3 Comparing Chemical and $\delta^{18}\text{O}$ Signals with Meteorological Observations	155
8.4	Meteorological Conditions Across All Seasons	156
	8.4.1 Local Meteorological Conditions	156
	<i>Summer Events</i>	156

	<i>Autumn Events</i>	156
	<i>Winter Events</i>	157
	<i>Spring Events</i>	158
8.4.2	Synoptic Meteorological Conditions	159
8.5	Summer Events Preserved in High Resolution Snow Pits and Firn Cores	160
8.5.1	Events that Concur with Expected Summer Chemical and Isotopic Signals	161
	$\delta^{18}O$	162
	<i>Marine Biogenic Indicators: MSA and Non-Sea Salt Sulphate</i>	162
	<i>Sea Salts</i>	163
	<i>Nitrate</i>	164
8.5.2	Events that Differ from Expected Summer Chemical and Isotopic Signals	164
	<i>Enhanced Summer Sea Salts (Events 1 and 25)</i>	164
	<i>Deviation Between MSA and Non-Sea Salt Sulphate (Event 21)</i>	165
	<i>Enhancement of Summer Marine Biological Indicators (Event 29)</i>	166
	<i>Low or Declining Marine Biological Indicators (Events 26 and 30)</i>	167
8.5.3	Concluding Remarks: Summer	169
8.6	Autumn Events Preserved in High Resolution Snow Pits and Firn Cores	171
8.6.1	Events that Concur with Expected Autumn Chemical and Isotopic Signals	172
	$\delta^{18}O$	173
	<i>Marine Biogenic Indicators: MSA and Non-Sea Salt Sulphate</i>	173
	<i>Sea salts</i>	173
	<i>Nitrate</i>	174
8.6.2	Events that Differ from Expected Autumn Chemical and Isotopic Signals	174
	<i>Low Autumn Sea Salts (Events 10, 11, 12, 14, 15, 37 and 51)</i>	174
	<i>Low Sea Salts – Slow Approach to Law Dome</i>	175
	<i>Low sea Salts – Low Latitude (Distant) Source Region</i>	175
	<i>Low Sea Salts – Coastline trajectory</i>	176
	<i>Enhanced Autumn Marine Biogenic Indicators (Events 16 and 17)</i>	176
	<i>Deviation Between MSA and Non-Sea Salt Sulphate (Event 38)</i>	177
8.6.3	Concluding Remarks: Autumn	178
8.7	Winter Events Preserved in High Resolution Snow Pits and Firn Cores	181
8.7.1	Events that Concur with Expected Winter Chemical and Isotopic Signals	182
	$\delta^{18}O$	182
	<i>Marine Biogenic Indicators: MSA and Non-Sea Salt Sulphate</i>	183

	<i>Sea salts</i>	183
	<i>Nitrate</i>	184
8.7.2	Events that Differ from Expected Winter Chemical and Isotopic Signals ..	184
	<i>Enhanced Winter $\delta^{18}O$ (Events 5, 6, 7, 24, 46, 47 and 48)</i>	184
8.7.3	Concluding Remarks: Winter	186
8.8	Spring Events Preserved in High Resolution Snow Pits and Firn Cores	188
8.8.1	Events that Concur with Expected Spring Chemical and Isotopic Signals ..	189
	<i>$\delta^{18}O$</i>	189
	<i>Marine Biogenic Indicators: MSA and Non-Sea Salt Sulphate</i>	190
	<i>Sea salts</i>	190
	<i>Nitrate</i>	191
8.8.2	Events that Differ from Expected Spring Chemical and Isotopic Signals...	191
	<i>Low Sea Salts and $\delta^{18}O$ (Event 2)</i>	191
	<i>Enhanced Spring Nitrate (Events 22, 44 and 45)</i>	192
	<i>Enhanced Spring Marine Biogenic Indicators (Events 31 and 43)</i>	193
8.8.3	Concluding Remarks: Spring	195
8.9	Concluding Remarks	196
8.9.1	Seasonal Considerations	196
	<i>Summer</i>	196
	<i>Autumn</i>	197
	<i>Winter</i>	198
	<i>Spring</i>	199
8.9.2	Implications for Interpreting Longer Law Dome Ice Core Records	200
	<i>Marine Biogenic Indicators: MSA and Non-Sea Salt Sulphate</i>	200
	<i>Sea Salts</i>	201
	<i>$\delta^{18}O$</i>	202
	<i>Nitrate</i>	202
	<i>Seasonal Variability in Meteorology</i>	203
	<i>Atmospheric Circulation Variability</i>	203
Chapter 9	Conclusions and Recommendations for Further Research	205
9.1	Conclusions	205
9.2	Areas for Further Research	208

Reference List	210
Appendix A Local and Synoptic Meteorological Conditions for Summer Events ...	224
Appendix B Local and Synoptic Meteorological Conditions for Autumn Events ...	242
Appendix C Local and Synoptic Meteorological Conditions for Winter Events	258
Appendix D Local and Synoptic Meteorological Conditions for Spring Events	274

List of Tables

2.1 Details of the four snow pits analysed in this research	26
2.2 Details of the thirteen firn cores analysed in this research	29
2.3 Concentrations of ions in a primary standard	36
2.4 Concentrations of six working standards	36
3.1 Mean deviations resulting from the seven line intra-pit comparison	45
4.1 Mean local meteorological conditions	86
5.1 Accumulation events preserved in <i>Matilda</i>	94
5.2 Accumulation events preserved in <i>DSS0102</i>	96
5.3 Accumulation events preserved in <i>Rama</i>	98
5.4 Accumulation events preserved in <i>S0k</i>	99
5.5 Significant events preserved in <i>S0k</i> and <i>DSS0102</i> used as event ties	109
7.1 Intercomparison of snow pit signals and meteorological conditions	143
8.1 Details of the snow pits and firn cores used in the event scale examination	153
8.2 Summer events preserved in Law Dome snow pits and firn cores	160
8.3 Autumn events preserved in Law Dome snow pits and firn cores	171
8.4 Winter events preserved in Law Dome snow pits and firn cores	181
8.5 Spring events preserved in Law Dome snow pits and firn cores	188

List of Figures

1.1 Simplified fractionation model for oxygen isotopes	3
1.2 Possible sources of natural sulphur preserved in polar ice	10
2.1 Location map for Law Dome	23
2.2 Location schematic for the snow pits and firn cores	24
2.3 Snow pit sampling probe and template	27
2.4 Schematic cross section of the <i>Rama</i> snow pit	28
2.5 Schematic cross section of the longitudinal cuts made in firn cores	30
2.6 Decontamination of a firn core sample	31
2.7 Cation separation	33

2.8	Anion separation	34
2.9	Calibration curve for sodium	35
3.1	Seven line intra-pit comparison for the <i>Rama</i> snow pit	40
3.2	Seven line intra-pit comparison for the <i>Rama</i> snow pit with an adjusted depth scale	43
3.3	Average chemical and $\delta^{18}\text{O}$ records for the <i>Rama</i> snow pit	44
3.4	Location schematic for the <i>Rama</i> , <i>Karioke</i> and <i>Paddy</i> snow pits	46
3.5	Inter-pit comparisons from the three snow pits	48
3.6	Location schematic for the firn cores	49
3.7	Inter-core $\delta^{18}\text{O}$ comparisons	51
3.8	Inter-core MSA comparisons	52
3.9	Inter-core nitrate comparisons	55
3.10	Inter-core non-sea salt sulphate comparisons	56
3.11	Inter-core sodium comparisons	58
3.12	Inter-core magnesium comparisons	59
4.1	Monthly air temperatures measured at Casey station and from AWS 1181	65
4.2	Daily average 4 m air temperature recorded from AWS 1181	66
4.3	Four year average temperature record	67
4.4	Tiled figure of daily average 4 m air temperatures	69
4.5	Daily average 4 m wind speed recorded from AWS 1181	70
4.6	Four year average wind speed record	71
4.7	Daily average wind direction recorded from AWS 1181	72
4.8	Four year average wind direction record	73
4.9	Correlation between wind direction and wind speed	74
4.10	Tiled figure of daily average 4 m wind speeds and wind directions	75
4.11	Daily average barometric pressure recorded from AWS 1181	77
4.12	Four year average barometric pressure record	78
4.13	Tiled figure of daily average barometric pressure	80
4.14	Total and net snow accumulation recorded from AWS 1181	82
4.15	Local meteorological conditions from AWS 1181	85
5.1	Total and net snow accumulation from AWS 1181	90
5.2	Total and net snow accumulation for <i>Rama</i> events	91
5.3	Total and net snow accumulation for <i>Matilda</i> events	92
5.4	Trace chemical and $\delta^{18}\text{O}$ signals for <i>Matilda</i> events	95
5.5	Trace chemical and $\delta^{18}\text{O}$ signals for <i>DSS0102</i> events	97

5.6	Trace chemical and $\delta^{18}\text{O}$ signals for <i>Rama</i> events	100
5.7	Trace chemical and $\delta^{18}\text{O}$ signals for <i>S0k</i> events	101
5.8	Snow pit density profiles	103
5.9	Firn core density profiles	104
5.10	MSA, sodium and $\delta^{18}\text{O}$ records preserved in <i>S0k</i>	105
5.11	MSA, sodium and $\delta^{18}\text{O}$ records preserved in <i>DSS0102</i>	107
5.12	MSA, sodium and $\delta^{18}\text{O}$ records preserved in <i>DSS0102</i> corrected for densification	108
6.1	MSA, sodium and $\delta^{18}\text{O}$ records preserved in <i>DSS0102</i> corrected for densification	116
6.2	Comparison between $\delta^{18}\text{O}$ and air temperatures for <i>DSS0102</i>	117
6.3	Linear correlation of $\delta^{18}\text{O}$ values and air temperatures	119
6.4	Comparison between $\delta^{18}\text{O}$ and pressure	122
6.5	Linear correlation of $\delta^{18}\text{O}$ and pressure	123
6.6	Comparison between MSA and air temperatures	123
6.7	Correlation of MSA and air temperatures	125
6.8	Comparison between nitrate and air temperatures	127
6.9	Linear correlation of nitrate and air temperatures	127
6.10	Comparison between non-sea salt sulphate and air temperatures	129
6.11	Correlation of non-sea salt sulphate and air temperatures	129
6.12	Comparison between sodium and wind speed	131
6.13	Linear correlation of sodium and wind speeds	132
6.14	Comparison between sodium and wind direction	132
6.15	10 day back trajectories for net accumulation events	134
7.1	Total and net accumulation from 21 December 1997 to 27 February 2000	140
7.2	Chemical and $\delta^{18}\text{O}$ records from <i>Rama</i>	141
7.3	Local meteorological conditions from 1 December 1999 to 27 February 2000	145
7.4	AVHRR satellite imagery associated with net accumulation periods	146
8.1	Local meteorological conditions from 1 December 1998 to 28 February 1999	225
8.2	Local meteorological conditions from 1 December 1999 to 29 February 1999	226
8.3	Local meteorological conditions from 1 December 2000 to 28 February 2001	227
8.4	Local meteorological conditions from 1 December 2001 to 31 December 2001 ...	228
8.5	AVHRR satellite imagery for Event 18	229
8.6	AVHRR satellite imagery for Event 19	230
8.7	AVHRR satellite imagery for Event 20	231
8.8	AVHRR satellite imagery for Event 27	232

8.9	AVHRR satellite imagery for Event 28	233
8.10	AVHRR satellite imagery for Event 41	234
8.11	AVHRR satellite imagery for Event 42	235
8.12	AVHRR satellite imagery for Event 1	236
8.13	AVHRR satellite imagery for Event 25	237
8.14	AVHRR satellite imagery for Event 21	238
8.15	AVHRR satellite imagery for Event 29	239
8.16	AVHRR satellite imagery for Event 26	240
8.17	AVHRR satellite imagery for Event 30	241
8.18	Local meteorological conditions from 1 March 1998 to 31 May 1998	243
8.19	Local meteorological conditions from 1 March 1999 to 31 May 1999	244
8.20	Local meteorological conditions from 1 March 2001 to 31 May 2001	245
8.21	AVHRR satellite imagery for Event 13	246
8.22	AVHRR satellite imagery for Event 50	247
8.23	AVHRR satellite imagery for Event 10	248
8.24	AVHRR satellite imagery for Event 11	249
8.25	AVHRR satellite imagery for Event 12	250
8.26	AVHRR satellite imagery for Event 14	251
8.27	AVHRR satellite imagery for Event 15	252
8.28	AVHRR satellite imagery for Event 16	253
8.29	AVHRR satellite imagery for Event 17	254
8.30	AVHRR satellite imagery for Event 37	255
8.31	AVHRR satellite imagery for Event 38	256
8.32	AVHRR satellite imagery for Event 51	257
8.33	Local meteorological conditions from 1 June 1998 to 31 August 1998	259
8.34	Local meteorological conditions from 1 June 1999 to 31 August 1999	260
8.35	Local meteorological conditions from 1 June 2000 to 31 August 2000	261
8.36	Local meteorological conditions from 1 June 2001 to 31 August 2001	262
8.37	AVHRR satellite imagery for Event 8	263
8.38	AVHRR satellite imagery for Event 9	264
8.39	AVHRR satellite imagery for Event 36	265
8.40	AVHRR satellite imagery for Event 49	266
8.41	AVHRR satellite imagery for Event 5	267
8.42	AVHRR satellite imagery for Event 6	268
8.43	AVHRR satellite imagery for Event 7	269

8.44 AVHRR satellite imagery for Event 24	270
8.45 AVHRR satellite imagery for Event 46	271
8.46 AVHRR satellite imagery for Event 47	272
8.47 AVHRR satellite imagery for Event 48	273
8.48 Local meteorological conditions from 1 September 1998 to 30 November 1998 ..	275
8.49 Local meteorological conditions from 1 September 1999 to 30 November 1999 ..	276
8.50 Local meteorological conditions from 1 September 2000 to 30 November 2000 ..	277
8.51 Local meteorological conditions from 1 September 2001 to 30 November 2001 ..	278
8.52 AVHRR satellite imagery for Event 3..	279
8.53 AVHRR satellite imagery for Event 4	280
8.54 AVHRR satellite imagery for Event 32	281
8.55 AVHRR satellite imagery for Event 33	282
8.56 AVHRR satellite imagery for Event 34	283
8.57 AVHRR satellite imagery for Event 35	284
8.58 AVHRR satellite imagery for Event 2	285
8.59 AVHRR satellite imagery for Event 22	286
8.60 AVHRR satellite imagery for Event 31	287
8.61 AVHRR satellite imagery for Event 43	288
8.62 AVHRR satellite imagery for Event 44	289
8.63 AVHRR satellite imagery for Event 45	290

Chapter 1

Introduction and Review of Relevant Literature

1.1 Overview

Ice core records from the world's glaciated regions have proven to be valuable tools for palaeoclimate reconstruction, recording both anthropogenic and natural changes in atmospheric composition. One of the most important questions facing physical scientists today involves separating the impact of humans on global climate from natural climate cycles. Anthropogenic effects such as global warming and the enhanced greenhouse effect are well known aspects of today's climate. Predicting the impact of these effects on the world's environment requires an inherent understanding of the natural variability of climate changes prior to human influence (~1800 A.D.). The acquisition of this knowledge is possible through the study of palaeoclimate records from tree-rings, corals, sediment cores and ice cores.

Glacial ice sheets are comprised of accumulated snowfall events, and thus preserve information about the atmosphere at the time of snowfall. Information about past climate conditions is preserved in the ice core as insoluble particles and air bubbles entrapped in the ice matrix, absorbed gases, dissolved trace ion species, and in the isotopic composition of the ice. Measurement of the chemical, isotopic, gaseous and physical properties of the ice provides a wealth of climate information about the ancient atmosphere, *e.g.* temperature, precipitation, chemistry and gas composition of the lower atmosphere, volcanic activity, solar variability, and sea surface biological activity (Bradley, 1999; Delmas, 1998; Legrand and Mayewski, 1997; Masson-Delmotte and others, 2004; Mayewski and others, 2004).

However, our ability to interpret ice core signals is limited by difficulties in understanding the relative importance of changes in source, transport and deposition

processes that influence a precipitating air mass. A relatively new avenue for ice core research is aimed at improving our understanding of the link between the ice core record and observed atmospheric conditions. These calibration studies require high resolution records of the firn and ice column, generally focussing on recently accumulated material and contemporaneous meteorological conditions. With the collective aim of improving our understanding of the ice core signal, a number of limited studies have been conducted using real time snowfalls (Wolff and others, 1998), atmosphere to snow transfer of particulates (Fuhrer and others, 1996; McConnell and others, 1997a) and comparisons between snow and firn core material and observed atmospheric conditions (McConnell and others, 1997b; Hardy and others, 1998; M^cMorrow and others, 2001; M^cMorrow and others, 2002; Naftz and others, 2002; Masson-Delmotte and others, 2003).

This study is concerned with further investigating the relationship between ice core signals and observed atmospheric conditions for Law Dome drilling site in East Antarctica. Law Dome has a valuable high resolution deep ice core that is used to reconstruct atmospheric conditions over the past ~90 000 years. This deep ice core provides a motivating factor for this study to enhance our understanding of the link between ice core signals and atmospheric conditions at Law Dome. Particular focus is given to examining the extent to which ultra high resolution records of the top 10 m of the snowpack at Law Dome, covering approximately 8 years, can be explained by observed meteorological conditions. The remainder of this chapter presents a literature review and discussion of relevant topics to provide background information on the issues examined in this work.

1.2 Oxygen Isotopes in the Antarctic

1.2.1 The Isotopic Composition of Precipitation

The analysis of the ratio between oxygen isotopes ^{16}O and ^{18}O ($\delta^{18}\text{O}$) preserved in polar firn and ice cores provides information relating to the isotopic composition of the water vapour in the atmosphere during precipitation. The isotopic composition of polar precipitation may be described by a simplified fractionation model (Fig. 1.1). Water molecules containing the heavier oxygen isotope, ^{18}O , contribute around 0.2% of all water (Faure, 1986). The oceans are relatively well mixed by currents and hence are

generally uniform in $\delta^{18}\text{O}$. When water evaporates from the surface of the ocean the water vapour is enriched in ^{16}O since H_2^{16}O has a higher vapour pressure compared to H_2^{18}O . The ratio of the vapour pressures between ^{18}O and ^{16}O defines the equilibrium fractionation factor described by Craig (1961) and Dansgaard (1964). In this equilibrium system fractionation of oxygen isotopes is dependent on air temperatures during evaporation and condensation (Horita and Wesolowski, 1994). Cooling of the air requires that condensation takes place to maintain relative humidity below saturation. During condensation of water vapour the subsequent liquid phase is enriched in ^{18}O and the remaining vapour phase is depleted in ^{18}O . As an air mass is transported the isotopic composition of the air mass becomes depleted in ^{18}O (Fig. 1.1). Additional cooling and precipitation leads to larger depletions of H_2^{18}O in the air mass and resulting precipitation.

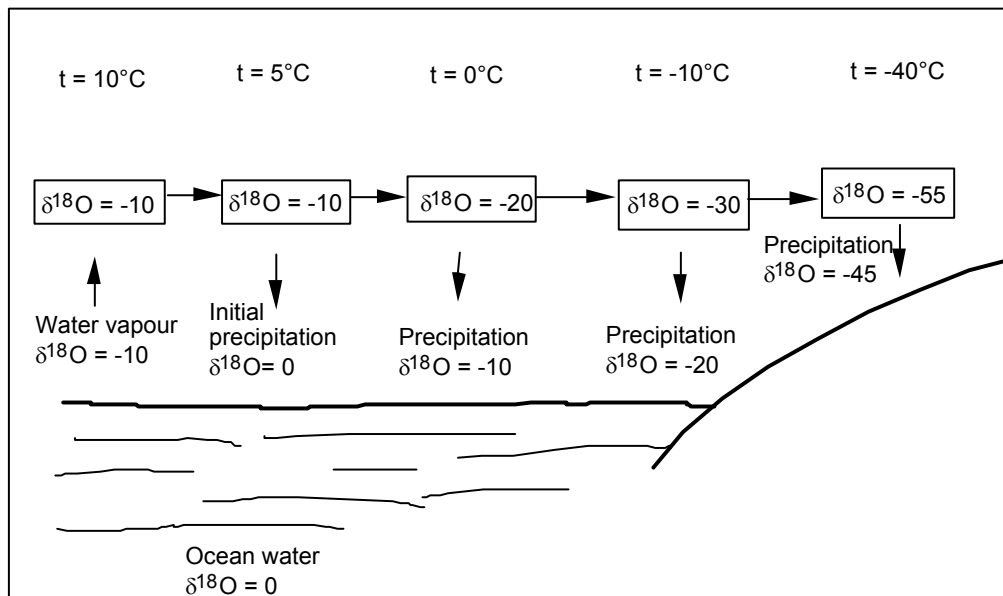


Figure 1.1: Simplified fractionation model for oxygen isotopes (modified from Bradley, 1999).

Isotope ratios in precipitation are reported as deviations in parts per thousand from Standard Mean Ocean Water (SMOW), a reference value adopted because the ratio found in oceanic water is relatively constant. This relationship is described by the following equation:

$$\delta^{18}\text{O} = ((\text{H}_2^{18}\text{O}_{\text{sample}} / \text{H}_2^{18}\text{O}_{\text{smow}}) - 1) \times 1000\%$$

Where $\text{H}_2^{18}\text{O}_{\text{sample}}$ and $\text{H}_2^{18}\text{O}_{\text{smow}}$ refer to the fractions of H_2^{18}O in the sample and SMOW respectively.

1.2.2 The Ice Core Palaeothermometer

The $\delta^{18}\text{O}$ value becomes progressively more negative as air masses are transported from the oceans in mid latitudes towards polar regions (Fig. 1.1). Temperature generally decreases as latitude increases, leading to a strong spatial correlation between the annual mean temperature at a site and the isotopic content of the precipitation at that site (Dansgaard, 1964; Araguas-Araguas, 2000; Schneider and others, 2005). While the fractionation of isotopes is dependent on temperature, the mass of water remaining in the air mass when it cools is also dependent on temperature through the saturation vapour pressure (Dansgaard, 1964). These two effects drive the observed relationship between $\delta^{18}\text{O}$ and temperatures in polar regions.

The strong dependence of $\delta^{18}\text{O}$ on air temperatures allows $\delta^{18}\text{O}$ records from polar firn and ice cores to be used as a source of proxy temperature data for palaeoclimate reconstruction (eg. Picciotto and others, 1960; Morgan, 1979; Bradley and Jones, 1993; Schotterer and others, 1997; van Ommen and Morgan, 1997; Mann and Jones, 2003). Reduction of observed isotope measurements to inferred temperatures relies on knowledge of this dependence, which is generally well approximated by a linear relationship:

$$\delta^{18}\text{O} = \alpha T + \beta$$

where T refers to temperature and the parameters $\alpha = d\delta/dT$ and β are the calibration constants for the isotope thermometer. This calibration is derived from either spatial variability, or from the temporal variation at a site. Spatially derived parameters have typically yielded slopes, α , of 0.6-0.7‰/°C (Dansgaard, 1964; Morgan, 1979).

Modelling of the physical process of fractionation as water vapour is progressively lost from a cooling air mass yields a similar slope of 0.7‰/°C (Dansgaard, 1964). However, the use of spatially derived parameters for a particular site may not be appropriate as other processes such as changes in air mass origin and transport may also influence the isotopic signal for that site. Therefore, temporal calibration of the isotope thermometer may be more appropriate. Recent temporal analyses for Law Dome have yielded slopes of 0.44‰/°C for long term (~700-year) $\delta^{18}\text{O}$ seasonality (van Ommen and Morgan, 1997) and 0.21‰/°C for an ultra high resolution, short term (~8 months) $\delta^{18}\text{O}$ record (McMorrow and others, 2001).

Although temperature is an important variable influencing the isotopic signature of polar snow, there are other factors which impact on the isotopic composition of precipitation. The effects of continentality on isotopic composition have been described by many studies (eg. Kato, 1978; Bromwich and Weaver, 1983; Zwally and others, 1998). As a parcel of air moves inland from a coastal location and condensation occurs, the moist marine air and resultant precipitation becomes increasingly depleted in the heavier ^{18}O . Altitude effects have also been investigated with $\delta^{18}\text{O}$ gradients larger over regions with high elevation mountain ranges (Siegenthaler and Oeschger, 1980; Zwally and others, 1998; Araguas-Araguas, 2000). As an air mass ascends over mountain ranges the water vapour will reach saturation relatively quickly and condensation will occur, resulting in isotopic rainout of the heavier ^{18}O isotopes. Continentality and altitude effects are intrinsically connected as continents are generally higher than oceanic surfaces, yet the altitude effect becomes increasingly important in areas with high elevation mountain ranges. East Antarctica is generally characterised by a narrow coastal strip which rises quickly to above 2 km in elevation on the inland plateau. Thus, continental and altitude effects are important in this region, yet it should be noted that both effects are also linked to temperature to some degree.

Extrapolating the physical principles which describe isotopic fractionation to reconstruct palaeoclimates from ice cores is not a simple matter. Although empirical studies have demonstrated that $\delta^{18}\text{O}$ records from ice cores may be used to reconstruct palaeotemperatures, the isotopic signal is influenced by processes which are inherently more complex than simple fractionation processes. A comprehensive understanding of the origin and circulation of air masses from which the precipitation is formed is required before variations in $\delta^{18}\text{O}$ preserved in the ice core can be reconstructed into a climate record.

1.3 Trace Ion Species in the Antarctic

The analysis of trace ion species preserved in polar snow provides a wealth of climatic information. However, the successful interpretation of trace ion records preserved in the ice core requires an inherent understanding of the source regions, transport and deposition mechanisms influencing each species. There are three main groups of ionic aerosol species found in the atmosphere of coastal Antarctic sites, and thus in the ice core record:

- Sea salt ions
- Marine biogenic sulphur compounds
- Nitrate.

1.3.1 Sea Salt Ions

The concentrations of sea salt ions preserved in Antarctic snow reflect the sea salt input for a particular site. Seawater is composed of pure water, dissolved inorganic salts, dissolved organic compounds from living organisms and dissolved gases. The majority of solid salt matter in seawater is inorganic (99.3%) and predominately composed of chloride (55.0%), sodium (30.6%), sulphate (7.7%), magnesium (3.7%), calcium (1%) and potassium (1%) (Wilson, 1975).

Sea Salt Particle Production

Sea salt particles in the atmosphere are produced mainly by the bursting of air bubbles from wave crest disruptions on the ocean surface when wind speeds exceed 3 ms^{-1} (Fitzgerald, 1991). Each bursting bubble produces between one and ten jet drops, which become sea salt particles, and up to several hundred smaller film drops which remain sea salt solution droplets. The total number of sea salt particles produced by bubble bursting depends on the size of the bubbles which in turn relies on the wind speed over the open ocean (Fitzgerald, 1991). The direct injection of large spray drops into the marine boundary layer also produces sea salt particles. This process is associated with white caps from breaking waves where wind speeds exceed $7 - 11 \text{ ms}^{-1}$ (O'Dowd and others, 1999). Thus, the concentration of sea salt aerosols is largely controlled by local wind speeds over the ocean surface. Gong and others (1997) have shown through modelling studies that about 99% of the sea salt aerosol mass generated by wind stress over the ocean falls back into the sea with the remaining 1-2% exported out of the original grid square (300 x 300 km). Furthermore, only 4% of the sea salt aerosols

which are exported are comprised of submicron particles that are likely to undergo long range transport.

In the Antarctic, sea salt particles are the only primary aerosols to be produced in significant quantities within the South Polar cell (Wagenbach and others, 1998a). Thus, these species may add a substantial fraction of the seawater sulphate to the total sulphate budget of this region. In addition, the low concentrations of ammonium in the modern Antarctic region make the sea salt ion an important alkaline counterpart for the more abundant acidic components such as non-sea salt sulphate, methansulphonic acid (MSA) and nitric acid (Wagenbach and others, 1998a).

Atmospheric sea salt particles are an important climate forcing due to their ability to act as condensation nuclei for other species (eg. bromide and iodide). These condensation nuclei have been shown to contribute to cloud processes and scattering of incoming radiation (Latham and Smith, 1990). Sea salt particles also participate in a series of heterogeneous air chemical processes which are responsible for large fluxes of hydrochloric acid (HCL) into the remote marine troposphere (McInnes and others, 1994).

Sea Salt Ions as Climate Indicators

Numerous sea salt records have been recovered from deep Antarctic ice cores and there is clear evidence for higher sea salt levels during glacial times (Petit and others, 1981; Legrand and Delmas, 1988; Clausen and Langway, 1989). These records are generally interpreted as indicating intensified sea salt production associated with higher cyclonic activity in the Southern Ocean during the glacial period. High resolution ice core records from recent (up to 200 years) accumulated material also show a strong link between sea salt concentrations and cyclonic activity. Coastal Antarctic sites generally exhibit a clear seasonal cycle in sea salt ions with higher concentrations during the austral winter, corresponding with a higher frequency of Southern Ocean cyclonic events intruding into the Antarctic region (Legrand and Delmas, 1984; Legrand and others, 1998; Minikin and others, 1994; Curran and others, 1998a; Wagenbach and others, 1998a). More recent research by Goodwin and others (2004) demonstrates a link between sea salts preserved in Antarctic ice cores and midlatitude winter atmospheric

variability in the Southern Ocean, with higher sea salt concentrations associated with increased meridional transport from midlatitude sources.

The winter maximum in sea salt concentrations preserved in ice cores represents a cycle which is out of phase of the open water fraction of the Southern Ocean resulting from seasonal sea ice growth and decay. This suggests that the main source of sea salt particles for Antarctic sites overcompensates the larger sea ice extent during the austral winter. A number of potential sources for the winter sea salt maxima have been identified in the literature. Coastal polynyas transiently opened by strong winds and ocean currents may provide a local source, although these sources cannot explain the large peaks observed in winter snow layers at high latitudes and high elevations. Moreover, coastal polynyas are often maintained by katabatic flow draining off the ice sheet (Worby and others, 1998), which would tend to direct sea salt aerosols away from the Antarctic continent. The increased production of spume drops from the surf zones prevailing at the rim of leads and ice floes under moderate wind speeds may also provide a local source. However, this mechanism doesn't explain winter peaks detected in inland and elevated ice core sites. Moreover, leads within the 10% open water fraction of winter sea ice typically show reduced wind speeds, suggesting reduced sea salt aerosol formation (Wagenbach and others, 1998a). Chemical sea salt fractionation from sulphate depletion during freezing of airborne sea water droplets at temperatures below -8°C may also explain winter sea salt maxima (Wagenbach and others, 1998a). However, this hypothesis does not explain the seasonal sea salt cycle observed in ice cores from coastal sites such as Law Dome where sea ice extent is only around 300 km off the coast, and percentage cover is often less than 70% (Gloersen and others, 1992). Finally, the formation of sea ice may itself provide a local source of sea salt for coastal Antarctic sites (Perovich and Richter-Monge, 1994; Rankin and others, 2000, Rankin and others, 2004; Kaleschke and others, 2004). As sea ice forms the salt is rejected from the ice crystals and forms a thin layer of brine of the surface of the ice. In low wind conditions frost flowers may develop from the surface brine. These frost flowers are thought to pull up brine from the surface layer by capillary action, and measurements of the salinity of the frost flowers have shown salinities similar to that of the brine layer (Perovich and Richter-Monge, 1994). Frost flowers only form during the winter on new sea ice when wind speeds are low. High wind speeds destroy the flowers or bury them with blowing snow (Rankin and others, 2000). Further research into potential source

regions and transport mechanisms are required to provide a more comprehensive understanding of the climate signals influencing the sea salt signal in ice cores.

1.3.2 Marine Biogenic Sulphur Compounds

There are two sulphur compounds observed in Antarctic firn and ice cores which are believed to indicate biological activity:

- Methansulphonate (MSA)
- Non-sea salt sulphate (nss SO₄).

The non-sea salt contribution of sulphate is usually calculated on the basis of sodium (Na) content in seawater using the following equation:

$$\text{nss SO}_4^{2-} = (\text{SO}_4^{2-}) - \chi(\text{Na})$$

where χ is the molar ratio of sulphate to sodium in seawater.

The Natural Sulphur Cycle

In addition to modern anthropogenic sulphur dioxide (SO₂) emissions, which on a global scale dominate the sulphur cycle, other sources of sulphur participate in the sulphur cycle. Figure 1.2 illustrates the many sources of atmospheric sulphate, including marine biogenic activity, oceanic sea salt aerosols, anthropogenic emissions, continental sources and volcanic emissions. Natural sources include volcanic emissions, mineral dust from continental regions and dimethylsulphide (DMS) emissions from marine biota. The production of DMS in the surface water of the oceans is caused by the decomposition of dimethylsulphoniopropionate (DMSP) which regulates the osmotic pressure of macroalgae (seaweeds) and phytoplankton cells (Anderson and others, 1995). DMS is released into the atmosphere via bubble bursting and gas to particle conversion processes (O'Dowd and others, 1997). From the atmosphere DMS is then oxidised by hydroxide (OH) and nitrate (NO₃) radicals. Final oxidation products include sulphate (SO₄²⁻) and methansulphonate (CH₃SO₃⁻, MSA) (Legrand, 1995; Allan and others, 1999). There is general agreement among researchers that non-sea salt sulphate in coastal Antarctic sites mainly originates from marine DMS emissions, with a small contribution from volcanic emissions in periods of reduced volcanic activity (Legrand, 1997; Minikin and others, 1998). Furthermore, due to the large oceanic sector within the Antarctic region, mineral dust sources of sulphate from continental regions remains low. Unlike non-sea salt sulphate, the only source of atmospheric MSA is the oxidation of DMS from marine biota.

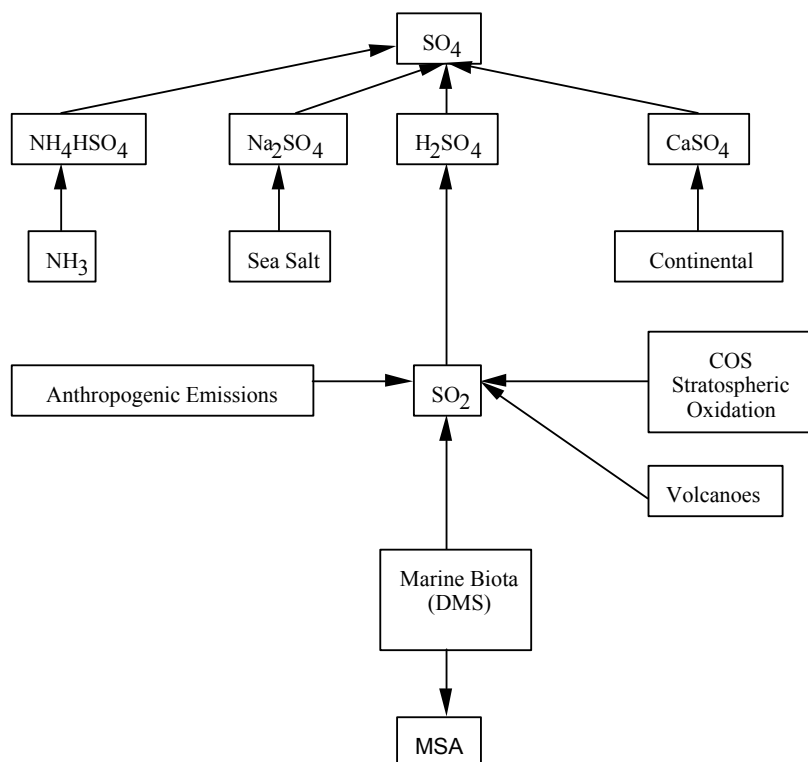


Figure 1.2: Possible sources of natural sulphur preserved in polar ice (Legrand, 1995).

The recent interest in sulphur compounds stems from the ability for these particles to act as cloud condensation nuclei and potential implications of a DMS-climate feedback loop (Charlson and others, 1987; Burgermeister and Georgii, 1991). The ability for DMS particles to nucleate cloud droplets has the effect of changing cloud albedo characteristics and cloud lifetime by changing the cloud droplet number and thus the amount of incoming solar radiation which reaches the planetary surface (Charlson and others, 1987). This in turn affects surface temperatures and other climate variables. Due to the complexity associated with interactions between the climate and oceanic biota, the overall impact of this feedback loop on the climate system remains uncertain.

Marine Biogenic Compounds as Climate Indicators

The extraction of non-sea salt sulphate and MSA records from deep ice cores enables a reconstruction of marine biogenic activity over time. Several studies have suggested that climate fluctuations on a variety of time scales will affect DMS production from marine emissions (eg. Legrand and others, 1991; Dibb and Whitlow, 1996; Legrand, 1997). Reconstruction of MSA and non-sea salt sulphate records from Vostok indicate increased oceanic emissions of DMS during the later stages of the glacial period compared with the more recent Holocene (Legrand and others, 1991). Shorter term

climate variations will also influence the marine biogenic sulphur records preserved in ice cores. Research suggests a tentative link between MSA concentrations and major El Niño Southern Oscillation (ENSO) events (Dibb and Whitlow, 1996; Isaksson and others, 2001). Furthermore, evidence has been presented for enhanced sea ice extent to be reflected in the ice core record through high MSA concentrations (Gibson and others, 1990; Welch and others, 1993; Minikin and others, 1998, Curran and others, 2003).

The seasonal cycles of non-sea salt sulphate and MSA for coastal Antarctic sites exhibit similar characteristics with a pronounced summer maximum and winter minima (Legrand, 1997; Curran and others, 1998a; Minikin and others, 1998). Firn core records from Law Dome reveal minimum levels of non-sea salt sulphate and MSA in August, which increase to a sharp peak in January (Curran and others, 1998a). This is in agreement with studies based on firn and ice cores retrieved from coastal West Antarctica (Peel and Mulvaney, 1992), the Antarctic plateau (Legrand and others, 1991), and the Antarctic Peninsula (Mulvaney and others, 1992). Aerosol samples of non-sea salt sulphate and MSA from three coastal Antarctic sites (Neumayer, Dumont D'Urville, Mawson) also indicate a broad winter trough and sharp summer peak (Minikin and others, 1998). Intersite differences occur in concentrations, although all three sites reach a maximum during January. Aerosol measurements from Cape Grim, Tasmania also show this strong seasonal cycle for sulphur compounds (Ayers and others, 1991).

The seasonal cycles of the sulphur compounds may be explained by phytoplankton blooms during the annual retreat of the winter sea ice. The release of sea ice algae into surface waters from melting ice floes during the austral spring provides an additional source of active phytoplankton growth into the Southern Ocean at this time (Smith and Nelson, 1991; Knox, 1994). The mid summer maxima in MSA and non-sea salt sulphate are likely to be sourced from DMS production during the decomposition of these spring phytoplankton blooms (Legrand and Pasteur, 1998).

The non-sea salt sulphate record for many sites often shows negative calculated values during the winter period (Hall and Wolff, 1998; Harder and others, 2000; Wagenbach and others, 1998a). These negative values generally correspond with high concentrations of sea salt in the aerosol or snow sample (Wagenbach and others,

1998a). Recent research has demonstrated that these negative non-sea salt sulphate values may reflect chemical fractionation of sulphate through frost flowers on newly formed sea ice (Rankin and others, 2000; Rankin and others, 2002). Frost flowers provide a source of sea salt that is depleted in sulphate, and are likely to dominate over open water production of sea salt in regions where there is at least 300 km of sea ice during the winter months and when temperatures are below -8°C (Rankin and others, 2000; Rankin and others, 2002).

1.3.3 Nitrate

Sources of Nitrate in Polar Snow

The atmospheric nitrogen cycle is highly complex and there are a wide range of factors which can influence the nitrate concentration in polar snow. Sources of nitrate in polar snow remain uncertain, and potential input from marine, terrestrial, atmospheric and anthropogenic sources have been considered in the literature.

The oceans contain large amounts of nitrogen species, mainly as dissolved organic nitrogen (DON), nitrate, nitrite and ammonium, with DON forming the largest component (Hu and Smith, 1998; Skoog and others, 2001). Terrestrial sources of nitrate include biomass burning, fossil fuel burning and natural soil release. Terrestrial sources dominate the production of nitrogen species within the troposphere, but their contribution to the Antarctic nitrogen budget remains limited (Legrand and Kirchner, 1990; Levy and others, 1999). This is due to the relative absence of anthropogenic activities in the Southern Hemisphere, the extensive oceanic coverage around the Antarctic region, and the efficient removal of nitrogen from the troposphere by deposition (Legrand and others, 1989).

The main sources of nitrogen originating within the atmosphere is caused by lightning in the troposphere and the oxidation of nitric acid in the stratosphere. Lightning has a significant effect on the global budget of nitrogen species, in particular the enhancements of odd-nitrogen species, nitric acid (N_2O) and peroxyacetyl nitrate (Tie and others, 2001). Although lightning occurs predominately in the low latitudes, it is believed to contribute to the Antarctic nitrate budget through diabatic transport through the stratosphere (Legrand and Delmas, 1986; Wolff, 1995). Recent estimates of the global production of lightning sourced nitrogen species suggest around

$10 - 15 \times 10 \text{ kg N yr}^{-1}$ (Pearce, 1997). The oxidation of N_2O is a major stratospheric source of nitrogen to the global atmosphere. Surface and tropospheric sources of N_2O include discharge from soils, release from the ocean, biomass burning, fossil-fuel combustion and artificial fertilisers (Legrand and others, 1989). Through advection of air in the tropics and midlatitudes, these surface and tropospheric sources of N_2O reach the stratosphere. In the stratosphere this species undergoes photodecomposition to produce nitrogen oxides through the following reaction (Warneck, 1988):



The oxidation of N_2O is a major atmospheric source of nitrogen and has been estimated to contribute around $0.5 - 1.0 \times 10 \text{ kg N yr}^{-1}$ (Legrand and Kirchner, 1990).

In the Antarctic region the transport of nitrogen species from the stratosphere to the troposphere occurs through the weakening of the polar vortex and subsequent downward mixing of air during spring and summer (Whitlow and others, 1992). During the austral summer the Antarctic stratosphere receives more solar radiation than lower latitudes and a weak easterly circulation results. From February, as solar heating reduces, the Antarctic stratosphere cools rapidly and an intense westerly vortex develops until the stratosphere warms again in the austral spring. The breakup of the westerly vortex in spring allows an increased exchange of tropospheric and stratospheric air, with greater intrusion of stratospheric aerosols into the troposphere (Shaw, 1988; König-Langlo and others, 1998). Temperatures within the polar vortex drop to very low levels in the stratosphere (-80°C) (Mulvaney and Wolff, 1993). At these temperatures, chemicals in the stratosphere freeze and form polar stratospheric clouds (PSCs). PSCs are composed mainly of nitric acid trihydrate and generally form during the weakening of the polar vortex (Legrand and Kirchner, 1990). The altitude of PSCs is lowest during winter-spring (July to October), resulting in an increased concentration of N_2O in the troposphere during these months (Mayewski and Legrand, 1990; Mulvaney and Wolff, 1993). Thus, the formation of PSCs provides an important source for odd-nitrogen species, particularly N_2O , for Antarctic snow.

Odd nitrogen species are also formed in polar regions by incident solar and geomagnetic charged particles. These particles follow the Earth's magnetic field into the polar atmosphere where they deposit their energy in the middle and upper atmosphere through chemical reactions with oxygen and nitrogen atoms, forming odd-nitrogen.

Changes in solar and geomagnetic activity such as auroral displays or solar particle events can drastically change the flux of the energetic particles (Vitt and Jackman, 1996). This leads to large variations in the formation of odd nitrogen in the polar atmosphere.

Nitrate as a Climate Indicator

Due to the complexity of the atmospheric nitrogen cycle the interpretation of nitrate records from deep ice cores remains uncertain. Evidence has been presented both for (Zeller and Dreschhoff 1995; Dreschhoff and Zeller, 1998; Wang and others, 2000; McCracken and others, 2001; Palmer and others, 2001) and against (Legrand and Kirchner, 1990; Mosely-Thompson and others, 1991) the preservation of a solar source of nitrate in long term records, although the most recent research suggests a positive correlation between nitrate and solar activity.

High resolution firn and ice core records reveal a distinct seasonal cycle in nitrate characterised by a sharp summer peak and a broad winter minimum (Legrand and Delmas, 1984; Minikin and others, 1994; Curran and others, 1998a; Kreutz and others, 1999; Wagenbach and others, 1998b). Previous studies on high resolution Law Dome firn cores show increasing nitrate concentrations from June until a spring shoulder is reached in November, with further sharp rises in concentrations until January (Curran and others, 1998a). Studies from Siple Dome, a low accumulation coastal site, indicate similar results but with a late spring rather than mid summer maximum in nitrate concentrations (Kreutz and others, 1999). Aerosol measurements of atmospheric nitrate from three coastal Antarctic stations (Mawson, Neumayer, Dumont D'Urville) show minimum concentrations between April and June, and late spring/early summer enhancement (Wagenbach and others, 1998b).

1.4 Deposition of Atmospheric Contaminants to Polar Snow

The transport of aerosol species to surface snow generally involves one of three main deposition mechanisms:

- Dry deposition of particles directly to the snow surface;
- Wet deposition with snow or ice crystals;
- Fog deposition.

Other factors may also influence the transfer of aerosol species to surface snow such as drifting or blowing snow and post depositional movement or loss of chemical species.

1.4.1 Dry Deposition

Dry deposition refers to the transport of particulate and gaseous contaminants from the atmosphere to the snow surface without precipitation (Davidson, 1989; Davidson and others, 1996). This process is believed to occur in three sequential steps, namely aerodynamic transport, boundary layer transport and interaction with the snow surface.

Aerodynamic transport refers to the process that occurs as the chemical contaminants are carried from the lowest layers of the atmosphere to the viscous sublayer of air just above the surface of the snow (Davidson and others, 1996). The principle mechanism for aerodynamic transport involves eddy diffusion where particles and gases are transported by wind eddies from regions of relatively high concentration to regions of lower concentration (Davidson and others, 1996).

Boundary layer transport involves the movement of contaminants across the viscous sublayer of air just above the snow surface. Davidson and others (1996) identified several mechanisms that occur during boundary layer transport:

- Diffusion of contaminants refers to the process where particles and gases are moved along a concentration gradient due to random thermal motion and turbulent wind eddies;
- Interception occurs when a particle on an air streamline passes within one particle radius of the surface;
- Inertial impaction refers to the movement of a particle along a streamline that is captured by a rapid change in direction after encountering rough surface elements such as ice needles;

- Turbulent inertial deposition occurs when a particle impacts the surface while influenced by a turbulent eddy which is moving perpendicular to the surface;
- Sedimentation refers to the gravitational settling of particles and generally influences particles with greater than 1 μm diameter; and
- Gas sorption occurs directly onto the snow crystals or onto a layer of liquid water on the crystals.

Finally, interaction of the particles and gases with the surface determines whether the particle or gas remains on the surface after penetrating the viscous sublayer, or is returned to the lower atmosphere. Particles can stick to the snow or rebound depending on their characteristics and the snow conditions (Davidson and others, 1996).

Previous studies at sites in central Antarctica have estimated the dry deposition flux for several chemical species and concluded that this process is the dominant deposition mechanism for inland sites where accumulation is low (Pourchet and others, 1983; Legrand, 1987). In contrast, dry deposition is generally considered to play a minor role for the transport of ions to surface snow for coastal Antarctic sites where accumulation is high (Wolff and others, 1998).

1.4.2 Wet Deposition

Wet deposition refers to the removal of gaseous and particulate contaminants from the atmosphere by precipitation (Davidson, 1989). Several processes are involved during wet deposition including nucleation, rime attachment, in-cloud scavenging and below-cloud scavenging (Wolff and others, 1998).

Nucleation occurs when contaminant particles are incorporated as nuclei in the ice crystals. In very low temperature regions clouds contain marine or continental aerosols that are conducive to the formation of ice. Once the aerosols become active nuclei, the resulting ice crystals coalesce to form snowflakes. Nucleation is considered an efficient deposition process with an individual snowflake containing up to 10^6 original ice crystals, each with a contaminant particle as a nucleus (Davidson, 1989). Rime attachment adds to the efficiency of nucleating and occurs when contaminants within supercooled liquid droplets attach to snowflakes and freeze (Davidson and others, 1996). Nucleation and rime attachment are believed to be the dominant removal

mechanisms for particles such as sea salts and marine biogenic compounds (Davidson and others, 1996; Minikin and others, 1994).

Scavenging by the collision of contaminants with cloud water or snowflakes (in-cloud) or by falling precipitation (below-cloud) also contributes to wet deposition. In polar regions in-cloud scavenging is thought to be the dominant method of wet deposition for gases (Möller, 1995; Davidson and others, 1996).

Wolff and others (1998) examined the role of deposition mechanisms for three high accumulation coastal Antarctic sites (Neumayer, Halley, Dumont D'Urville). Results showed that wet deposition was the dominant process in transferring particulates from the atmosphere to the snow surface.

1.4.3 Fog Deposition

Fog may occur in polar regions either as ice fog (presence of water in the ice crystal phase) or fog (presence of water as liquid droplets at the surface) (Davidson and others, 1996). During fog deposition the contaminants diffuse into the fog droplets and are deposited as the fog settles. The flux of chemical removal through fog deposition depends on the settling velocity of the fog droplets and the chemical concentration in the fog. It has previously been recorded that the concentrations of chemical species in fog can exceed those in the snow (Davidson and others, 1996). Results from fog studies at Summit, Greenland demonstrated that mean concentrations were higher in collected fog than in collected fresh snow by factors of 4.7 for sulphate and 1.7 for sodium (Bergin and others, 1995). Thus, fog may have a disproportionate effect on chemical deposition to the snow surface.

Recent work by Wolff and others (1998) at the coastal Halley station, Antarctica found that fog deposition contributed to a small proportion (3%) of the total chemical deposition to the snow surface. This finding was mainly due to the rarity of fogs at Halley as fogs were only present for around 5% of the year.

1.4.4 Drifting and Blowing Snow

Blowing snow is defined as wind-borne snow of sufficient depth and density to impair visibility at or above the height of an observer's head, while drifting snow refers to wind-borne snow not reaching this height (King and Turner, 1997). Drifting and blowing snow can affect the chemical concentration of the snow in three ways:

- Scavenging particles from the lower levels of the atmosphere;
- Sublimation of water vapour from drifting snow leading to enhanced chemical concentrations; and
- Movement of snow leading to redistribution of snow or removal of snow from the accumulation record (Wolff and others, 1998).

Snow drift can scavenge particles from the lower levels of the atmosphere and deposit these particles onto the surface when snow drift ceases. Wolff and others (1998) estimated that the flux to the surface from snow drift scavenging amounts to approximately 0.1% of the annual deposition in accumulating snow a suite of chemical ions for a coastal Antarctic station (Halley). Similar results were presented for South Pole using modelling techniques (Harder and others, 1996). These studies suggest that direct scavenging by drifting and blowing snow has a negligible influence on the annual flux of chemical impurities.

Sublimation of water vapour from drifting snow has the potential to lead to considerable enhancement of the chemical concentration in surface snow (Wolff and others, 1998). Modelling studies by Pomeroy and Jones (1996) calculated a sublimation rate of 244 mm water equivalent per year for coastal Antarctica. However, calculations from meteorological observations at Halley station, Antarctica estimate sublimation rates from blowing snow to be considerably lower (3.71 mm water equivalent for a 6-month period from autumn to winter) (King and others, 1996). Observations suggest that when blowing snow occurs, the lowest few metres of the atmosphere are very close to saturation with respect to ice, and this causes relatively low sublimation rates (King and others, 1996; Wolff and others, 1998).

Redistribution of snow or snow removal from blowing or drifting snow will have a significant effect on chemical concentrations at a given site. The removal of entire snowfalls from an accumulation record has been reported at a number of ice coring sites

(Hardy and others, 1998; Wolff and others, 1998; M^cMorrow and others 2002). In addition, snowfalls that did not take place at a coring site may have been blown into the record. The quantification of snow redistribution by wind remains uncertain, yet the effects may be considered in comparing well dated high resolution records with wind speed and direction data. For example, at coastal Antarctic sites it is expected that sea salt concentrations in surface and buried snow are higher at sites close to the oceanic source. Thus, blowing or drifting snow carried inland is expected to increase the sea salt concentrations for the more inland site.

1.4.5 Post Depositional Modification of Chemical Species

A number of studies have reported post depositional movement or loss of chemical species within the snow. Of the suite of chemical and isotopic species examined in this work, four have been demonstrated to be affected by post depositional modification.

Hydrogen peroxide (H_2O_2) is the clearest example of a species that undergoes diffusive smoothing throughout the firn layer (Sigg and Neftel, 1991). Post depositional diffusion is caused by movement of H_2O_2 in the vapour phase through the pore space (Wolff, 1996). The $\delta^{18}\text{O}$ signal is also subject to post depositional diffusion, although the rate of diffusion is slower (Whillans and Grootes, 1985).

The deposition of nitrate is proposed to be severely affected by post depositional loss of nitric acid, where up to 70% of surface nitrate may be lost during burial (Mulvaney and Wolff, 1993; Mulvaney and others, 1998). Ice core records from low accumulation sites in Antarctica show dramatic decreases in nitrate concentrations in the first metre of core (Mayewski and Legrand, 1990; Wagon and others, 1999). However, nitrate losses in the surface layer of firn from moderate to high accumulation sites is more difficult to determine. Mulvaney and others (1998) found no evidence for a consistent loss of nitrate over the timescales of a few days at Halley station, Antarctica. Rather, both uptake and loss of nitrate in the near surface snow were observed over a timescales from 24 hours to one week (Mulvaney and others, 1998). Furthermore, clear seasonal cycles in nitrate are preserved in high resolution ice cores at other coastal Antarctic sites (eg. Curran and others, 1998a; Mulvaney and Wolff, 1993). The equilibrium uptake and loss of nitrate at the surface over the course of days, with loss predominating over uptake for sites where the surface layer is exposed for timescales from weeks to months leads to

nitrate loss in the surface layer. This mechanism allows the preservation of clear seasonal cycles in nitrate records from moderate to high accumulation sites (Mulvaney and others, 1998). At low accumulation sites the snow layer may remain within 1 – 2 metres of the snow surface for up to 5 – 10 years. In this case there is net nitrate loss until very low nitrate concentrations are preserved and the seasonal cycle becomes indistinct. A number of potential processes for nitrate loss in surface snow layers have been identified in the literature. These include photochemical decomposition of nitrate, wind scouring of the surface layer, volatilisation of nitric acid and scavenging of nitrate by other particulates or gases aided by wind pumping of the snowpack (Wolff, 1996; Mulvaney and others, 1998; Wagenbach and others, 1998b).

Movement of MSA has been reported from firn core studies from Antarctica coring sites including the Dolleman Islands (Pasteur and Mulvaney, 2000), the Filchner-Ronne Ice Shelf (Minikin and others, 1994), Siple Dome (Kreutz and others, 1998) and Law Dome (Curran and others, 2002, Smith and others, 2004). The exact mechanism for movement of MSA is not clearly understood. Simple diffusion, percolation and other gravitational forces are not likely to produce movement since MSA appears to concentrate as new peaks in winter layers (Kreutz and others, 1999; Pasteur and Mulvaney, 2000; Curran and others, 2002). High resolution studies of the MSA record from Law Dome indicate a distinct relationship between MSA movement, accumulation rates, and the concentration of acidic species such as nitrate and sodium surrounding elevated concentrations of MSA. MSA is believed to migrate into the acidic sea salt layer and form a stable cation salt through a metathesis reaction (Kreutz and others, 1999; Pasteur and Mulvaney, 2000; Curran and others, 2002). This reaction removes MSA from solution and creates a gradient from which more MSA may migrate. Curran and others (2002) have suggested that there is a limit to the migration distance along which MSA can penetrate into the sea salt layer, with this limit determined by the sea salt concentration gradient.

1.5 Chapter Summary and Thesis Outline

The work presented in this thesis involves a detailed investigation of the link between isotopic and chemical signals preserved in polar snow and meteorological observations. High resolution records of $\delta^{18}\text{O}$, sea salt ions (sodium, chloride, magnesium), marine biogenic compounds (MSA, non-sea salt sulphate) and nitrate are obtained from a series of snow pits and shallow firn cores from the high accumulation site near Law Dome summit, East Antarctica. This chapter provides a review of relevant literature important for understanding the chapters that follow. This includes a discussion of the source, transport and deposition mechanisms of the isotopic and trace chemical species analysed in this research, as well as their application to palaeoclimate reconstruction from ice cores.

Chapter 2 presents the physical and climatological characteristics of the sampling site near Law Dome summit, as well as the sample retrieval, preparation and analysis for the $\delta^{18}\text{O}$ and trace ion records. *Chapter 3* investigates a high resolution spatial comparison at Law Dome in order to examine the extent to which isotopic and chemical signals are retained in different firn core records. A detailed description of the local meteorology at the sampling site using automatic weather station data over a 4 year period is provided in *Chapter 4*. *Chapter 5* details the techniques used for dating the high resolution snow pit records, including a discussion on the effect of densification on the top 6 m of the snowpack. *Chapter 6* provides an examination of ultra high resolution seasonality of trace ion species and the oxygen isotope ratio over a 4 year period. *Chapter 7* details the results from a pilot study that directly compares chemical and $\delta^{18}\text{O}$ signals and meteorological observations for three accumulation periods preserved in a Law Dome snow pit. Further detailed investigations of meteorological events preserved in the high resolution snow pit records are presented in *Chapter 8*. This includes discussion on meteorological links with the isotopic and chemical signals, as well as analysis on potential source regions for particular signals through synoptic cloud tracking using satellite imagery and back trajectory modelling. Finally, conclusions and recommendations for future work are detailed in *Chapter 9*.

Chapter 2

Site Characteristics, Sample Retrieval, Preparation and Analysis

2.1 Overview

Climate information retained in the top 10 m section of the Antarctic snowpack may be accessed through a variety of techniques. The technique chosen for a particular study depends on the physical characteristics of the site, the desired sample resolution and the type of analysis being conducted. In particular, snow accumulation rates and wind speeds will affect the density of the snowpack material being analysed, and thus influence the sampling technique used.

This chapter details the site characteristics of the Law Dome summit region, with particular focus on the physical and climatic conditions of the sampling site. The techniques for sample retrieval and preparation of both the snow pit and firn core samples are presented. In addition, the various chemical and isotopic analysis methods used in this research are described. Unless otherwise noted, all firn cores and snow pit samples were collected and analysed by the author.

2.2 Physical and Climatological Conditions of Dome Summit South (DSS), Law Dome

Law Dome is situated at the edge of the main East Antarctic ice sheet (Fig. 2.1). It is a small ice cap (200 km diameter) with ice flow independent of the main East Antarctic ice sheet (Morgan and others, 1997). The Dome Summit South (DSS) sampling site has been the focus of a deep (~1200 m) ice core retrieved between 1987

and 1993 (Morgan and others, 1997), as well as other shallow drilling projects aimed at improving our interpretation of the deeper record. The DSS site lies 4.6 km south-southwest of the summit of Law Dome (Fig. 2.1), has an elevation of 1379 m and is situated on mainly level bedrock resulting in undisturbed ice flow (Morgan and others, 1997).

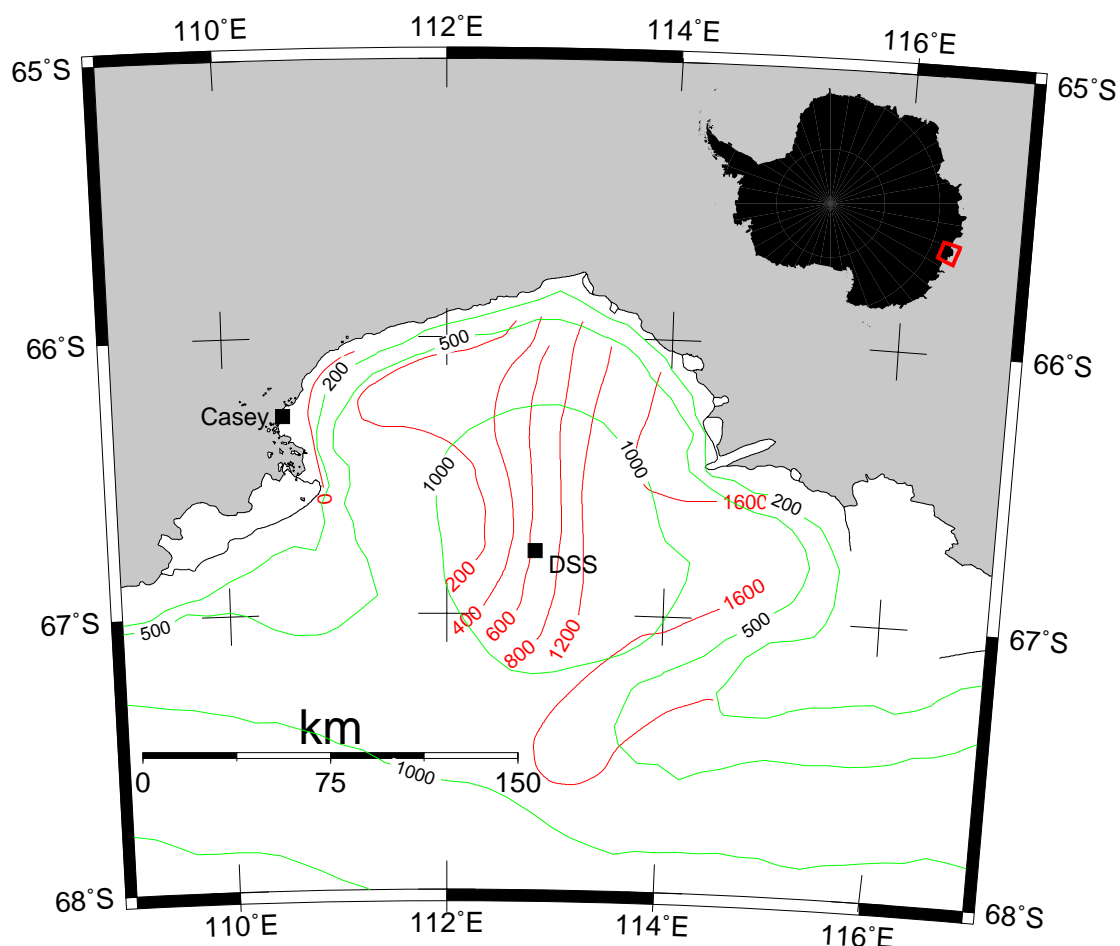


Figure 2.1: Location map for Law Dome with DSS sampling site and Casey station marked. Elevation (green) and accumulation (red) contours are shown.

This project draws on shallow material retrieved from the DSS site, extending up to 4 km to the north and 7 km to the south of the deep ice core borehole (Fig. 2.2). The DSS site was chosen for this study to further improve our interpretation of the deep record retrieved at DSS. Snow pit and firn core samples were collected over 2 field seasons (austral summer 1999/2000 and austral summer 2001/2002) and up to 11 km apart.

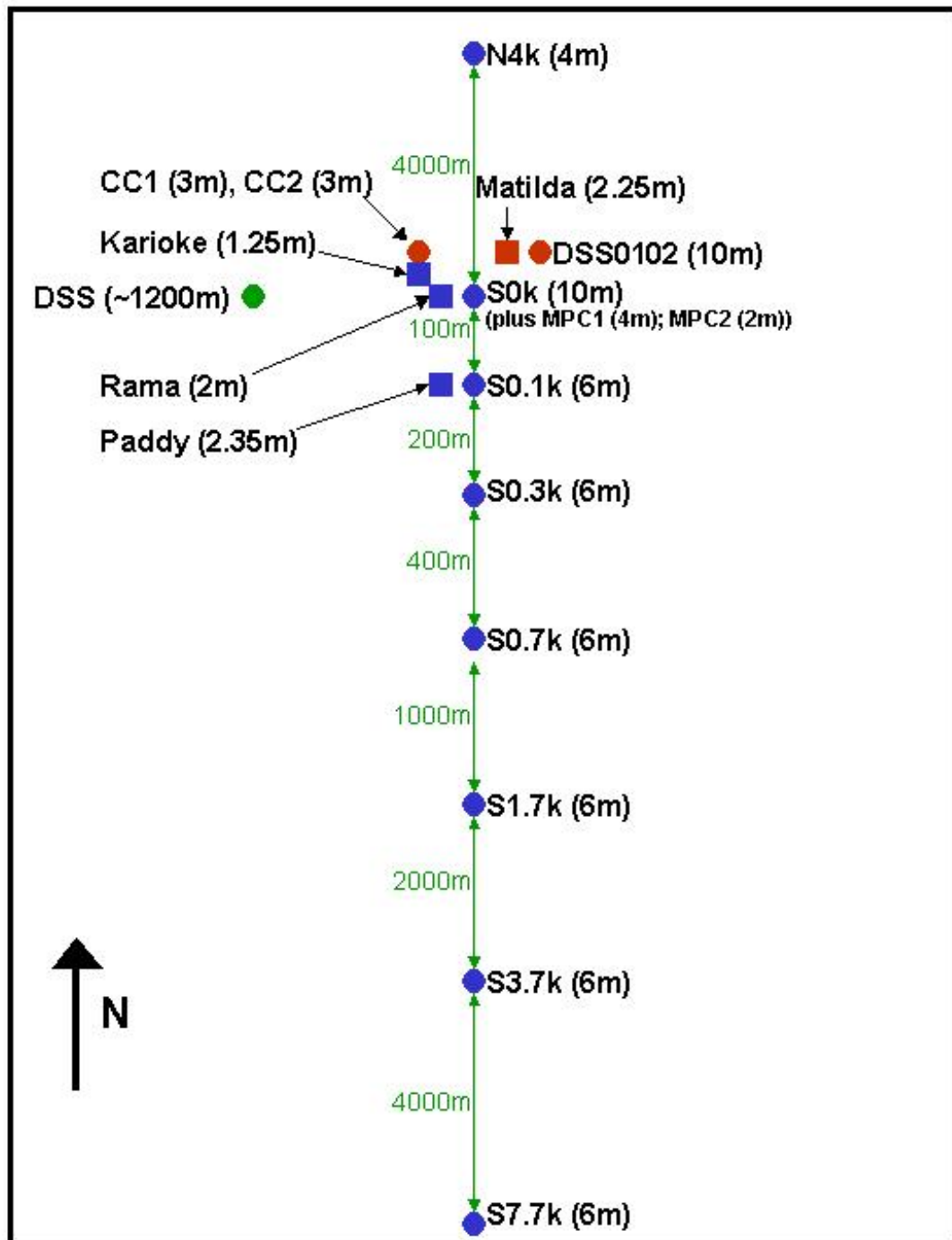


Figure 2.2: Location schematic for the snow pits sampled and firn cores collected from the DSS sampling site during the course of this research. Pits and cores collected during the first field season (Austral Summer 1999/2000) are coloured blue, while pits and cores collected in the second season (Austral Summer 2001/2002) are coloured red. Squares denote snow pits and circles denote firn cores with appropriate depths labelled. The deep DSS ice core borehole is indicated as a green circle.

The climatology of the Law Dome region is well suited to the extraction of records for high resolution studies of the climate signals preserved in the snowpack. Previous studies have shown that peak cyclone densities occur in the region to the northwest of Law Dome (55-60° S, 60-90° E) (Jones and Simmonds, 1993). Well structured cyclonic systems tend to form in this region and travel southeast before dissipating to the east of Law Dome. These systems produce predominately easterly maritime circulation for Law Dome, resulting in high accumulation on the eastern side of Law Dome (up to 1.2 m ice per year), with accumulation dropping to approximately 0.67 m ice per year for DSS (Morgan and others, 1997). The high annual accumulation at DSS leads to the deposition of thick annual layers, allowing the extraction of chemical and isotopic records with intra-annual resolution. The absence of high wind gusts at Law Dome (Adams, 1996) minimises mixing and redistribution of surface snow, and low mean summer temperatures (-12.6 °C) (Allison and others, 1993) preclude summer melt. These conditions limit disturbance of the chemical archive preserved in the snowpack.

The characteristics of the synoptic-scale meteorology of the Law Dome region make it an interesting site for examining the impact of meteorology on ice core signals. Jones and Simmonds (1993) identified a seasonal variation in the peak values of cyclogenesis and cyclolysis in the circumpolar trough north of this region of East Antarctica, with a general intensification of cyclone density during the winter months (June – August). A semi-annual variation in atmospheric pressure has also been observed in East Antarctica with low pressure recorded in spring (September – November) and autumn (March – May) (Schwerdtfeger, 1984; Allison and others, 1993; King and Turner, 1997). The frequent intrusion of cyclonic events over Law Dome also provides a mechanism for connections with lower latitudes. Meteorological reanalysis has shown that cyclonic activity, storm tracks and general circumpolar circulation in this region are influenced by atmospheric ridging and blocking from low latitudes in Australasia (Cullather and others, 1998; Pook and Cowled, 1999; Pook and Gibson, 1999).

2.3 Snow Pit Sample Retrieval

Four snow pits were sampled during the course of this research, three during the first field season and the remaining pit sampled during the second field season. Table 2.1 outlines the details of the snow pits. The high annual accumulation at DSS (allowing low density material to be retained at depth), coupled with the requirement of accurate high resolution records, determined the use of snow pits for sample retrieval for this project.

Table 2.1: Details of the four snow pits analysed in this research

Snow Pit	Date Sampled	No. Lines	Depth (m)	Sample Resolution (cm)	Approx. Record Start	Approx. Record End
Rama	1-Mar-00	7	2	2.5	Summer 99/00	Winter 98
Karioke	29-Feb-00	3	1.25	2.5	Summer 99/00	Summer 98/99
Paddy	28-Feb-00	3	2.35	2.5	Summer 99/00	Winter 98
Matilda	24-Dec-01	3	2.25	2.5	Summer 01/02	Summer 00/01

Throughout the snow pit sampling procedure clean techniques were adopted to allow the extraction of trace ion samples free from contamination. All instruments used in the digging and sampling of the snow pits were washed prior to transportation to the field with deionised Milli-Q water (resistivity $> 18 \text{ M}\Omega\text{-cm}$). Snow pit personnel wore clean suits, at least two sets of polyethylene gloves, and dust masks to minimise contamination from human interference. Initial digging of the snow pits to a depth of approximately 1 m was done using cleaned stainless steel shovels. A further 20 cm of the wall was removed with a number of scrapers to ensure an uncontaminated sampling wall. Just before sampling, a further 2 cm was scraped away using a clean microtome blade. A cleaned metal template was then fastened to the wall using steel pins, and two samples for each depth interval were extracted using steel square tube probes. Further digging of the snow pits to their final depth (2 – 2.5 m) was done by cutting blocks of firn from the pit floor using the stainless steel shovels. The wall was then decontaminated by scraping as described above before sampling commenced.

Sample resolution was 2.5 cm, and the template ensured millimetre depth accuracy (Fig. 2.3). Samples were collected for $\delta^{18}\text{O}$ and trace ion chemical species. Three lines of samples (approx. 30 cm apart) were collected from each snow pit along the full depth of the pit wall. An additional four lines of samples were collected from *Rama* covering a depth range 0.25 – 1.25 m (Fig. 2.4). Snow pit samples were then transported frozen back to Australia. The snow pit sampling technique extracted 8 – 10 mL of sample available for analysis.



Figure 2.3: Snow pit sampling probe and template. Samples were collected for $\delta^{18}\text{O}$ and trace ion species simultaneously for each depth range. The use of the template ensured consistent 2.5 cm resolution with millimetre depth accuracy.

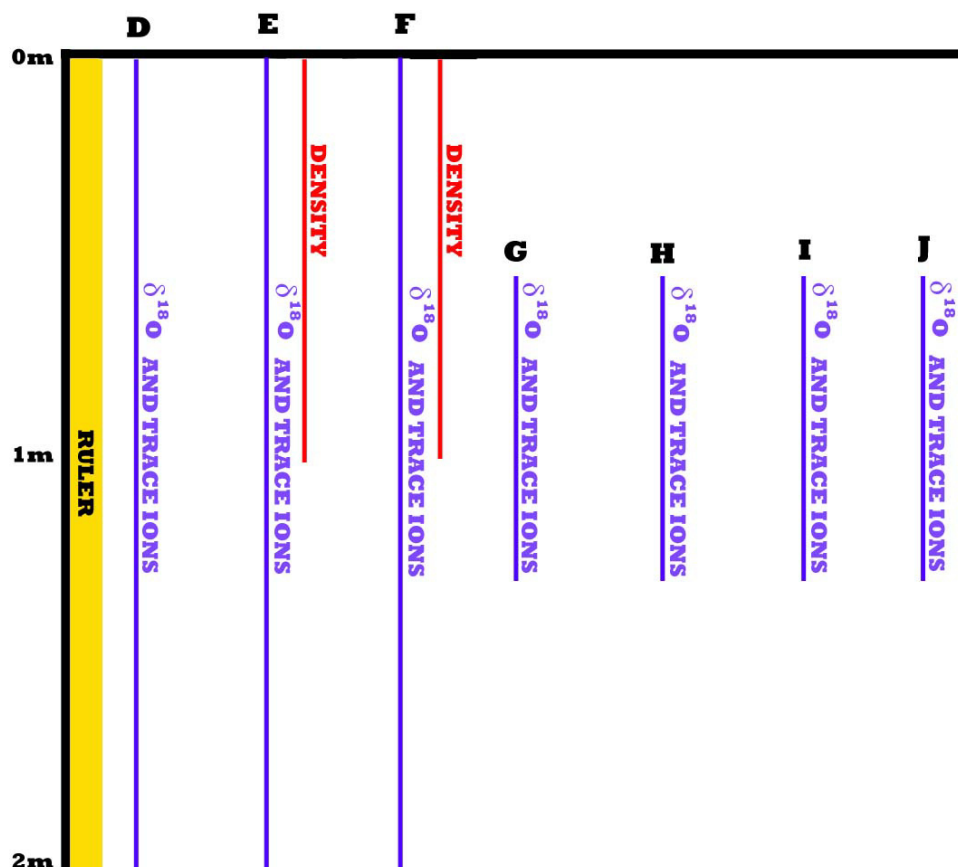


Figure 2.4: Schematic cross section of the Rama snow pit showing the 7 lines sampled for $\delta^{18}\text{O}$ and trace ions down the pit wall. The 2 density lines are also shown.

The snow pits were also sampled for density using a 3 x 3 cm stainless steel square probe. Two lines of density samples were collected for *Rama*, *Karioke* and *Matilda* from approximately 0 – 1 m with a sample resolution of 3 cm. These samples were weighed in the field, and density measurements recorded.

2.4 Firn Core Retrieval and Sample Preparation

Thirteen shallow firn cores were collected from DSS during this research varying in depth from 2 – 10 m (Table 2.2). All cores were drilled using a hand auger with special care taken to preserve the top 0.3 m section of friable material. Cores were collected to extend the snow pit records further back in time where the increased density prevented snow pit sampling. Cores were drilled within approximately 0.5 m of the snow pit wall, and at regular intervals along the north/south accumulation isopleth that crosses the main snow pit (*Rama*)

(Fig. 2.2). Polyethylene gloves were worn during core handling in the field to minimise contamination and all cores were transported frozen back to Australia.

Table 2.2: Details of the thirteen firn cores analysed in this research

Firn Core	Date Drilled	Depth (m)	Sample Resolution (cm)	Distance/ Direction from DSS	Approx. Record Start	Approx. Record End
N4k	1-Mar-00	4	2.5	4km north	Summer 99/00	Summer 97/98
DSS0102	24-Dec-01	10	2.5	0km	Summer 01/02	Summer 94/95
CC1	24-Dec-01	3	2.5	0km	Summer 01/02	Summer 99/00
CC2	24-Dec-01	3	2.5	0km	Summer 01/02	Summer 99/00
S0k	29-Feb-00	10	2.5	0km	Summer 99/00	Winter 92
MPC1	29-Feb-00	4	2.5	0km	Summer 99/00	Summer 97/98
MPC2	29-Feb-00	2	2.5	0km	Summer 99/00	Winter 98
S0.1k	29-Feb-00	6	2.5	0.1km south	Summer 99/00	Summer 95/96
S0.3k	28-Feb-00	6	2.5	0.3km south	Summer 99/00	Summer 95/96
S0.7k	28-Feb-00	6	2.5	0.7km south	Summer 99/00	Summer 95/96
S1.7k	28-Feb-00	6	2.5	1.7km south	Summer 99/00	Summer 95/96
S3.7k	28-Feb-00	6	2.5	3.7km south	Summer 99/00	Summer 95/96
S7.7k	29-Feb-00	6	2.5	7.7km south	Summer 99/00	Summer 95/96
Matilda	24-Dec-01	2.25	2.5	0km	Summer 01/02	Summer 00/01

Firn core processing was conducted in a freezer laboratory at -18°C within the Antarctic CRC. Polyethylene gloves were always worn when handling the cores to minimise contamination. The cores were sampled for $\delta^{18}\text{O}$, hydrogen peroxide and trace ion chemicals using established techniques (Curran and Palmer, 2001). Stratigraphy was recorded prior to sampling (eg. core breaks, clear bands of ice indicating melt layers or wind crusts) and the core was cut longitudinally into four sections using a band saw (Fig. 2.5). Half the core (section A) was re-bagged for potential further analysis, while the two outer core sections (sections B and C) were sampled at 2.5 cm resolution for $\delta^{18}\text{O}$ and hydrogen peroxide. The inner core stick (section D) was used for trace ion analysis, with the outer edge of the stick cut using the band saw and discarded (red shading). The stick was then scored at 2.5 cm resolution and the top and bottom depths of each sample recorded. The stick was

placed in a clean vice within a laminar flow hood, which directs clean filtered air over the firn. The outer 2 – 4 mm of firn was removed along the length of each sample by scraping with a pre-cleaned microtome blade (Fig. 2.6). Each sample was then knocked into a 10 mL accuvette (Coulter) using the microtome blade and stored in the freezer laboratory. The firn core decontamination process resulted in 4 – 7 mL clean sample available for analysis depending on the density of the firn. Blank ice was prepared from deionised Milli-Q water (resistivity > 18 MΩ-cm) as a system check to determine if the decontamination procedure was effective. Three blank ice samples were prepared using the same techniques described above for every (approx.) 1 m firn core section. Blank ice was also used to clean the band saw and microtome blade prior to sampling the firn cores.

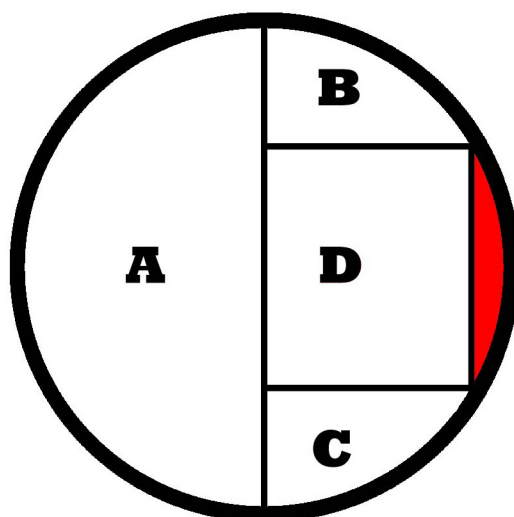


Figure 2.5: Schematic cross section of the longitudinal cuts made on the firn cores. Part of the core was re-bagged for potential future analysis (A), while the other sections were analysed for $\delta^{18}\text{O}$ (B), hydrogen peroxide (C) and trace ion species (D). Red shading indicates core section which was discarded.



Figure 2.6: Decontamination of a firn core sample by removing the outer 2 – 4 mm of firn using a pre-cleaned microtome blade (photo courtesy of Mark Curran, AAD).

2.5 Sample Analysis

2.5.1 Oxygen Isotope Ratios

Oxygen isotope analysis was conducted using a Stable Isotope Mass Spectrometer at the Central Sciences Laboratory, University of Tasmania. Isotope results were provided by V. Morgan from the Antarctic CRC.

2.5.2 Hydrogen Peroxide

Hydrogen Peroxide (H_2O_2) concentrations were measured using a commercial diffraction grating type fluorescence detector and the enzymatic fluorimetric analysis described by Sigg and Neftel (1988). H_2O_2 analysis was conducted within the Antarctic CRC (L. van Ommen) and results provided by T. van Ommen.

2.5.3 Trace Ion Chemical Species

Since the late 1980s ion chromatography (IC) has become a popular technique for obtaining trace ion chemical records from firn and ice cores (eg. Mayewski and others, 1990; Minikin and others, 1994; Mulvaney and Wolff, 1994; Curran and Palmer 2001). The multi-species analysis, low detection limits and low sample volumes of IC make this technique well suited to the detection of trace ion records in firn and ice cores. The trace ion concentrations of the snow pit and firn core samples prepared in this research were analysed using chemical-suppressed IC (Curran and Palmer, 2001). This technique allows detection of part-per-billion, or micro-gram per litre ($\mu\text{g L}^{-1}$) concentrations. The IC system used in this research was a DX500 microbore (2 mm) ion chromatograph with a CD20 conductivity detector and GP40 gradient pump (Dionex, California). Cation analysis was conducted using Ionpac CG12A guard and CS12A analytical columns (Dionex, California) with carboxylic/phosphonic acid functional groups. Ionpac AG14 guard and AS14 analytical columns (Dionex, California) with quaternary ammonium functional groups were used for anion separation. Snow pit and firn core samples were melted at room temperature for at least 2 hours before being transferred to autosampler polyvials using a micropipette (Eppendorf) within a laminar flow hood. The polyvials were then loaded into the IC system from an AS40 automated sampler (Dionex, California). Samples were analysed for magnesium, sodium, potassium, calcium, nitrate, sulphate, methanesulphonic acid (MSA) and chloride.

Methods

During the course of this research there were some changes in the IC system for the analysis of trace ions. Approximately one third of all samples were analysed using two separate systems for cations and anions at different times, with the remaining two thirds analysed using a dual system. During the dual system analysis both anions and cations were analysed from the same polyvial injection, with the cation sample analysed first from the bleed line.

All cations (sodium, potassium, magnesium, calcium) were analysed using an isocratic elution and 11 mM sulphuric acid eluent. This method was developed initially by Zwart (1997) and Palmer (1997) and modified to increase the amount of

sample injected by increasing the sample loop size to 250 μL (Palmer 2002). A cation run of 10 mins allowed the elution of all cations with excellent separation (Fig. 2.7). All anions were analysed using a two step isocratic elution method using a 4 mm anion concentrator column, which allowed 5 mL of sample to be preconcentrated. The first step involved an eluent concentration of 9.2 mM sodium tetraborate which eluted MSA and chloride on a flat baseline. During the second stage of analysis the eluent concentration was increased to 4.0 mM sodium tetraborate which allowed nitrate and sulphate to be eluted on a flat baseline. An anion run of 20 mins allowed the elution of all anions with excellent separation, with very low levels of MSA able to be detected in the presence of relatively high concentrations of chloride in the winter firn samples (Fig. 2.8).

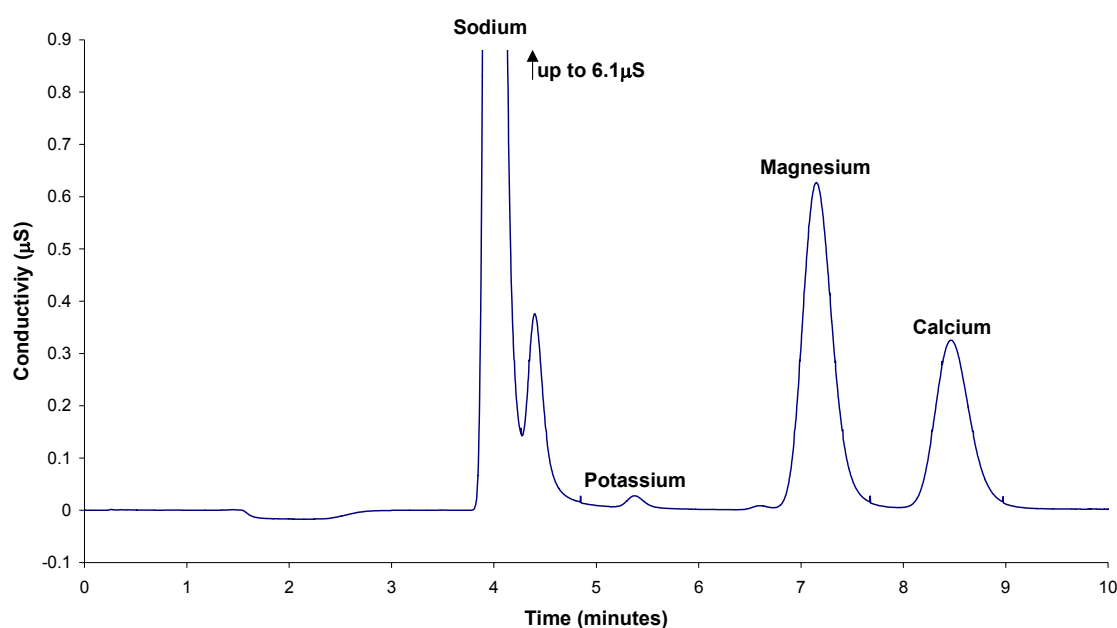


Figure 2.7: Cation separation with sodium, potassium, magnesium and calcium peaks detected.

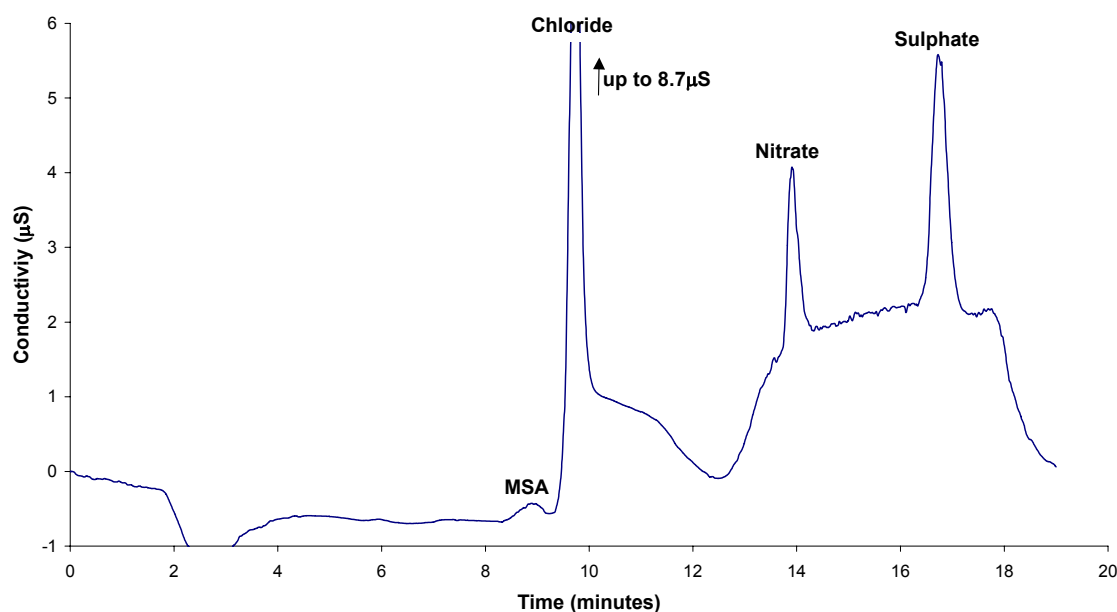


Figure 2.8: Anion separation with MSA, chloride, nitrate and sulphate peaks detected.

Standards and Sample Calibration

A primary standard, containing all the ions of interest (Table 2.3), was diluted to give six working calibration standards for analysis (Table 2.4). The IC system was calibrated throughout sample analysis with a full calibration conducted approximately every 60 samples, and a partial calibration (low and high standard) conducted every 20 samples. Deionised Milli-Q water samples (resistivity > 18 MΩ-cm) were also analysed at the beginning and end of every calibration (full and partial) as a system check to ensure no contamination has occurred during the analysis procedure. All chromatograms were checked manually to ensure each peak was labelled correctly and peak areas detected accurately. A calibration curve (Fig. 2.9) was obtained from the standards analysed using the peak areas detected from the IC. The calibration curve was used to calculate the concentration of the snow and firn samples using the following equation:

$$C_{\text{sample}} = \frac{\text{peakarea} - \text{intercept}}{\text{slope}}$$

where *peak area* refers to the area detected by the IC for the sample, and *slope* and *intercept* are calculated from the calibration curve.

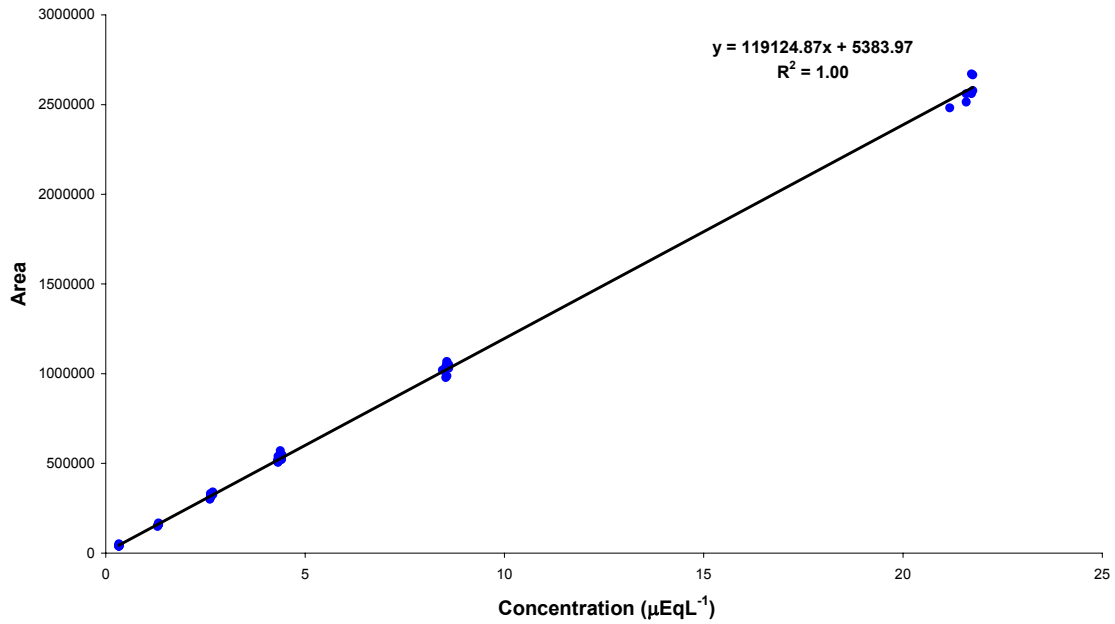


Figure 2.9: Calibration curve for sodium.

Many of the firn core samples were limited in volume due to the low density material associated with shallow cores and the high (2.5 cm) sample resolution. Where sample volume was less than the 6 mL required for analysis, the samples were diluted using a working standard. Concentrations of these samples were calculated using the following equation:

$$C_{\text{sample}} = \frac{V_{\text{total}} \times C_{\text{total}} - (C_{\text{standard}} \times (V_{\text{total}} - V_{\text{sample}}))}{V_{\text{sample}}}$$

where C and V denotes concentration and volume respectively. The subscripts refer to the snow or firn sample (*sample*), the total liquid analysed by the IC (*total* – 6 mL) and the working standard (*standard*) used in the dilution.

Table 2.3: Concentrations of ions in a primary standard

Ion	Concentration (μEqL^{-1})
MSA	0.872
Chloride	58.401
Nitrate	8.166
Sulphate	7.273
Sodium	43.896
Potassium	7.273
Magnesium	8.166
Calcium	14.504

Table 2.4: Concentrations of six working standards (μEqL^{-1})

Ion	Standards					
	1	2	3	4	5	6
MSA	0.442	0.175	0.086	0.053	0.027	0.007
Chloride	30.363	12.033	5.922	3.665	1.823	0.460
Nitrate	4.197	1.663	0.819	0.507	0.252	0.064
Sulphate	3.795	1.504	0.740	0.458	0.228	0.058
Sodium	22.909	9.079	4.468	2.765	1.376	0.347
Potassium	3.795	1.504	0.740	0.458	0.228	0.058
Magnesium	4.197	1.663	0.819	0.507	0.252	0.064
Calcium	7.454	2.954	1.454	0.900	0.448	0.113

It is important to note the precision of the IC system used in analysing trace ion species. Precision is defined as the ability of the analytical procedure to produce the same result for the same sample (Howard and Statham, 1993). Curran and Palmer (2001) conducted an intense study on the precision of the IC system used in this research, with precision values for 20 repeats of a standard ranging from 0.6% (chloride) up to 12% (calcium), with values less than 10% generally accepted. Similarly, detection limits for all the ions were calculated in Curran and Palmer (2001) and ranged between $0.001 \mu\text{EqL}^{-1}$ (MSA) and $0.03 \mu\text{EqL}^{-1}$ (magnesium), within acceptable ranges for the concentrations expected from the samples.

2.6 Concluding Remarks

The Law Dome region provides an excellent site for the extraction of high resolution records aimed at examining the impact of meteorology on climate signals preserved in the snowpack. The combination of snow pit and firn core sampling from near the summit of Law Dome produced a series of accurate high resolution records for $\delta^{18}\text{O}$, trace ion species and hydrogen peroxide (firn cores only). The snow pit sampling technique enabled a very accurate high resolution record to be extracted, with individual sample volumes of approximately 8 – 10 mL and no breaks in the record. This is in contrast to the firn core samples where volumes ranged from 4 – 7 mL and multiple core breaks interfered with the record. This chapter also shows the ion chromatography methods used for analysis of the trace ion samples and demonstrates that the sensitivities and precision are within acceptable ranges.

Chapter 3

High Resolution Spatial Comparison Across Law Dome

3.1 Overview

In order to reconstruct past climatic conditions from chemical and isotopic data recorded in Law Dome ice cores, it is important to understand the spatial and temporal variability across Law Dome. This chapter presents an ultra high resolution spatial comparison across Law Dome to assess the spatial reproducibility of chemical and isotopic signals, and to identify regional accumulation events preserved in the snowpack. Section 5.3 (Chapter 5) provides an analysis of the temporal variability of chemical and isotopic signals at Law Dome.

The ultra high resolution nature of this study requires the identification of regional accumulation events within the snow pit and firn core records. If variations in the chemical and isotopic signals are not observed in records across Law Dome, then the signals may be the result of accumulation differences between drilling sites rather than regional snowfall events. This would prevent the establishment of confident ties between snowfall events and chemical and isotopic signals. Regional accumulation events are recorded at different depths in the snow pit or firn core records due to:

- a. accumulation differences between sites;
- b. different sampling/drilling dates;
- c. loss of surface snow at the time of sampling/drilling;
- d. surface snow redistribution by wind;
- e. surface irregularity; and
- f. local firn density variations.

Some of these factors can be corrected when comparing records through simple depth offsets or scaling factors (a, b, c). Other factors introduce stochastic variations between

depth scales which cannot be corrected (d, e, f). These stochastic variations will influence the extent that regional events are preserved in the snow pit and firn core records. The identification of regional events preserved in the records allows a more comprehensive investigation of the regional meteorology associated with these events. This chapter examines the spatial reproducibility of signals preserved in the snowpack at Law Dome across a range of scales, with the aim of assessing the extent to which regional accumulation events are preserved in the records, and allowing further comparisons between the chemical and isotopic signals, and meteorological events.

3.2 Intra-Pit Spatial Variability (30 cm to 2 m)

3.2.1 The *Rama* Snow Pit

Seven lines of trace chemical and $\delta^{18}\text{O}$ samples were collected from the *Rama* snow pit with a vertical resolution of 2.5 cm and a horizontal spacing of 30 cm between the lines (Fig. 2.4; Chapter 2). Three lines (D, E, F) were sampled from 0 – 2 m depth, and the additional four lines (G, H, I, J) were sampled over the depth range 0.25 – 1.25 m. A total of 400 samples were collected from the *Rama* snow pit using a 2.5 cm template that assured millimetre depth accuracy. The samples were analysed for $\delta^{18}\text{O}$ and trace chemical species including MSA, nitrate, sulphate, sodium, chloride, magnesium, calcium and potassium. Further details on the analysis of the snow pit samples are contained in Chapter 2 of this thesis.

The seven line intra-pit comparison highlights the minimal impact that surface irregularities over spatial scales from 30 cm to approximately 2 m has on snow pit records at Law Dome (Fig. 3.1). Major features in the trace ion and $\delta^{18}\text{O}$ records are represented in all or most of the sample lines for $\delta^{18}\text{O}$, MSA, nitrate, non-sea salt sulphate and the sea salt ions (represented by sodium and magnesium). These reproducible features indicate regional accumulation events that can be used for further analysis and comparison with meteorological events. The $\delta^{18}\text{O}$, MSA and non-sea salt sulphate records show excellent agreement at this spatial scale. The sea salt ions (sodium, magnesium) also show good agreement at low concentrations, although spatial variability increases when concentrations are high. These results are consistent with results reported by Steffensen and others (1996) for snow pits sampled at Summit, Greenland. However, in contrast to Steffensen and others (1996), nitrate profiles presented here show considerable variability when concentrations are low, but good

agreement when concentrations are higher. Finally, the calcium and potassium records show poor agreement between the sample lines, indicating considerable variability throughout the snow pit. These results are consistent with previous studies from Law Dome ice core records (Curran and others, 1998a), and snow pits sampled at Summit, Greenland (Steffensen and others, 1996), where noisy calcium and potassium records were reported. The analysis presented in Figure 3.1 confirms that calcium and potassium are poor indicators of regional events.

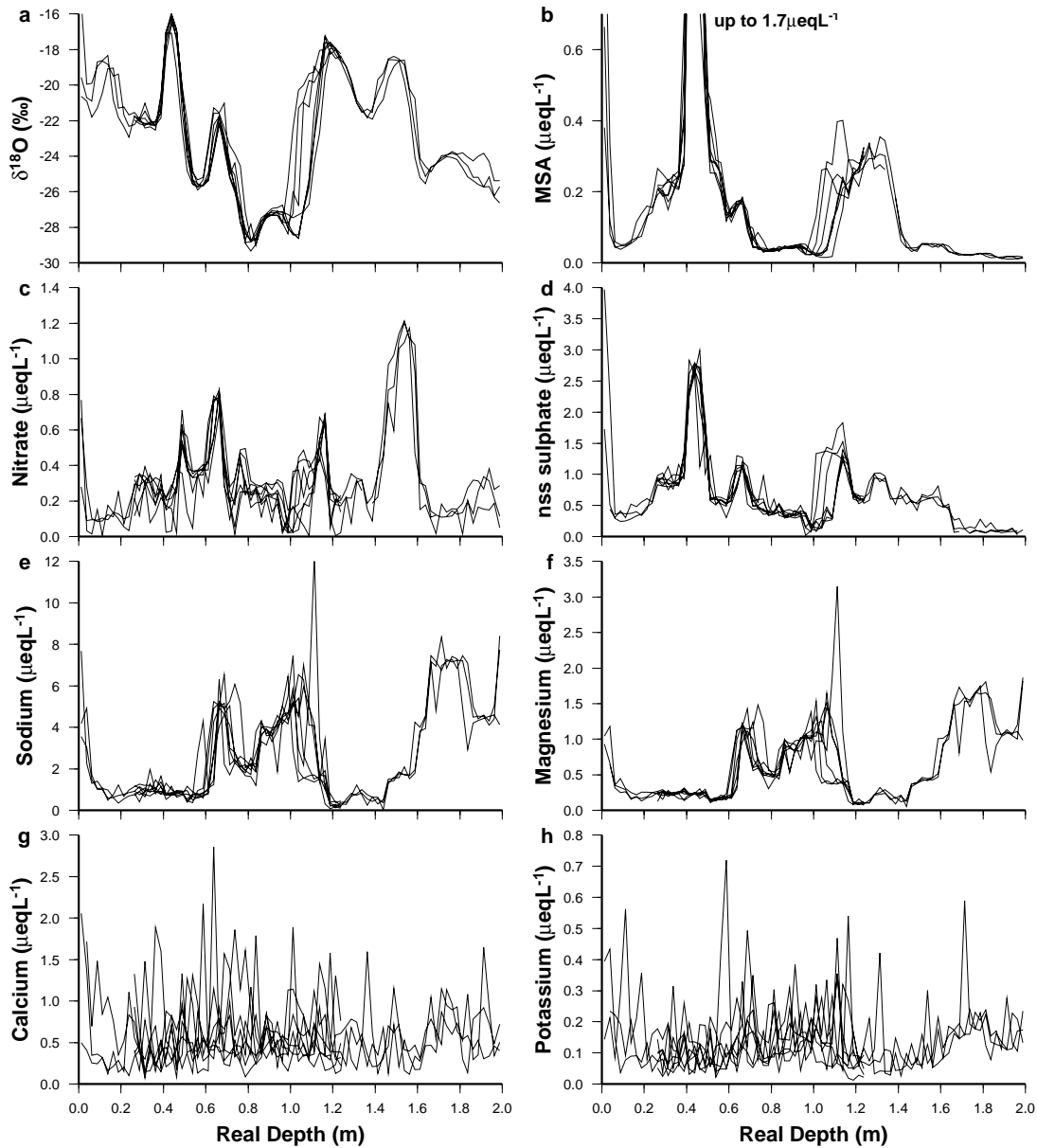


Fig. 3.1: Seven line intra-pit comparisons for the *Rama* snow pit. (a) $\delta^{18}\text{O}$, (b) MSA, (c) nitrate, (d) non-sea salt (nss) sulphate, (e) sodium, (f) magnesium, (g) calcium, (h) potassium.

Law Dome ice core records are generally characterised by elevated levels of $\delta^{18}\text{O}$, MSA, non-sea salt sulphate and nitrate during summer, and peaks in sea salts during

winter (Morgan and van Ommen, 1997; Curran and others, 1998a). A clear seasonal signal can be seen in the *Rama* snow pit over two annual cycles for $\delta^{18}\text{O}$, MSA, nitrate, non-sea salt sulphate, sodium and magnesium, with summer species peaking around 0.5 and 1.3 m, and winter species peaking around 0.9 and 1.7 m (Fig. 3.1). The potassium lines show a weak seasonal signal that is similar to the signal preserved in the sodium and magnesium records. This is consistent with a potassium signal influenced by sea salt input, however the potassium seasonal cycle is weak due to erratic concentrations. Potassium is a species that is easily contaminated through human interference during the sampling or analysis phases. In addition, potassium concentrations are close to the detection limit of the ion chromatograph. These two factors combined may explain the erratic concentrations of potassium in the *Rama* snow pit. Finally, calcium is a minor component of the sea salt aerosol, and is also an indicator of terrestrial dust (Mulvaney and Wolff, 1994). The calcium records presented in this study do not show a seasonal cycle and all seven snow pit lines are represented by a noisy signal. A definitive cause for the erratic calcium records is not clear, yet may be attributed to sample contamination during the sampling or analysis phases.

It is interesting to note that all species show high concentrations at the very surface of the snow pit, corresponding to late February 2000 when the snow pit was sampled. This event is discussed in detail in Chapter 7 of this thesis. In addition to seasonal cycles, the 2.5 cm resolution at this high accumulation site has captured many sub-seasonal phenomena (eg. multiple $\delta^{18}\text{O}$ peaks during summer deposition, non-summer elevated levels of MSA, and double peaks in winter sodium levels) (Fig. 3.1). These events are also discussed in more detail in Chapter 7.

Statistical Analysis of the Spatial Reproducibility

Figure 3.1 presents a spatial comparison of the snow pit sample lines on a ‘real depth’ scale. Real depth refers to the depth of the snow pit sample as recorded in the field. No adjustments were made to the depth scale to account for differences between the sample lines due to surface irregularity or surface redistribution of snow. The results indicate that major features are reproduced in the sample lines for most of the chemical and isotopic records. In order to conduct a more rigorous spatial reproducibility test by comparing the seven profiles on a sample by sample basis, it is necessary to minimise effects from surface irregularity and local firn density variations. These effects are minimised by slightly shifting the sample lines relative to one another. The depth scale

of the D profile remains unchanged, and the depth scales of the other sample lines are adjusted so that their $\delta^{18}\text{O}$ profiles align with the $\delta^{18}\text{O}$ profile of the D sample line. The $\delta^{18}\text{O}$ signal is used for the adjustment due to the number of clear signals that can be used to 'tie' the other sample lines. The 'ties' are created by shifting the sample profiles by inserting gaps in the sequence, and by stretching or compacting the records using a multiplier in the depth scale. This technique has been used in other studies (eg. McMorrow and others, 2001; Steffensen and others, 1996), and provides a mechanism for a more rigorous comparison of the chemical and isotopic features.

Figure 3.2 illustrates the adjusted $\delta^{18}\text{O}$ and trace chemical profiles, and shows similar results to those discussed above. $\delta^{18}\text{O}$, MSA and non-sea salt sulphate indicate excellent agreement between the sample lines, nitrate and the sea salt ions show good agreement, and potassium and calcium show poor agreement. The depth scale adjustment allows a tightening of the records, with a clearer indication of the regional features.

The mean $\delta^{18}\text{O}$ and trace ion records from the adjusted spatial comparison are shown in Figure 3.3. The error bars represent the maximum deviation from the mean across all seven sample lines at each depth point, and are plotted in the depth range where all seven lines overlap (0.25 – 1.25 m). The mean records and the error bars thus show the signal to noise ratio for individual species. The figure again shows the excellent agreement in the intra-pit comparison for $\delta^{18}\text{O}$, MSA and non-sea salt sulphate. The sea salt ions (sodium, magnesium) are also characterised by good agreement, with increased variability when concentrations are high. The error bars for the nitrate records also indicate good agreement, with higher variability when concentrations are low. Finally, the large error bars associated with the calcium and potassium records indicate poor agreement within the snow pit.

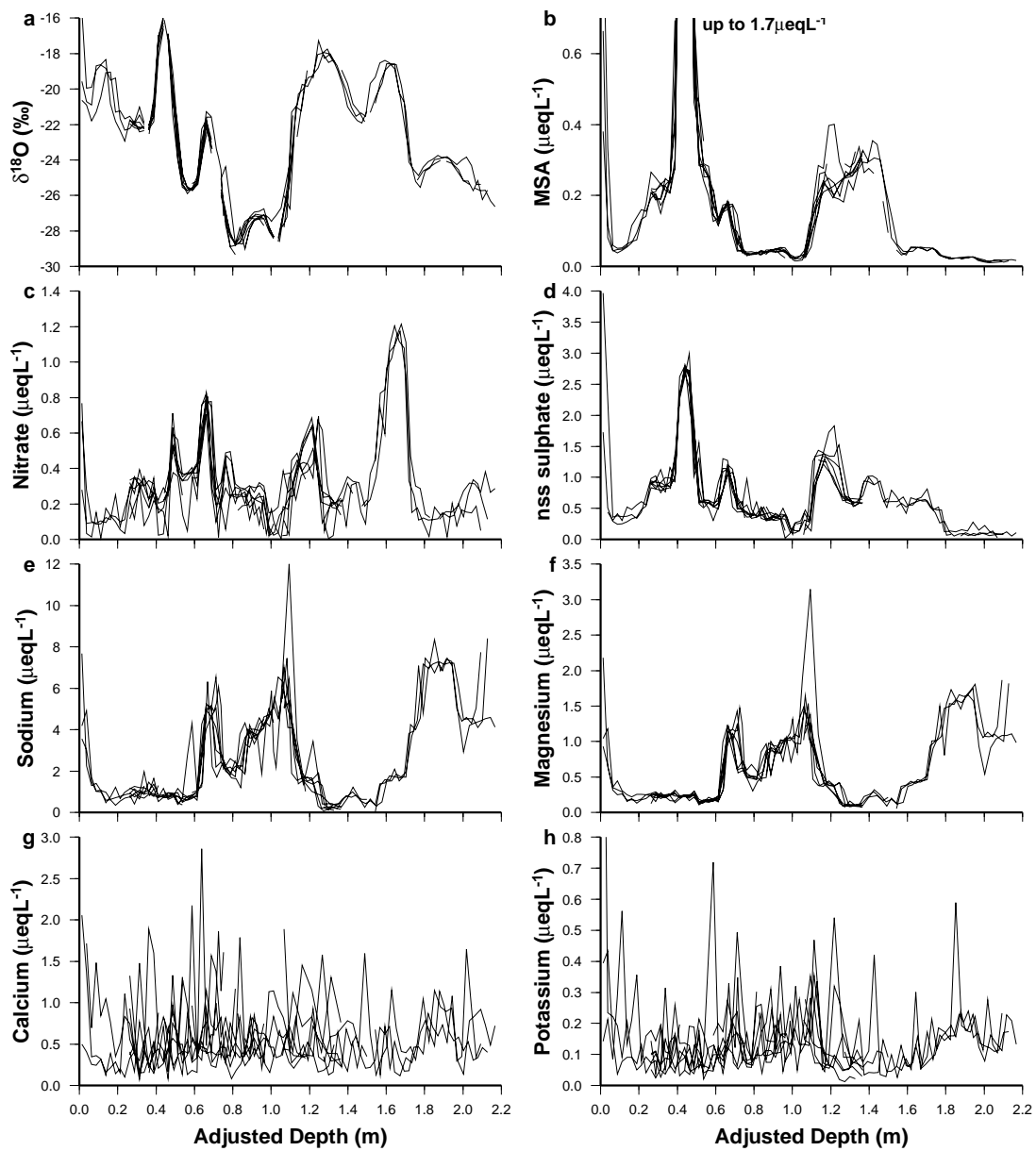


Fig. 3.2: Seven line intra-pit comparisons for the *Rama* snow pit with an adjusted depth scale. The depth scale was adjusted by interpolation of similar $\delta^{18}\text{O}$ signals. (a) $\delta^{18}\text{O}$, (b) MSA, (c) nitrate, (d) non-sea salt (nss) sulphate, (e) sodium, (f) magnesium, (g) calcium, (h) potassium.

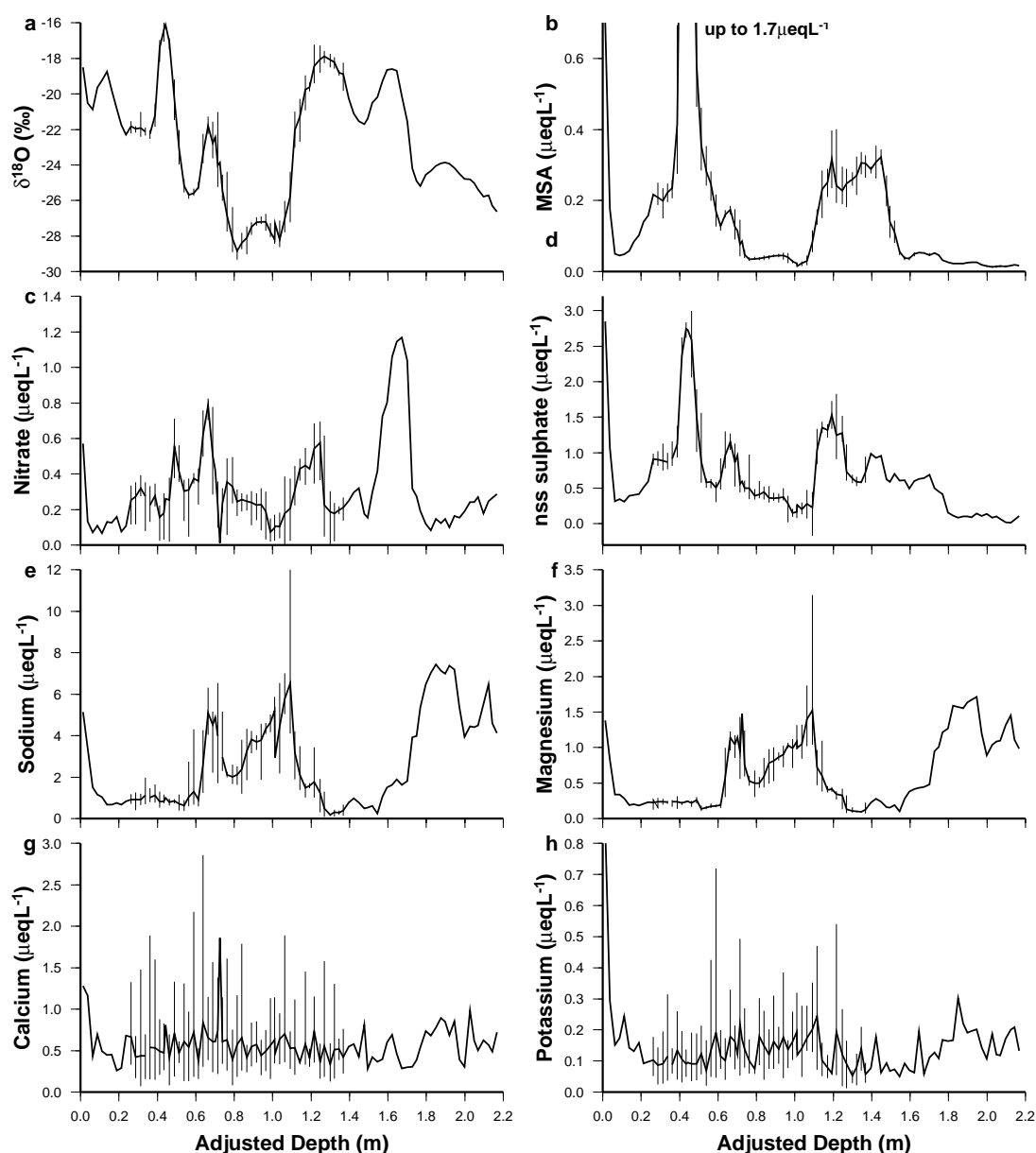


Fig. 3.3: Average chemical and $\delta^{18}\text{O}$ records for the *Rama* snow pit. Error bars represent the maximum deviation from the mean at each depth point. (a) $\delta^{18}\text{O}$, (b) MSA, (c) nitrate, (d) non-sea salt sulphate, (e) sodium, (f) magnesium, (g) calcium, (h) potassium.

Table 3.1 gives a comparison of the mean error bars for the chemical and isotopic records. As expected, the mean deviation from the mean for the $\delta^{18}\text{O}$ signal is extremely low (2.54 – 3.06%). This results from using the $\delta^{18}\text{O}$ signals as ‘ties’ for the other pit profiles during the depth adjustment. It should be noted that if the depth adjustment is performed using another chemical species, the resulting statistics reported in Table 3.1 will differ. The lowest mean deviation will equate with the chemical or isotopic species used to ‘tie’ the other records. However, the position or ‘rank’ of the mean deviations for the other species is expected to remain the same.

The relatively low mean deviations for MSA (16.13 – 17.63%) and non-sea salt sulphate (17.25 – 22.09%) indicate these species exhibit a low spatial variability at Law Dome. In other words, if another snow pit record was sampled in close vicinity of the seven lines then the likelihood that this new profile would fall within the region defined by the error bars is between 82.37 – 83.87% for MSA and 77.91 – 82.75% for non-sea salt sulphate. The sea salt ions of sodium and magnesium indicate mid-range spatial variability, with mean deviations between 30.45 – 38.71% (sodium) and 22.46 – 29.38% (magnesium). It should be noted that deviations for the sea salt ions show a greater variation for concentrations above the mean records, consistent with the finding reported earlier that sea salt records exhibit greater spatial variability when concentrations are high. The nitrate signal is also characterised by mid-range spatial variability, with mean deviations ranging from 34.60 – 41.87%. In contrast to the sea salt ions, the nitrate deviations are greater for values below the mean, indicating greater spatial variability when concentrations are low. Finally, the mean deviations for calcium (53.34 – 98.97%) and potassium (54.78 – 91.38%) clearly show these species exhibit poor spatial variability. The figures indicate that there is a less than 2% (calcium) and 9% (potassium) likelihood that another profile would fall in the error range for these species.

Table 3.1: Mean deviations resulting from the seven line intra-pit comparison from the *Rama* snow pit. Concentrations of the ionic species are in μEqL^{-1} , and $\delta^{18}\text{O}$ values are in ‰.

Signal	Mean	Mean Deviation				Likelihood new profile would fall in error range	
		above mean	below mean	above mean (%)	below mean (%)	above mean (%)	below mean (%)
$\delta^{18}\text{O}$	-23.10	0.71	0.59	3.06	2.54	96.94	97.46
MSA	0.28	0.04	0.05	16.13	17.63	83.87	82.37
Nitrate	0.29	0.10	0.12	34.60	41.87	65.40	58.13
Non-sea salt sulphate	0.86	0.19	0.15	22.09	17.25	77.91	82.75
Sodium	2.27	0.88	0.69	38.71	30.45	61.29	69.55
Magnesium	0.56	0.16	0.13	29.38	22.46	70.62	77.54
Calcium	0.57	0.57	0.31	98.97	53.34	1.03	46.66
Potassium	0.13	0.12	0.07	91.38	54.78	8.62	45.22

Summary

This section compared seven chemical and $\delta^{18}\text{O}$ profiles from the *Rama* snow pit on a spatial scale from 30 cm to 2 m. The intra-pit comparison enabled an investigation of the impact of local depositional noise and/or post depositional modification of the chemical and isotopic signals. $\delta^{18}\text{O}$, MSA and non-sea salt sulphate records showed

excellent agreement between profiles. The sea salt ions, represented by sodium and magnesium, indicated good agreement, particularly when concentrations are low. Nitrate signals also indicated good agreement between the profiles, with better spatial reproducibility for higher concentrations. Finally, calcium and potassium records showed poor agreement between the profiles, possibly due to sample contamination. These species are unlikely to represent regional events and are not considered further in this chapter or thesis. The remaining sections of this chapter expand the intra-pit comparisons and investigate the reproducibility of chemical and $\delta^{18}\text{O}$ signals across larger spatial scales.

3.3 Inter-Pit Spatial Variability (50 m to 100 m)

3.3.1 The *Rama*, *Karioke* and *Paddy* Snow Pits

The *Rama*, *Karioke* and *Paddy* snow pits were all sampled between 28 February to 1 March 2000, and represent records up to approximately 100 m apart (Fig. 3.4). All snow pits were sampled using the same technique, resulting in 2.5 cm sample resolution and millimetre depth accuracy. Seven lines were sampled from the *Rama* snow pit (see Section 3.2), and three lines from the *Karioke* and *Paddy* snow pits. Further details on the sampling and analysis of the snow pits are contained in Chapter 2 of this thesis.

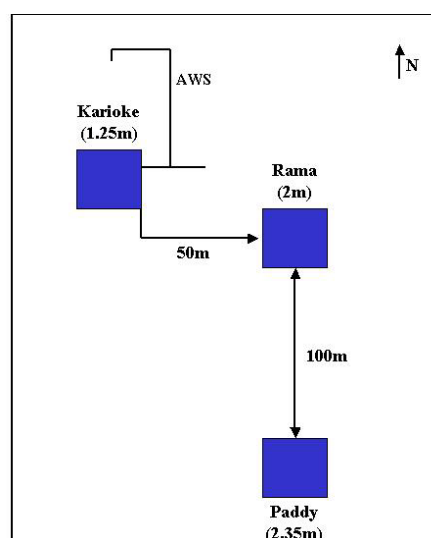


Figure 3.4: Location schematic for the *Rama*, *Karioke* and *Paddy* snow pits. Depths of each snow pit are indicated. The *Karioke* snow pit was sampled directed beneath the AWS accumulation sensor.

Figure 3.5 illustrates the inter-pit comparison between *Rama*, *Karioke* and *Paddy* using a representative line from each pit. In this figure, only the depth scale for the *Paddy*

snow pit has been adjusted with a simple depth offset to account for an earlier sampling date. The comparisons indicate that similar chemical and isotopic features are preserved in all three pits, and complement the conclusions drawn from the intra-pit comparisons described in Section 3.2. $\delta^{18}\text{O}$ and MSA records indicate the best spatial reproducibility between the pits, with only subtle differences in concentrations for regional events. Non-sea salt sulphate is also characterised by good agreement between the pits, with many features reproduced across pits. The non-sea salt sulphate comparisons show some variability, for example, the *Paddy* snow pit indicates a sharp spike in non-sea salt sulphate at approximately 1.2 m depth that is absent in the *Rama* snow pit (and beyond the depth range for the *Karioke* snow pit). Inter-pit comparisons for nitrate also indicate enhanced variability compared to the intra-pit comparisons reported in Section 3.2, although most of the features are represented across all three pits. It is interesting to note that a sharp nitrate spike in the *Paddy* snow pit at approximately 1.3 m depth is not reproduced in the other pits. This feature coincides with the non-sea salt sulphate spike preserved in *Paddy* at 1.3 m depth. Co-deposition of nitrate and non-sea salt sulphate outside the summer season has been documented in other Law Dome firn and ice cores, and may reflect a stratospheric input during these events (Curran and others, 1998a; McMorrow and others, 2003). The preservation of this distinct co-deposition of nitrate and non-sea salt sulphate event in *Paddy* while it is absent in *Rama* illustrates that on occasions, the pit and core records may not preserve snowfall events across Law Dome. Stochastic variations such as surface redistribution or removal of snow through wind scouring will lead to the absence of the event in some snow pits or cores. In order to conduct a robust comparison of snow pit and meteorological conditions, it is necessary to determine that the signals examined are regional events and are preserved in many locations across Law Dome. Although absent from *Rama*, the co-deposition event preserved in *Paddy* is also preserved in some of the firn cores drilled across Law Dome (Figs. 3.9 – 3.10). This indicates the event is regional, and may be used in the comparison with meteorological conditions.

Finally, the sea salt ions (sodium, magnesium) indicate good spatial reproducibility across the snow pits, with major features preserved in all pits. Variations between the snow pit records tend to occur in the relative concentrations of sea salts, for example, the sharp spike in sea salts at approximately 1.1 m depth is characterised by a lower concentration in the *Rama* snow pit compared to the *Karioke* and *Paddy* snow pits.

However, the shape of the features compare well between pits, suggesting sea salt signals are good indicators of regional events.

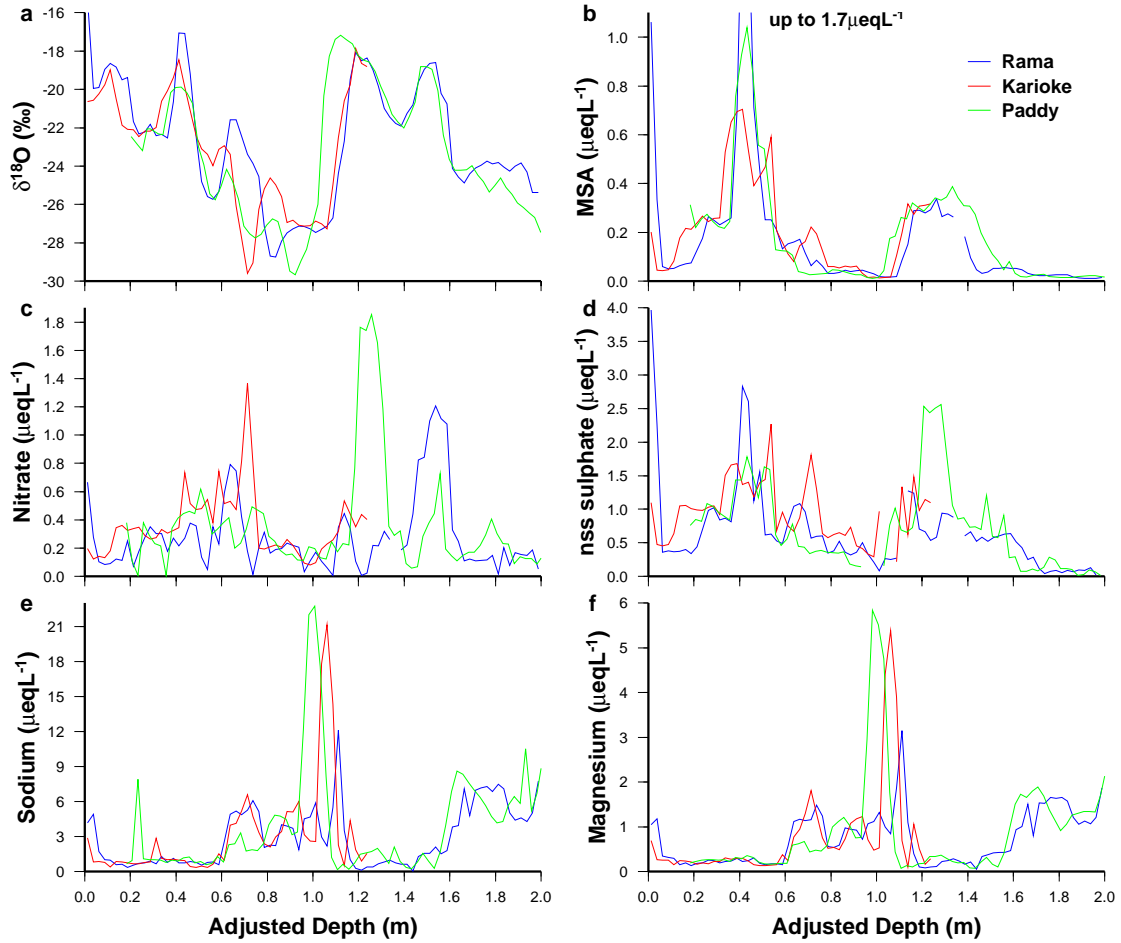


Fig. 3.5: Inter-pit comparisons from three snow pits: Rama (blue), Karioke (red), Paddy (green). The depth scale for Paddy was offset by 17 cm to reflect an earlier sampling date for this pit. (a) $\delta^{18}\text{O}$, (b) MSA, (c) nitrate, (d) non-sea salt (nss) sulphate, (e) sodium, (f) magnesium.

3.4 Inter-Core Spatial Variability (100 m to 11.7 km)

Comparisons between chemical and $\delta^{18}\text{O}$ records at spatial scales from 100 m to 11.7 km are made using inter-core comparisons. Figure 3.6 illustrates a location schematic for the inter-core comparison. The firn cores were drilled to a depth of 6 m (10 m for *S0k*, 3 m for *N4k*) and collected within a 16 day period to minimise drilling-date differences. Accumulation differences were minimised by drilling along the same accumulation isopleth. It should be noted that although the firn cores were drilled along a constant accumulation gradient, this accumulation gradient may not have been located in a similar pattern in the past. Further research using Law Dome ice core records extending further back in time would be useful to investigate the spatial coherence of

chemical signals along geographic orientations to determine whether the accumulation isopleths have changed over time.

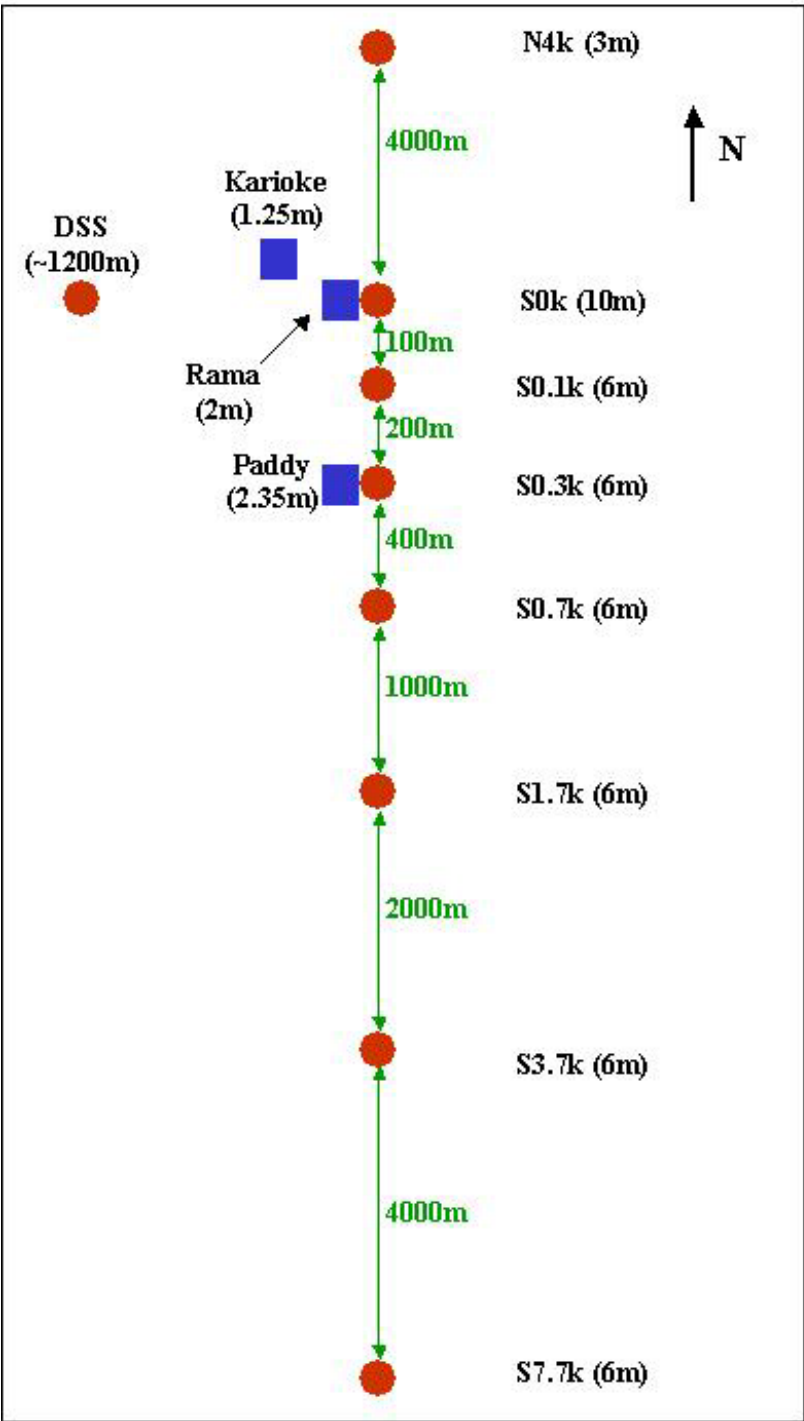


Figure 3.6: Location schematic for the firm cores used in the inter-core comparison. Firm cores are represented by red circles and snow pits are represented by blue squares. Names and depths of pits and cores are indicated. The deep DSS ice core borehole is also indicated.

Comparisons between firm core records up to 11.7 km show excellent agreement at this spatial scale (Figs. 3.7 – 3.12). Major seasonal and sub-seasonal signals are preserved in

all cores, allowing the identification of regional events for further analysis and comparison with meteorological conditions.

Figure 3.7 shows the inter-core comparison for the $\delta^{18}\text{O}$ signal. Major features in the $\delta^{18}\text{O}$ records are represented in all cores. For example, the smooth and distinct peak of summer 1997/1998 (approximately 3 m depth) is clearly preserved in each firn core. The range in maximum $\delta^{18}\text{O}$ values between cores for this peak is small (-18.5 to -17‰) and the shape of the peak is similar. The deep, narrow trough in $\delta^{18}\text{O}$ preserved during winter 1999 (approximately 1 m depth) provides another example of excellent agreement in the $\delta^{18}\text{O}$ signal across all cores. In contrast, some of the features that are present in each core differ slightly in shape or isotopic composition between cores. For example, the warm $\delta^{18}\text{O}$ signal preserved during winter 1997 (approximately 3.5 m depth) is evident in each core, yet the shape and isotopic composition varies between cores. The warm winter signal is more clearly defined in some cores (*S0.7k*, *S1.7k*, *S3.7k*, *S7.7k*) where the peak is sharper and maximum isotopic values are higher, compared to other cores where the peak is smaller and characterised by a multiple peak signal (*S0k*, *S0.1k*, *S0.3k*).

The MSA inter-core comparison shows similar results with major features preserved in all cores (Fig. 3.8). Compared to the $\delta^{18}\text{O}$ records, the MSA signal involves sharper features and less variability throughout the record. The relatively smooth signals preserved in the $\delta^{18}\text{O}$ records are caused by isotopic diffusion in the firn (Whillans and Grootes, 1985). The absence of diffusion in MSA (and other trace ion records) leads to a sharper, more jagged appearance in the signals. In addition, the MSA record is driven mainly by seasonal fluctuations in the biological activity in the Southern Ocean, while the $\delta^{18}\text{O}$ record is influenced by a variety of conditions including seasonal variations in temperature, continental and altitude effects, and the intrusion of strong cyclonic events (Kato, 1978; Siegenthaler and Oeschger, 1980; Zwally and others, 1998; McMorrow and others, 2001). This results in MSA records characterised mainly by summer maxima and winter minima, while the $\delta^{18}\text{O}$ records show more variability within the seasonal cycle. The strong seasonal driver for MSA is reflected by clear, narrow summer peaks and broad winter troughs in the inter-core comparison (Fig. 3.8).

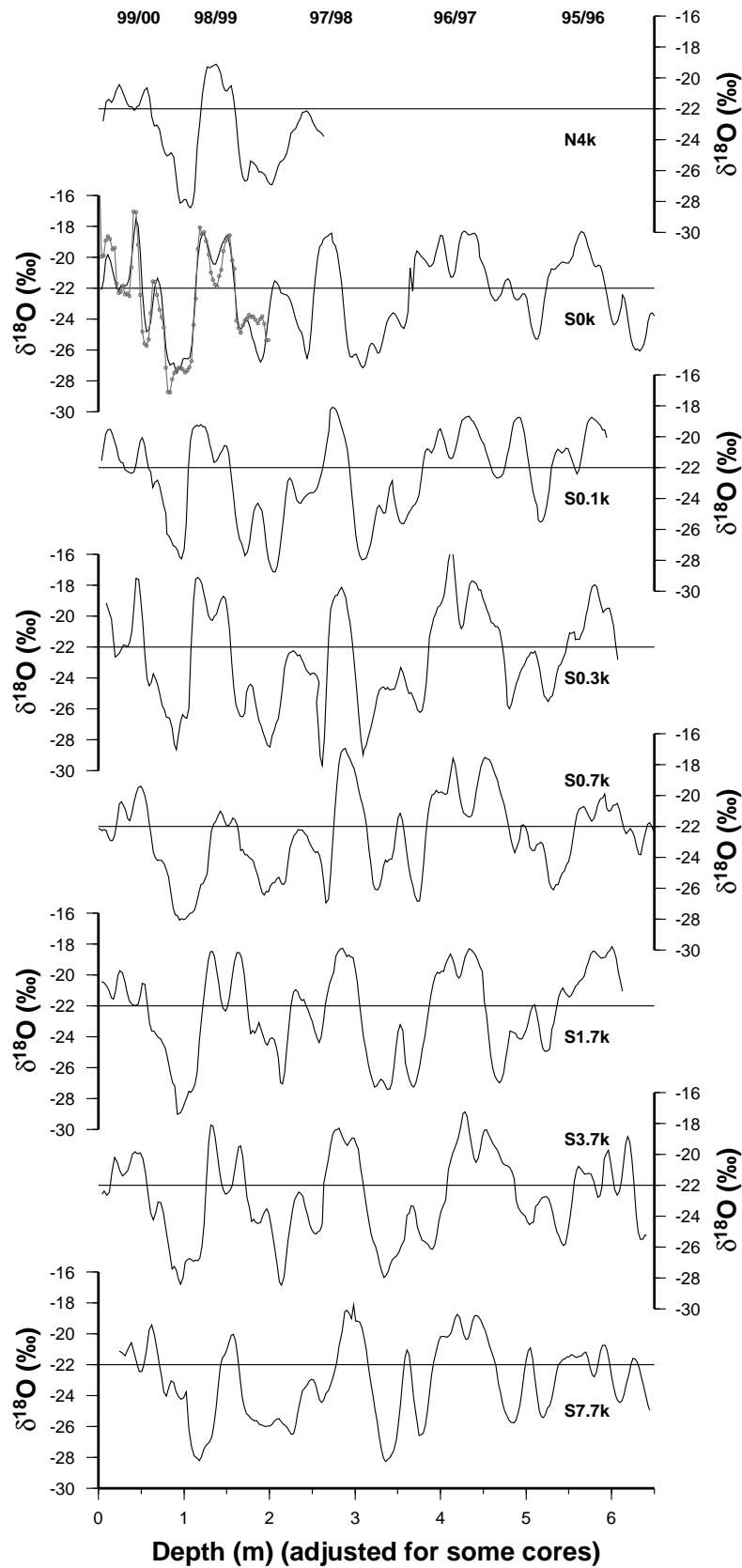


Fig. 3.7: Inter-core $\delta^{18}\text{O}$ comparisons from drilling sites. Top to bottom: *N4k* (4 km north of *Rama*), *S0k* (co-located with the *Rama* snow pit; *Rama* $\delta^{18}\text{O}$ record is shown as dotted line), *S0.1k* (0.1 km south of *Rama*), *S0.3k* (0.3 km south of *Rama*), *S0.7k* (0.7 km south of *Rama*), *S1.7k* (1.7 km south of *Rama*), *S3.7k* (3.7 km south of *Rama*), *S7.7k* (7.7 km south of *Rama*). The depth scale for *S0.7k* was adjusted due to the earlier drilling date of this core.

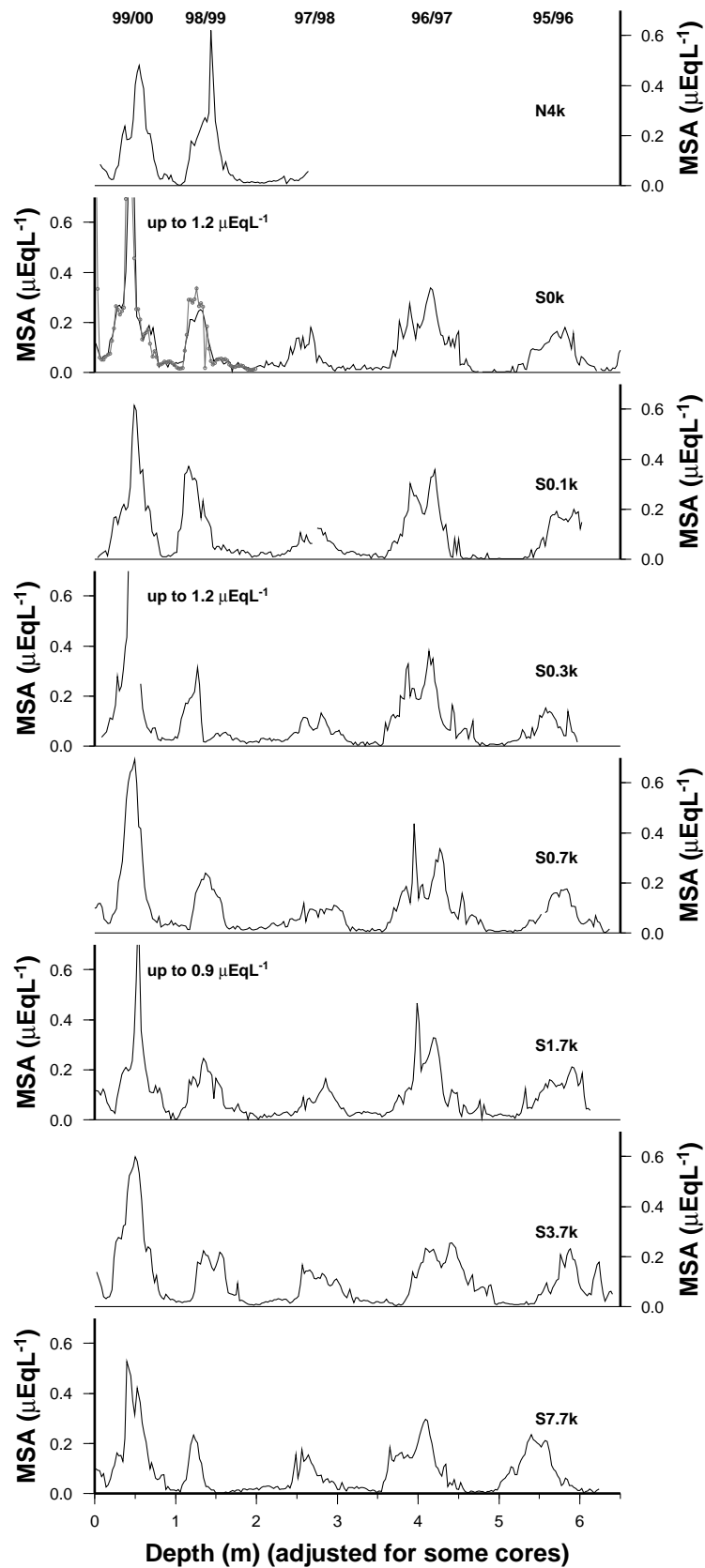


Fig. 3.8: Inter-core MSA comparisons from drilling sites. Top to bottom: *N4k* (4 km north of *Rama*), *S0k* (co-located with the *Rama* snow pit; *Rama* δ¹⁸O record is shown as dotted line), *S0.1k* (0.1 km south of *Rama*), *S0.3k* (0.3 km south of *Rama*), *S0.7k* (0.7 km south of *Rama*), *S1.7k* (1.7 km south of *Rama*), *S3.7k* (3.7 km south of *Rama*), *S7.7k* (7.7 km south of *Rama*). The depth scale for *S0.7k* was adjusted due to the earlier drilling date of this core.

The MSA inter-core comparison also shows excellent representation of the variability between years (Fig. 3.8). For example, the 1999/2000 summer (approximately 0.5 m depth) is characterised by a narrow peak and high MSA concentrations. Maximum concentrations for the 1999/2000 summer range from $0.5 \mu\text{EqL}^{-1}$ (*N4k*) up to $1.2 \mu\text{EqL}^{-1}$ (*S0k*, *S0.3k*). In contrast, the 1997/1998 summer (approximately 2.5 m depth) is characterised by a broader peak and lower MSA concentrations ($0.1 - 0.2 \mu\text{EqL}^{-1}$). The preservation of consistent inter-year variability in MSA across cores up to 11.7 km apart implies MSA is an excellent indicator of regional events. However, it should be noted that on some occasions the MSA signals differ between cores. For example, the multi-peaked summer of 1996/1997 (approximately 3.8 – 4.3 m depth) shows some variability between cores. The shape of the second peak (approximately 4.2 m depth) is similar between cores, while the first peak (approximately 3.9 m depth) varies between cores. *S0.3k*, *S0.7k* and *S1.7k* show a very narrow peak at approximately 3.9 m with MSA concentrations reaching $0.4 - 0.5 \mu\text{EqL}^{-1}$. In contrast, *S0k*, *S0.1k*, *S3.7k* and *S7.7k* preserve a smaller and broader peak at approximately 3.9 m depth with concentrations reaching $0.2 - 0.3 \mu\text{EqL}^{-1}$.

The nitrate records show more variability between cores, particularly when concentrations are low (Fig. 3.9). However, the major nitrate features are represented in most cores, implying that nitrate records from Law Dome are good indicators of regional accumulation events. Major nitrate features, although evident, differ slightly in shape and concentration between each core. For example, the spring/early summer peak preserved during 1998/1999 (approximately 1.5 m depth) is clearly preserved in each core, yet maximum concentrations vary from $0.7 \mu\text{EqL}^{-1}$ (*N4k*) to $1.5 \mu\text{EqL}^{-1}$ (*S0k*).

Increased variability in the reproducibility of nitrate features between cores tends to occur when concentrations are low (Fig. 3.9). This result is consistent with the finding reported earlier in the intra-pit comparison (Section 3.2), where snow pit profiles showed increased variability when nitrate concentrations were low. On occasion, some major nitrate events are not preserved in all cores. For example, the late summer/autumn peak during 1998/1999 (approximately 1.2 m depth) is evident in *S0.1k*, *S0.3k*, *S1.7k* and *S3.7k*, yet is absent from *N4k*, *S0k*, *S0.7k* and *S7.7k*. This event, where preserved in the cores, coincides with a distinct non-sea salt sulphate peak (Fig. 3.10). The event was also identified in the inter-pit comparison (Section 3.3), preserved in the *Paddy* snow pit yet absent from the *Rama* snow pit (and beyond the depth scale for the *Karioke* snow

pit). The preservation of this distinct co-deposition of nitrate and non-sea salt sulphate event in some records across Law Dome illustrates that on occasions, the pit and core records may not preserve snowfall events across Law Dome. Stochastic variations such as surface redistribution or removal of snow through wind scouring will lead to the absence of the event in some records. These results suggest that nitrate records may be more susceptible to surface redistribution or removal than other chemical or isotopic signals. The cause of this variability for nitrate between records is uncertain, yet increased wind scouring during autumn or spring when wind speeds are generally higher may provide an explanation. However, the preservation of nitrate events in at least some of the records across Law Dome indicates the event is regional, and allows further analysis into potential source regions and transport paths through comparisons with meteorological conditions.

The non-sea salt sulphate inter-core comparison shows similar results to MSA with excellent reproducibility between cores (Fig. 3.10). The non-sea salt sulphate signals tend to coincide with MSA signals, illustrating the strong marine biogenic influence on non-sea salt sulphate at Law Dome. This results in a clear seasonal cycle in non-sea salt sulphate with summer maxima and winter minima. Similar to the MSA comparison, the non-sea salt sulphate comparisons also capture variability between years. For example, the 1999/2000 summer (approximately 0.5 m depth) is characterised by a narrow peak and high concentrations of non-sea salt sulphate. Maximum concentrations for this summer peak range from $1.6 \mu\text{EqL}^{-1}$ (*S0.7k*) to $2.9 \mu\text{EqL}^{-1}$ (*S0k*). In contrast, the 1997/1998 summer (approximately 2.5 m depth) is characterised by a broader peak and lower non-sea salt sulphate concentrations ($0.8 - 1.6 \mu\text{EqL}^{-1}$). The preservation of consistent inter-year variability in non-sea salt sulphate across cores up to 11.7 km apart implies non-sea salt sulphate is an excellent indicator of regional events.

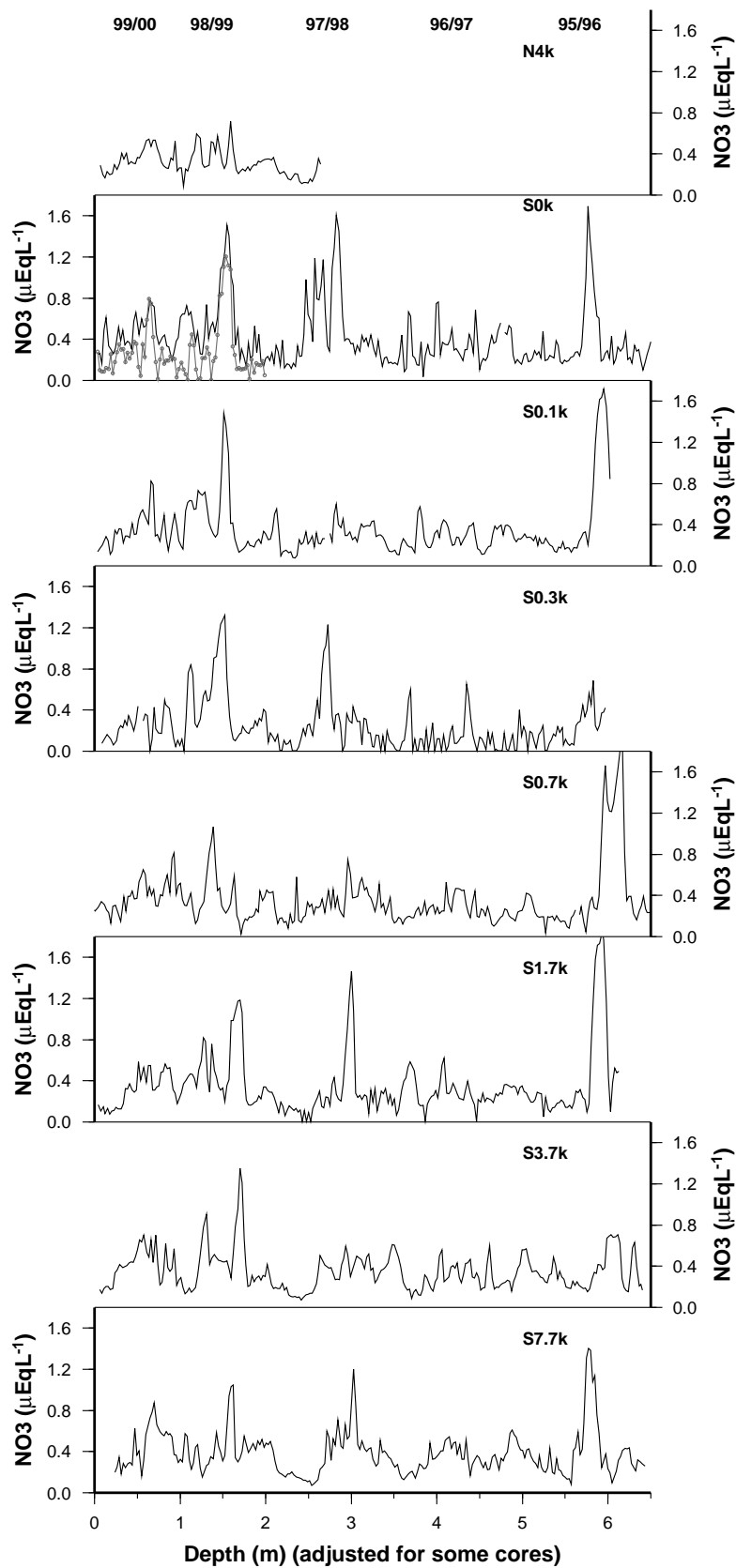


Fig. 3.9: Inter-core nitrate comparisons from drilling sites. Top to bottom: *N4k* (4 km north of *Rama*), *S0k* (co-located with the *Rama* snow pit; *Rama* $\delta^{18}\text{O}$ record is shown as dotted line), *S0.1k* (0.1 km south of *Rama*), *S0.3k* (0.3 km south of *Rama*), *S0.7k* (0.7 km south of *Rama*), *S1.7k* (1.7 km south of *Rama*), *S3.7k* (3.7 km south of *Rama*), *S7.7k* (7.7 km south of *Rama*). The depth scale for *S0.7k* was adjusted due to the earlier drilling date of this core.

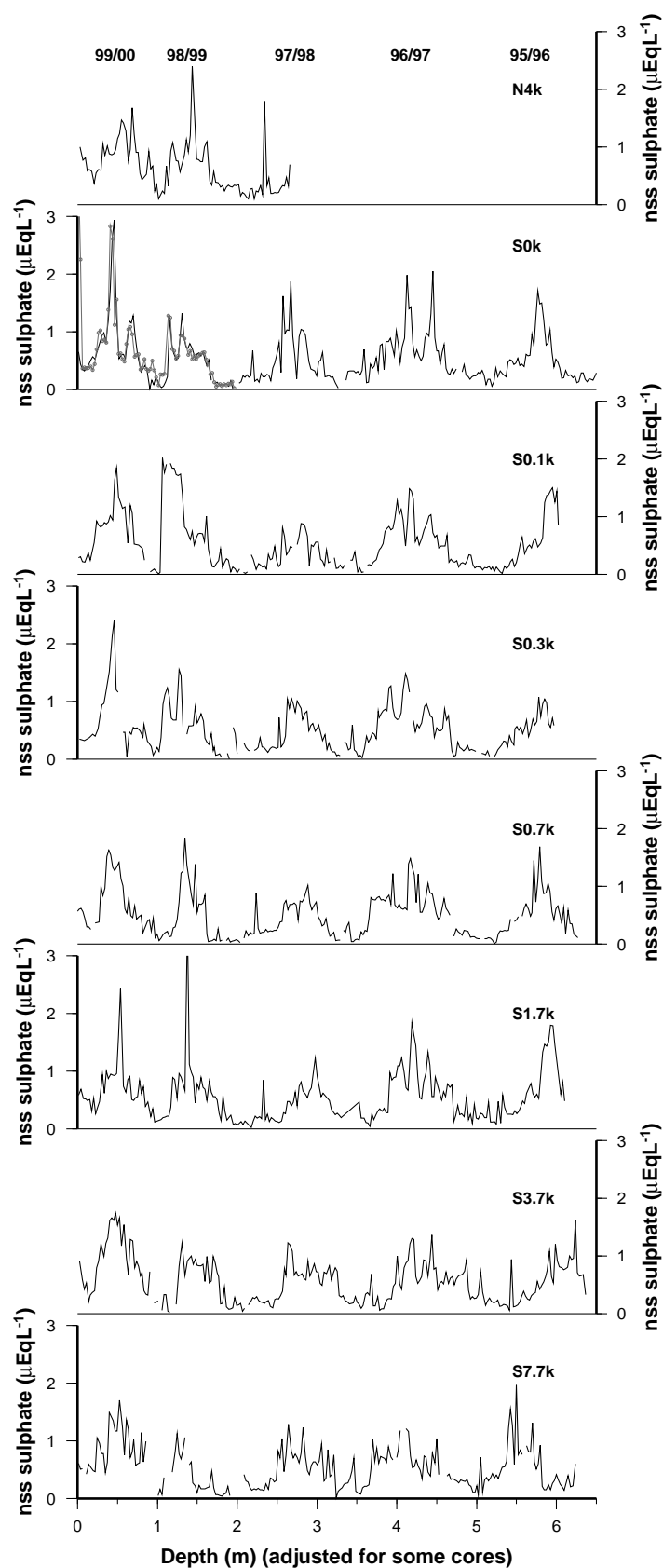


Fig. 3.10: Inter-core non-sea salt (nss) sulphate comparisons from drilling sites. Top to bottom: *N4k* (4 km north of *Rama*), *S0k* (co-located with the *Rama* snow pit; *Rama* $\delta^{18}\text{O}$ record is shown as dotted line), *S0.1k* (0.1 km south of *Rama*), *S0.3k* (0.3 km south of *Rama*), *S0.7k* (0.7 km south of *Rama*), *S1.7k* (1.7 km south of *Rama*), *S3.7k* (3.7 km south of *Rama*), *S7.7k* (7.7 km south of *Rama*). The depth scale for *S0.7k* was adjusted due to the earlier drilling date of this core.

However, outside the main summer peak in non-sea salt sulphate there is increased variability in the reproducibility of signals between cores (Fig. 3.10). For example, at approximately 1.2 m depth some cores show a non-sea salt sulphate peak that shoulders the main summer peak (*N4k*, *S0k*, *S0.3k*, *S1.7k*, *S3.7k*), while the feature is unclear or absent in other cores (*S0.1k*, *S0.7k*, *S7.7k*). In some of the cores, this shouldering peak coincides with the nitrate event discussed earlier, and although the signal is not represented in all records across Law Dome, the preservation of the distinct co-deposition of nitrate and non-sea salt sulphate in at least some of the cores suggests the event is regional. However, due to higher variability in the reproducibility of non-sea salt sulphate events outside the main summer peak, it is recommended these events are identified in a number of cores before conducting further analysis into potential source regions and transport paths through comparisons with meteorological conditions.

Finally, the sea salt ions, represented by sodium and magnesium, indicate good spatial reproducibility of events in the inter-core comparison (Figs. 3.11 – 3.12). The major features in the sea salt records are reproduced in each core. For example, the large autumn/winter peak during 1999 (approximately 1 m depth) is clearly preserved in each core. However the maximum concentrations for this peak varies between cores, with *N4k*, *S0k*, *S0.1k*, *S1.7k*, *S3.7k* and *S7.7k* recording high concentrations, and *S0.3k* and *S0.7k* recording lower concentrations. The distinct double-peaked winter of 1997 (approximately 3 – 4 m depth) provides another example of significant sea salt features reproduced in a number of cores. *S3.7k* and *S7.7k* provide the clearest examples of these high peaks, while the double-peak tends to be less clear in the remaining cores due to the preservation of lower concentrations. The sea salt records are inherently more noisy compared to the other chemical and $\delta^{18}\text{O}$ records, and the signals tend to be more numerous and narrower throughout the record. This leads to increased difficulty in identifying specific events preserved across the cores, yet figures 3.10 and 3.11 indicate that significant signals are easily identified in at least some of the cores across Law Dome.

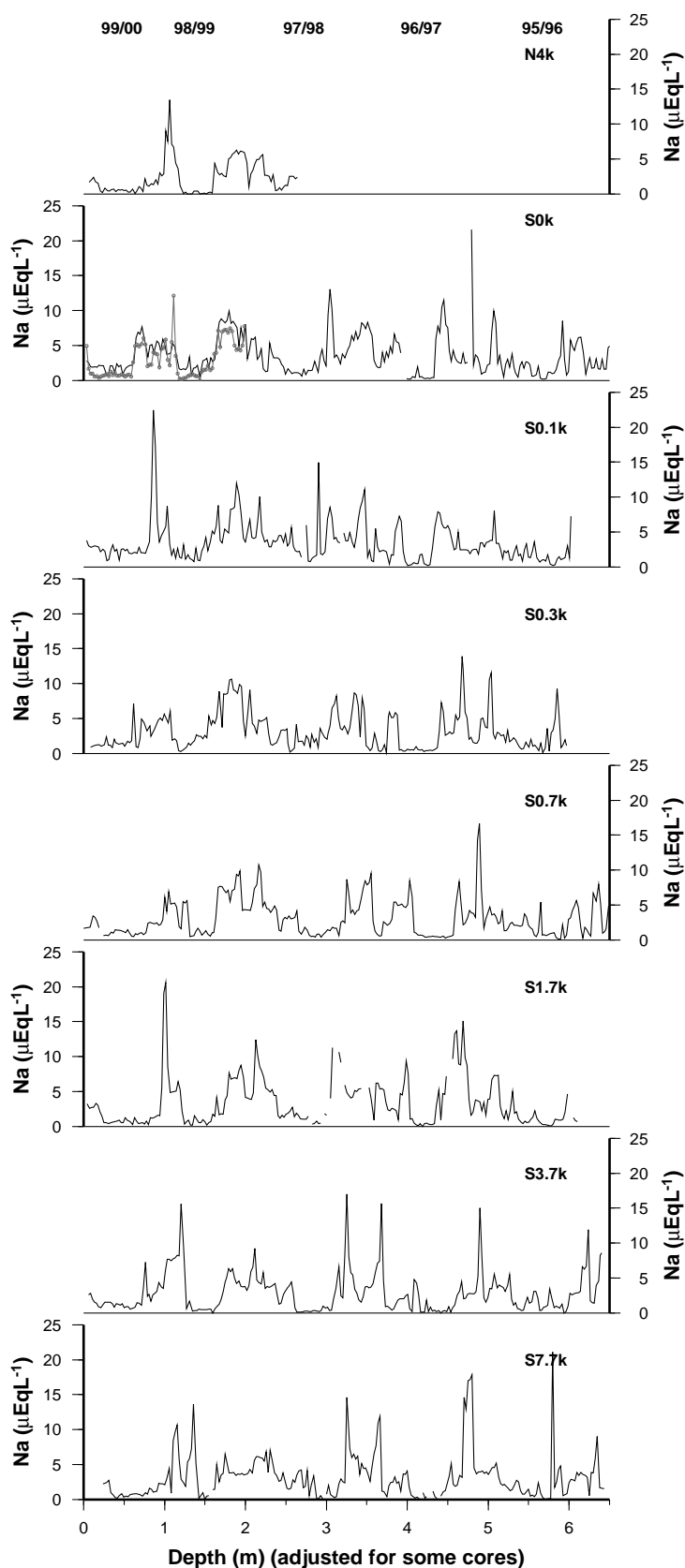


Fig. 3.11: Inter-core sodium comparisons from drilling sites. Top to bottom: *N4k* (4 km north of *Rama*), *S0k* (co-located with the *Rama* snow pit; *Rama* $\delta^{18}\text{O}$ record is shown as dotted line), *S0.1k* (0.1 km south of *Rama*), *S0.3k* (0.3 km south of *Rama*), *S0.7k* (0.7 km south of *Rama*), *S1.7k* (1.7 km south of *Rama*), *S3.7k* (3.7 km south of *Rama*), *S7.7k* (7.7 km south of *Rama*). The depth scale for *S0.7k* was adjusted due to the earlier drilling date of this core.

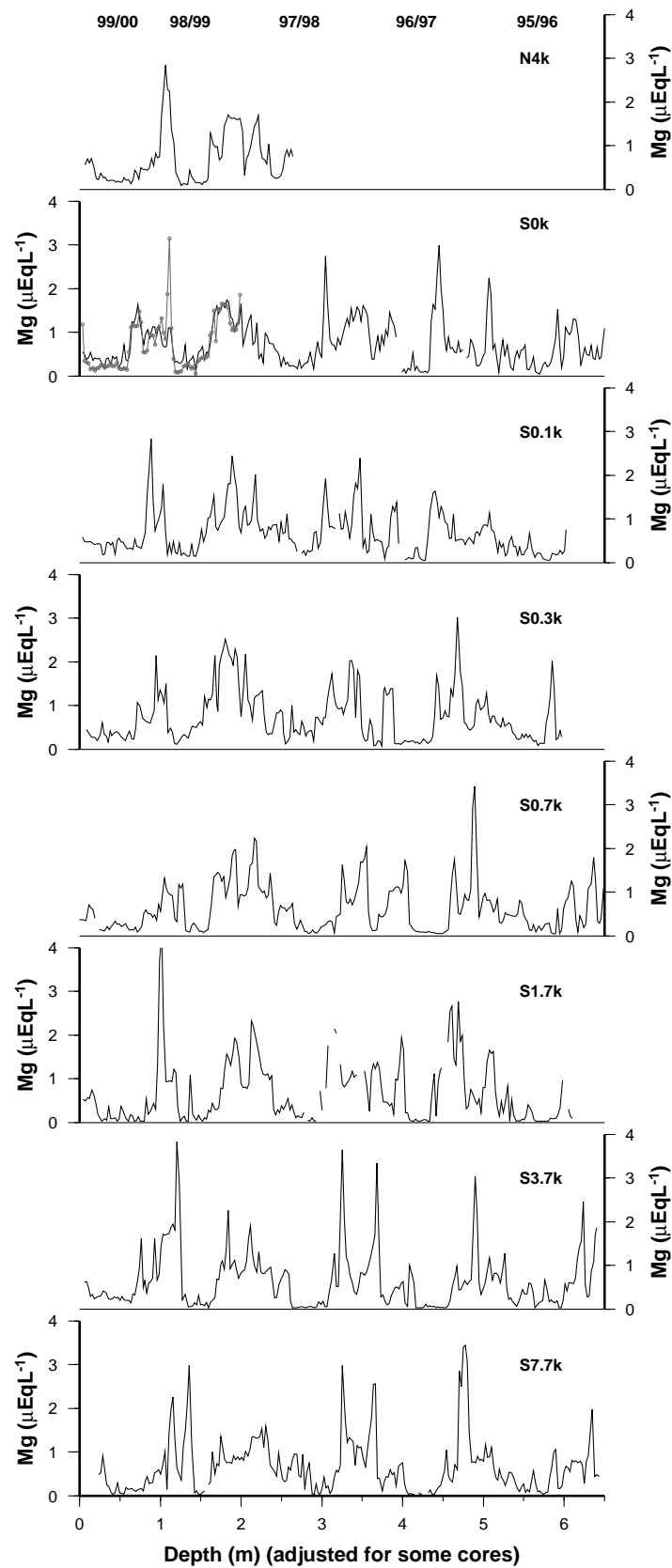


Fig. 3.12: Inter-core magnesium comparisons from drilling sites. Top to bottom: *N4k* (4 km north of *Rama*), *S0k* (co-located with the *Rama* snow pit; *Rama* $\delta^{18}\text{O}$ record is shown as dotted line), *S0.1k* (0.1 km south of *Rama*), *S0.3k* (0.3 km south of *Rama*), *S0.7k* (0.7 km south of *Rama*), *S1.7k* (1.7 km south of *Rama*), *S3.7k* (3.7 km south of *Rama*), *S7.7k* (7.7 km south of *Rama*). The depth scale for *S0.7k* was adjusted due to the earlier drilling date of this core.

3.5 Concluding Remarks

In order to compare chemical and isotopic signals from snow pits with meteorological conditions at the event scale, it is necessary to assess the spatial reproducibility of the signals to ensure the signals represent regional accumulation events. This chapter presented an ultra high resolution spatial comparison of chemical and isotopic signals preserved in snow pits and firn cores across a range of spatial scales at Law Dome.

The intra-pit comparison across seven vertical profiles from the *Rama* snow pit and representing records up to 2 m apart allowed an investigation of the impact of local depositional noise and/or post depositional modification on each of the chemical and isotopic species. Results indicated the $\delta^{18}\text{O}$, MSA and non-sea salt sulphate records showed excellent agreement at this spatial scale. The sea salt ions, represented by sodium and magnesium, also revealed good agreement at low concentrations, although spatial variability increased when concentrations were high. In contrast, nitrate profiles showed good agreement when concentrations were high, yet spatial variability increased when concentrations were low. Finally, the calcium and potassium records showed poor agreement between the sample profiles, indicating considerable variability throughout the snow pit and implying these species are poor indicators of regional events. Calcium and potassium were not considered further in this chapter, or in this thesis.

Increasing the spatial scale through inter-pit comparisons (up to 100 m apart) and inter-core comparisons (up to 11.7 km apart) revealed similar results. $\delta^{18}\text{O}$, MSA and non-sea salt sulphate were shown to be excellent indicators of regional events, although in some cases the shape and concentrations of signals varied between records. Spatial variability in non-sea salt sulphate was higher outside the main summer peak, possibly due to increased snow removal from wind scouring in autumn and spring when wind speeds are generally higher. Results from nitrate comparisons revealed this species is a good indicator of major features in the nitrate signal, although on occasion some events were absent from some records. The cause of this higher variability for nitrate is unclear, and may be the result of increased snow removal from wind scouring in autumn and spring. It is recommended that nitrate events are examined on a case-by-case basis to ensure the features are represented in at least some of the cores across Law Dome. Finally, the sea salt ions, represented by sodium and magnesium, revealed good agreement in the inter-pit and inter-core comparisons. The noisy nature of sea salt

records at times caused some difficulty in identifying specific events. However, the major features were clearly evident in all records, providing evidence that this species is a good indicator of regional events.

In general, the spatial comparisons across a range of scales at Law Dome revealed excellent results for the major chemical and isotopic species examined in many ice core studies at Law Dome. Results indicate that drilling a single core on Law Dome will give a good representation of regional signals, thus providing further evidence that interpretation of the deep DSS ice core is based on regional climatological variations. In addition, the results provide confidence that high and ultra high resolution studies, including the research presented in further chapters of this thesis, are based on regional meteorological events.

Chapter 4

Local Meteorology at DSS, Law Dome

4.1 Overview

The ice core record provides a record of past climatic events which have influenced a particular site. Interpretation of the deep ice core record requires an inherent understanding of the modern meteorological conditions for the ice core site. This chapter examines the local meteorology of DSS, Law Dome using data extracted from an automatic weather station (AWS) over a four year period. The seasonality of meteorological parameters such as temperature, wind speed and direction and atmospheric pressure are examined. Inter-year variability in the local meteorology is investigated for the four year period. Finally, potential meteorological bias in the ice core is investigated by comparing meteorological conditions on accumulation and non-accumulation days over the four year period.

4.2 Antarctic Meteorology

The Antarctic continent is generally split into two distinct meteorological patterns. The continental interior is characterised by a permanent anticyclone, producing stable meteorological conditions. Temperatures in the interior vary from around -30°C in summer to -65°C in winter (King and Turner, 1997). Precipitation in the interior is extremely low (almost zero), with precipitation in the form of ice crystals falling from thin, isolated cloud or even from an apparently clear sky ('diamond dust') (King and Turner, 1997). Strong cooling over the surface of the dome-shaped interior generates a persistent katabatic circulation, with cold surface air flowing out from the interior towards the coasts.

In contrast, coastal Antarctic sites are generally characterised by the passage of large synoptic scale cyclonic systems that develop and decay in the Southern Ocean. These systems are often weak or declining by the time they reach the Antarctic coastline, and produce precipitation of slight intensity (no more than 0.5 mm water equivalent per hour) (King and Turner, 1997). The tendency for Antarctic precipitation to be of lower intensity is also a result of the limited capacity of air to hold moisture at temperatures close to and below freezing. Sites which are characterised by moderate or heavy precipitation are usually influenced by more active fronts reaching the coastal region at the leading edge of warm air masses being advected southwards. Law Dome is an elevated coastal site which is frequently influenced by these active fronts. Well structured cyclonic systems tend to form in the region to the northwest of Law Dome (55-60° S, 60-90° E), and then travel southeast before dissipating to the east of Law Dome (Jones and Simmonds, 1993). These systems produce predominately easterly maritime circulation for Law Dome, resulting in high accumulation on the eastern side of Law Dome (up to 1.2 m ice per year), with accumulation dropping to approximately 0.67 m ice per year for sites near the summit (Morgan and others, 1997).

4.3 Automatic Weather Stations in the Antarctic and at Law Dome

Due to the sparseness of the meteorological network and the large effort required for maintaining manned research stations in the Antarctic, the use of unmanned and remotely sensed data for meteorological analysis has always been an attractive option. Automatic observing systems within the Australian National Antarctic Research Expeditions (ANARE) began in their infancy in the 1950s (Allison and others, 1993). These observations were used primarily for research and climatological investigations since it was not possible to receive the data in real time. By the late 1970s, improved satellite technology enabled AWS transmissions to be relayed by satellite, and hence enabled the retrieval of meteorological data from remote locations in real or near-real time (Allison and Morrissy, 1981). The first Antarctic AWSs that transmitted data through a satellite link were deployed during early 1980 and formed a chain between Dome C and Dumont D'Urville station in East Antarctica (Allison and others, 1993). The first Australian AWSs were designed by the Australian Antarctic Division in the

early 1980s (Allison and Morrissey, 1981). Since that time there have been approximately 120 AWSs deployed by numerous nations around the Antarctic continent, establishing a wide coverage of meteorological data for this remote region of the earth (King and Turner, 1997).

The AWS observations are collected via the French designed ARGOS system, carried by the National Oceanographic and Atmospheric Administration (NOAA) series of near-polar orbiting satellites. The ARGOS system receives information uplinked by the AWSs at a frequency of 401.65 MHz during overpasses of the satellites. These data are sent as 256 bit data words transmitted over a 1 second period and repeated every 200 seconds (Allison and others, 1993). The data transmitted are updated every 10 minutes which defines the highest frequency of observations that can be collected (King and Turner, 1997). The orbiting time of the NOAA satellites south of 75°S is about 104 minutes, and at high latitudes there is generally a large overlap of the field of view of successive orbits (Allison and others, 1993). With at least two NOAA satellites normally in orbit, it is possible to obtain direct observations approximately every 52 minutes in polar regions, even if the AWS has no storage capacity (Allison and others, 1993).

AWS 1181 was installed at DSS, Law Dome on 19 December 1997. This station is part of the Series 98 fleet of AWSs installed in Australian Antarctic Territory. For more information on Series 98 weather stations and data manipulation conducted prior to this work see Appendix 1. AWS 1181 measures a full suite of meteorological parameters including air temperature, sub-surface temperature, wind speed and direction, atmospheric pressure, relative humidity, radiation and snow accumulation. Two other AWSs have operated on Law Dome, one with limited sensors (air temperature, wind speed, barometric pressure) which operated from May 1986 to June 1998, and one with the full suite of meteorological sensors which operated from May 1997 to February 1998. This research focuses on AWS 1181 only, with particular reference to the time period from December 1997 through to December 2001. This time frame was chosen to overlap with the period covered by the snow pit and firn core records also analysed in this research.

4.4 Features of Local Meteorology at DSS

4.4.1 Air Temperature

The AWS is fitted with three air temperature sensors (1 m, 2 m, 4 m). These temperature heights are correct at the time of installation of the AWS but the sensors will become progressively buried as snow accumulates over time. The AWS was raised twice during the course of this study, November 1999 and October 2000. The 4 m arm was the only arm to remain above the snow surface during the full four year period studied in this project.

Comparisons between air temperatures from the AWS and air temperatures observed at Casey station show that seasonal variability in Casey temperatures are replicated at Law Dome (Fig. 4.1). In addition, figure 4.1 indicates that the four years examined in this research represent ‘normal’ meteorological conditions observed in this region.

The mean air temperature at Casey station during the four year period (1998 – 2000; -9.67°C) compares well with the mean air temperature at Casey from 1965 – 2000 (-9.23°C).

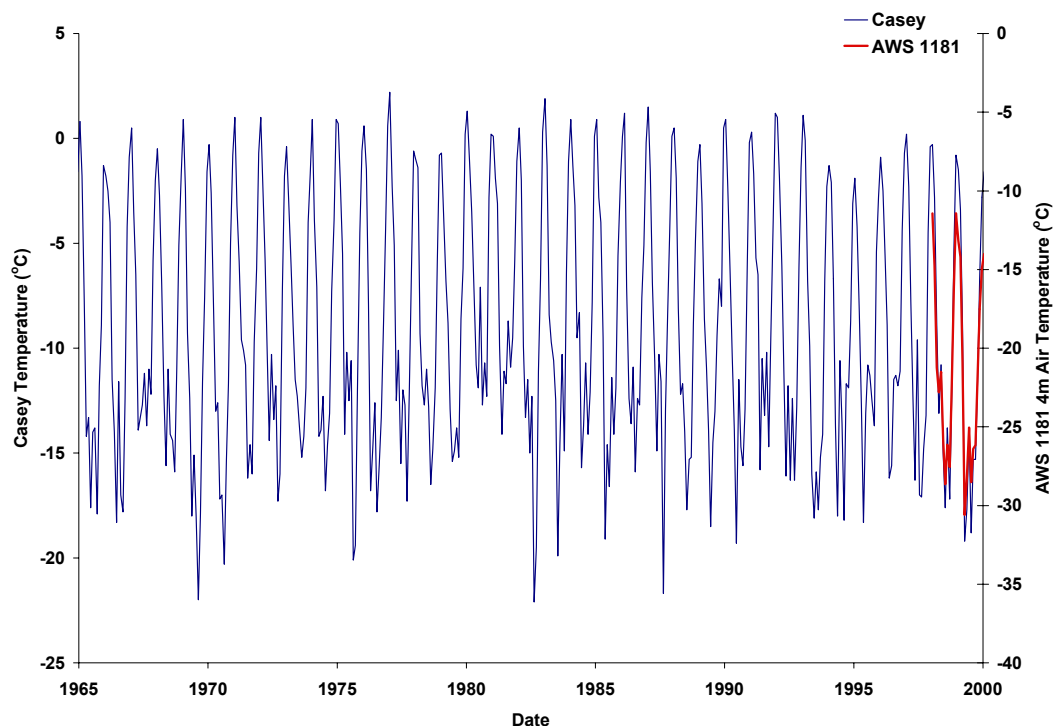


Figure 4.1: Monthly air temperatures measured at Casey station from 1965 to 2000, with monthly 4m air temperatures measured from AWS 1181 from 1998 to 2000 also shown.

Air temperatures at Law Dome show a distinct seasonal cycle with summer maxima (mean $-13.16 \pm 6.36^{\circ}\text{C}$) and winter minima (mean $-25.99 \pm 3.63^{\circ}\text{C}$) (Fig. 4.2, 4.3). The temperature ranged through the four years between -1.84°C and -47.54°C although these extremes were not sustained long enough to be recorded in the daily average presented in figure 4.2. All four years show a narrow summer peak and broad coreless winter trough with no distinct minima. Maximum temperatures are recorded in early January and all years show a sharp decrease in temperatures at the end of February, a long winter trough and a more gradual increase back to summer levels beginning early to mid October (Fig. 4.4). During the broad winter trough there are often large scale winter “peaks” where temperatures rise and then drop back to winter levels. These peaks generally last between 20 and 70 days.

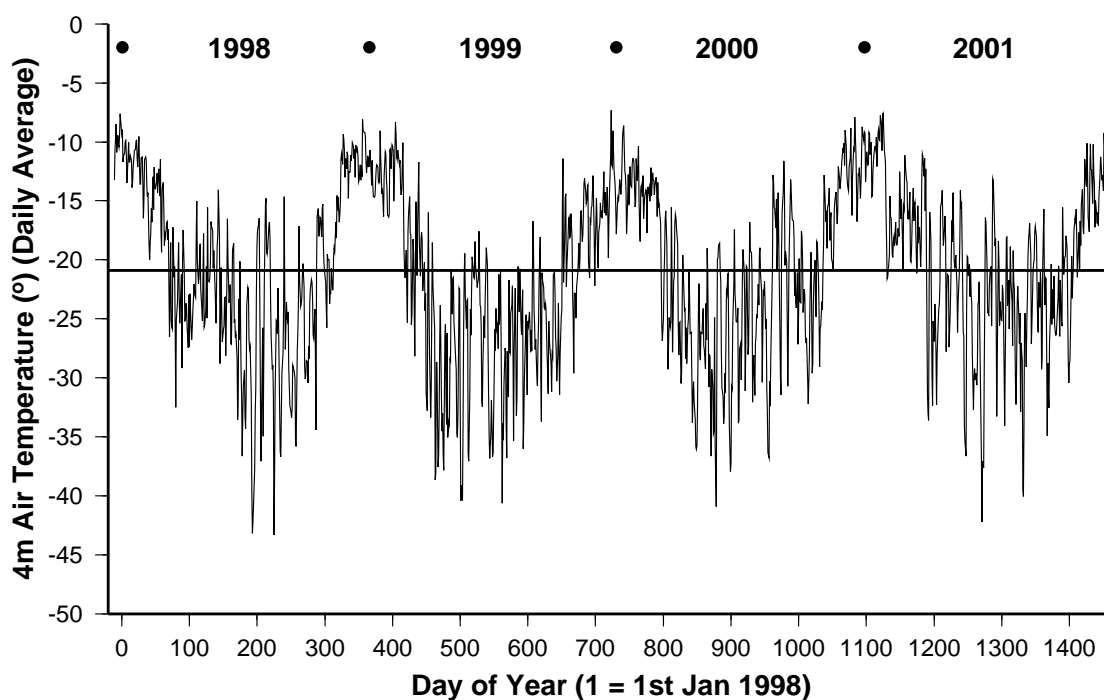


Figure 4.2: Daily average 4 m air temperature recorded from AWS 1181 from 19 December 1997 (Day of Year (1998) -11) to 31 December 2001 (Day of Year (1998) 1461). The mean temperature through this period is plotted as a solid horizontal line through the record. Each year is labelled and solid circles represent 1 January.

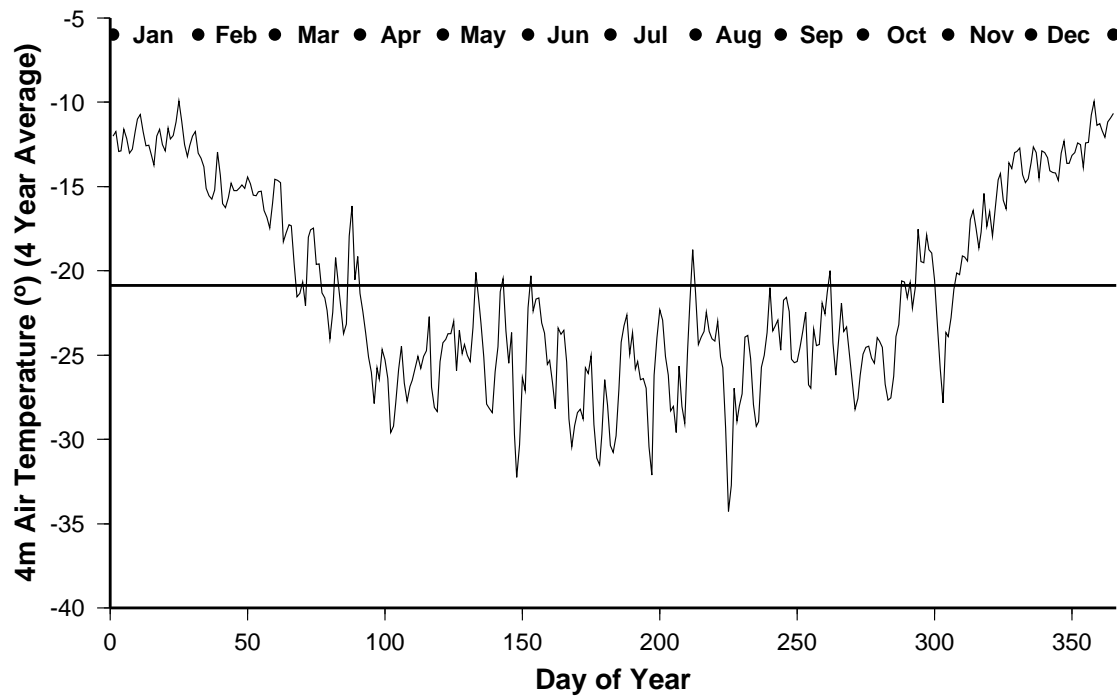


Figure 4.3: Four year average temperature record calculated from the daily averages of the 4 m air temperatures from 1 January 1998 to 31 December 2001. The mean temperature through this period is plotted as a solid horizontal line through the record. Months are labelled and solid circles represent 1st day of each month.

The main differences between each of the four years occur in the structure of the colder months (autumn to early spring) (Fig. 4.4). During 1998 one large scale winter peak is evident with temperatures rising from -30°C in mid April, up to -14°C at the end of May and dropping back to -40°C at the end of June. 1999 shows less structure during the colder months with more erratic variations in temperature. Autumn temperatures during 1999 (mean $-26.41 \pm 7.36^{\circ}\text{C}$) are significantly lower than the mean autumn temperature for all four years ($-23.34 \pm 6.64^{\circ}\text{C}$). This feature is also maintained through winter with mean winter temperatures in 1999 ($-26.99 \pm 5.62^{\circ}\text{C}$) lower than the winter mean for all four years ($-25.99 \pm 6.36^{\circ}\text{C}$). Similarly, 2000 recorded lower than average autumn temperatures (mean for 2000 $-25.06 \pm 6.29^{\circ}\text{C}$, mean for all years $-23.34 \pm 6.64^{\circ}\text{C}$) but in contrast to 1999, winter temperatures in 2000 (mean $-25.09 \pm 6.08^{\circ}\text{C}$) are slightly higher than the mean for all four years ($-25.99 \pm 6.36^{\circ}\text{C}$). Temperatures begin to rise early in 2000 (mid August) but drop back to mean winter levels in early October before rising again in mid October and reaching a maximum in early January. During 2001 the temperature record for the

colder months shows more structure compared to the other years. There are distinct oscillations in air temperatures, with four large scale peaks of warmer temperatures recorded, and each peak lasting between 30 and 60 days. Autumn temperatures during 2001 (mean $-20.14 \pm 6.25^{\circ}\text{C}$) are significantly higher than the mean autumn temperature for all four years ($-23.34 \pm 6.64^{\circ}\text{C}$). Winter ($-25.06 \pm 6.21^{\circ}\text{C}$) and spring ($-21.23 \pm 5.53^{\circ}\text{C}$) temperatures during 2001 are also higher compared to the seasonal averages for all four years (winter, $-25.99 \pm 6.36^{\circ}\text{C}$; spring, $-21.42 \pm 6.13^{\circ}\text{C}$), yet not to the same extent as autumn.

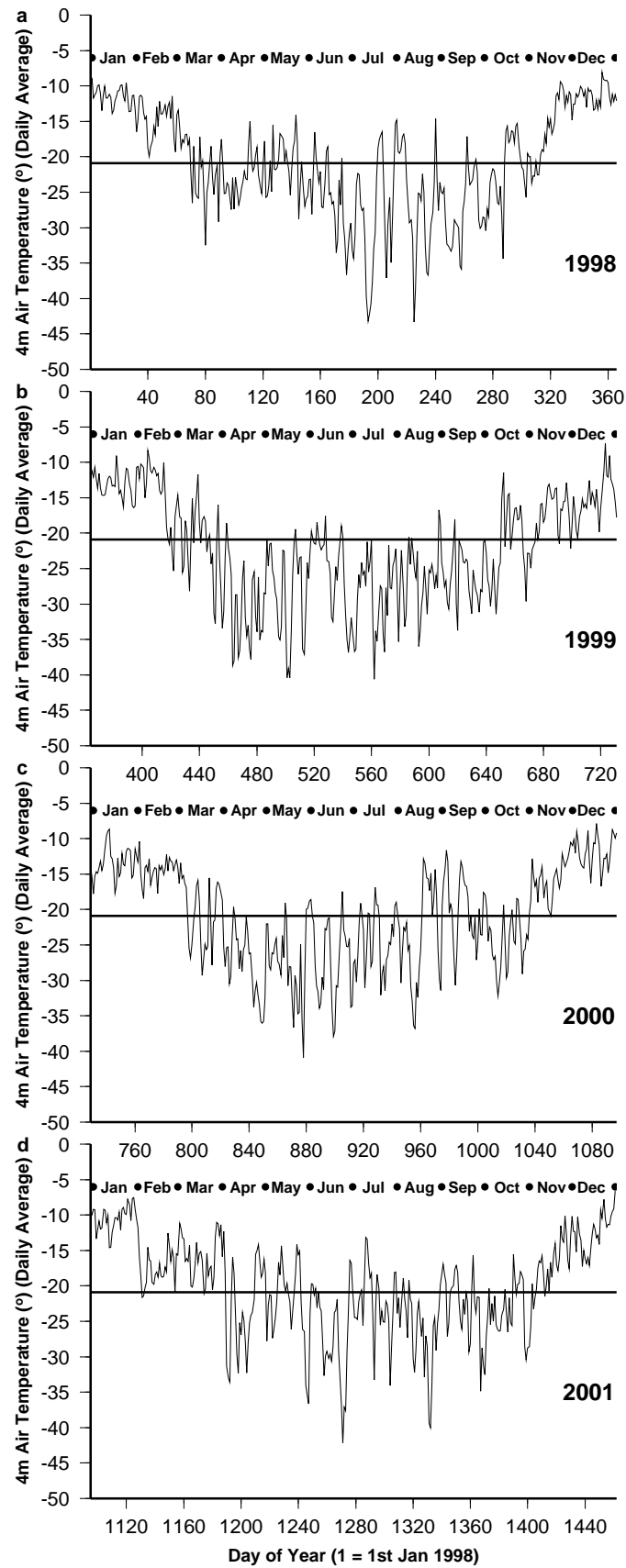


Figure 4.4: Tiled figure of daily average 4 m air temperatures for (a) 1998; (b) 1999; (c) 2000; (d) 2001. The mean temperature through this period is plotted as a solid horizontal line through the record. Months are labelled and solid circles represent 1st day of each month.

4.4.2 Wind Speed and Direction

The AWS is fitted with three anemometers to measure wind speed (1 m, 2 m, 4 m) and one wind direction sensor (4 m). These wind sensors are sensitive and there are lengthy periods through the four year period where the sensors failed to record observations. This occurred more frequently during the colder months, and could be due to freezing and a build up of hoar frost on the sensors as this phenomenon was observed by personnel during field work seasons.

A weak seasonal cycle in wind speeds is evident from the four year record with wind speeds generally higher and more erratic during winter months (May to September) (Fig. 4.5, 4.6). However, this data needs to be interpreted with caution as the lengthy periods where the anemometer failed to record observations may bias the results. If sensor failure is caused by freezing and a build up of hoar frost then this is more likely to occur during colder periods with low wind speed, resulting in a bias towards high wind speed observations during winter.

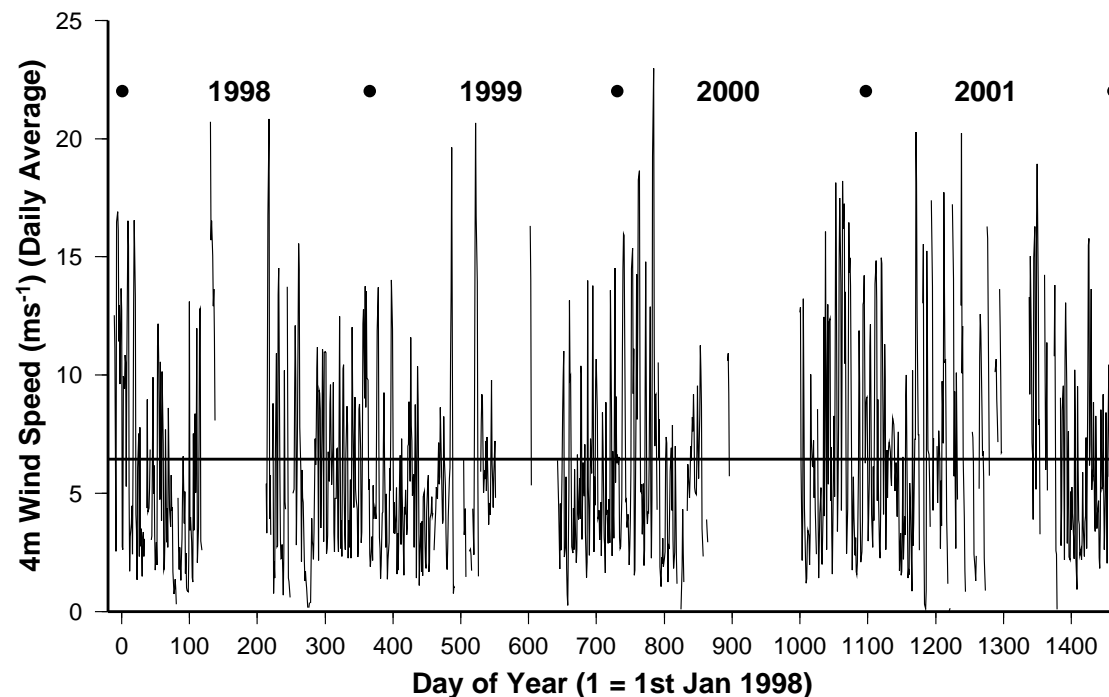


Figure 4.5: Daily average 4 m wind speed recorded from AWS 1181 from 19 December 1997 (Day of Year (1998) –11) to 31 December 2001 (Day of Year (1998) 1461). The mean wind speed through this period is plotted as a solid horizontal line through the record. Each year is labelled and solid circles represent 1 January.

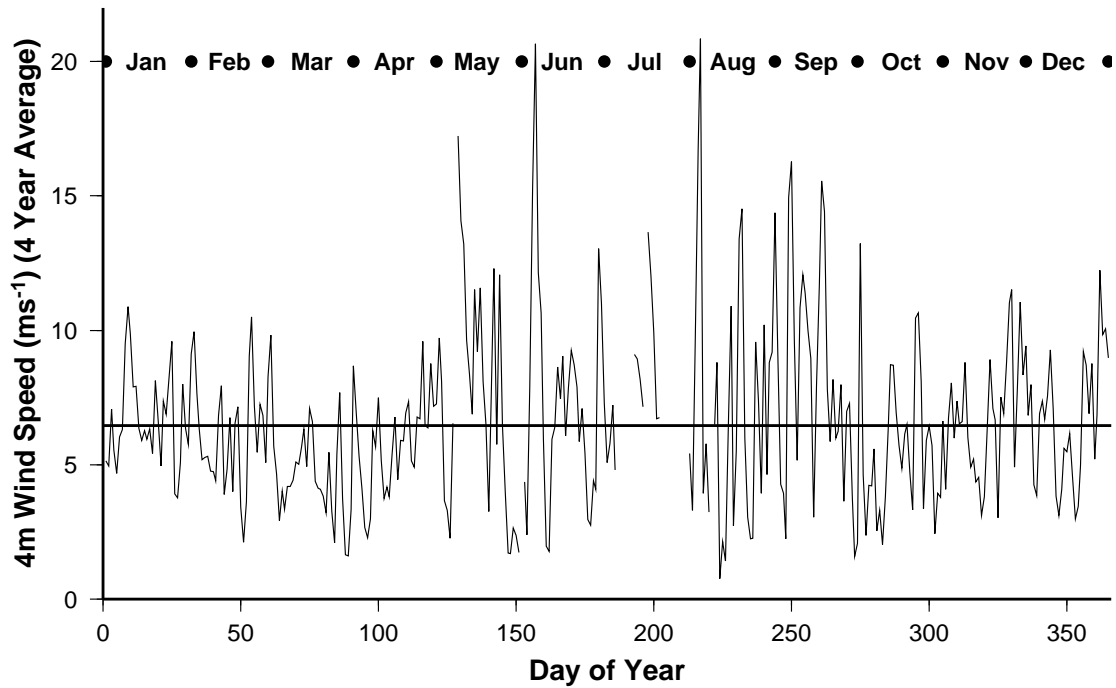


Figure 4.6: Four year average wind speed record calculated from the daily averages of the 4 m wind speed from 1 January 1998 to 31 December 2001. The mean wind speed through this period is plotted as a solid horizontal line through the record. Months are labelled and solid circles represent 1st day of each month.

The wind speed record is characterized by numerous sharp peaks generally lasting two to three days (Fig. 4.7). These strong wind events are most likely caused by the passage of cyclonic systems over the Law Dome region. Wind speeds over the four year period averaged $6.45 \pm 4.62 \text{ ms}^{-1}$, the relatively large standard deviation reflecting the high frequency of strong wind events. The maximum wind gust recorded over the four year period reached 24.9 ms^{-1} and the maximum daily average was 22.96 ms^{-1} on the same day (23 February 2000, Day of Year (1998) (DoY) 784). Autumn recorded the lowest mean wind speeds ($5.87 \pm 4.57 \text{ ms}^{-1}$) compared to summer ($6.65 \pm 4.61 \text{ ms}^{-1}$) and spring means ($6.39 \pm 4.59 \text{ ms}^{-1}$). These results are in contrast to many Antarctic sites where minimum wind speeds occur in summer and maxima occur during autumn and winter (Allison and others, 1993). The strong temperature difference between the Antarctic continent and the surrounding oceans during the colder months provides the mechanism for strong katabatic flow for many sites in Antarctica, producing high wind speeds in the colder months. Although Law Dome is an elevated site, it's proximity to the ocean results in a mainly maritime climate, with wind speeds dominated by the incursion of cyclonic events rather than

katabatic flow. This explains the weak seasonal signal and highly erratic wind speed record for Law Dome compared to other sites.

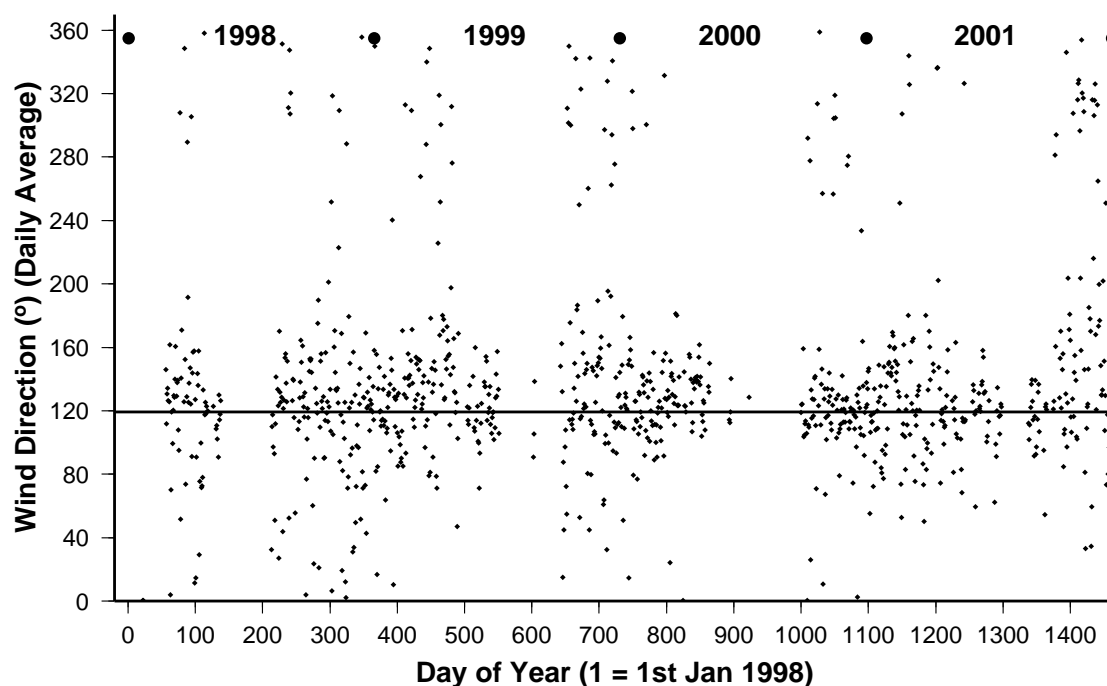


Figure 4.7: Daily average wind direction (weighted for wind speed) recorded from AWS 1181 from 19 December 1997 (Day of Year (1998) –11) to 31 December 2001 (Day of Year (1998) 1461). The mean wind direction through this period is plotted as a solid horizontal line through the record. Each year is labelled and solid circles represent 1 January.

Wind direction at DSS is predominately east to south easterly with a four year mean of $119.1 \pm 55.02^\circ$ (weighted for wind speed)) (Fig. 4.7, 4.8). A weak seasonal cycle is evident with wind direction during winter (May to July) tending more towards the four year average of 119.1° and a larger spread in wind directions outside these months. However, like the wind speed record, this data needs to be interpreted with caution due to sensor failure during the colder months. The wind direction at DSS is dominated primarily by the quasi-stationary cyclonic system situated to the north west of Law Dome. As cyclonic systems pass from west to east through the Law Dome region wind direction at DSS will change from north east to south east, with south easterly winds associated with strong wind events and snowfalls at DSS in the wake of the cyclone. These events are examined in more detail in section 4.4 of this chapter. Seasonal means for the four year period are relatively uniform, although winter wind directions appear to have a more easterly component (mean $114.4 \pm 55.63^\circ$) compared

to other seasons (summer mean $118.7 \pm 54.44^\circ$, autumn mean $121.4 \pm 55.55^\circ$, spring mean $119.7 \pm 54.70^\circ$). This could either reflect the more frequent passage of cyclonic systems across Law Dome during winter, or a bias in observations recorded during high wind, easterly component wind events compared to sensor failure during low wind events.

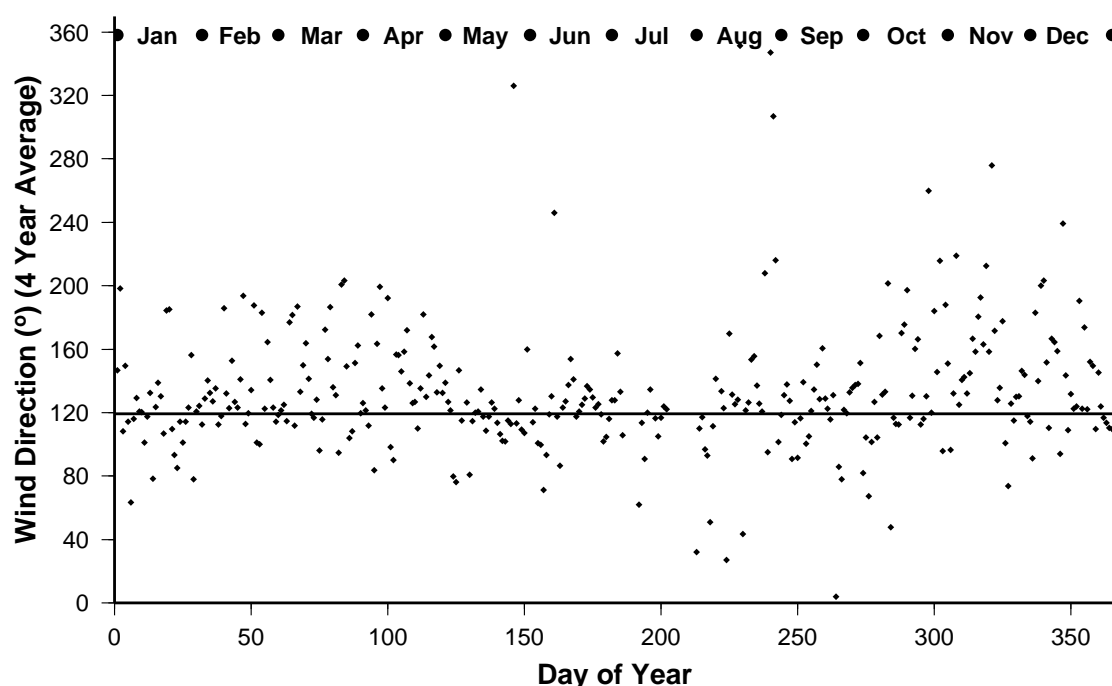


Figure 4.8: Four year average wind direction record calculated from the daily averages of wind directions (weighted for wind speed) from 1 January 1998 to 31 December 2001. The mean wind direction through this period is plotted as a solid horizontal line through the record. Months are labelled and solid circles represent 1st day of each month.

There is a distinct correlation between wind speed and direction at DSS (Fig. 4.9) with wind direction becoming increasingly easterly as wind speeds rise. There appears to be a critical level of wind speed (around 6 ms^{-1}) above which a linear correlation between wind speed and direction becomes evident. Below this critical level the relationship between wind speed and direction is more erratic with a large spread in wind directions recorded. It is important to note that strong wind events are exclusively associated with wind directions from the east to south east sector. This is consistent with the frequent incursion of storm events onto Law Dome associated with the passage of cyclonic systems through the region.

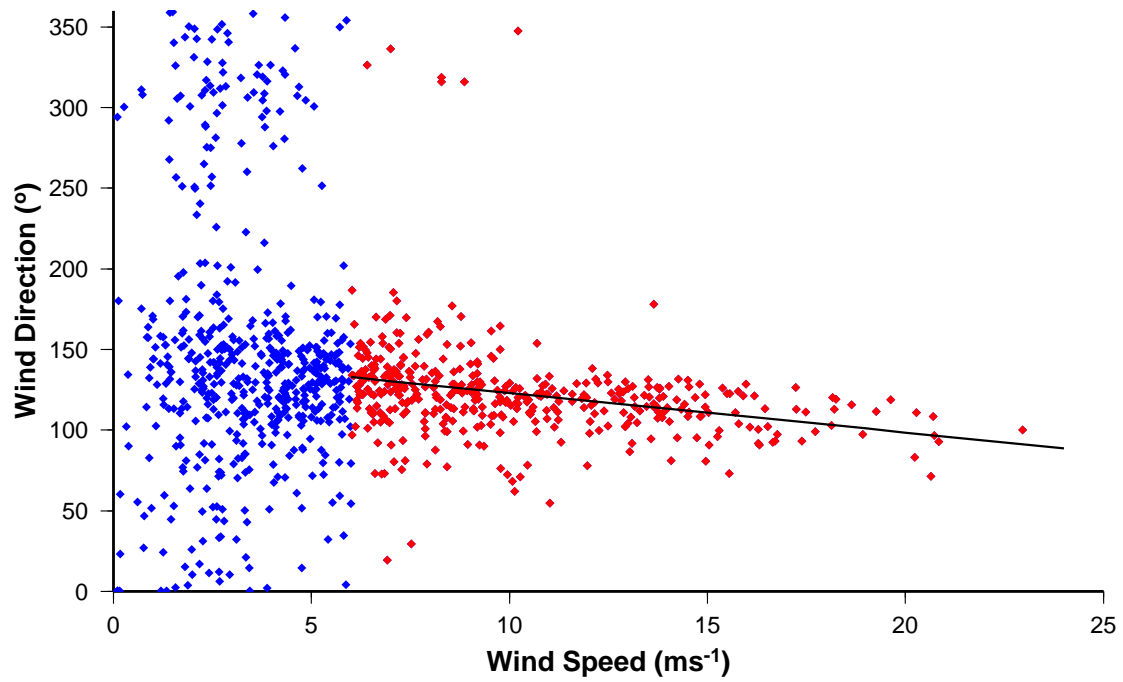


Figure 4.9: Correlation between wind direction and wind speed for the four year period 1 January 1998 to 31 December 2001. A linear correlation ($R^2 = 0.0681$) is calculated on wind speed/wind direction combinations where wind speeds are greater than 6 ms^{-1} (red points, black line).

The main differences in wind characteristics between each of the four years lies in the frequency of strong wind events with south easterly wind direction (Fig. 4.10). Wind speeds during 1998 averaged $6.37 \pm 4.73 \text{ ms}^{-1}$, similar to the total average over the four years (6.45 ms^{-1}). Strong wind events during this year occurred frequently at regular intervals. These strong wind events generally lasted two to three days, followed by another four to five days of low wind speeds before wind strength increased again. There were two extreme wind events (daily averages greater than 20 ms^{-1}) recorded during 1998, the first occurred on 11 May (DoY 131) and the second on 5 August (DoY 217). There were also two periods of extended low wind speeds (daily averages less than 2 ms^{-1}), 17 to 30 March (DoY 76 – 89) and 26 September to 10 October (DoY 269 – 283). Wind directions during 1998 were consistently near the four year mean of 119.1° , and reflect the regular occurrence of strong wind events driving these east to south easterly winds. Wind directions diverged away from the east to south easterly average when wind speeds were low. Most of these rogue wind directions had a strong northerly or southerly component with only a few observations recorded from the westerly sector.

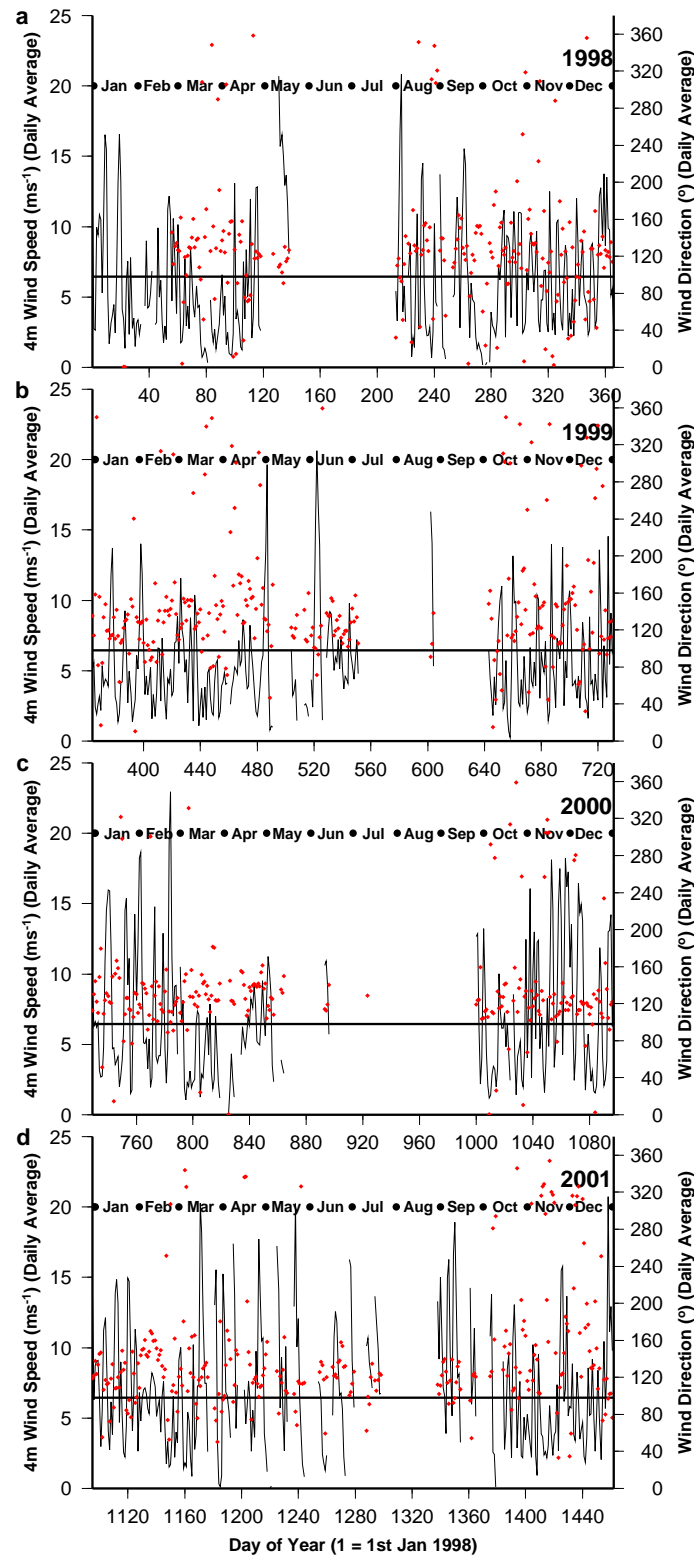


Figure 4.10: Tiled figure of daily average 4 m wind speeds (black line) and wind directions (red points) for (a) 1998; (b) 1999; (c) 2000; (d) 2001. The mean wind speed through this period is plotted as a solid horizontal black line through the record. The mean wind direction through this period is plotted as a solid horizontal red line through the record. Months are labelled and solid circles represent 1st day of each month.

In contrast to 1998, 1999 was characterised by mean wind speeds significantly lower ($5.46 \pm 3.78 \text{ ms}^{-1}$) than average levels for the four year period (6.45 ms^{-1}). Two extreme wind events were recorded during the year, the first reaching a daily average maximum of 19.63 ms^{-1} (2 May, DoY 487) and the second reaching a daily average maximum of 20.65 ms^{-1} (6 June, DoY 522). A larger spread in wind direction was recorded for 1999, consistent with the general lower wind speeds recorded for this year.

The wind direction record for 2000 shows a distinct difference to 1999 with very little spread in wind direction from the four yearly average. Strong wind events were frequent, particularly later in the year (November to December). Numerous strong wind events reaching wind speeds around 18 ms^{-1} were recorded, including an extreme event with a daily average of 22.96 ms^{-1} on 23 February (DoY 784). It is interesting to note that wind speeds during autumn were lower than average, yet winds maintained south easterly directions.

In contrast, wind directions during 2001 were more erratic with a larger spread from the 119.1° four year average. Early in the year wind direction tended more easterly with summer and autumn averages $109.2 \pm 52.13^\circ$ and $110.0 \pm 56.90^\circ$ respectively. During winter and spring the average wind direction tended more towards the four yearly average of 119.1° . Frequent strong wind events were registered, particularly during autumn and spring. Three extreme wind events with daily averages greater than 20 ms^{-1} were recorded, with an additional ten events recording daily average wind speeds greater than 15 ms^{-1} .

4.4.3 Atmospheric Pressure

The barometric pressure transducer is mounted on the 4 m arm of the AWS and measures atmospheric pressure at DSS (elevation 1379 m) (Fig. 4.11, 4.12). A semi-annual oscillation in atmospheric pressure is evident in the four year record with pressure minima in spring (mean $819.47 \pm 9.51 \text{ hPa}$) and autumn (mean $820.02 \pm 9.33 \text{ hPa}$). This phenomena has been reported for other sites in Antarctica (van Loon, 1967; Allison and others, 1993) and indicates that there is a maximum of cyclonic activity during the equinoctial months. The position of the circumpolar trough is

closest to the Antarctic continent during these months, and cyclonic depressions report the lowest pressure centres (King and Turner, 1997). The main pressure maximum at DSS is found in summer months (mean 826.00 ± 7.72 hPa) and a secondary maximum in winter (mean 821.37 ± 9.54 hPa).

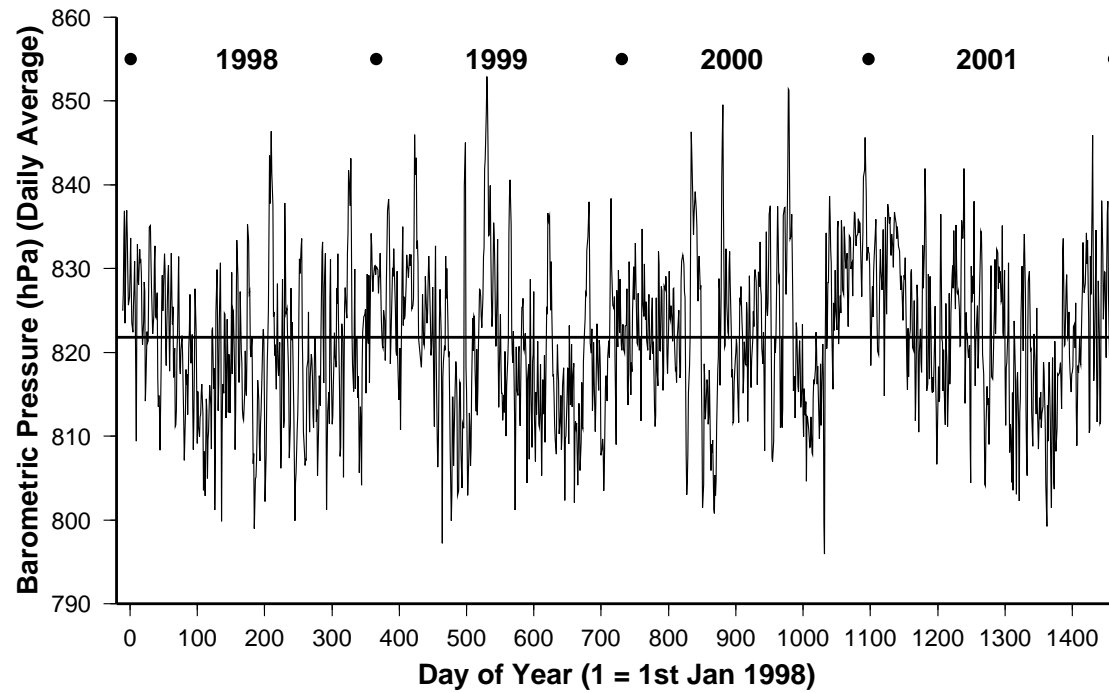


Figure 4.11: Daily average barometric pressure recorded from AWS 1181 from 19 December 1997 (Day of Year (1998) –11) to 31 December 2001 (Day of Year (1998) 1461). The mean pressure through this period is plotted as a solid horizontal line through the record. Each year is labelled and solid circles represent 1 January.

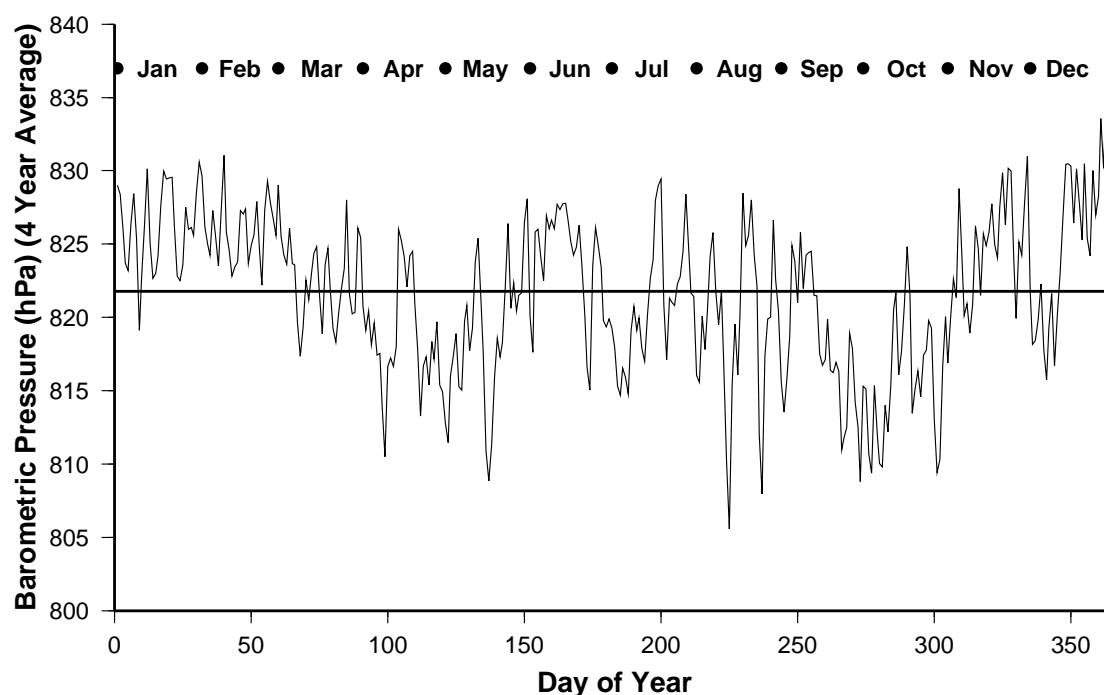


Figure 4.12: Four year average barometric pressure record calculated from the daily averages of pressures from 1 January 1998 to 31 December 2001. The mean pressure through this period is plotted as a solid horizontal line through the record. Months are labelled and solid circles represent 1st day of each month.

Although all four years record this semi-annual oscillation there are some differences in the structure of the pressure record for individual years (Fig. 4.13). Atmospheric pressures during 1998 record a weak semi-annual oscillation with the autumn minimum (late April) clearly defined but spring pressures more erratic. An extreme pressure event was recorded during midwinter (26 – 31 July, DoY 207 – 212) where pressures increased to 846 hPa. A similar spike in pressure occurred in late November (20 – 25 November, DoY 324 – 329) with pressure levels reaching 843 hPa. The pressure record for 1999 shows more structure throughout the year with numerous pressure spikes superimposed on a clear seasonal cycle. Distinct pressure minima are evident during late April and late September, with the primary maximum occurring in June rather than January. A large peak in high pressure from 9 – 20 June (DoY 525 – 536) forms the midwinter primary maximum with pressure levels reaching 853 hPa. A clear semi-annual oscillation is evident during 2000 with distinct pressure minima in May and October. The autumn minimum occurs later than other years and is characterised by a sharp narrow trough. This is in contrast to the broader trough of low pressure recorded during September and October. Pressure levels are generally

low during January and February compared to the clear peak in atmospheric pressure during November and December. A more subtle seasonal cycle is evident during 2001 with less variation in atmospheric pressure throughout the year. Pressure minima occur in April and late September with the spring trough deeper than autumn pressure levels. The winter maximum occurs in May with a general decline in atmospheric pressure throughout winter and spring before rising again in early October towards the summer maximum in late December.

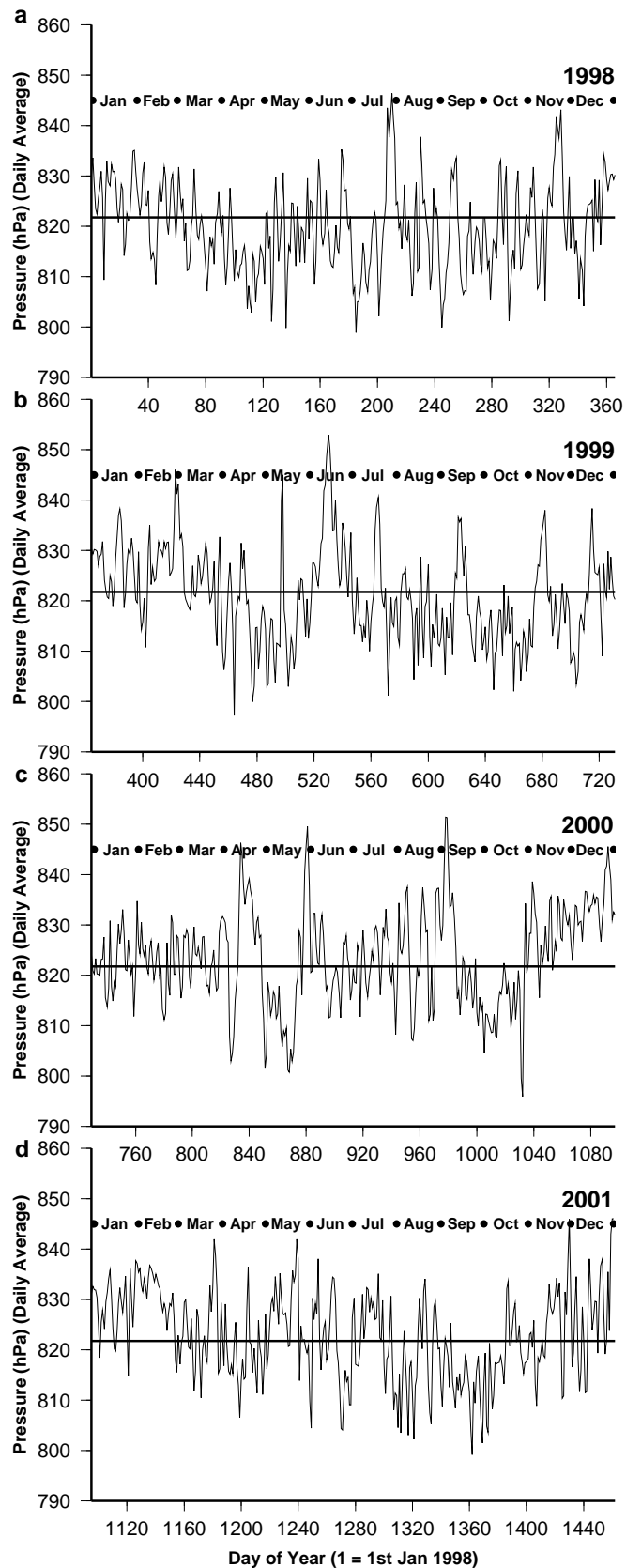


Figure 4.13: Tiled figure of daily average barometric pressure for (a) 1998; (b) 1999; (c) 2000; (d) 2001. The mean pressure through this period is plotted as a solid horizontal line through the record. Months are labelled and solid circles represent 1st day of each month.

4.5 Meteorological Bias in Ice Core Records

4.5.1 Snow Accumulation

Snow accumulation at DSS is measured from the AWS using a downward pointing ultrasonic sounding at approximately hourly intervals. Figure 4.14 shows the snow accumulation record from 19 December 1997 (DoY –11) to 31 December 2001 (DoY 1461). Net accumulation of snow is made up of accumulated snowfall events and subsequent snow removal through ablation and wind scouring of the surface. In addition, compaction of the snowpack results in a perceived loss of snow for the AWS accumulation sensor. The ice core record is comprised of accumulation events, excluding snow removal events from ablation and wind scouring, but including the perceived loss of snow through snowpack compaction. Net accumulation recorded from the AWS (red line, Fig. 4.14) can be used to identify accumulation events which are retained in recent snow pit or firn core records. However, this technique of dating needs to be used with caution as the rate of densification will affect the identification of net accumulation events which make up the core. More information regarding densification and identification of events is contained in Chapter 5 of this thesis. At this stage, potential uncertainties in the identification of events preserved in the core are alleviated by examining net accumulation at the seasonal resolution.

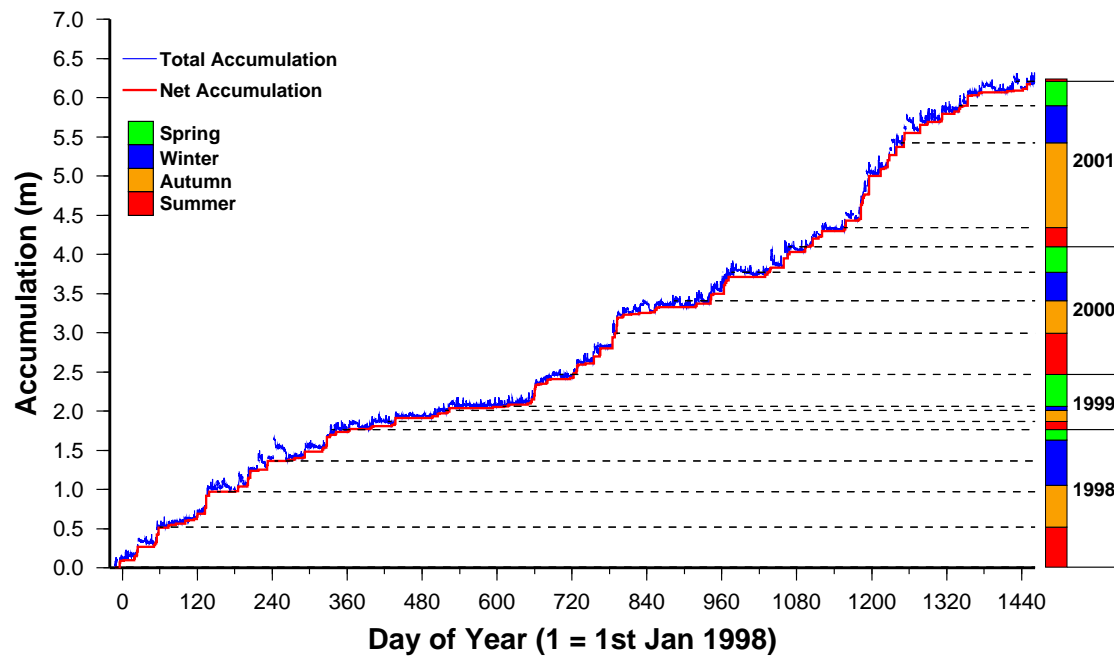


Figure 4.14: Total and net snow accumulation recorded from AWS 1181 from 19 December 1997 (Day of Year (1998) –11) to 31 December 2001 (Day of Year (1998) 1461). Net accumulation amounts preserved during each year and each calendar season are illustrated.

The most notable feature of figure 4.14 is the variability in accumulation over the four year period. Interpretation of the deeper ice core record, particularly for sites that resolve sub-annual cycles, often relies on the assumption of uniform accumulation throughout the year. Indeed, sub-annual analysis on the deep record at DSS (~1200 m) has often adopted this assumption (van Ommen and Morgan, 1996; Morgan and van Ommen, 1997b; Curran and others, 1998). Further analysis on the deep DSS ice core has shown that *on average* accumulation at DSS is uniform throughout the year (van Ommen and Morgan, 1997), yet figure 4.14 highlights that for any particular year accumulation may vary significantly through the year. This will not significantly affect long term studies which determine seasonality in the ice core record by averaging annual cycles of many years, but may affect studies which examine seasonality using high resolution short term records. Variability in accumulation within and between years will also affect studies which examine a particular year or epoch in detail. In these cases the accumulation variability may bias the analysis unless independent accumulation records are available and considered in the ice core interpretation.

The net accumulation record presented in figure 4.14 clearly shows the extent of accumulation variability both within and between years for the four year period. Accumulation during 1998 preserved uniform accumulation at the seasonal resolution with each calendar season receiving approximately equal amounts of net accumulation. At the onset of summer 1998/99 Law Dome appeared to move into drought conditions with very little accumulation recorded by the AWS. These conditions were maintained through autumn and winter of 1999 with winter showing the most extreme drought conditions and only 6 cm of net accumulation recorded. Accumulation events began to pick up again during spring 1999 and by the end of summer 1999/00 conditions were similar to 1998. Autumn, winter and spring of 2000 recorded approximately equal amounts of net accumulation although were generally lower than seasonal amounts recorded for 1998. Summer 2000/01 also recorded lower net accumulation compared to both summer 1997/98 and summer 1999/00. In contrast, autumn 2001 recorded significantly more accumulation compared to any other single season. The remainder of 2001 showed characteristics similar to 1998 and 1999 with comparable amounts of accumulation recorded for winter and spring.

Long term studies on the deep DSS ice core have calculated an average annual accumulation of 0.7 m ice or 1.2 m snow per year based on the 700 year record (Morgan and others, 1997). Annual accumulation for the four year period analysed in this research averaged 1.5 m of snow, slightly higher than the 700 year record. 2001 recorded the highest annual accumulation of 2.01 m, followed by 1998 (1.85 m), 2000 (1.56 m) and 1999 only preserving 0.69 m.

4.5.2 Local Meteorology of Accumulation Events at Law Dome

The potential for meteorological bias in ice core records has often been highlighted in ice core research but the impact of this potential bias on palaeoclimate interpretation has yet to be fully investigated. Ice core records are comprised of accumulated snowfall events and thus record information about the atmosphere at the time of snowfall. Therefore, the ice core preserves meteorological conditions associated specifically with snowfall events. Furthermore, the ice core only preserves *net* snowfall events, with many accumulation events lost through ablation or wind scouring. This leads to the preservation of only a sample of climate conditions

retained in the ice core record, and the extent to which this sample is biased towards certain meteorological conditions is considered in figure 4.15 and table 4.1.

Figure 4.14 compares the local meteorology associated with net accumulation events which are retained in the ice core record with the complete daily meteorological record for the four year period 19 December 1997 to 31 December 2001. The net accumulation events (red circles) show a distinct but subtle bias in meteorological conditions compared to the complete record (blue line). This bias is also reflected in the mean meteorological conditions associated with days with a range of accumulation characteristics (table 4.1). Temperatures are generally higher during accumulation events, and this warm bias is more pronounced during events which produce larger accumulation events. Events which recorded more than 10 cm of accumulation in a single day averaged -16.73° , 4.15° warmer than the mean for the complete record, and 4.68° warmer than the mean for zero or negative accumulation days. Similarly, large accumulation events recorded higher than average wind speeds with more easterly component wind direction. Events which recorded more than 10 cm of accumulation in a single day clearly show this high wind (mean 11.18 ms^{-1}), easterly component (mean 111.93°) bias. However, net accumulation events with average wind speeds of 8.21 ms^{-1} , higher than the average for the complete record (6.45 ms^{-1}), generally recorded wind directions nearer the mean wind direction for the complete record (119.1°). This suggests there is a distinct bias towards high wind speeds during net accumulation events preserved in the ice core, yet wind directions appear less sensitive and on average are not significantly biased in the ice core. Atmospheric pressure at DSS is relatively stable between the various accumulation groupings with pressures around 821 hPa. Local pressure is higher during large accumulation events which record greater than 10 cm of accumulation in a single day (mean pressure 823.84 hPa). This result is surprising as large accumulation events which are associated with high wind speeds and easterly wind directions are likely to be caused by the situation of a well developed low pressure system to the north of Law Dome. An intense low pressure system in close proximity to Law Dome is expected to cause lower than average local pressures at DSS. Relative humidity also shows a distinct bias with relative humidity rising as the amount of daily accumulation increases. This result is consistent with the intrusion of a moist air mass onto Law Dome during large accumulation events.

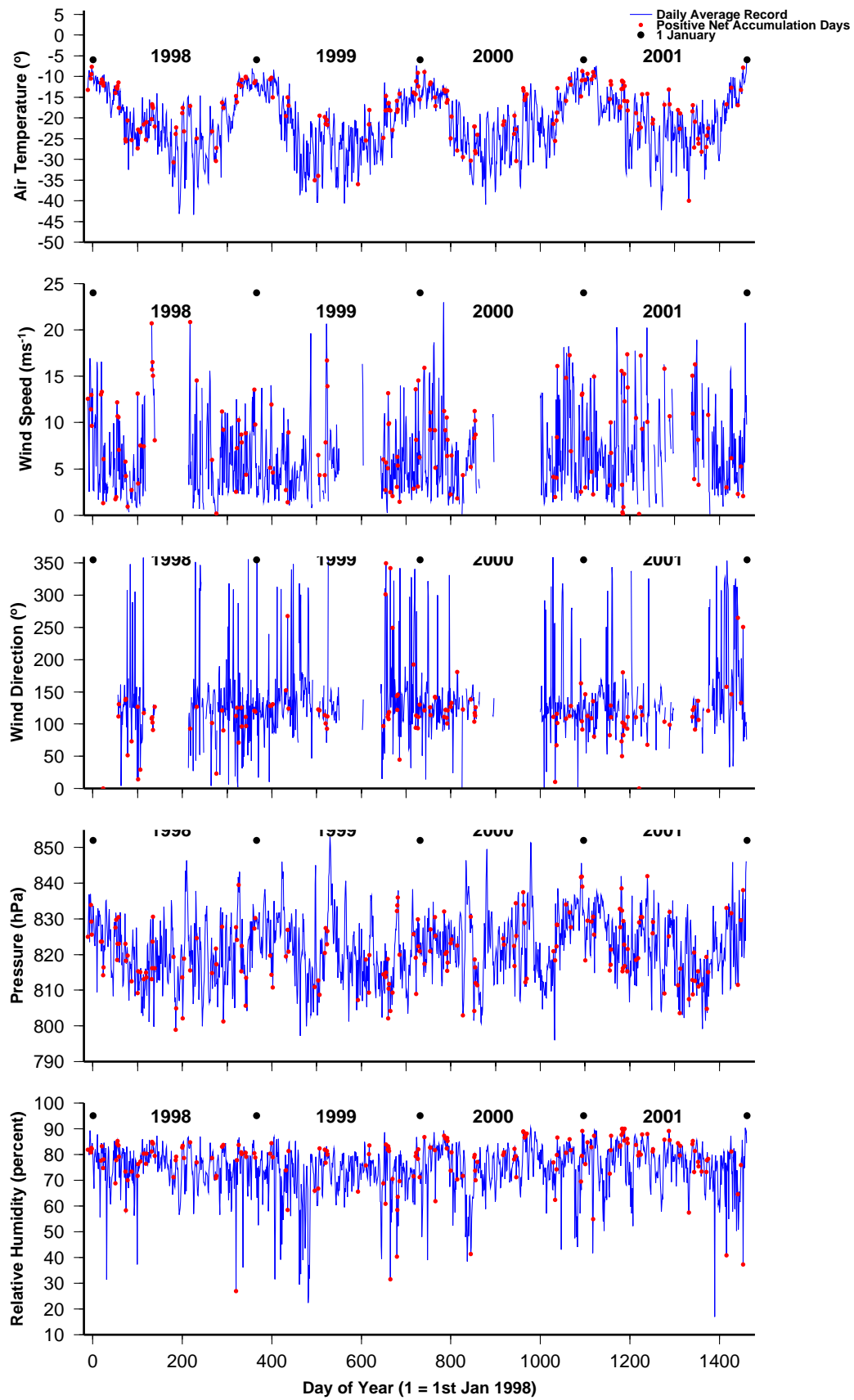


Figure 4.15: Local meteorological conditions from 19 December 1997 (Day of Year (1998) –11) to 31 December 2001 (Day of Year (1998) 1461) with local meteorology during net accumulation days also plotted (red circles).

Table 4.1: Mean local meteorological conditions for days with various accumulation characteristics

Accumulation Days	Number of Days	Mean Temperature (°)	Mean Wind Speed (ms⁻¹)	Mean Wind Direction (°)	Mean Pressure (hPa)	Mean Relative Humidity (%)
Total Acc > 0 cm	539	-20.18	6.46	133.10	821.83	76.03
Total Acc > 2 cm	352	-19.57	7.20	126.48	821.83	77.67
Total Acc > 3 cm	229	-18.77	8.14	121.89	821.67	79.17
Total Acc > 5 cm	118	-17.57	9.34	117.46	821.83	80.62
Total Acc > 10 cm	48	-16.73	11.18	111.93	823.84	82.09
Net Acc > 0 cm	178	-17.97	8.21	119.11	820.73	77.53
≤ 0 cm	908	-21.41	6.16	139.24	821.76	73.59
All Days	1473	-20.88	6.45	119.11	821.78	74.60

4.6 Concluding Remarks

This chapter presented a detailed investigation of the meteorological conditions of DSS, Law Dome using data extracted from an AWS situated within 100 m of the deep DSS ice core. The high resolution four year meteorology record examined here, extending from 19 December 1997 to 31 December 2001, corresponds with the time period covered by the snow pit and firn core records also analysed in this research.

The results show a clear seasonal cycle in temperatures with a narrow summer peak and broad coreless winter trough. The wind speed and wind direction records show more erratic observations and a subtle seasonal cycle with higher wind speeds and more easterly component winds during winter. Wind directions are predominately east to south easterly at DSS and there is a distinct correlation between wind speed and direction with wind direction tending more easterly as wind speed rises. A semi-annual oscillation in atmospheric pressure is evident at DSS with pressure minima in spring and autumn, consistent with the more southerly position and lower pressures reported for the circumpolar trough during the equinoctial months.

Inter-year variability in the local meteorology at DSS is evident in the four year record and has a direct impact on the ice core record. Snow accumulation during 1998 was high with relatively uniform accumulation through the year. In sharp contrast, 1999 was characterised by very low accumulation. The local meteorology during 1999 recorded generally lower air temperatures and low wind speeds with a larger spread in wind directions compared to 1998. Accumulation during 2000 exhibited similar characteristic to 1998 with high and relatively uniform accumulation through the year. Wind directions were consistently east to south easterly with little spread and numerous high wind gusts. The highest annual accumulation occurred during 2001 and was attributed to very high accumulation during autumn. Temperatures were generally warmer in 2001 compared to other years and many high wind gusts were recorded.

A subtle meteorological bias in the ice core record at Law Dome is evident from the results presented here. Snow accumulation events which are preserved in the ice core record are generally characterised by warmer air temperatures and higher relative humidity compared to the complete daily meteorology record. In addition, events with higher wind speeds and east to south easterly wind direction tend to be preserved in the ice core. Potential meteorological bias in the ice core should be considered when interpreting palaeoclimate records. The results presented in this chapter indicate that Law Dome ice core records may typically record events characterised by strong, east to south easterly winds and warmer, more humid air masses compared to average climate signals.

Chapter 5

High Resolution Dating of the Snow Pit Records

5.1 Overview

A key task in interpreting the ice core record lies in accurate dating of the core. The temporal resolution of the ice core chronology depends on the time scale under investigation. Ice core records extending back to the last glacial period may only require millennial-scale resolution. In contrast, studies which aim to compare contemporary meteorological records with ice core signals typically require annual or better resolution. Various methods are used for dating ice cores including annual layer counting of seasonal variations in isotope ratios and chemistry signals and electroconductivity measurements, reference horizons and stratigraphy studies.

Only a few studies have attempted to identify individual snowfall events preserved in snow pit or firn core records. McConnell and others (1997b) used snow accumulation stakes over a seven year period to investigate the episodic nature of accumulation at South Pole. However, difficulties arose in accurate dating due to the low accumulation and high wind speeds at the site, as well as infrequent (monthly) stake measurements. A more sophisticated method of identifying accumulation events preserved in the snowpack was conducted by Hardy and others, (1998) and Vuille and others, (1998) at Sajama, Bolivia. In this study snowfall events were identified using an automated weather station equipped with a snow accumulation sensor. Preliminary results provided atmospheric circulation information relating to 17 precipitation events preserved in a snow pit within a 5 month period (Vuille and others, 1998). Hardy and others (1998) report that accumulation at this site was revealed to be more episodic in nature than previously believed.

The results presented in this chapter detail the high resolution dating techniques developed in this work and are an extension of the methods outlined in M^cMorrow and others (2001). Dating scales are determined independently for two snow pit records sampled over different field seasons. Effects of densification of the snowpack on the dated records are also discussed.

5.2 Identification of Net Accumulation Events

Identification of accumulation events preserved in the snow pit records is determined using net accumulation recorded from the co-located AWS. Snow accumulation is measured from the AWS using a downward pointing ultrasonic sounding at approximately hourly intervals. Snow pits were sampled directly beneath the snow accumulation sensor to minimise uncertainties caused by surface roughness. Figure 5.1 shows the snow accumulation record (blue line) from the date of installation of the AWS (19 December 1997 (DoY -11)) to the sampling date of the final snow pit (*Matilda*, 24 December 2001 (DoY 1454)). Date of sampling of the first snow pit (*Rama*, 28 February 2000 (DoY 789)) is also illustrated. Net accumulation of snow (red line) is made up of accumulated snowfall events and subsequent snow removal through ablation and wind scouring of the surface. In addition, compaction of the snowpack results in a perceived loss of snow for the AWS accumulation sensor. The ice core record is comprised of net accumulation events, thus the net accumulation record provides the first step to identifying accumulation events preserved in the snow pit records.

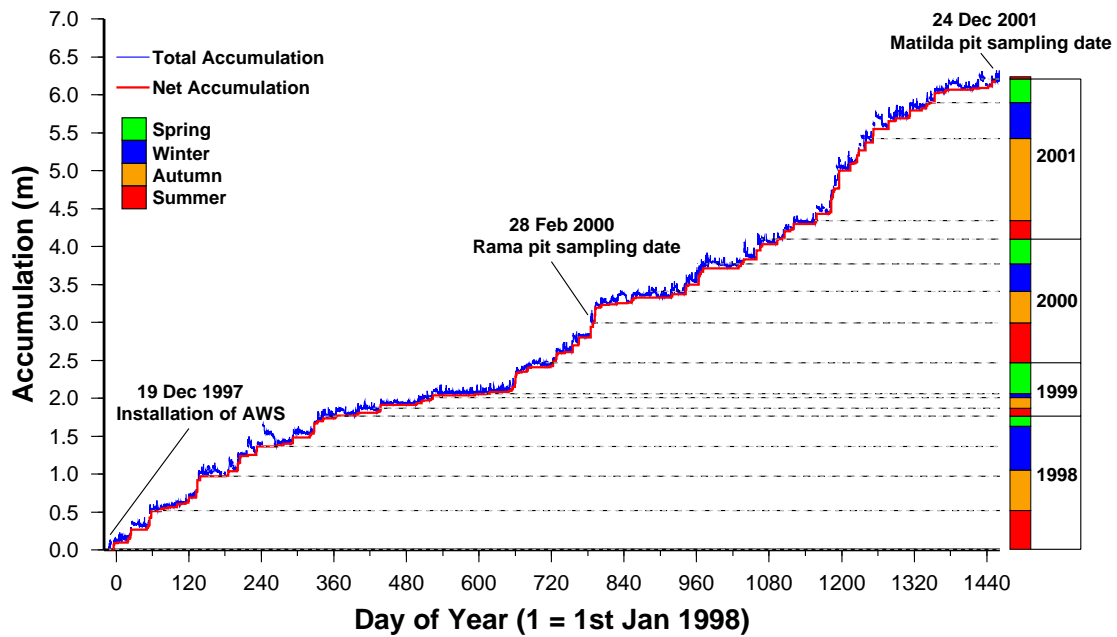


Figure 5.1: Total and net snow accumulation recorded from AWS 1181 from date of installation of the AWS (19 Dec 1997 (DoY -11)) to the sampling date of the final snow pit (*Matilda*, 24 Dec 2001 (DoY 1454)). Date of sampling of the first snow pit (*Rama*, 28 Feb 2000 (DoY 789)) is also illustrated.

5.2.1 Defining Events in the *Rama* and *Matilda* Snow Pits

Comparisons between chemical and isotopic signals preserved in the snow pits and contemporaneous meteorological conditions requires identification of net accumulation events. The net accumulation record (red line, Fig. 5.1) provides the first step to identifying these events yet physical processes such as wind redistribution of snow and densification of the snowpack will introduce uncertainties in the absolute dating of some events. This section describes the process of refining the net accumulation record and identifying net accumulation events preserved in the *Rama* and *Matilda* snow pits that are used in the comparative studies.

The *Rama* snow pit was sampled on 28 February 2000 (DoY 789) to a depth of 2 m. Figure 5.2 illustrates the accumulation and net accumulation records for the time period corresponding to the *Rama* snow pit. The net accumulation record (red line, Fig. 5.2) shows 92 specific net accumulation steps in the *Rama* record. These net accumulation steps are defined as the difference between snow accumulation and snow removal as perceived by the AWS accumulation sensor. The *Matilda* snow pit was sampled on 23 December 2001 (DoY 1454) to a depth of 2.25 m. 72 net accumulation steps are identified in *Matilda* from the net accumulation record (red

line, Fig. 5.3). The amount and distribution of snow preserved in each pit highlights the inter-annual variability of accumulation at this site. The 2 m of snow preserved in *Rama* represents accumulation over an 18 month period, while the 2.25 m of snow preserved in *Matilda* only covers a 12 month period. The drought conditions of autumn and winter 1999 (*Rama*, Fig. 5.2) are in sharp contrast to the large snowfalls preserved during autumn 2001 (*Matilda*, Fig. 5.3). More information relating to snow accumulation variability is detailed in Chapter 4 of this thesis.

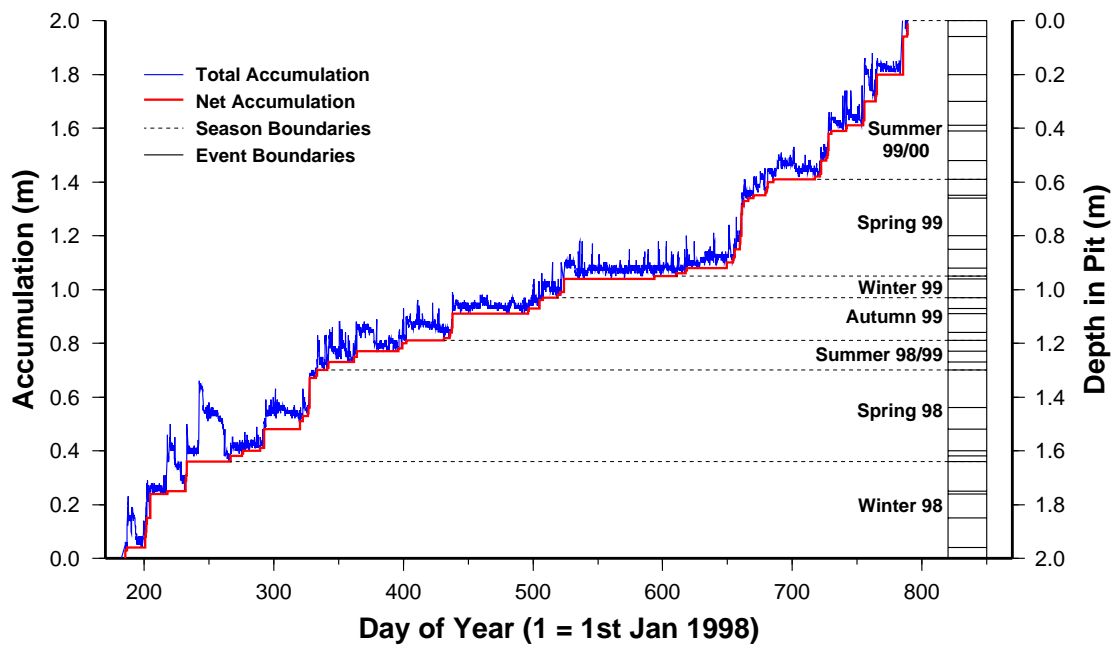


Figure 5.2: Total and net snow accumulation records for events preserved in the *Rama* snow pit.

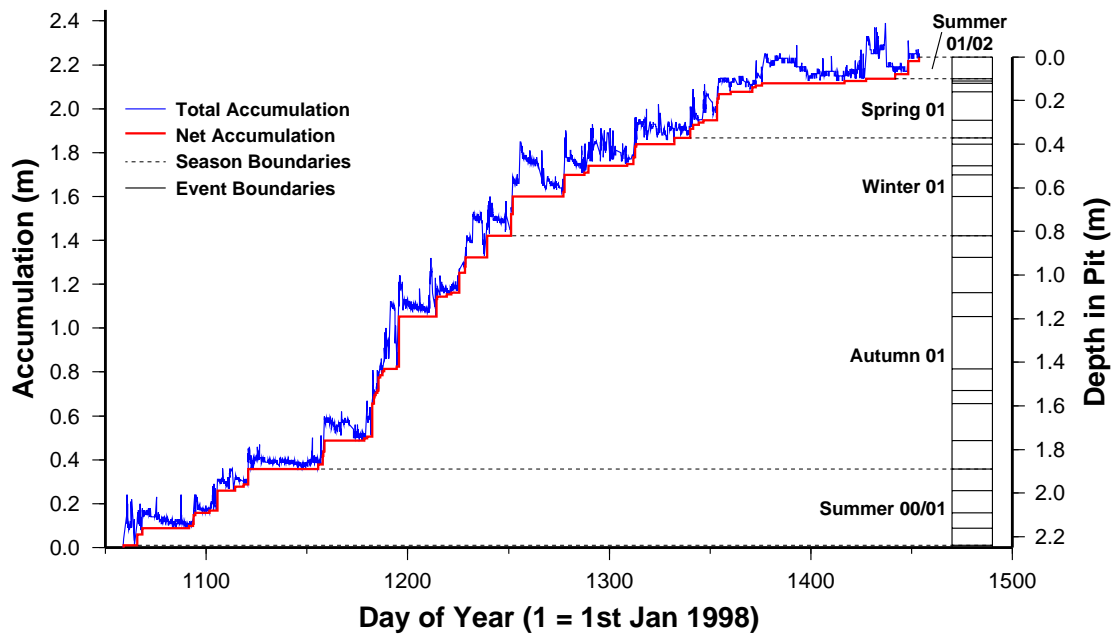


Figure 5.3: Total and net snow accumulation records for events preserved in the *Matilda* snow pit.

Net accumulation steps preserved in the snow pit records are grouped into events using two considerations. First, accumulation steps which occur close together in time (less than a week) and from a particular synoptic situation are grouped into a single event. Second, the chemical and isotopic signature for each accumulation step is examined. Sharp changes in chemical or isotopic signals within a short time period are separated into distinct events. This separation allows the investigation of sharp changes in the chemical or isotopic record that occur over consecutive days or within a particular synoptic system. Accumulation events that are used in the comparative studies in the remainder of this thesis are thus defined using these two considerations. Moreover, events that result in net accumulation of less than 3 cm are excluded from the analysis to minimise uncertainties associated with the dating technique.

Grouping the accumulation events using these techniques identifies 25 events preserved in *Rama* (Fig. 5.2) and 21 events preserved in *Matilda* (Fig. 5.3). In addition, the snow pit records are extended further back in time using firn cores drilled within 0.5 m of the pit walls. Due to the increased uncertainty associated with dating deeper records, only significant or large events preserved in the firn cores are included in the analysis. Three significant events are identified in the *DSS0102* core, extending the *Matilda* record back to winter 2000, and two events are identified in the *S0k* core, extending the *Rama* record back to winter 1998.

5.2.2 Accumulation Events

Accumulation events are numbered in reverse chronology (ie. down-core direction), with Event 1 corresponding to the most recent time period sampled (summer 2001/2002) and the top section of the *Matilda* snow pit, extending down to Event 51 identified in *S0k* and snow preserved during winter 1998.

Matilda Events

Table 5.1 summarises the 21 accumulation events preserved in *Matilda*. Many of the events are characterised by large net accumulation (greater than 10 cm), allowing confidence in the accuracy of the dating. The events are preserved over a single annual cycle, with sampling of the snow pit occurring during summer 2001/2002 and the dated record extending back to summer 2000/2001. The net accumulation preserved during this single annual cycle was 2.25 m, with a significant amount of accumulation preserved during autumn.

Table 5.1: Accumulation events preserved in *Matilda*

Event Number	Date Start	Date Finish	Date(s) with most Net Accumulation	Net Accumulation (cm)
1	11 Dec 2001	23 Dec 2001	18 Dec 2001	10
2	2 Oct 2001	6 Oct 2001	All days	4
3	14 Sep 2001	21 Sep 2001	14 Sep 2001	13
4	1 Sep 2001	7 Sep 2001	1 Sep 2001	8
5	24 Aug 2001	24 Aug 2001	24 Aug 2001	3
6	31 Jul 2001	5 Aug 2001	4 Aug 2001	10
7	10 Jul 2001	12 Jul 2001	All days	4
8	30 Jun 2001	30 Jun 2001	30 Jun 2001	10
9	4 Jun 2001	5 Jun 2001	All days	18
10	23 May 2001	23 May 2001	23 May 2001	10
11	9 May 2001	12 May 2001	All days	16
12	28 Apr 2001	5 May 2001	28 Apr 2001	11
13	8 Apr 2001	9 Apr 2001	9 Apr 2001	24
14	30 Mar 2001	2 Apr 2001	30 Mar 2001	11
15	28 Mar 2001	29 Mar 2001	All days	6
16	23 Mar 2001	27 Mar 2001	27 Mar 2001	17
17	28 Feb 2001	3 Mar 2001	3 Mar 2001	13
18	18 Jan 2001	24 Jan 2001	24 Jan 2001	10
19	5 Jan 2001	9 Jan 2001	9 Jan 2001	10
20	26 Dec 2000	29 Dec 2000	28 Dec 2000	7
21	30 Nov 2000	3 Dec 2000	All days	8

Figure 5.4 illustrates the trace chemical and $\delta^{18}\text{O}$ signals associated with the 21 accumulation events preserved in *Matilda*. In addition to seasonal (dotted) and event (pink) boundaries, the amount of net accumulation occurring on specific days within the events is also shown (grey lines). This indicates the number of days that make up the net accumulation event, and clearly shows events that are dominated by a single day of accumulation.

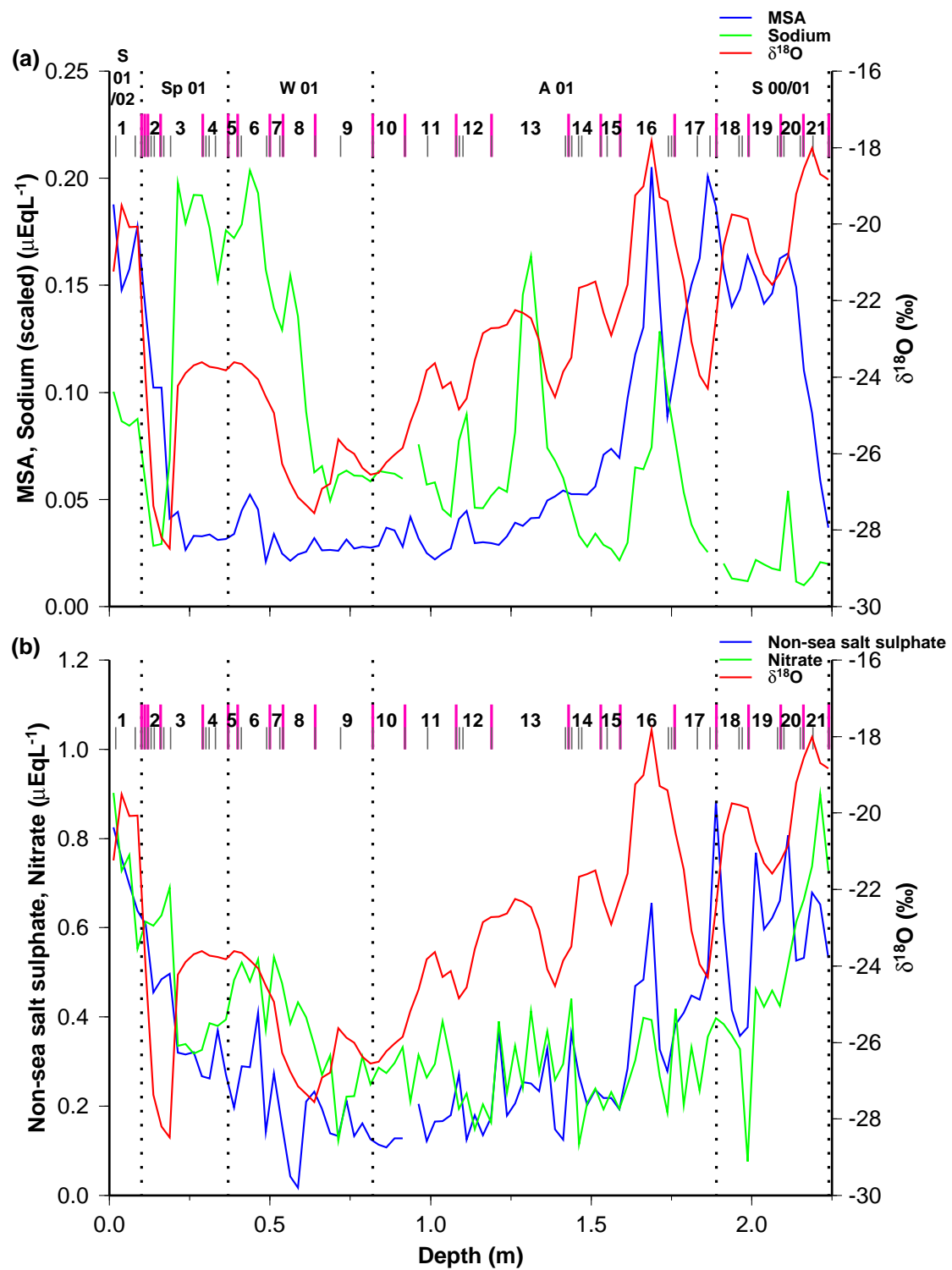


Figure 5.4: Trace chemical and $\delta^{18}\text{O}$ signals associated with the 21 accumulation events preserved in *Matilda*: (a) MSA, Sodium (scaled by a factor of 0.025) and $\delta^{18}\text{O}$; (b) Non-sea salt sulphate, Nitrate and $\delta^{18}\text{O}$. Seasonal (dotted), event (pink) and event day (grey) boundaries are also shown.

Clear seasonal signals in $\delta^{18}\text{O}$, MSA, sodium, nitrate, non sea-salt sulphate are apparent for the single annual cycle preserved in *Matilda*. The traditional summer

species ($\delta^{18}\text{O}$, MSA, nitrate, non sea-salt sulphate) show higher concentrations during late spring, summer and early autumn periods, with lower concentrations during winter. In contrast, sodium concentrations are greatest during late winter and early spring. Other chemical and $\delta^{18}\text{O}$ features are also apparent in the record, including winter and autumn $\delta^{18}\text{O}$ peaks (events 5, 6, 11, 13), autumn deposition of MSA, $\delta^{18}\text{O}$, non sea-salt sulphate and sodium (event 16), and high nitrate concentrations during winter deposition (events 6, 7).

Extending Matilda – DSS0102 Events

The high quality firn core (*DSS0102*) drilled within 0.5 m of the *Matilda* pit wall allows the investigation of events preserved at depths greater than the *Matilda* record. Table 5.2 details 3 events that are preserved in *DSS0102* that extend the record back through spring and winter 2000. Although the accuracy of the dating technique is reduced for material preserved in deeper sections of the core, the large net accumulation associated with each of these events allows confidence in dating these events.

Table 5.2: Accumulation events preserved in *DSS0102*

Event Number	Date Start	Date Finish	Date(s) with most Net Accumulation	Net Accumulation (cm)
22	23 Nov 2000	23 Nov 2000	23 Nov 2000	12
23	25 Oct 2000	3 Nov 2000	All days	12
24	19 Aug 2000	27 Aug 2000	20 Aug 2000	21

Figure 5.5 shows the trace chemical and $\delta^{18}\text{O}$ signals preserved in *DSS0102*. Of particular interest is the very high nitrate concentration preserved during spring 2000 (events 22, 23), and the warm $\delta^{18}\text{O}$ signal preserved during winter 2000 (event 24).

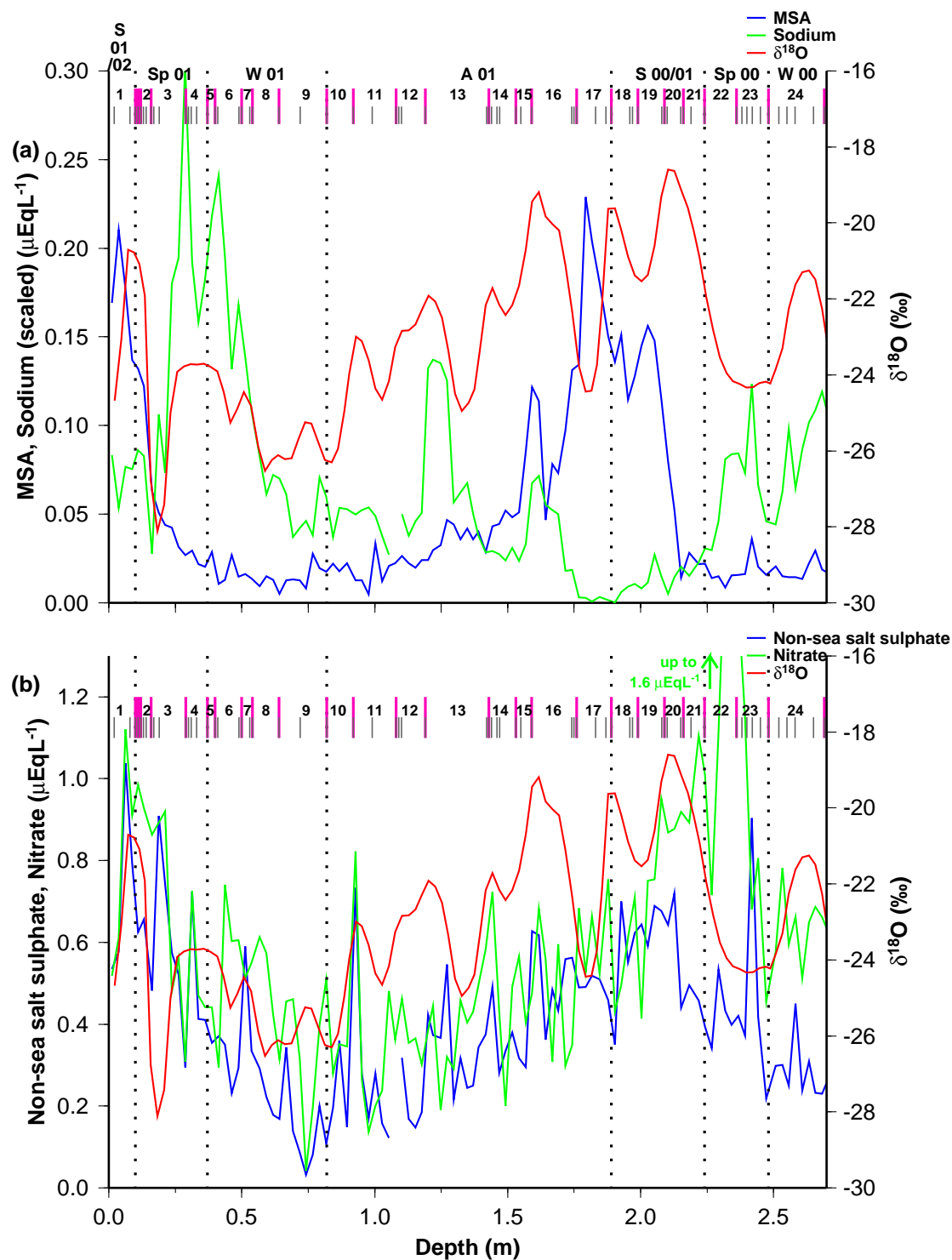


Figure 5.5: Trace chemical and $\delta^{18}\text{O}$ signals associated with the 24 accumulation events preserved in DSS0102: (a) MSA, Sodium (scaled by a factor of 0.025) and $\delta^{18}\text{O}$; (b) Non-sea salt sulphate, Nitrate and $\delta^{18}\text{O}$. Seasonal (dotted), event (pink) and event day (grey) boundaries are also shown.

Rama Events

Details of the 25 events preserved in *Rama* are outlined in Table 5.3. In contrast to *Matilda*, events preserved in *Rama* are generally characterised by lower amounts of net accumulation enabling a longer time frame preserved in the pit. Sampling of *Rama* occurred at the end of February 2000, and the 2 m record extends back to winter 1998.

Table 5.3: Accumulation events preserved in *Rama*

Event Number	Date Start	Date Finish	Date(s) with most Net Accumulation	Net Accumulation (cm)
25	27 Feb 2000	27 Feb 2000	27 Feb 2000	6
26	24 Feb 2000	24 Feb 2000	24 Feb 2000	14
27	3 Feb 2000	4 Feb 2000	4 Feb 2000	10
28	24 Jan 2000	25 Jan 2000	25 Jan 2000	9
29	27 Dec 1999	31 Dec 1999	28 Dec 1999	11
30	18 Dec 1999	23 Dec 1999	23 Dec 1999	7
31	10 Nov 1999	16 Nov 1999	11, 12 Nov 1999	6
32	22 Oct 1999	27 Oct 1999	22 Oct 1999	14
33	21 Oct 1999	21 Oct 1999	21 Oct 1999	5
34	11 Oct 1999	17 Oct 1999	All days	7
35	2 Sep 1999	10 Sep 1999	All days	3
36	2 Jun 1999	8 Jun 1999	7, 8 Jun 1999	7
37	19 May 1999	22 May 1999	19 May 1999	4
38	13 Mar 1999	13 Mar 1999	13 Mar 1999	7
39	7 Mar 1999	11 Mar 1999	11 Mar 1999	3
40	31 Jan 1999	6 Feb 1999	All days	4
41	27 Dec 1998	29 Dec 1998	All days	4
42	7 Dec 1998	8 Dec 1998	All days	3
43	23 Nov 1998	29 Nov 1998	23 Nov 1998	14
44	16 Nov 1998	22 Nov 1998	All days	8
45	16 Oct 1998	19 Oct 1998	19 Oct 1998	8
46	20 Aug 1998	20 Aug 1998	20 Aug 1998	11
47	23 Jul 1998	23 Jul 1998	23 Jul 1998	9
48	19 Jul 1998	20 Jul 1998	All days	11
49	29 Jun 1998	5 Jul 1998	4 Jul 1998	7

The trace chemical and $\delta^{18}\text{O}$ signals associated with the 25 events preserved in *Rama* are illustrated in Figure 5.6. Each species exhibits clear seasonal cycles with high concentrations of MSA, $\delta^{18}\text{O}$, nitrate and non sea-salt sulphate during summer, late

spring and early autumn, and high concentrations of sea salt during winter and spring. Interesting features preserved in *Rama* include extremely high marine biogenic compounds preserved during summer 99/00 (event 29), late summer and late spring deposition of MSA, $\delta^{18}\text{O}$, non sea-salt sulphate, nitrate and sodium (events 25, 32), and high $\delta^{18}\text{O}$ and nitrate signals preserved during early spring 1998 (events 44, 45).

Extending Rama – S0k Events

The high quality firn core (*S0k*) drilled within 0.5 m of the *Rama* pit wall allows the investigation of events preserved at depths greater than the *Rama* record. Table 5.4 details 2 events that are preserved in *S0k* that extend the record back through autumn 1998. These 2 events are interesting as they preserve a warm $\delta^{18}\text{O}$ signal during autumn snowfalls (events 50, 51; Fig. 5.7). Although most of the accumulation occurs between just two days (12 and 14 May 1998), the sodium record shows high concentrations during 14 May, and low concentrations during 12 May, indicating the snowfalls are derived from different events.

Table 5.4: Accumulation events preserved in *S0k*

Event Number	Date Start	Date Finish	Date(s) with most Net Accumulation	Net Accumulation (cm)
50	14 May 1998	18 May 1998	14 May 1998	20
51	11 May 1998	13 May 1998	12 May 1998	8

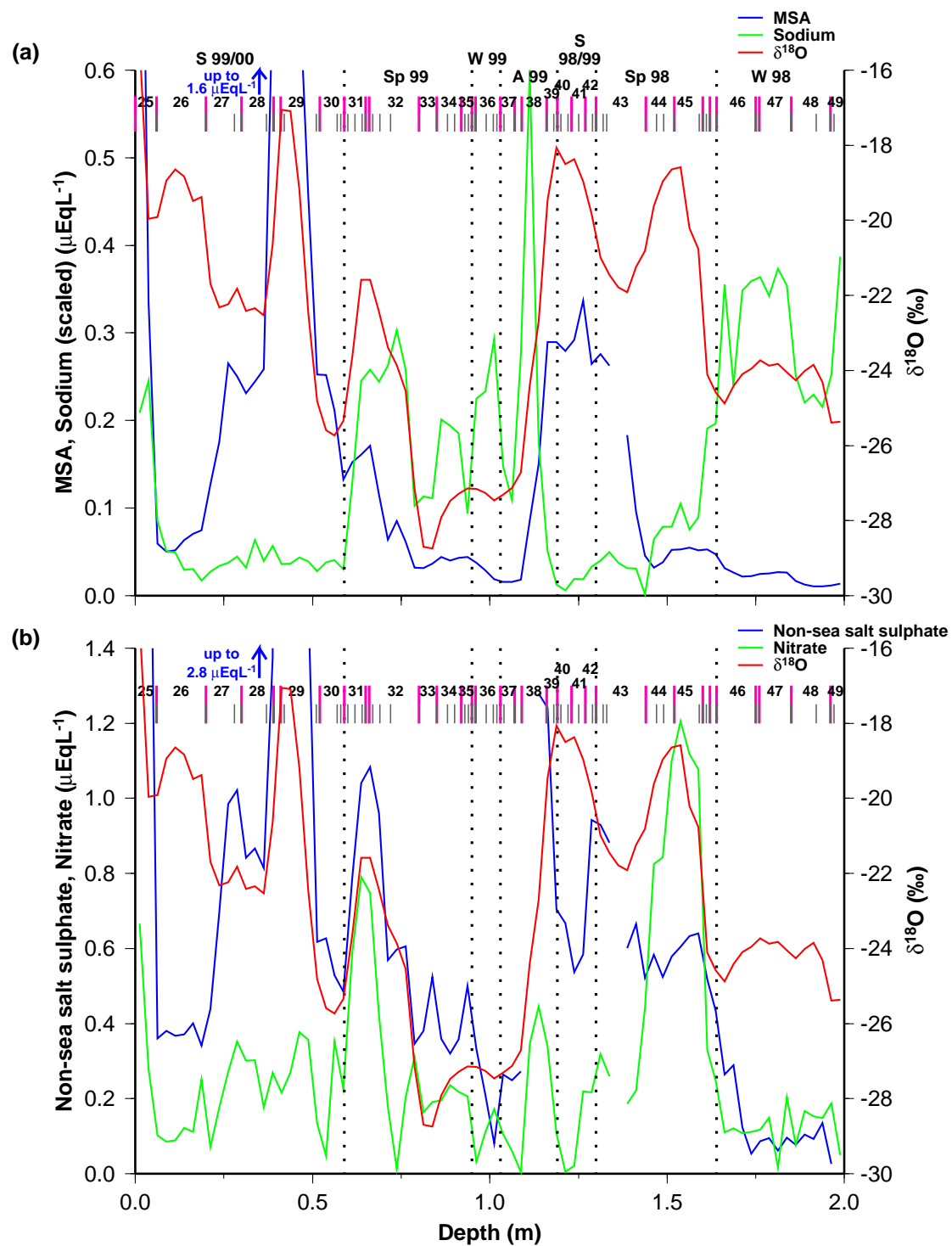


Figure 5.6: Trace chemical and $\delta^{18}\text{O}$ signals associated with the 24 accumulation events preserved in Rama: (a) MSA, Sodium (scaled by a factor of 0.025) and $\delta^{18}\text{O}$; (b) Non-sea salt sulphate, Nitrate and $\delta^{18}\text{O}$. Seasonal (dotted), event (pink) and event day (grey) boundaries are also shown.

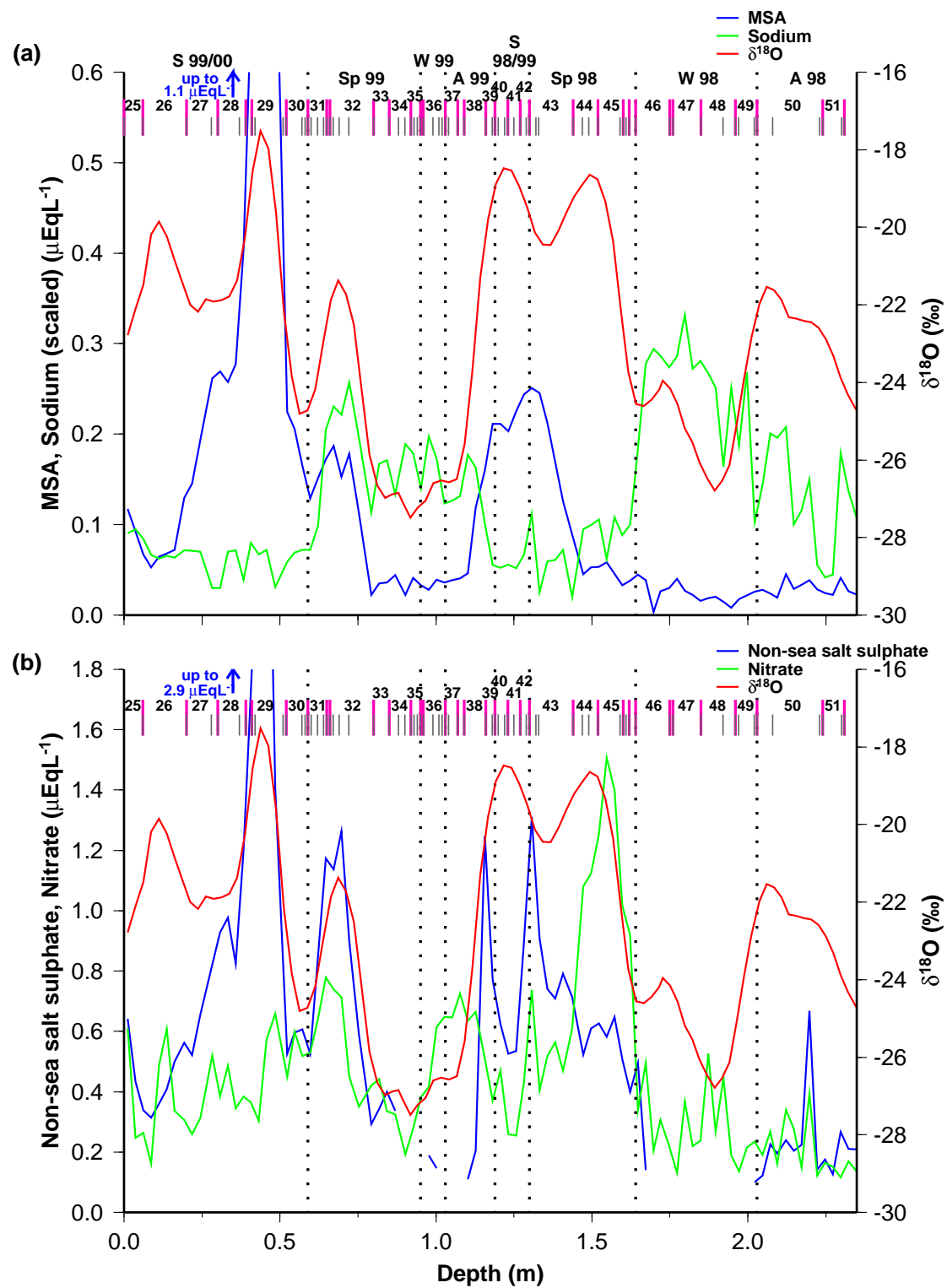


Figure 5.7: Trace chemical and $\delta^{18}\text{O}$ signals associated with the 24 accumulation events preserved in *S0k*: (a) MSA, Sodium (scaled by a factor of 0.025) and $\delta^{18}\text{O}$; (b) Non-sea salt sulphate, Nitrate and $\delta^{18}\text{O}$. Seasonal (dotted), event (pink) and event day (grey) boundaries are also shown.

Summary

The identification of accumulation events preserved in each snow pit and co-located firn cores allows the analysis of meteorological conditions associated with specific chemical and isotopic signatures. The following chapters present a detailed investigation of the local and synoptic meteorology associated with a selection of the 51 events identified in this section. Uncertainties in the dating technique are minimised wherever possible through grouping daily snowfalls into events that cover a period of time and the exclusion of very low net accumulation events (less than 3 cm).

5.3 Densification of the Snowpack

The deposition of snow on the ice sheet is an episodic process, and over time the snow accumulation compresses the snow beneath it. Densification involves the process of transformation from snow to firn, and then to ice. This has the potential to introduce large uncertainties in dating high resolution snow pit and firn core records. Densification results in a perceived loss of snow from the snow accumulation sensor mounted on the AWS, yet the compacted snow is retained in the snow pit and firn core records. The following discussion investigates the effects of densification on the records analysed in this research.

5.3.1 Density Profiles

Density profiles were generated for the top 0 – 5 m of the snowpack using two techniques. Density samples were collected *in situ* from snow pits sampled during both field seasons using a 3 x 3 cm stainless steel square probe. Three lines of density samples were collected from *Rama* and two lines from *Matilda* between 0 and 1.3 m with a sample resolution of 3 cm. An additional line of density was collected from the *Karioke* snow pit, sampled during the first field season and located approximately 50 m from *Rama*. Density profiles were also extracted from firn cores up to 5 m depth collected during both field seasons. Core density samples were prepared from inner core sections and shaped into cylinders using a lathe. Cylinder dimensions and weights were noted and the corresponding densities calculated. Sample resolution averaged 3 cm although the shaping technique resulted in discontinuous profiles with

approximately 2 cm breaks every three samples. Detailed information on the sampling techniques of the density records are outlined in chapter 2 of this thesis.

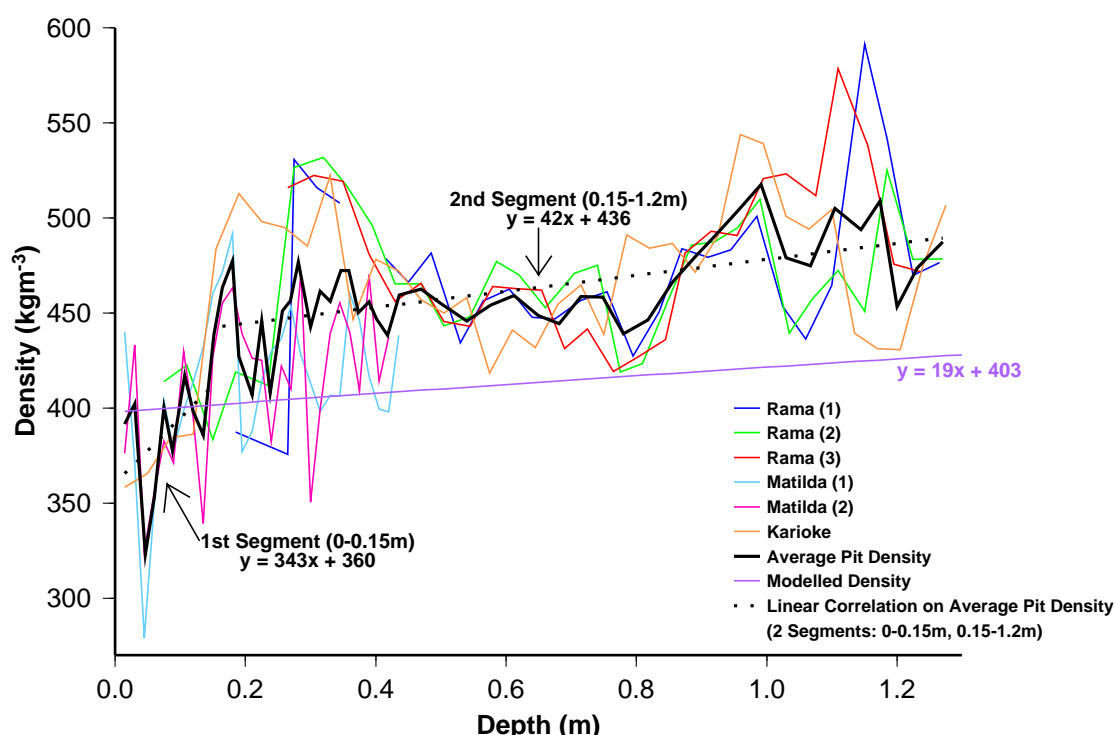


Figure 5.8: Snow pit density profiles from samples collected over two field seasons. Samples from *Rama* and *Karioke* were collected during the 99/00 austral summer, while samples from *Matilda* were collected during the 01/02 austral summer. Linear correlations from two depth segments (0-0.15m, 0.15-1.2m) are compared with a modelled density profile calculated from an empirical fit of density measurements from the deep DSS ice core.

Figure 5.8 illustrates the snow pit density profiles collected over the two field seasons. The figure shows a dual segmented linear relationship between density and depth for the top 1.2 m of the snowpack. For the surface layers of snow (0 – 0.15 m), density increases with depth with a mean slope of 343 kg m^{-4} . However, for depths between 0.15 and 1.2 m, the mean slope for the linear relationship between density and depth declines to 42 kg m^{-4} . The slope of the second segment compares well with a firm density model calculated from an empirical fit of density measurements from the deep DSS ice core (van Ommen and others, 1999). The firn core density measurements analysed in this research compare well with modelled densities from the deep DSS ice core (Fig. 5.9). The slope of the linear relationship between firn density and depth from the core samples averages 18 kg m^{-4} , compared to the modelled slope of 19 kg m^{-4} . The excellent agreement between the pit and core densities analysed in this

research and the empirical modelled densities generated from the deep ice core indicate consistent densification at the sampling site. Even with different sampling techniques, the high resolution pit and core density records from separate seasons show comparable profiles. Moreover, the sampled profiles compare well with the modelled density profile and confirm the accuracy of the model in representing the density characteristics of the top section of the snowpack.

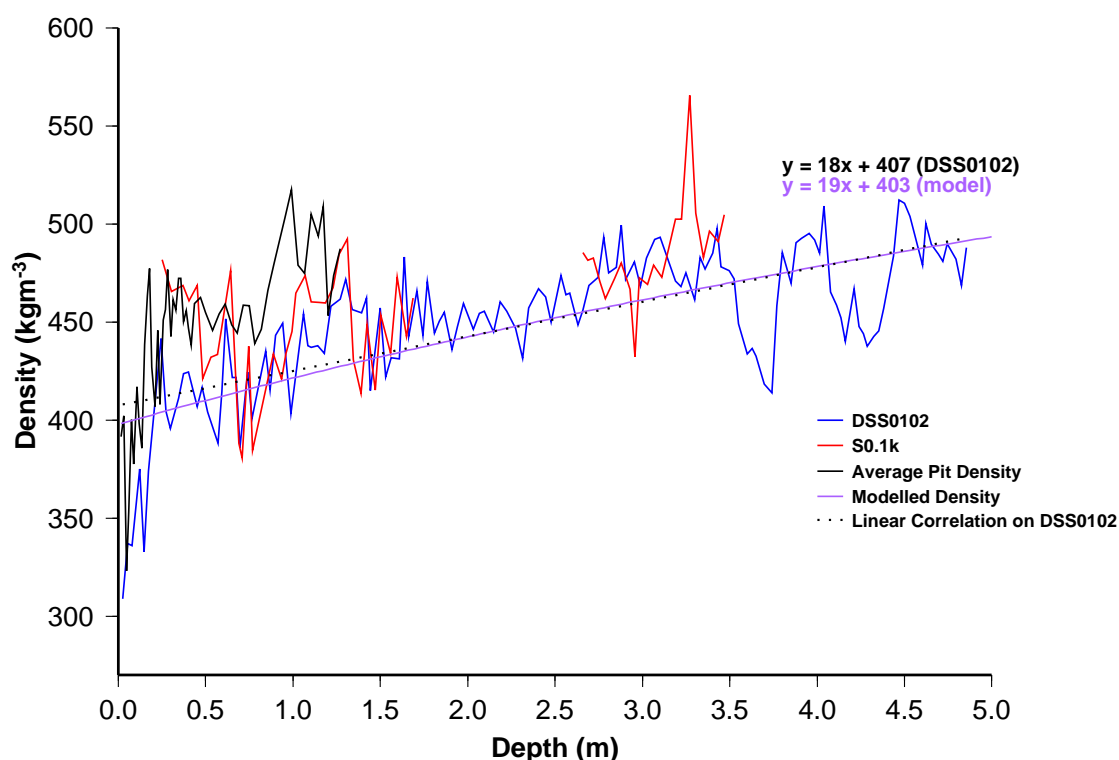


Figure 5.9: Firn core density profiles from samples collected over two field seasons. Samples from *S0.1k* were collected during the 99/00 austral summer, while samples from *DSS0102* were collected during the 01/02 austral summer. The linear correlation from *DSS0102* samples are compared with a modelled density profile calculated from an empirical fit of density measurements from the deep DSS ice core.

5.3.2 Density Effects on the Extended Firn Core Records

Extending the snow pit records using co-located firn cores enables the identification of accumulation events deeper than the 2 – 2.25 m pit profiles. However, identification of events at depth needs to be interpreted with caution due to the potential impact of densification. The collection of firn cores from two distinct seasons that cover the same time period allows the investigation of potential density effects on the dated records.

Season 1 – S0k

The top 3 m of the *S0k* firn core, collected during the first season and the sampling of *Rama*, preserves material from summer 99/00 back to the installation of the AWS during summer 97/98 (Fig. 5.10). This core section preserves chemical and isotopic signals consistent with two seasonal cycles identified from the AWS dating scale. Traditional summer species ($\delta^{18}\text{O}$, MSA, nitrate (not shown) and non-sea salt sulphate (not shown)) are in phase with the summer periods of the AWS dating scale, while sea salt concentrations (sodium, chloride (not shown) and magnesium (not shown)) are preserved during winter deposition layers (Fig. 5.10). This is consistent with previous high resolution studies that resolve the seasonal cycle of ice core signals both at the Law Dome site (Curran and others, 1998) and other Antarctic sites (Legrand and Delmas, 1984; Minikin and others, 1994; Kreutz and others, 1999). The results suggest that densification over the top 3 m of the snowpack does not significantly affect the dating of events at the seasonal scale.

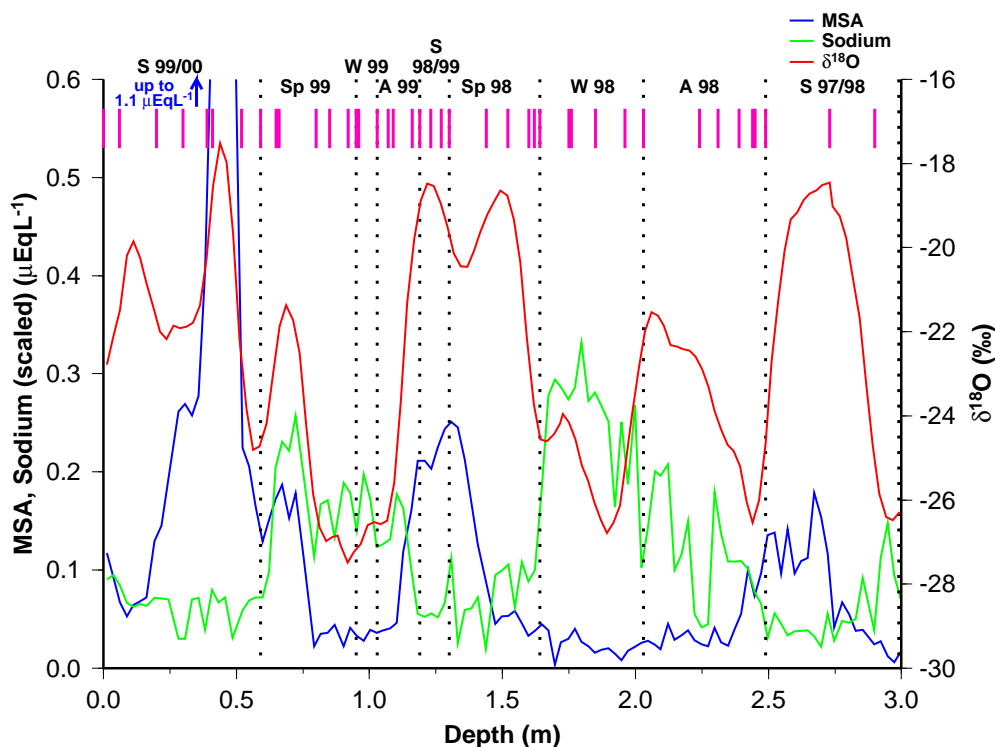


Fig. 5.10: MSA, sodium and $\delta^{18}\text{O}$ records preserved in *S0k* for the 0-3 m depth range. Seasonal (dotted) and event (pink) boundaries determined from the AWS are also shown.

Season 2 – DSS0102

The *DSS0102* firn core was collected two years later than *S0k* and the top 6 m of *DSS0102* covers the time period from summer 01/02 back to the installation of the AWS during summer 97/98 (Fig. 5.11). The core section 3 – 6 m in *DSS0102* overlaps with the time period preserved in the core section 0 – 3 m in *S0k*. This allows an investigation of the effects of densification on specific events after a two year period.

Figure 5.11 illustrates that for the top 3 m of the snowpack, the seasonal cycles of the chemical and isotopic signals are in phase with the AWS dating scale. For example, the summer species of $\delta^{18}\text{O}$ and MSA are peaking in the summer periods as determined from the AWS dating scale. This is consistent with the results presented in figure 5.10 and confirms that the top 3 m of the snowpack is not significantly affected by densification at the seasonal time scale. However, for depths greater than 3 m the impact of densification becomes increasingly more pronounced and the firn core record compacts significantly compared to the AWS dating scale (Fig. 5.11). This is indicated by the seasonal signals in the firn core becoming out of phase with the seasonal boundaries identified in the AWS dating scale. For example, at a depth of 5.3 m $\delta^{18}\text{O}$ and MSA show a pronounced peak, indicating summer deposition. However, at this depth the AWS dating scale identifies these peaks as occurring during autumn 1998.

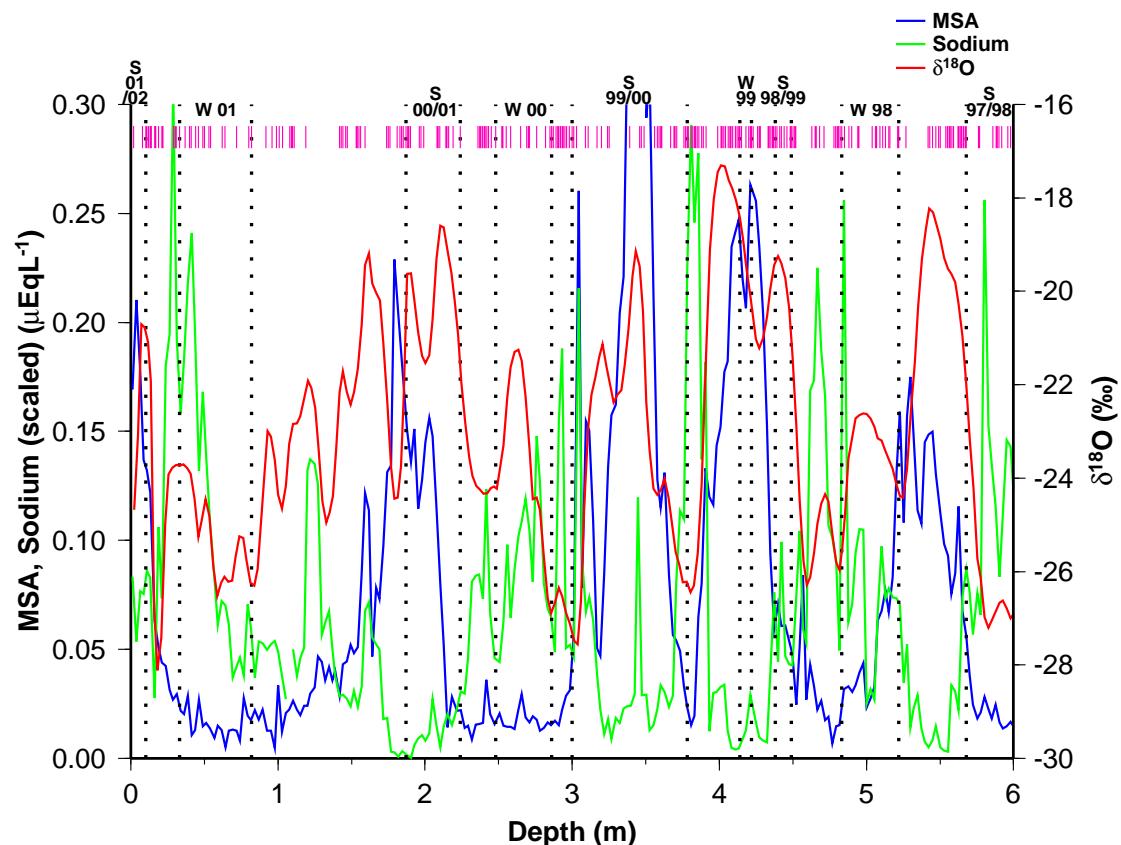


Fig. 5.11: MSA, sodium and $\delta^{18}\text{O}$ records preserved in *DSS0102* for the 0-6 m depth range. Seasonal (dotted) and event (pink) boundaries determined from the AWS are also shown.

Correcting for Densification – DSS0102

The AWS dating scale may be “corrected” for depths greater than 3 m by considering the amount of densification for events preserved in both the *S0k* and the *DSS0102* firn cores. Figure 5.12 illustrates the effect of compacting the AWS dating scale for *DSS0102* to bring the seasonal signals in the firn core in phase with seasons identified from the AWS net accumulation record. For example, the summer signals preserved in *DSS0102* at around 5.3 m depth, indicated by elevated levels of $\delta^{18}\text{O}$ and MSA, are now dated by the AWS as occurring during summer 1997/1998 (Fig. 5.12) rather than autumn 1998 before correcting for densification (Fig. 5.11).

The AWS dating scale “correction” was calculated using interpolation between nineteen significant chemical and $\delta^{18}\text{O}$ events preserved in both firn cores (Table 5.5). The technique involved a simple linear interpolation of the AWS dating scale using the depths of each significant event in *S0k* and *DSS0102* as the known input ranges.

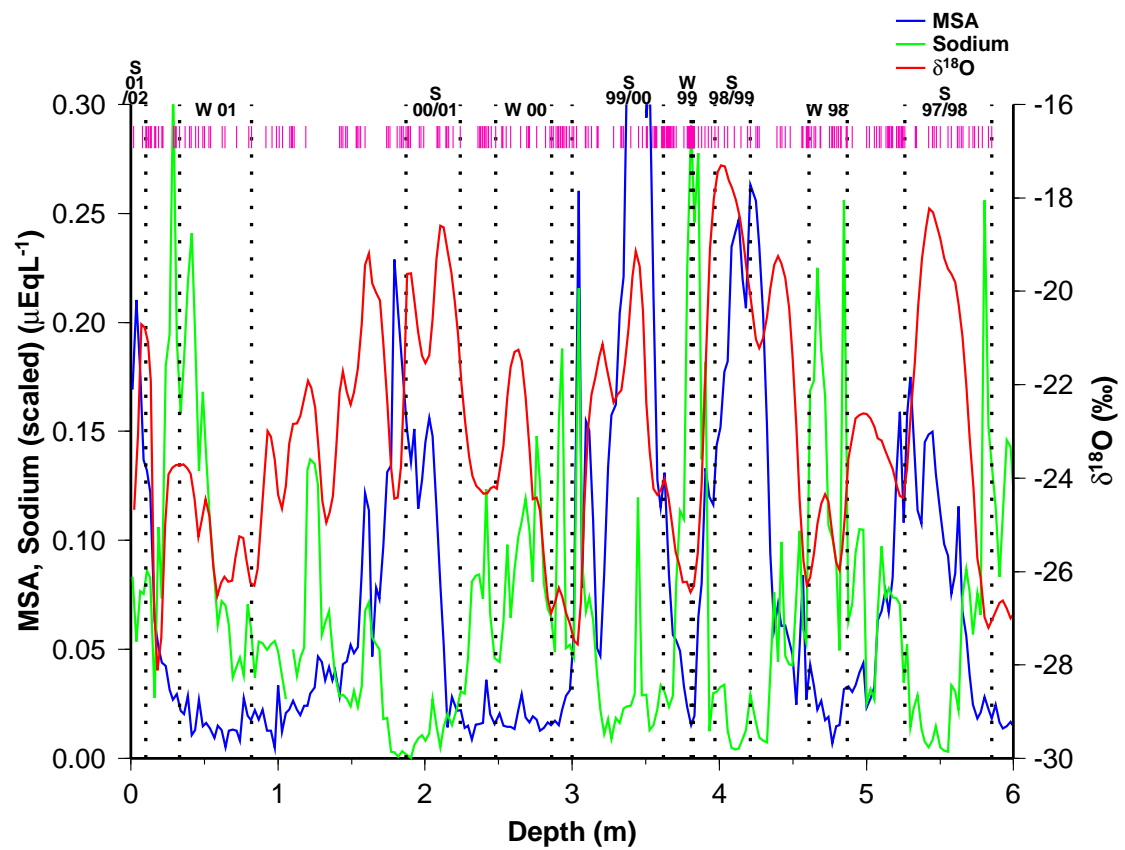


Fig. 5.12: MSA, sodium and $\delta^{18}\text{O}$ records preserved in *DSS0102* for the 0-6 m depth range. Seasonal (dotted) and event (pink) boundaries determined from the AWS but corrected for densification are also shown.

Table 5.5: Significant events preserved in *S0k* and *DSS0102* used as event ties

Event Number	Species	Event Description	Depth in <i>S0k</i> (m)	Depth in <i>DSS0102</i> (m)
1	MSA	increase	0.01	3.18
2	$\delta^{18}\text{O}$	peak start	0.06	3.13
3	$\delta^{18}\text{O}$	peak end	0.21	3.28
4	MSA	peak start	0.37	3.40
5	MSA	peak end	0.52	3.50
6	MSA	decrease start	0.80	3.76
7	MSA	decrease end	0.82	3.78
8	MSA	increase start	1.09	3.83
9	MSA	increase end	1.14	3.86
10	MSA	peak start	1.30	4.21
11	MSA	peak end	1.31	4.25
12	sodium	increase start	1.60	4.57
13	sodium	increase end	1.61	4.59
14	sodium	trough start	2.23	5.01
15	sodium	trough end	2.28	5.05
16	MSA	peak start	2.67	5.42
17	MSA	peak end	2.69	5.43
18	$\delta^{18}\text{O}$	trough start	2.98	5.83
19	$\delta^{18}\text{O}$	trough end	2.99	5.85

5.4 Concluding Remarks

This chapter aimed to develop a reliable technique for dating high resolution snow pit records at the event scale. Accurate and independent dating is essential for studies that intend to compare snow pit and firn core records with contemporaneous meteorological observations.

The dating technique uses high resolution snow accumulation data from an AWS co-located with the snow pit records. Net accumulation steps are identified using the net snow accumulation record, defined as the difference between snow accumulation and snow removal as perceived by the AWS. These net accumulation steps are then grouped into events that cover a number of days close together in time and from a particular synoptic situation. In addition, events characterised by a sharp change in chemical or isotopic signals are separated into distinct events. Grouping the

accumulation events using these methods reduces possible uncertainties associated with surface redistribution of snow and densification of the snowpack. This technique provides, for the first time, accurate event scale dating of snow pit records that is independent of the ice core signals under investigation.

The dating technique identifies 25 events preserved in the *Rama* snow pit and 21 events preserved in the *Matilda* snowpit. These events are used in the comparative studies presented in Chapters 6 and 7 of this thesis. In addition, a further 5 events are confidently dated from the firn cores co-located with the snow pits, resulting in a total of 51 events identified in this research. The identification and dating of the 51 events preserved in the snow pit and firn core records enables confident comparisons between the chemical and $\delta^{18}\text{O}$ signals, and contemporaneous meteorological conditions.

The high resolution snow pit and snow accumulation records also allowed an examination of the impact of densification on the top 6 m of the snowpack at Law Dome. Densification of the snowpack has the potential to introduce uncertainties in high resolution snow pit and firn core dating. The results presented in this chapter show that densification does not significantly affect dating of events over the top 3 m of the snowpack. Comparisons between chemical and isotopic signals over the 3-6 m section of the *DSS0102* firn core with the same events preserved two years earlier in the 0-3 m section of *S0k* firn core show that densification does effect the dating of events preserved at depths below 3 m. The effects of densification may be “corrected” for depths below 3 m using a technique of identifying significant event ties that are preserved in a firn core record that was drilled two years earlier, and applying a linear interpolation to compact the deeper (3-6 m) section of the record. The ability to accurately date a 0-6 m firn core at Law Dome provides an important tool for conducting further analysis on the high resolution record. The technique for dating *DSS0102* is unique compared to previous high resolution studies in that it was develop using net accumulation measurements independent of the seasonal cycle of the chemical and $\delta^{18}\text{O}$ signals. This allows, for the first time, the examination of exact timings in the seasonality of the chemical and isotopic signals.

Chapter 6

Seasonal Characteristics of High Resolution Firn Core Signals

6.1 Overview

The use of the AWS accumulation record to accurately date high resolution snow pit and firn core records provides a unique opportunity to examine the seasonality of chemical and isotopic signals preserved in the ice core. Previous studies aimed at interpreting the seasonality of species in the ice core have determined chronologies using the annual cycle of well understood species such as $\delta^{18}\text{O}$ (Whitlow and others, 1992), or by calculating composite seasonal signals by stacking data from cores covering a number of years (Palmer, 2002; Curran and others 1998; Morgan and van Ommen). In contrast, the chronology of *DSS0102* presented here is unique in that it was developed using net accumulation measurements independent of the seasonal cycle of the chemical or isotopic signals under investigation. This allows, for the first time, the examination of exact timings in the seasonality of each species.

The following chapter aims to enhance our understanding of the seasonality of chemical and isotopic signals preserved in Law Dome ice cores. The research explores the seasonal characteristics of chemical and isotopic species preserved in Law Dome ice cores using a combination of techniques and datasets. First, a brief discussion of the literature on seasonality in ice cores is presented to review the current status on seasonality research. Second, seasonal signals are examined over a 4 year period using the well dated high resolution firn core *DSS0102*. Third, local meteorological conditions recorded during net accumulation events are compared with the chemical and isotopic signals preserved in the firn core. Finally, potential

source regions and transport paths for the seasonal signals are considered by examining back trajectories associated with net accumulation events during each season.

6.2 Summarised Literature Review for Seasonality Studies of $\delta^{18}\text{O}$ and Trace Chemical Species in Antarctic Ice Cores

6.2.1 $\delta^{18}\text{O}$

High resolution records from Antarctic firn and ice cores reveal a clear seasonal cycle in $\delta^{18}\text{O}$ characterised by a pronounced summer maximum and broad winter minima (eg. Bradley and Jones, 1993; Morgan and van Ommen, 1997). The theoretical processes that describe $\delta^{18}\text{O}$ fractionation define a strong dependence of $\delta^{18}\text{O}$ on air temperatures (Craig, 1961; Dansgaard, 1964; Araguas-Araguas, 2000). This dependence allows $\delta^{18}\text{O}$ records from polar firn and ice cores to be used as a source of proxy temperature data for palaeoclimate reconstruction. The $\delta^{18}\text{O}$ record has been shown to consistently reflect the annual temperature cycle on time periods covering just a few years (McMorrow and others, 2001), to records that extend back through the Holocene (Bradley and Jones, 1993; Morgan and van Ommen, 1997). However, studies have also reported that the $\delta^{18}\text{O}$ signal in ice cores is affected by a number of physical processes in addition to air temperature. For example, distance from the ocean and altitude of the ice core site will also influence the $\delta^{18}\text{O}$ signal preserved in the ice (Kato, 1978; Siegenthaler and Oeschger, 1980; Zwally and others, 1998; Araguas-Araguas, 2000). Moreover, the speed and transport path of the air mass has been shown to impact on the $\delta^{18}\text{O}$ signal preserved in the ice (McMorrow and others, 2001, McMorrow and others, 2003). A comprehensive understanding of the origin and circulation of air masses from which the precipitation is formed will enhance our understanding of when the $\delta^{18}\text{O}$ signal is recording temperature variations, and when the signal is indicating another process.

6.2.2 Marine Biogenic Sulphur Compounds

Antarctic aerosol, firn and ice core studies of the marine biogenic sulphur compounds (methansulphonic acid (MSA), non-sea salt sulphate) generally indicate a seasonal variation with enhanced concentrations during summer months and winter minima

(Legrand, 1997; Curran and others, 1998; Minikin and others, 1998). Firn core records from Law Dome reveal minimum levels of non-sea salt sulphate and MSA in August, which increase to a sharp peak in January (Curran and others, 1998). This is in agreement with studies based on firn and ice cores retrieved from other coastal and inland Antarctic sites (Peel and Mulvaney, 1992; Legrand and others, 1991; Mulvaney and others, 1992). Aerosol samples of non-sea salt sulphate and MSA from three coastal Antarctic sites (Neumayer, Dumont D'Urville, Mawson) also indicate a broad winter trough and sharp summer peak (Minikin and others, 1998).

The seasonal cycles of the sulphur compounds may be explained by phytoplankton blooms during the annual retreat of the winter sea ice. The release of sea ice algae into surface waters from melting ice floes during the austral spring provides an additional source of active phytoplankton growth into the Southern Ocean at this time (Smith and Nelson, 1986; Knox, 1994). The mid summer maxima in MSA and non-sea salt sulphate are likely to be sourced from DMS production during the decomposition of these spring phytoplankton blooms (Legrand and Pasteur, 1998).

6.2.3 Nitrate

There are numerous sources of odd nitrogen (the precursors of nitrate) in the Antarctic atmosphere. The major contributors are thought to be nitrous oxide oxidation in the stratosphere and lightning activity in the tropics (Legrand and Kirchner, 1990; Tie and others, 2001). Other potential contributors include anthropogenic pollution (Levy and others, 1999), dissolved organic nitrogen in the oceans (Hu and Smith, 1998; Skoog and others, 2001) and high energy solar particles (Vitt and Jackman, 1996; Vitt and others, 2000).

Previous high resolution studies of nitrate seasonality generally show similar structure with concentrations peaking in summer, relative maxima during spring and late summer and minimum levels during winter months (Legrand and Delmas, 1984; Savoie and others, 1993; Minikin and others, 1994; Curran and others, 1998; Wagenbach and others, 1998b; Kreutz and others, 1999). Winter nitrate concentrations at three coastal Antarctic sites (Neumayer, Dumont D'Urville, Mawson) were observed to be relatively constant and a common continental source region for this time period was suggested (Wagenbach and others, 1998b). The study

of atmospheric tracers revealed nitrate concentrations were derived from stratospheric origin with various transport mechanisms determining the timing of the nitrate peaks (Wagenbach and others, 1998b). In this study the spring nitrate relative maximum was attributed to the descent of stratospheric air to the troposphere through sedimentation of polar stratospheric clouds made up primarily of nitrate acid and water. The main summer peak was attributed to leakage of odd nitrogen through the tropopause and the late summer maximum was linked to air mass exchange across the tropopause.

The nitrate cycle preserved in Antarctic firn and ice is further complicated by the volatile nature of this species. Many firn and ice core studies have reported post depositional loss of nitrate, particularly in the top 1 m of the core (Mayeweski and Legrand, 1990; Wagon and others, 1999). However, nitrate losses in the surface layer of firn from moderate to high accumulation sites is more difficult to determine. Mulvaney and others (1998) and found no evidence for a consistent loss of nitrate over the timescales of a few days at Halley station, Antarctica. Moreover, Curran and others (1998) report the preservation of clear seasonal cycles in nitrate from the high accumulation Law Dome site. This suggests post depositional loss of nitrate does not significantly affect the ice core record from Law Dome.

6.2.4 Sea Salts

High resolution aerosol, firn and ice core studies from Antarctica of the major sea salt species (chloride, sodium, sulphate, magnesium) indicate a general seasonal cycle dominated by enhanced concentrations during winter and minima during summer (Legrand and Delmas, 1984; Legrand and others, 1998; Minikin and others, 1994; Curran and others, 1998; Wagenbach and others, 1998a). The primary mechanism for sea salt aerosol formation is the bursting of air bubbles by wave action at the ocean surface, and thus the concentration of sea salt aerosols is directly related to the local surface wind speeds over the ocean (O'Dowd and others, 1997; Gong and others, 1997). The winter maximum in sea salt concentrations preserved in ice cores represents a cycle which is out of phase of the open water fraction of the Southern Ocean resulting from seasonal sea ice growth and decay. This suggests that the main source of sea salt particles for Antarctic sites overcompensates the larger sea ice extent during the austral winter. A number of potential local sources for the winter sea salt maxima have been identified in the literature including coastal polynas, increased

production of spume drops from the surf zones prevailing at the rim of leads and ice floes under moderate wind speeds, chemical sea salt fractionation from sulphate depletion during freezing of airborne sea water droplets (Wagenbach and others, 1998a), and the formation of frost flowers on new sea ice when wind speeds are low (Perovich and Richter-Monge, 1994; Ranikin and others, 2000). Alternatively, more distant oceanic sources for high winter sea salt concentrations in Antarctic ice cores have also been considered (Bodhaine, 1996; Curran and others, 1998; McMorrow and others, 2001). The intensification of cyclonic activity in the Southern Ocean during the austral winter provides a mechanism for elevated oceanic winds speeds. This is consistent with enhanced bubble bursting over the ocean and associated increases in sea salt aerosols during these storm events. Meridional transport of the aerosols to the ice core sites is facilitated by the cyclonic circulation associated with the storm events. Further research is required to determine the relative importance of local and distant sources of sea salt for specific ice core sites.

6.3 Seasonality of $\delta^{18}\text{O}$ and Trace Ion Species over 4 Annual Cycles at Law Dome

The top 6 m of the *DSS0102* firn core provides a high resolution record of trace chemical species and $\delta^{18}\text{O}$ over 4 annual cycles at Law Dome (Fig. 6.1). Accurate dating of the record, obtained from the AWS accumulation record and adjusted for densification of the snowpack (see Chapter 5), enables a detailed examination of the seasonal characteristics of the firn core signals. The chronology of *DSS0102* is unique compared to previous seasonality studies in that it was developed using net accumulation measurements independent of the seasonal cycle of the chemical or isotopic signals. This allows, for the first time, the examination of exact timings in the seasonality of each species.

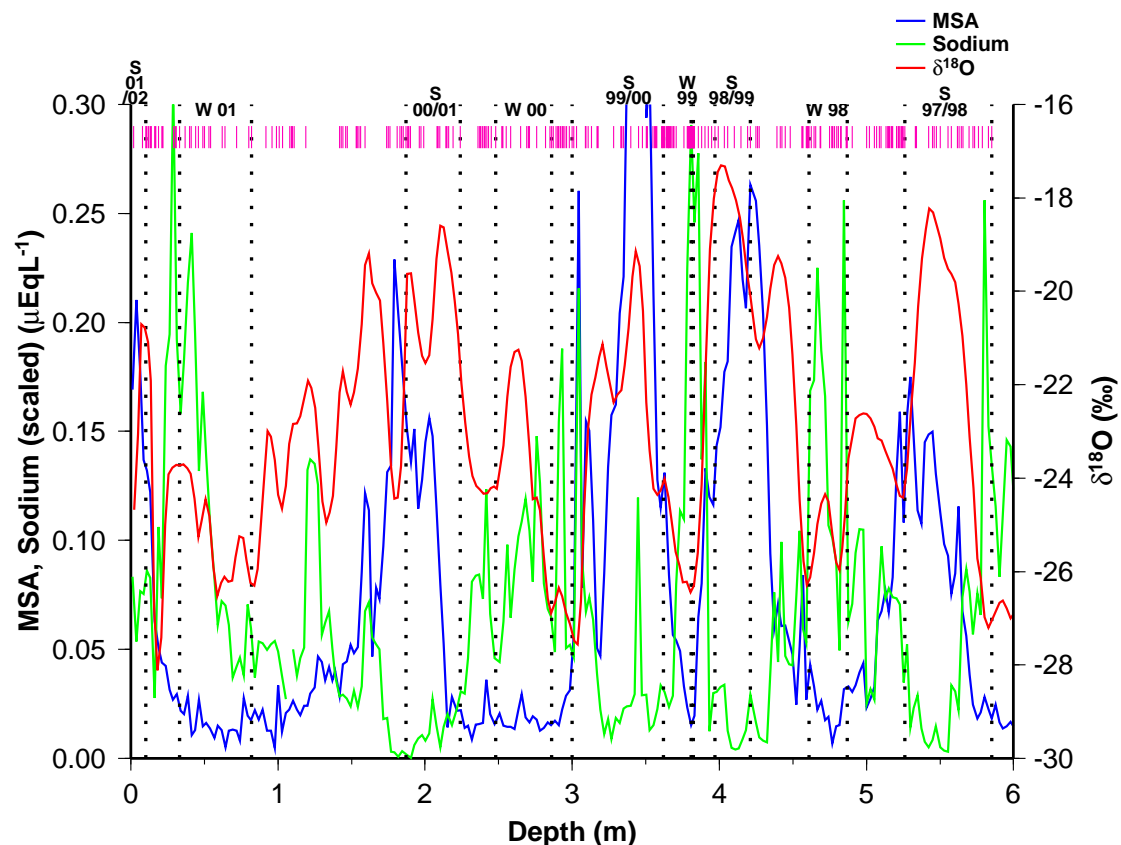


Fig. 6.1: MSA, sodium and $\delta^{18}\text{O}$ records preserved in *DSS0102* for the 0-6 m depth range. Seasonal (dotted) and event (pink) boundaries determined from the AWS but corrected for densification are also shown.

6.3.1 $\delta^{18}\text{O}$

Seasonal Cycle

The seasonal signal in $\delta^{18}\text{O}$ preserved in *DSS0102* is generally characterised by a narrow summer peak and broad winter trough (Fig. 6.1). All 4 years presented in figure 6.1 show a maximum in $\delta^{18}\text{O}$ occurring during mid-summer, with smaller peaks occurring periodically throughout the seasonal cycle. These smaller $\delta^{18}\text{O}$ peaks will diffuse over time and result in a smoothed record characterised by a broad seasonal signal in $\delta^{18}\text{O}$ for deeper ice core records. The seasonal cycle in $\delta^{18}\text{O}$ presented in figure 6.1 is in agreement with longer term ice core studies (Schotterer and others, 1997; van Ommen and Morgan, 1997) and compares well with the annual cycle in temperature for the East Antarctic region (Allison and others, 1993).

Non-summer peaks in $\delta^{18}\text{O}$ (ie. ^{18}O enrichments) often occur during periods of enhanced sea salt concentrations (Fig. 6.1), and indicate a common source of $\delta^{18}\text{O}$ and

sea salt unrelated to the seasonal cycle in temperature. Potential sources for the link between non-summer ^{18}O enrichments and sea salt peaks include the intrusion of strong cyclonic events onto the Antarctic continent (McMorrow and others, 2001). The results presented in McMorrow and others (2001) suggest that cyclonic events facilitate the rapid advection of marine air from lower latitudes onto Law Dome. This rapid advection of low latitude air is consistent with the enhanced non-summer $\delta^{18}\text{O}$ signals, while strong winds associated with the cyclone direct sea salt aerosols over the sampling site.

Temperature and $\delta^{18}\text{O}$

Figure 6.2 compares the $\delta^{18}\text{O}$ record from *DSS0102* with associated air temperatures recorded by the co-located AWS. The temperature records correspond to daily averages for net accumulation days determined from the AWS accumulation record and thus represent a discontinuous record in time. More information on techniques for identifying the net accumulation days and applying the dating scale to the *DSS0102* firn core can be found in Chapter 5 of this thesis.

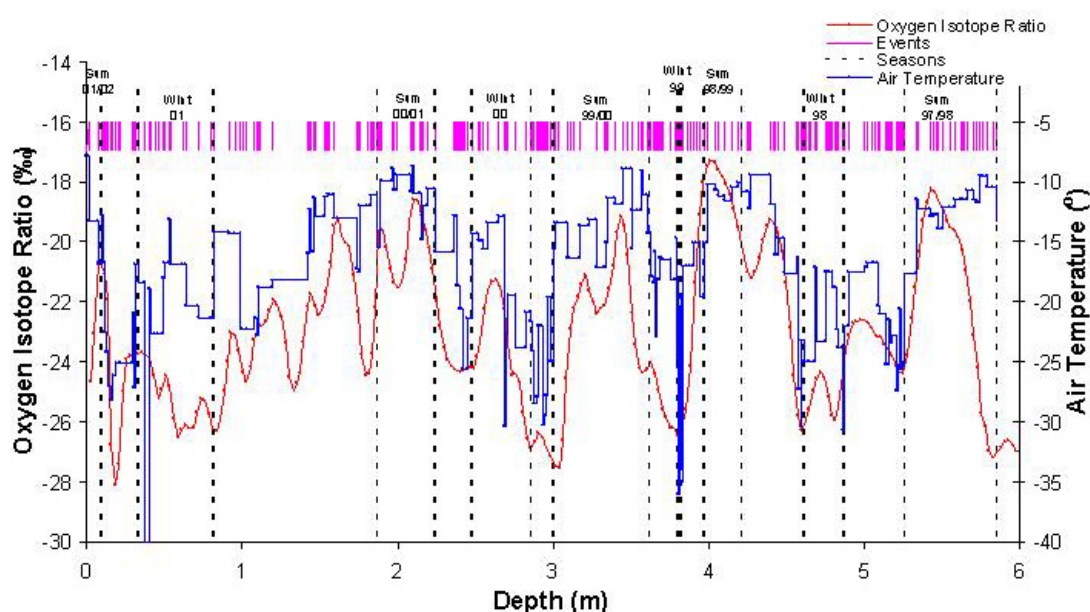


Fig. 6.2: Comparison between $\delta^{18}\text{O}$ and associated air temperatures for *DSS0102*. The temperature record is drawn from the 4 m air temperatures recorded by the co-located AWS. The temperatures represent daily averages for net accumulation days determined from the AWS net accumulation record.

Variations in $\delta^{18}\text{O}$ preserved over the 4 annual cycles show a reasonable agreement ($R^2=0.33$) with observed variations in temperature at the coring site (Fig. 6.2). The narrow summer peak and broad winter trough in $\delta^{18}\text{O}$ for all 4 years is reflected in the AWS air temperature observations. In addition, many non-summer peaks in $\delta^{18}\text{O}$ are also accompanied by peaks in air temperatures. This suggests a strong relationship between $\delta^{18}\text{O}$ and air temperatures at Law Dome. The results are in agreement with Morgan and van Ommen (1997), who compare $\delta^{18}\text{O}$ values from a composite seasonal signal calculated from 700 years of Law Dome data with a modern 5 year composite in air temperatures from an AWS 5 km north of the drilling site. However, this longer term study only considers the broad seasonal cycle in $\delta^{18}\text{O}$ as fine resolution features such as non-summer peaks are smoothed by $\delta^{18}\text{O}$ diffusion in the deep ice record. Figure 6.2 indicates a strong relationship between $\delta^{18}\text{O}$ and air temperatures at Law Dome at a resolution finer than the annual cycle. In addition, figure 6.2 provides a direct comparison between contemporaneous $\delta^{18}\text{O}$ and site temperature observations on an event-by-event basis. This is in contrast to the comparison between composite $\delta^{18}\text{O}$ cycles from a 700 year ice core record and modern 5 year temperature records considered in Morgan and van Ommen (1997). Thus, the results presented here provide further evidence for the use of $\delta^{18}\text{O}$ from deep ice cores as a proxy for palaeotemperatures. Deviations between $\delta^{18}\text{O}$ and temperature occur infrequently in the 4 year record. Specific events are characterised by $\delta^{18}\text{O}$ signatures that appear to be anti-correlated with air temperatures. These events are examined in more detail in chapter 7 of this thesis.

The relationship between $\delta^{18}\text{O}$ measurements and observed site temperatures can be used to calibrate the ice core palaeothermometer. The dependence of observed $\delta^{18}\text{O}$ measurements on temperature is generally well approximated by a linear relationship:

$$\delta^{18}\text{O} = \alpha T + \beta$$

The calibration slope (α) is derived from either spatial variability over a region, or from temporal variations at a site. A spatially derived slope of 0.6-0.7‰/°C has been determined for the Law Dome region (Morgan, 1979), and a temporally derived slope of 0.44‰/°C has been calculated from 700 years of annual cycles in $\delta^{18}\text{O}$ at Law

Dome (van Ommen and Morgan, 1997). More recent studies from a short length of Law Dome firn core examined the correlation between $\delta^{18}\text{O}$ and temperature values on an event-by-event basis (McMorrow and others, 2001). In this study, a first attempt was made to account for the episodic nature of net accumulation and potential temperature biases preserved in the ice core. The temporal calibration determined from McMorrow and others (2001) yields a $\delta^{18}\text{O}$ temperature slope of $0.21\text{‰}/^{\circ}\text{C}$, and agrees with the finding from van Ommen and Morgan (1997) that temporally derived calibrations give lower slopes than spatially derived calibrations. This lower slope could be ascribed to the fact that the seasonal temperature cycle during accumulation events is much smaller than for non-accumulation events.

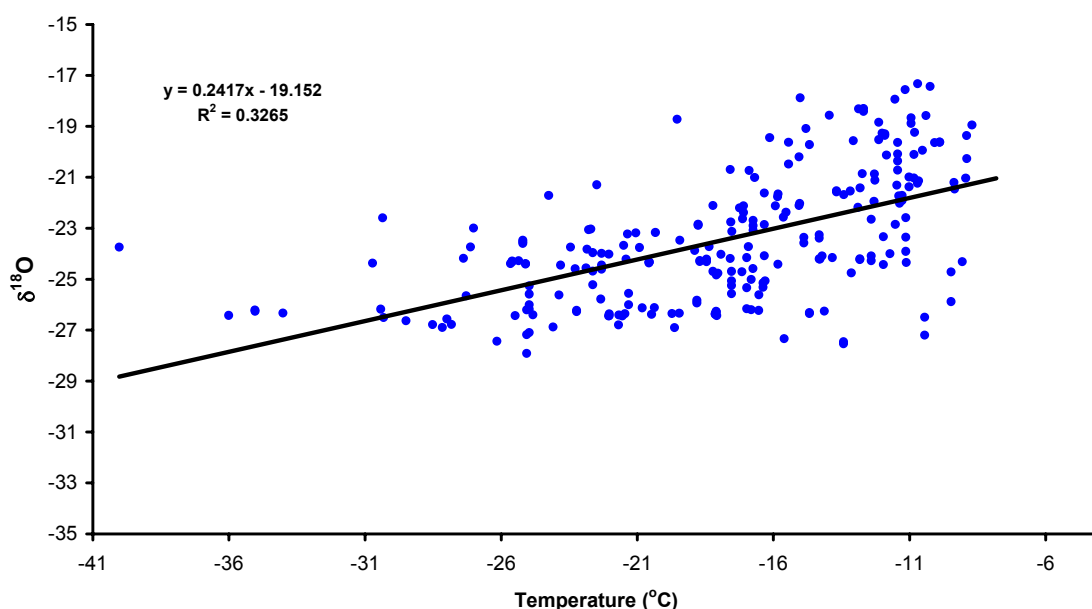


Fig. 6.3: Linear correlation of $\delta^{18}\text{O}$ values from the *DSS0102* firn core over 4 annual cycles and associated air temperatures recorded from the co-located AWS (4 m temperature record).

Figure 6.3 illustrates the linear correlation of $\delta^{18}\text{O}$ values from the *DSS0102* firn core over 4 annual cycles and site temperatures recorded from the co-located AWS. The results show a strong positive correlation between $\delta^{18}\text{O}$ and temperature (Student's t , 10.79; probability of no correlation for 1 tailed Student's t test, 1.12×10^{-22}). The slope of the temporal calibration ($0.24\text{‰}/^{\circ}\text{C}$) is significantly smaller than the temporal slope derived by van Ommen and Morgan (1997), yet remarkably similar to the value calculated using a very shallow firn core at the event scale (McMorrow and others, 2001). The similarity between the values calculated in this work and

McMorrow and others (2001) indicate consistency in event scale calibration between $\delta^{18}\text{O}$ and temperature. The short length of firn core considered in McMorrow and others (2001) covers just 0.3 m of core, corresponding to 8 months of accumulation, while the material analysed in this research covers 6 m of core and 4 annual cycles. The similar calibration coefficients calculated in each study provides evidence for the accuracy in determining temporal $\delta^{18}\text{O}$ temperature calibrations using this event-by-event technique.

The observed slope of temporal calibrations will be influenced by isotopic diffusion in the firn column, which reduces the amplitude of the annual cycle in $\delta^{18}\text{O}$. The calibration coefficients developed in McMorrow and others (2001) and this work are not corrected for isotopic diffusion in the firn. The degree to which diffusion affects $\delta^{18}\text{O}$ values at shallow depths is not well understood, but may have decreased the amplitude of the $\delta^{18}\text{O}$ annual cycle by up to 30%, which is the integrated effect over the full firn column at DSS (van Ommen and Morgan, 1997). Therefore, the 0.24‰/°C calibration determined here may be corrected upwards by a corresponding factor. Correcting the 0.24‰/°C calibration upwards by 30% yields a maximum corrected coefficient of 0.31‰/°C. This value is still considerably lower than the temporally derived value of 0.44‰/°C (corrected for diffusion) determined by van Ommen and Morgan (1997). Thus, correlating $\delta^{18}\text{O}$ and temperature at the event level appears to reflect a genuine difference in the $\delta^{18}\text{O}$ temperature calibration compared to longer term, lower resolution studies.

The difference between the two temporal calibration techniques invites speculation as to the appropriate coefficient to use for interpretation of the longer term $\delta^{18}\text{O}$ record. Assuming that diffusion effects in the shallow firn core material used in this work can correct the event scale coefficient of 0.24‰/°C upwards by a maximum of 30%, then another explanation for the difference between this coefficient and the longer term temporal calibration calculated by van Ommen and Morgan (1997) is required. A number of factors have been identified as likely contributors to lower temporal than spatial values for the $\delta^{18}\text{O}$ temperature calibration, and these factors may also explain differences in temporal values. First, snowfall typically occurs when the temperature is warmer than average and this has been shown to affect the temporal calibration

(Peel, 1992). Perhaps the event scale temporal calibration determined in this work accentuates the effects of such a temperature bias in the firn core. Chapter 4 of this thesis investigates the temperature bias observed over 4 annual cycles. The results show that temperatures are generally higher during snowfall events, and this warm bias is more pronounced during events which produce larger accumulation events. Events which recorded more than 10 cm of accumulation in a single day averaged -16.73°C , 4.15°C warmer than the mean for the 4 annual cycles, and 4.68°C warmer than the mean for days without accumulation. The temporal calibration of $0.44\text{‰}/^{\circ}\text{C}$ determined by van Ommen and Morgan (1997) uses 700 years of annual cycles in $\delta^{18}\text{O}$ at Law Dome and 5 years of modern AWS temperature data. No attempt was made to distinguish the temperatures associated with snowfall events and the potential warm bias preserved in the $\delta^{18}\text{O}$ record. In contrast, the event-by-event calibration of $0.24\text{‰}/^{\circ}\text{C}$ does consider the potential warm bias in temperatures as only temperatures associated with net accumulation events preserved in the firn core are used in the calculation. This will have the effect of increasing temperatures compared to $\delta^{18}\text{O}$ values in the calibration, thus reducing the overall calibration coefficient.

Another important factor that will influence temporal $\delta^{18}\text{O}$ temperature calibrations involves temperature variations at the moisture source. A reduction in temperature at the source will reduce the relative temperature variation and lead to reduced fractionation and smaller fluctuations in the $\delta^{18}\text{O}$ signal. The short term study conducted here (4 annual cycles) samples the modern climate regime for the Law Dome region. Temporal calibrations from long term ice core records sample a wide range of different climate regimes with greater variations in moisture source and deposition temperatures. Thus, these longer term coefficients will include more fluctuations in climate cycles and may be more appropriate for calibrating the long term isotope palaeothermometer. The short term calibration provides greater insight into the relationship between modern $\delta^{18}\text{O}$ and temperature signals on an event-by-event basis, which in turn will enhance our understanding of the palaeotemperature signal.

Cyclonic Precipitation and $\delta^{18}\text{O}$

Studies by Kato (1978) have shown high $\delta^{18}\text{O}$ values associated with falling atmospheric pressure resulting from the approach of a cyclone. However, this relationship is not generally observed in the 4 year *DSS0102* record (Fig. 6.4). In contrast, falling atmospheric pressure at the coring site appears to be associated with lower $\delta^{18}\text{O}$ values, although the general trend is reasonably erratic. There are more deviations between $\delta^{18}\text{O}$ and pressure compared to the temperature comparison, suggesting only a weak link exists between $\delta^{18}\text{O}$ and site pressure at Law Dome. This result is further indicated by the high scatter associated with the linear correlation between $\delta^{18}\text{O}$ and pressure (Fig. 6.5). Although a positive correlation is identified from the dataset, the low significance (Student's *t*, 4.92; probability of no correlation for 1 tailed Student's *t* test, 8.08×10^{-7}) indicates only a weak correlation between $\delta^{18}\text{O}$ and atmospheric pressure.

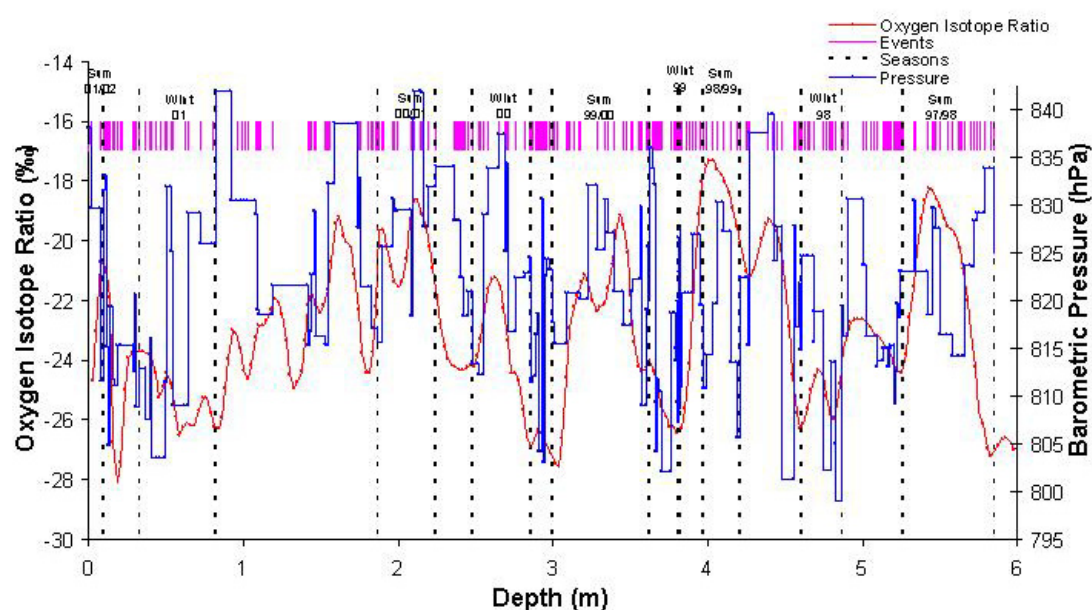


Fig. 6.4: Comparison between $\delta^{18}\text{O}$ and associated pressure for *DSS0102*. The pressure record is drawn from observations recorded by the co-located AWS. The pressure readings represent daily averages for net accumulation days determined from the AWS net accumulation record.

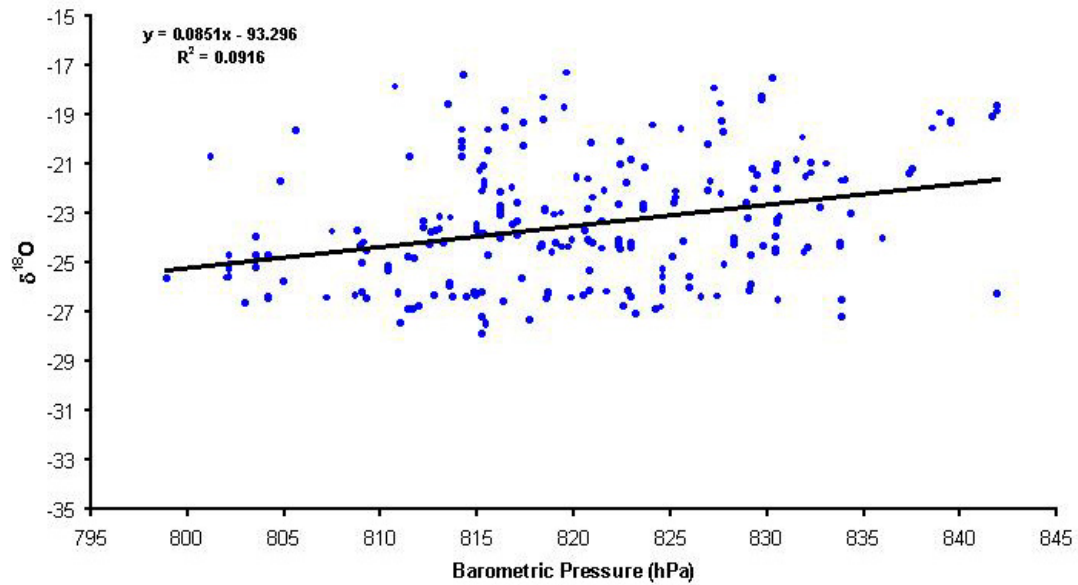


Fig. 6.5: Linear correlation of $\delta^{18}\text{O}$ values from the *DSS0102* firn core over 4 annual cycles and associated pressure recorded from the co-located AWS.

The extent to which atmospheric pressure observations at the coring site on Law Dome reflects the approach of cyclonic events needs to be established before this parameter can be used to infer a relationship between cyclonic precipitation and $\delta^{18}\text{O}$. Perhaps a more useful approach is to compare $\delta^{18}\text{O}$ signals with the observation of cyclonic events at the synoptic scale. Chapter 7 of this thesis will investigate these synoptic events in more detail.

6.3.2 MSA

Seasonal Cycle

The marine biogenic signal represented by MSA in *DSS0102* shows a clear seasonal signal for the 4 annual cycles with maximum concentrations occurring during summer and minima during autumn, winter and spring (Fig. 6.1). The record is characterised by sharp boundaries either side of the summer peak with few additional peaks preserved through the remaining annual cycle. The main summer MSA peak tends to occur simultaneously with the main mid-summer $\delta^{18}\text{O}$ peak, consistent with a link between MSA and $\delta^{18}\text{O}$ cycles. These results are consistent with MSA sourced from DMS production during the summer annual decomposition of spring phytoplankton blooms. Non-summer MSA peaks are much smaller and confined to either late

summer/early autumn or spring events. These events are also generally characterised by elevated levels in $\delta^{18}\text{O}$, sea salt and nitrate (Fig. 6.1). Previous studies have attributed similar events to the intrusion of low latitude air through strong cyclonic systems (McMorrow and others, 2001). Chapter 7 will examine these non-summer MSA peaks in more detail.

Temperature and MSA

Due to the strong relationship between MSA and $\delta^{18}\text{O}$ it is not unexpected that there is also a link between MSA and site temperature (Fig. 6.6). However, the positive relationship tends to be constricted to summer accumulation where high MSA concentrations correspond with warm temperatures. Warm temperature events outside the summer season are not generally accompanied by peaks in MSA. This indicates the link between MSA and temperature is largely driven by seasonal cycles in temperature rather than specific events. However, the small non-summer MSA peaks that frequently occur during late summer/early autumn or spring also tend to correspond with warm temperature events. This suggests that these MSA signals are driven by more specific meteorological events rather than the large scale seasonal cycle. The correlation between temperature and MSA represents an “exponential-shaped” relationship where high MSA concentrations are associated with high temperatures, yet the link between low MSA concentrations and temperature is more erratic (Fig. 6.7). This result supports the suggestion that MSA cycles are largely driven by seasonality rather than specific temperature events.

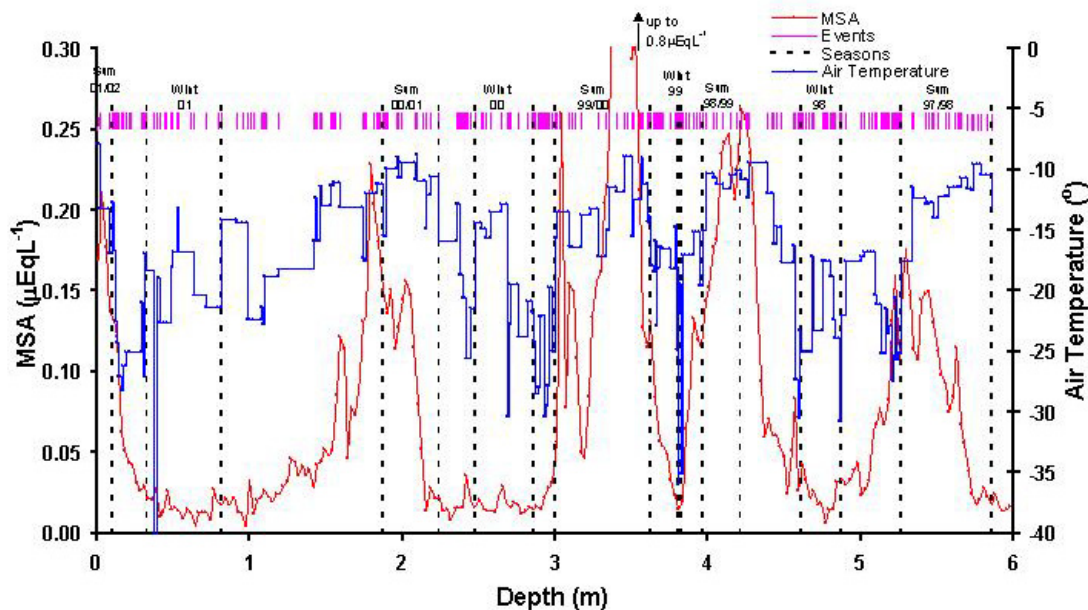


Fig. 6.6: Comparison between MSA and associated air temperatures for *DSS0102*. The temperature record is drawn from observations recorded by the co-located AWS. The temperature record is drawn from the 4 m air temperatures recorded by the co-located AWS. The temperatures represent daily averages for net accumulation days determined from the AWS net accumulation record.

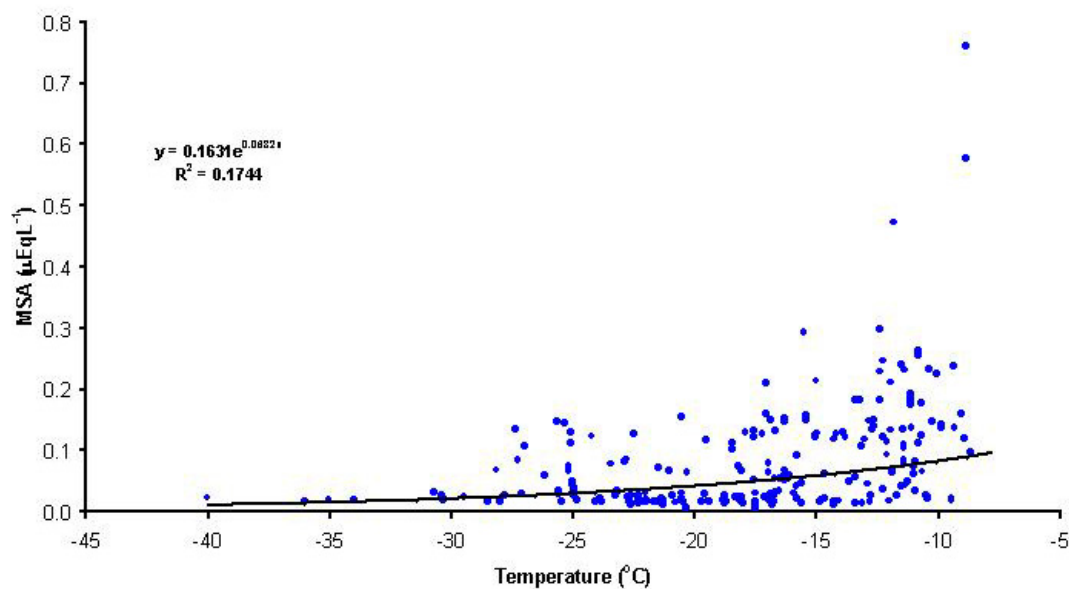


Fig. 6.7: Correlation of MSA values from the *DSS0102* firn core over 4 annual cycles and associated air temperatures recorded from the co-located AWS (4 m temperature record).

6.3.3 Nitrate

Seasonal Cycle

Nitrate shows a more erratic seasonal cycle characterised by narrow peaks during spring and early summer and lower levels during late summer, autumn and winter (Fig. 6.1). Previous studies from Law Dome nitrate records have suggested that nitrate concentrations increase from June until a relative maximum is reached in November, with further sharp rises in concentrations until an absolute maximum is attained in January (Curran and others, 1998). However, the results presented here indicate nitrate maxima occurs earlier in the year, and precedes the main mid-summer $\delta^{18}\text{O}$ and MSA peaks (Fig. 6.1). Similarly, high resolution records from Siple Dome (Kruetz and others, 1999) and the coastal Antarctica stations of Mawson, Neumayer and Dumont D'Urville (Wagenbach and others, 1998b) show late spring/early summer enhancement of nitrate. Spring enhancement of nitrate is consistent with the transport of nitrogen species from the stratosphere to the troposphere through the weakening of the polar vortex at this time of year. These results suggest the nitrate signal preserved in Law Dome ice cores is sourced from the stratosphere rather than local regions.

Temperature and Nitrate

The comparison between nitrate signals and associated air temperatures provides further evidence that the nitrate seasonal cycle is driven by seasonal variability rather than specific meteorological events (Fig. 6.8). Linear correlation of these parameters yields a weak positive relationship (Student's t , 4.25; probability of no correlation for 1 tailed Student's t test, 1.56×10^{-5}) (Fig. 6.9). This positive correlation is mainly attributed to seasonal variations in nitrate and temperature where winter is characterised by low nitrate concentrations and low temperatures, while the spring nitrate peaks correspond with warmer temperatures. Figure 6.9 indicates that the warmest temperature values, generally corresponding to mid-summer, are not associated with the highest nitrate concentrations. This is consistent with a seasonal cycle in nitrate that peaks in spring/early summer rather than mid-summer.

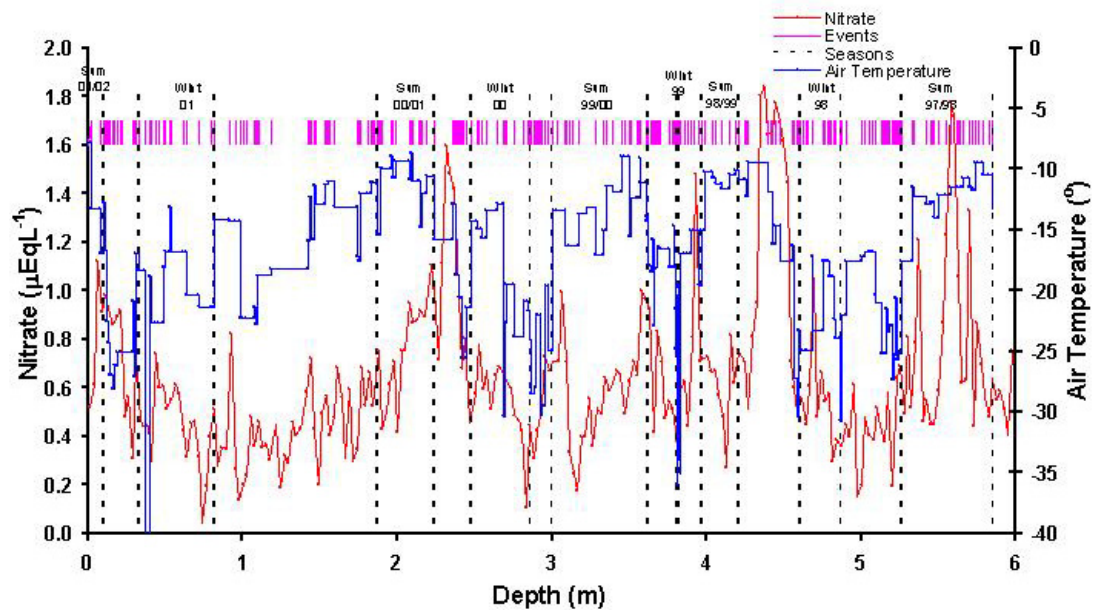


Fig. 6.8: Comparison between nitrate and associated air temperatures for *DSS0102*. The temperature record is drawn from observations recorded by the co-located AWS. The temperature record is drawn from the 4 m air temperatures recorded by the co-located AWS. The temperatures represent daily averages for net accumulation days determined from the AWS net accumulation record.

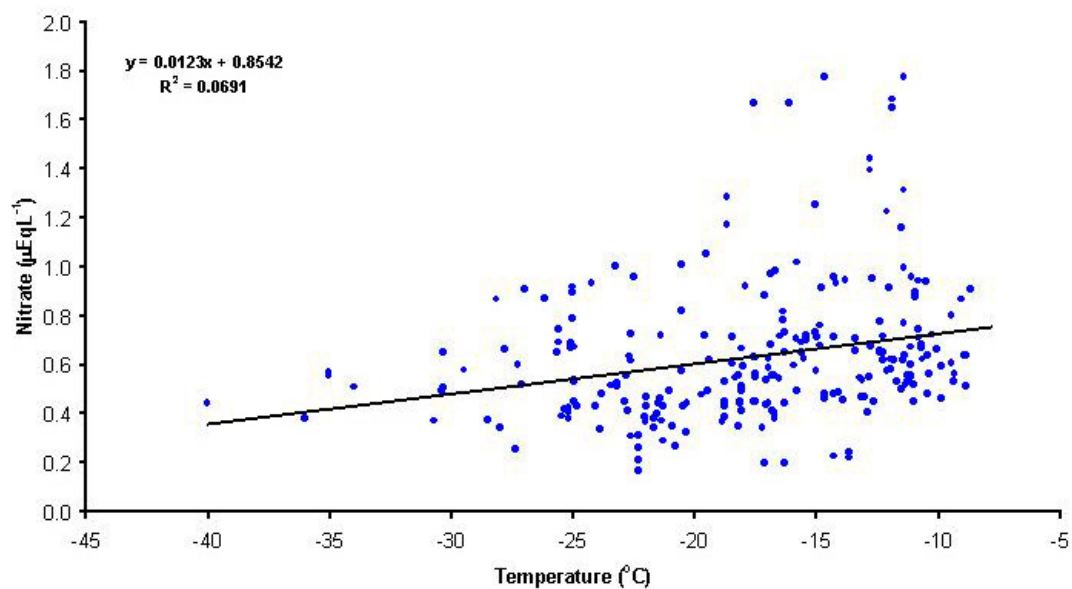


Fig. 6.9: Linear correlation of nitrate values from the *DSS0102* firn core over 4 annual cycles and associated air temperatures recorded from the co-located AWS (4 m temperature record).

6.3.4 Non-Sea Salt Sulphate

Seasonal Cycle

The non-sea salt sulphate record preserved in *DSS0102* shows a clear seasonal cycle with a pronounced mid-summer maximum and lower concentrations during winter (Fig. 6.1). The summer maximum coincides with the main mid-summer peaks in MSA and $\delta^{18}\text{O}$, and is consistent with marine biogenic sulphur compounds dominating the non-sea salt sulphate signal at this time of year. However, outside the main mid-summer peak the non-sea salt sulphate signal is more comparable to the nitrate record (Fig. 6.1). This indicates a common source for non-sea salt sulphate and nitrate during spring, autumn and winter, with potential sources including the downward mixing of stratospheric air.

Temperature and Non-Sea Salt Sulphate

The non-sea salt sulphate seasonal cycle appears to be driven by a combination of biological activity and incursions of stratospheric air, causing peaks in the non-sea salt sulphate record during spring and mid-summer accumulation. Comparisons between non-sea salt sulphate and air temperatures reflect this spring/summer dominance in the non-sea salt sulphate signal where peaks correspond with warm temperatures (Fig. 6.10). The positive relationship between non-sea salt sulphate and temperatures is strongest during spring and summer and warm temperature events outside these seasons are not generally accompanied by peaks in non-sea salt sulphate. This indicates, similar to MSA and nitrate signals, the link between non-sea salt sulphate and temperature is largely driven by seasonal cycles in temperature rather than specific events. The correlation between non-sea salt sulphate and temperature is similar to that between MSA and temperature and reflects an exponential relationship (Fig. 6.11). High non-sea salt sulphate concentrations are associated with warmer temperatures, yet the link between low non-sea salt sulphate and temperature is more erratic. This result supports the suggestion that non-sea salt sulphate cycles are largely driven by seasonality rather than specific temperature events.

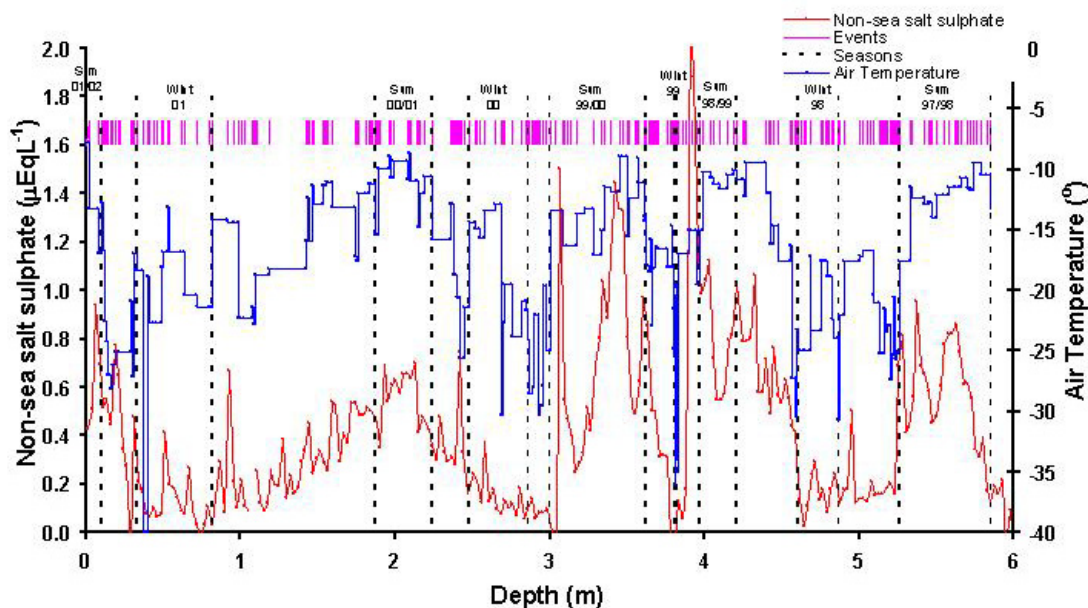


Fig. 6.10: Comparison between non-sea salt sulphate and associated air temperatures for *DSS0102*. The temperature record is drawn from observations recorded by the co-located AWS. The temperature record is drawn from the 4 m air temperatures recorded by the co-located AWS. The temperatures represent daily averages for net accumulation days determined from the AWS net accumulation record.

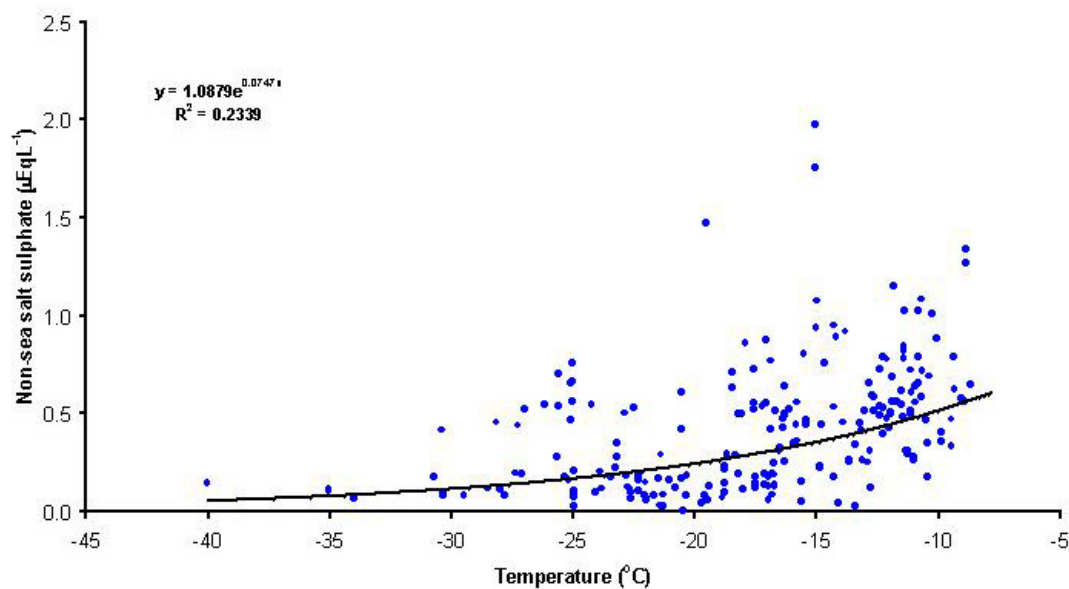


Fig. 6.11: Correlation of non-sea salt sulphate values from the *DSS0102* firn core over 4 annual cycles and associated air temperatures recorded from the co-located AWS (4 m temperature record).

6.3.5 Sea Salts

Seasonal Cycle

The major sea salt species (sodium, chloride, magnesium) preserved in *DSS0102* reflect a noisy record although maximum concentrations tend to be preserved during spring, winter and autumn and minimum levels during summer (Fig. 6.1). This is in general agreement with previous studies from coastal Antarctic sites where higher levels of sea salts are preserved during the austral winter (Minikin and others, 1994; Curran and others, 1998; Wagenbach and others, 1998a). The noisy nature of the sea salt species indicates the record is driven by specific events rather than the broad seasonality in climate conditions. High winter sea salt concentrations are consistent with increased frequency of cyclonic events in the Antarctic region during winter (King and Turner, 1997). The fine resolution sampling of *DSS0102*, coupled with the accurate, independent dating scale, allows the extension of the sea salt seasonal cycle to include maximum concentrations preserved during spring and autumn. This result is consistent with the synoptic scale meteorology for these seasons. Meteorological studies for the East Antarctic region report a semi-annual variation in atmospheric pressure with minimum pressures observed in the austral spring and autumn (Schwerdtfeger, 1984; Allison and others, 1993; King and Turner, 1997).

Atmospheric pressure minima in the Southern Ocean produce more intense cyclonic systems characterised by stronger surface winds. These strong winds provide the mechanism for producing enhanced sea salt concentrations in the ice core record.

Wind Speed, Direction and Sea Salts

Previous studies have suggested the seasonal cycle in sea salts is driven by oceanic wind speeds caused by the seasonal variation in position and intensity of cyclonic events in the Southern Ocean (Curran and others, 1998). Figure 6.12 illustrates the relationship between local wind speeds during net accumulation events and sea salt concentrations over 4 annual cycles at Law Dome. The comparison reflects a positive relationship between wind speeds and sea salt concentrations, although the noisy nature of both records produces an erratic correlation (Fig. 6.13). This feature is accentuated during the austral winter where wind speeds have been shown to be more erratic from May to September (Chapter 4, this thesis), and the sea salt record is also noisier during these seasons (Fig. 6.1). High local wind speed events tend to be associated with strong cyclonic systems passing over the Law Dome region. In

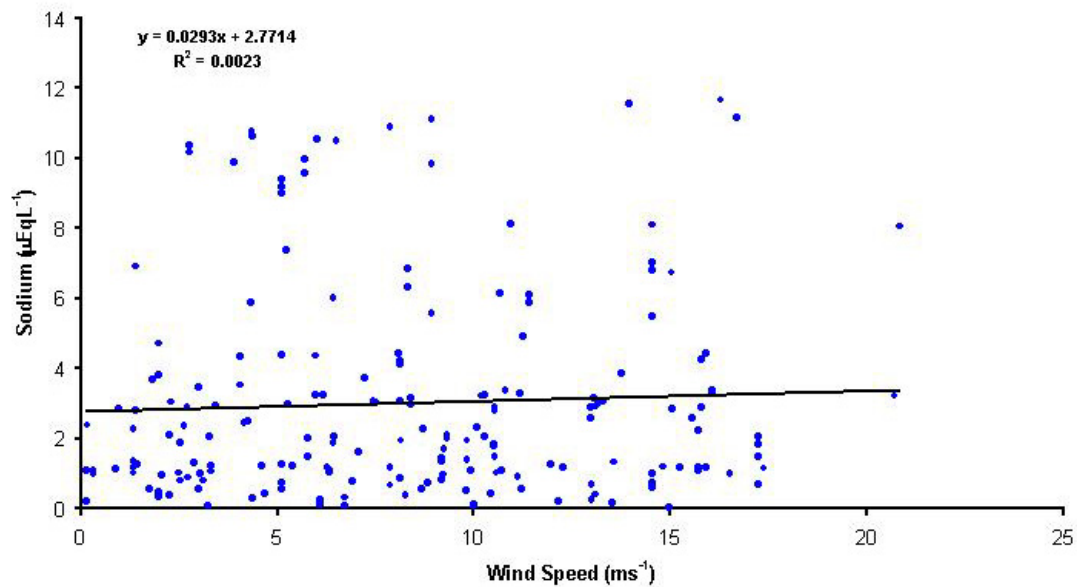


Fig. 6.13: Linear correlation of sodium values from the *DSS0102* firn core over 4 annual cycles and associated wind speeds recorded from the co-located AWS (4 wind speed record).

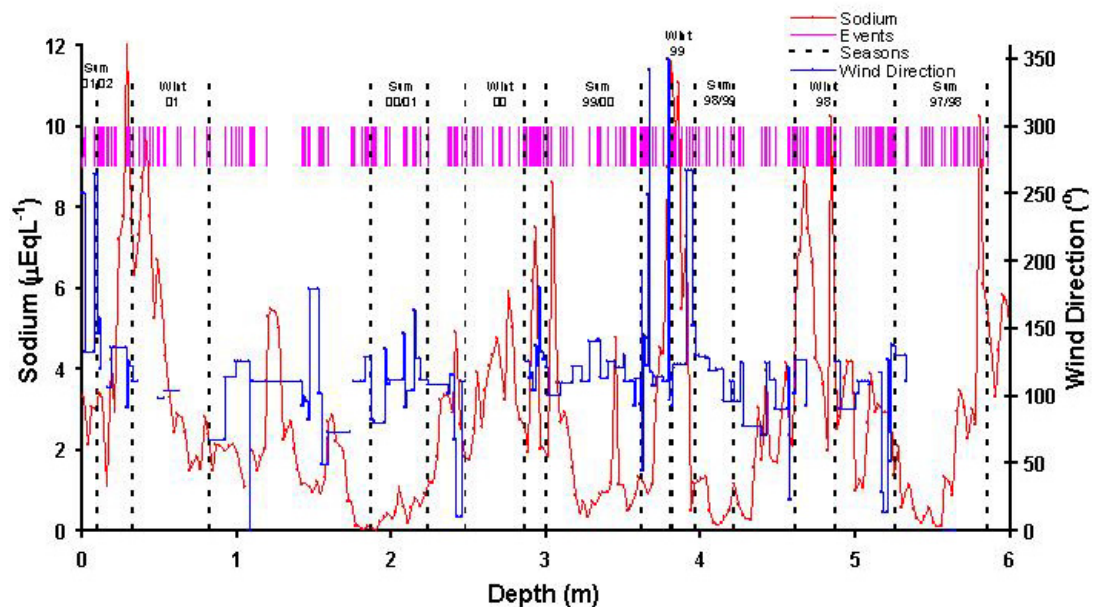


Fig. 6.14: Comparison between sodium and associated site wind direction for *DSS0102*. The wind direction record is drawn from observations recorded by the co-located AWS. The wind directions represent daily averages for net accumulation days determined from the AWS net accumulation record.

The reasonable link between wind speed and direction at Law Dome and sea salt concentrations provides a greater understanding of the transport and deposition mechanisms influencing the seasonal sea salt cycle. Although all three records are erratic in nature, suggesting both the meteorological and sea salt signals are largely influenced by specific events, the general seasonality in the position and intensity of cyclonic depressions in the Southern Ocean drives the annual cycle in sea salt concentrations. The sea salt signals thus provide valuable information relating to the seasonality of cyclonic systems in the Southern Ocean. However, it also captures specific and often unusual climatic events in the ice core. Such events are examined in more detail in Chapter 7 of this thesis.

6.4 Sources Regions for Seasonal Signals Preserved in Law Dome Ice Cores

The source region for climate signals preserved in ice cores is determined by the atmospheric circulation associated with net accumulation events. The climatology of Law Dome is dominated by frequent incursions of cyclonic depressions that make up the circumpolar trough. These cyclonic depressions produce high accumulation events at Law Dome, allowing the preservation of climate signals in the ice core that are associated with the depressions. Peak cyclone densities occur in the region to the northwest of Law Dome (55-60° S, 60-90° E), and the systems tend to travel southeast and then dissipate to the east of Law Dome (Jones and Simmonds, 1993). Thus, atmospheric circulation associated with net accumulation events at Law Dome is generally characterised by the cyclonic (clockwise) circulation of the system.

The source region for climate signals associated with individual cyclonic events can be traced using back trajectories from the Law Dome sampling site. Figure 6.15 shows the back trajectories associated with the net accumulation events preserved in *DSS0102* and covering 4 annual cycles. Back trajectories were obtained from the Bureau of Meteorology general circulation model (GASP modelled data) and provided by Ian Simmonds from the University of Melbourne (Ian Simmonds, pers. comm., 2003). They are calculated using the 500 hPa level wind speed and direction from the GASP model of atmospheric conditions from the source region (Law Dome

drilling site), and back calculated for 10 days. The back trajectories indicate both the transport path and the speed of transport of the air masses influencing net accumulation events. The accuracy of the back trajectory decreases as time from the source input values increase. Therefore, faster trajectories are generally more accurate further back in time than slower trajectories.

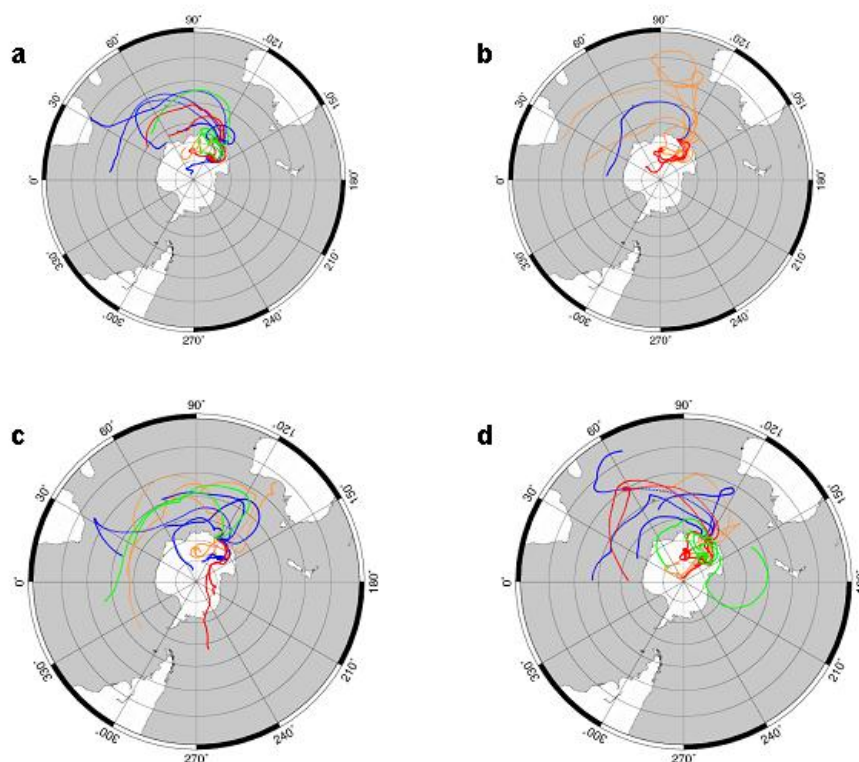


Fig. 6.15: 10 day back trajectories from the 500 hPa level associated with the net accumulation events preserved in *DSS0102* and covering 4 annual cycles. Back trajectories were obtained from the Bureau of Meteorology general circulation model (GASP modelled data) and provided by the University of Melbourne. (a) Austral summers (Blue, 1998/1999; Red, 1999/2000; Green 2000/2001; Orange, 2001/2002); (b) Austral autumns (Blue, 1998; Red, 1999; Green, 2000; Orange, 2001); (c) Austral winters (Blue, 1998; Red, 1999; Green, 2000; Orange, 2001); (d) Austral springs (Blue, 1998; Red, 1999; Green, 2000; Orange, 2001).

The back trajectories for the net accumulation events show a general trend in atmospheric circulation dominated by cyclonic circulation (Fig. 6.15). Most air parcel trajectories show zonal circulation in the mid-latitude region north of 55° E and west of 90° E, before travelling southeast and hooking around towards Law Dome from the east of Law Dome. This is consistent with westerly air circulation dominating in the mid-latitudes and the air mass following the cyclonic depressions associated with the

region of cyclogenesis northwest of Law Dome (55-60° S, 60-90° E). These events also tend to be characterised by faster transport paths and stronger wind speeds than other trajectories (Fig. 6.15). Events that do not pass through the region of cyclone development still tend to show easterly trajectories immediately prior to reaching Law Dome. These events are characterised by slower transport paths and weaker wind speeds, and are generally sourced from inland areas of Antarctica. However, the source regions further back in time for these trajectories further need to be interpreted with caution due to increased uncertainty associated with slower trajectories.

6.4.1 Seasonality in Atmospheric Circulation for Net Accumulation Events

Figure 6.15 shows the seasonal distribution of back trajectories associated with net accumulation events preserved over the 4 annual cycles. Of the 18 events that are preserved during the austral summer (December, January, February), 5 events follow the general trend of cyclonic circulation originating from the mid-latitude area to the northwest of Law Dome, 3 events also indicate cyclonic circulation but with higher latitude source regions, and the remaining 10 events show weaker trajectories with slower transport paths and inland source regions. In contrast, only 4 out of the 14 events that are preserved during the austral autumn (March, April, May) indicate cyclonic circulation and each trajectory shows a different latitude source region. 3 events are dominated by strong meridional transport from lower latitudes (30-40° S, 90-120° E), and the remaining 7 events show weaker trajectories and inland source regions. Events preserved during the austral winter (June, July, August) generally show a strong cyclonic circulation with a wide range of latitude source regions. 17 events are preserved during the austral winter and 7 events show weak trajectories and inland source regions. 5 events are sourced from the lower latitudes directly to the north of Law Dome (40-50° S, 120-150° E) and the remaining 5 can be traced from the mid to high latitude regions to the northwest of Law Dome. Finally, events preserved during the austral spring (September, October, November) are generally characterised by strong cyclonic circulation originating from the northwest of Law Dome, or by weak trajectories and inland source regions. Of the 21 events preserved during spring, 8 events indicate strong cyclonic circulation, 3 events show a source region along the Antarctic coastline due west of Law Dome, and the remaining 10 events indicate weak trajectories and inland source regions.

The main differences in the atmospheric circulation associated with each season lies with the strength of the cyclonic systems. Summer trajectories tend to show a consistent circulation pattern dominated by source regions directly to the northwest of Law Dome. In contrast, autumn, winter and spring trajectories are characterised by a wider range of transport paths. Source regions for these trajectories are extended to include lower latitudes compared to summer trajectories. This is consistent with the northward location of the circumpolar trough and the general increase in cyclonic activity during autumn, winter and spring (Allison and others, 1993; King and Turner, 1997). Larger storm events produce strong circulation patterns and allow the advection of low latitude air towards the pole. In contrast, smaller cyclonic systems formed during summer will limit advection of air from lower latitudes and result in a more consistent source region close to the area of cyclogenesis.

The back trajectories illustrated in figure 6.15 only show a sample of the events that influence the Law Dome region. These trajectories were chosen to reflect the net accumulation events that make up the ice core record over the 4 annual cycles. They provide insight into the seasonal variability of atmospheric circulation for specific events that are associated with ice core signals. More detailed investigation of the atmospheric circulation associated with particular ice core signals is contained in Chapter 7 of this thesis.

6.5 Concluding Remarks

This chapter explored the seasonal characteristics of chemical and isotopic species preserved in the high resolution *DSS0102* Law Dome ice core over 4 annual cycles. Accurate dating of *DSS0102*, obtained from the AWS accumulation record and adjusted for densification of the snowpack, enabled a detailed examination of the seasonal characteristics of the firm core signals. The chronology of *DSS0102* is unique compared to previous seasonality studies in that it was developed using net accumulation measurements independent of the seasonal cycle of the chemical and isotopic signals. This allowed, for the first time, the examination of exact timings in the seasonality of each species. The traditional summer-maximum species of $\delta^{18}\text{O}$ and MSA show consistent relative phasing during mid-summer over the 4 annual cycles.

Nitrate shows an erratic seasonal cycle with a general trend characterised by narrow peaks during spring and early summer, preceding the mid-summer peaks in $\delta^{18}\text{O}$ and MSA. Non-sea salt sulphate cycles indicate similar characteristics to MSA signals during summer, but are more comparable to nitrate signals during spring, autumn and winter. This suggests the summer non-sea salt sulphate signal is driven by biological activity, although this species appears to be linked with nitrate signals outside the summer season. Finally, the sea salt species indicate a seasonal cycle characterised by maximum concentrations during spring, winter and autumn.

Local meteorological conditions recorded during net accumulation events were compared directly with the firn core signals preserved in *DSS0102*. A strong relationship between $\delta^{18}\text{O}$ and local air temperature was established at the event scale, providing evidence that Law Dome $\delta^{18}\text{O}$ signals are driven by specific temperature events. In contrast, the relationship between air temperature and the marine biogenic species (MSA, non-sea salt sulphate) shows a positive relationship during the summer months, and a more erratic correlation outside the summer season. This indicates the link between marine biogenic activity and temperature is largely driven by seasonal cycles in temperature rather than specific events. Similarly, the comparison between nitrate signals and associated air temperatures yields a weak positive relationship with high nitrate concentrations corresponding with warm temperatures. The warmest temperature values, generally coinciding with mid-summer, are not associated with the highest nitrate concentrations. This is consistent with the a seasonal cycle in nitrate that peaks in spring/early summer rather than mid-summer. The weak positive relationship between nitrate and air temperatures provides further evidence that the nitrate seasonal cycle is driven by seasonal variability rather than specific meteorological events. Finally, a strong link between sea salt concentrations and wind speed and direction was established at the event scale. The erratic nature of all three records suggest both the sea salt and meteorological signals are largely influenced by specific events. However, the results show that the general seasonality in the position and intensity of cyclonic depressions in the Southern Ocean drives the annual cycle in sea salt concentrations. The sea salt signals thus provide valuable information relating to the seasonality of cyclonic systems in the Southern Ocean, while also capturing specific and often unusual climatic events in the ice core.

Potential source regions for the seasonality in the firn core signals were considered using back trajectories associated with net accumulation events. The trajectories show a general trend in atmospheric circulation dominated by cyclonic circulation. Most air parcel trajectories show zonal air circulation in the mid-latitude region north of 55° E and west of 90° E, before travelling southeast and hooking around towards Law Dome from the east of Law Dome. The main differences in the atmospheric circulation associated with each season lies with the strength of the cyclonic systems. Summer trajectories tend to show a consistent circulation pattern dominated by source regions directly to the northwest of Law Dome. In contrast, autumn, winter and spring trajectories are characterised by a wider range of transport paths. Source regions for these trajectories are extended to include lower latitudes compared to summer trajectories.

The use of a range of glaciological and meteorological tools to examine the seasonality of ice core signals enables a greater understanding of the application of these signals for the interpretation of palaeoclimate signals preserved in deeper ice core records. The following chapter provides further examination of the meteorological conditions associated with particular ice core signals at the event scale.

Chapter 7

Pilot Study – Examination of Three Accumulation Periods in the *Rama* Snow Pit

7.1 Overview

Ultra high resolution studies of the snowpack facilitate a greater understanding of the source regions and transport mechanisms influencing climate signals that are preserved in ice cores. In the previous chapter, discussion was centred around the seasonal cycles in chemical and $\delta^{18}\text{O}$ signals preserved over four annual cycles in near-surface firn at Law Dome. This chapter takes that seasonality discussion one step further down to the event scale, and directly compares chemical and $\delta^{18}\text{O}$ events with contemporaneous meteorological observations.

This chapter uses a pilot study to develop the techniques for directly comparing chemical and isotopic signals with observed meteorology at the event scale. Methods for directly comparing Law Dome ice core signals and meteorological conditions at the event scale are drawn from the preliminary techniques described in McMorrow (1998) and McMorrow and others (2001). In this preliminary study a shallow firn core that comprised seven months of snow accumulation was used to directly compare ice core signals and meteorological events.

The preliminary techniques described in the above references are further developed in this chapter with a pilot study that focuses on three accumulation periods preserved in the top 0.5 m of the *Rama* snow pit. The *Rama* snow pit was sampled on 1 March 2000 for trace chemical and $\delta^{18}\text{O}$ signals at 2.5 cm resolution and extending to 2 m depth. The pilot study aims to develop the techniques used to compare chemical and isotopic signals with contemporaneous local and synoptic meteorological conditions at the event scale. The results from this pilot study are reported in McMorrow and others (2002), and form the basis for the techniques used to extend the analysis to signals preserved in other snow pit and firn core records (Chapter 8).

7.2 Chemical and Isotopic Signals

The AWS net accumulation record indicates three main periods of accumulation preserved in the *Rama* snow pit during summer 1999/2000 (P1 – P3) (Fig. 7.1). These accumulation periods comprise the top 0.5 m of *Rama* and the corresponding chemical and $\delta^{18}\text{O}$ signals are represented in Figure 7.2. Densification effects may lead to uncertainties in the registration of events as depth increases, and the following analysis is restricted to major changes in the top 0.5 m of the record to minimise these depth uncertainties. However, it should be noted that results from Section 5.3 of this thesis indicate that densification effects in the top 0 – 3 m of the snowpack do not significantly affect the dating of events. This result provides confidence in the accuracy of event-scale dating snow pit and firn core records in the 0 – 3 m depth range.

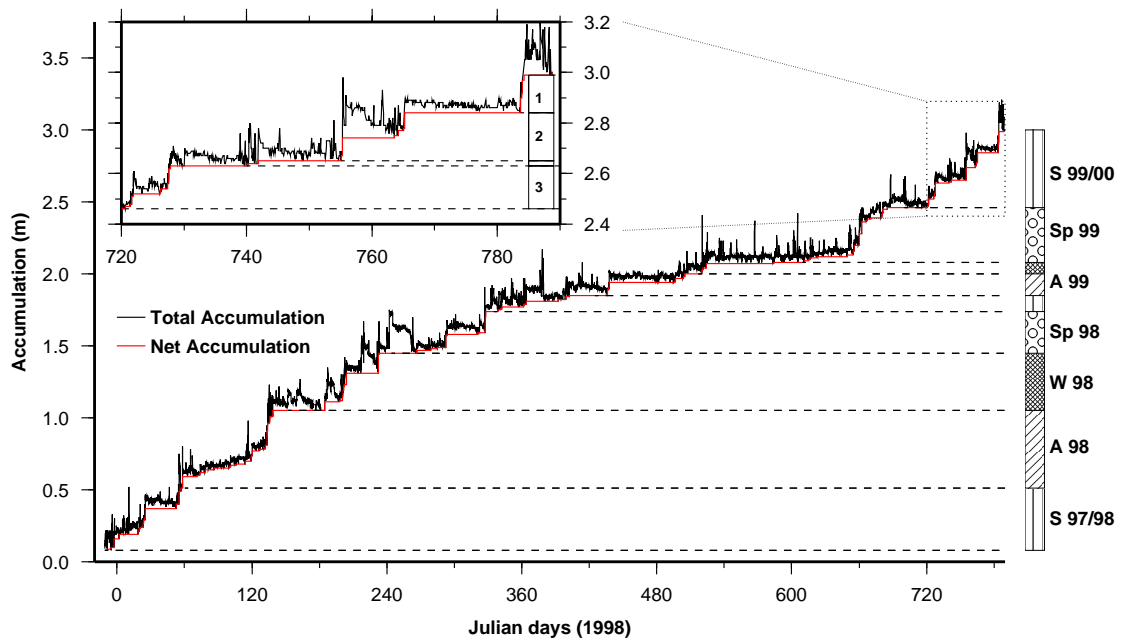


Figure 7.1: Total and net accumulation recorded from the AWS from 21 December 1997 (Julian day –10) to 27 February 2000 (Julian day 788). Net accumulation from each austral season is shown (summer (S), autumn (A), winter (W), spring (Sp)), and accumulation periods (P1-P3) from summer 1999/2000 is also illustrated.

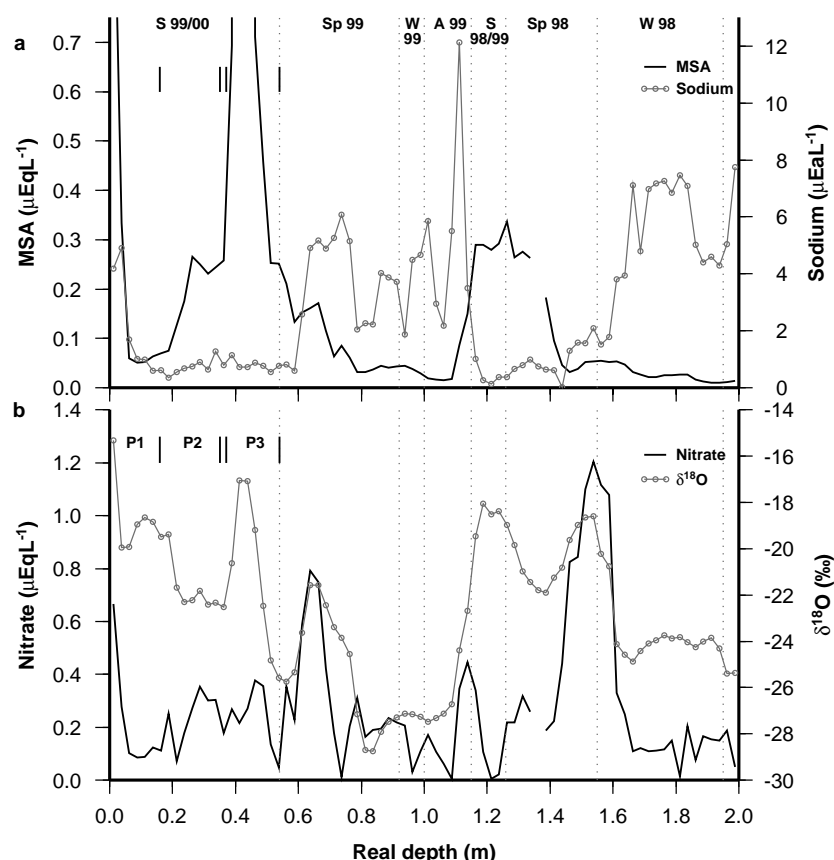


Figure 7.2: Chemical and $\delta^{18}\text{O}$ records from a representative line from *Rama*, with dating scale illustrated. (a) MSA and sodium, (b) nitrate and $\delta^{18}\text{O}$. Dotted lines indicate austral season boundaries defined by the AWS net accumulation record. Period boundaries for summer 1999/2000 (P1-P3) are also illustrated.

The three net accumulation periods identified in Figure 7.1 are characterised by similar amounts of accumulated material (0.16 – 0.19 m) (Fig. 7.1; Table 7.1) yet the chemical and isotopic signatures observed in each period are varied (Fig. 7.2; Table 7.1). The snow pit signals associated with P1 (late summer) include elevated MSA, $\delta^{18}\text{O}$, sodium and nitrate concentrations. The deposition of MSA, $\delta^{18}\text{O}$ and sea salts outside the mid-summer MSA peak is also observed in deeper records at Law Dome (Curran and others, 2002), and current research is being directed towards explaining these events. It is interesting to note that all chemical and $\delta^{18}\text{O}$ records show a large spike at the very surface of the snow pit, and there is a distinct sharp change in concentrations within P1. The cause of these elevated surface concentrations is not clear, and closer examination of the meteorological conditions associated with P1 may provide an explanation. However, it should be noted that in this case, the sharp change in chemical and isotopic species in surface samples may indicate these species undergo rapid post depositional modification or loss within the snow. The high concentrations observed in the surface samples may reflect the chemical and $\delta^{18}\text{O}$ signal prior to post depositional

modification. Of the key species examined in this pilot study, nitrate is proposed to be severely affected by post depositional loss (Mulvaney and Wolff, 1993; Mulvaney and others, 1998), and the elevated surface nitrate concentrations may reflect conditions prior to loss of nitric acid in the snow. $\delta^{18}\text{O}$ has been shown to be affected by post depositional diffusion in the firn, although the rate of diffusion is expected to be slower than the sharp change indicated in the *Rama* snow pit (Whillans and Grootes, 1985). MSA has also been shown to migrate in firn and ice cores (Wolff, 1996; Kreutz and others, 1998; Pasteur and Mulvaney, 2000; Curran and others, 2002), yet the processes driving MSA migration are unlikely to occur in the top few metres of the snowpack (Curran and others, 2002). Non-volatile sea salt species (eg. sodium) are not expected to undergo post depositional modification (Kreutz and others, 1998; Wolff and others, 1998). All these results suggest that the concurrent elevated levels of MSA, $\delta^{18}\text{O}$, sodium and nitrate in the top 0.1 m of the *Rama* snow pit are probably reflecting the signature of a specific snowfall event rather than indicating these species undergo rapid post depositional modification or loss. The following analysis will therefore assume P1 is characterised by relatively high chemical and $\delta^{18}\text{O}$ signals.

The snow pit signals observed during P2 show levels of MSA, nitrate, $\delta^{18}\text{O}$ and sodium comparable to average summer concentrations at Law Dome. In contrast, P3 is characterised by a very narrow and pronounced peak in MSA and $\delta^{18}\text{O}$. MSA concentrations peak at $1.7\ \mu\text{EqL}^{-1}$, significantly higher than average summer levels from deeper records at Law Dome ($0.10\mu\text{EqL}^{-1}$; Anne Palmer, pers. comm., 2005).

Table 7.1: Intercomparison of snow pit signals and meteorological conditions for summer accumulation periods 1, 2 and 3 preserved in the *Rama* snow pit.

<i>Period</i>	<i>P1</i>	<i>P2</i>	<i>P3</i>
Dates	22 – 27 Feb 00	25 Jan 99 – 4 Feb 00	21 – 28 Dec 99
Julian Days (1998)	783 – 788	755 – 765	720 – 727
Net Accum. (m)	0.17	0.19	0.16
Snow Pit Signal	Co-deposition of MSA, $\delta^{18}\text{O}$, sodium, nitrate	Average summer signals, no distinct peaks	Narrow and pronounced MSA and $\delta^{18}\text{O}$ peaks
Local Pressure	2 sharp troughs	Sharp trough	2 sharp troughs
Local Air Temperature	Steady at -12°C	-11°C to -17°C (variable)	Sharp rise from -22°C to -2°C
Local Wind Speed	Sharp peak (20.6ms ⁻¹)	2 sharp peaks (19.9ms ⁻¹ , 22.2ms ⁻¹)	2 sharp peaks (24.9ms ⁻¹ , 14.5ms ⁻¹)
Local Wind Direction	Easterly	Variable, but tending easterly	Easterly and tending northerly
Synoptic-scale Meteorology	Large cyclonic system	Weak and disorganised cloud systems	2 large cyclonic systems
Approximate Source of System(s)	45°S, 90°E	55°S, 90°E	50°S, 70°E

7.3 Local Meteorological Conditions

Local meteorological conditions recorded by the AWS during summer 1999/2000 are illustrated in Figure 7.3. The three accumulation periods are all marked by a sharp decline in atmospheric pressure and pronounced peaks in wind speed (Fig. 7.3). There is also evidence of elevated temperatures during the periods, especially for P3. In addition, these conditions are reflected in the meteorology at Casey station (located 110 km from DSS), indicating the influence of large-scale atmospheric systems. Precipitation events at Law Dome are usually caused by the passage of cloud bands associated with cyclonic systems located in the oceanic region to the north of Law Dome. These systems result in strong easterly winds, falling atmospheric pressure and elevated temperatures at Law Dome (Schwerdtfeger, 1984; Callaghan and Betts, 1987; Bromwich, 1998). The conditions recorded by the AWS and Casey station during the net accumulation periods (P1 – P3) are consistent with these studies. In

addition, there is a period in the summer record where the AWS measured local pressure and temperature conditions similar to the net accumulation periods (Julian days 738 – 743; Fig. 7.3), yet only 0.02 m of accumulation is retained in the record (Fig. 7.1). Significant snowfalls are recorded during this period, but the majority of material was lost, probably through wind scouring (Fig. 7.1). Snow removal through wind scouring is consistent with the sustained high levels of wind speeds recorded by the AWS during this period, in contrast to the other net accumulation periods (P1 – P3) which are characterised by sharp spikes in wind speed followed by lower wind speeds. The reduction of wind speeds during an accumulation event provides a mechanism for the snowfalls to accumulate and be retained in the snow pit record (Fig. 7.3).

7.4 Synoptic Scale Meteorological Conditions

Advanced Very High Resolution Radiometer (AVHRR) infrared imagery illustrates differences in source and transport mechanisms influencing each of the accumulation periods (Fig. 7.4; Table 7.1). All periods are characterised by cyclonic systems passing over Law Dome, yet the intensity, travel path and speed of travel of the cyclones vary between periods. P1 is characterised by a large cyclonic system that began to develop on 20 February 2000 (Julian day 781) around 45°S, 90°E (Fig. 7.4a) and then intensified and moved due south onto Law Dome early on 22 February 2000 (Julian day 783) (Fig. 7.4b). This system continued to influence Law Dome until around 27 February 2000 (Julian day 788). P2 is characterised by a series of weak and disorganised cyclonic systems that decayed quickly while passing over Law Dome through the period. An example of one of these systems is given in Figure 7.4c and 7.4d. In contrast, AVHRR imagery for P3 shows two large cyclonic systems passing over Law Dome in quick succession. System 1 is sourced from the Heard/McDonald Island region (50°S, 70°E) around 20 December 1999, and travelled southeast and onto Law Dome on 22 December 1999 (Julian day 721) (Fig. 7.4e and 7.4f). System 2 followed a similar path, passing over Law Dome on 27 December 1999 (Julian day 726), although cloud cover indicates a less intense system (not shown).

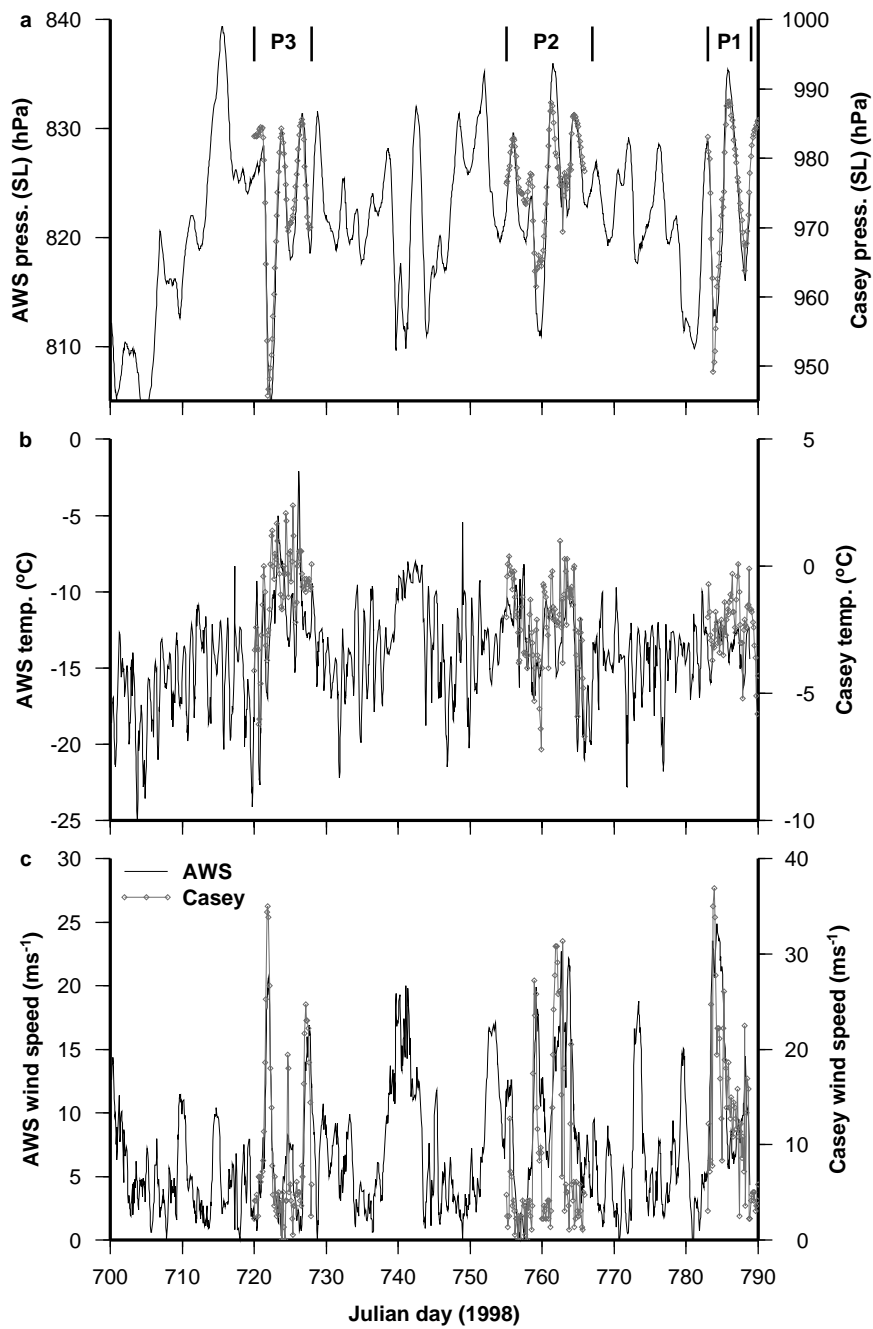


Figure 7.3: Local meteorological conditions recorded by the AWS from 1 December 1999 (Julian day 700) to 27 February 2000 (Julian day 788). (a) Station-level (SL) pressure, (b) air temperature, (c) wind speed. Net accumulation (P1-P3) are illustrated, and meteorological conditions recorded at Casey station during accumulation periods are also plotted.

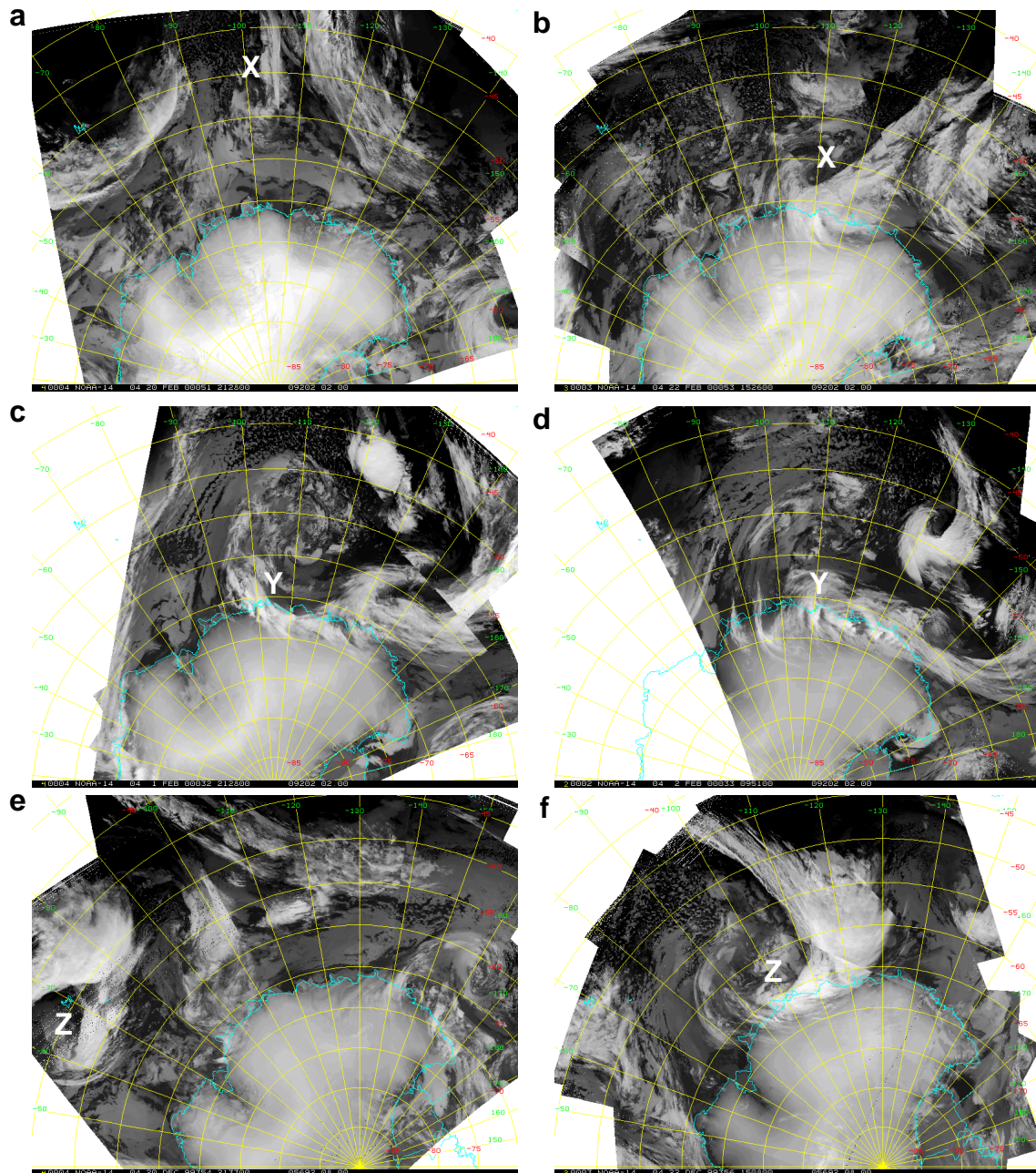


Figure 7.4: AVHRR satellite imagery showing cyclonic systems associated with net accumulation periods P1 (a,b), P2 (c,d) and P3 (e,f); (a) Cyclonic system (X) at 2128 UTC 20 February 2000 (Julian day 781); (b) Cyclonic system (X) at 1526 UTC 22 February 2000 (Julian day 783); (c) Cyclonic system (Y) at 2128 UTC 1 February 2000 (Julian day 762); (d) Cyclonic system (Y) at 0951 UTC 2 February 2000 (Julian day 762); (e) Cyclonic system (Z) at 0148 UTC 21 December 1999 (Julian day 720); (f) Cyclonic system Z at 1508 UTC 22 December 1999 (Julian day 721).

7.5 Source Regions and Transport Mechanisms for the Snow Pit Signals

The late-summer deposition of MSA, $\delta^{18}\text{O}$ and sea salts observed during P1 is consistent with rapid poleward transport of an air mass driven by a strong cyclonic system located in the midlatitudes (Fig. 7.4; Table 7.1). ‘Rapid’ transport is determined for this air mass using a combination of storm tracking using AVHRR, and comparing the speed of the back trajectory for this system with other back trajectories examined in this research (see Chapter 8). Rapid advection of warm marine air from the midlatitudes, where there is an expected source of dimethylsulphide (DMS) from marine biota at this time of year (Curran and Jones, 2000), provides an explanation for the enhanced MSA concentrations in the snow pit record. Limited fractionation of $\delta^{18}\text{O}$ due to the short time available for precipitation of heavy oxygen isotopes (^{18}O) during rapid transport of the air mass explains the high levels of $\delta^{18}\text{O}$ preserved in the record. Finally, increased uptake of sea salts from the ocean during the storm event is consistent with enhanced concentrations of sodium in the snow pit.

In contrast, the average summer levels of MSA, $\delta^{18}\text{O}$, nitrate and sodium observed during P2 are consistent with a series of weak, local cyclonic systems passing over Law Dome in close succession during this period. Analysis of the AVHRR satellite imagery (not shown) indicates that the systems all developed in close proximity to Law Dome and travelled over the sea ice before reaching Law Dome (Table 7.1). The sea ice zone is an important source of MSA for summer deposition at Law Dome (Curran and Jones, 2000), and differs from the implied source region of MSA observed during the late summer period (P1). This suggests that mid-summer signals at Law Dome may be the result of weak cyclonic systems that develop close to the coast of Antarctica, while MSA peaks outside the mid-summer peaks may be caused by stronger cyclonic systems sourced from lower latitudes. The low sodium signals observed during P2, similar to average summer levels from deeper DSS ice cores, may be explained by limited sea salt production from the weak cyclonic activity, and supports a local source region for chemical signals during P2.

Finally, the enhanced mid-summer levels of MSA observed during P3 may be explained by the rapid advection of an air mass laden with MSA aerosols from a known area of DMS production. Both cyclonic systems influencing Law Dome during P3 are sourced from the Heard/McDonald Island region (50°S, 70°E) (Table 7.1). This region is an expected source of

MSA due to documented high levels of DMS productivity from marine biota (Curran and others, 1998b).

The arguments outlined above represent one set of hypotheses for the chemical and isotopic signals observed during the three accumulation periods. Although plausible, other mechanisms for driving the snow pit signature cannot be ruled out. For example, the elevated levels of MSA preserved during P1 and P3 may be the result of increased DMS production in the local sea ice zone, or increased DMS air sea transfer through high surface winds over the ocean, rather than rapid transport of DMS laden air from the midlatitudes. Section 7.3 will investigate a larger number of accumulation events in order to provide a more robust analysis of potential source regions and transport mechanisms influencing the chemical and isotopic signals. However, the three-period comparison shows the techniques are useful in facilitating a discussion on potential source regions and transport mechanisms influencing chemical and isotopic signals.

7.6 Concluding Remarks

The preceding discussion presents results from a direct comparison between snow pit signals and meteorological conditions for three summer accumulation periods. Late summer deposition of MSA, $\delta^{18}\text{O}$ and sea salts appears to be associated with rapid advection of air from low latitudes where DMS production is high at this time of year. Further analysis of the meteorological conditions associated with similar chemical and isotopic signals is needed before concluding whether this mechanism is influencing non-summer peaks in MSA observed in deeper Law Dome ice core records. In addition, a pronounced mid-summer peak in MSA, higher than concentrations observed in deeper records at Law Dome, is associated with strong cyclonic systems sourced from a known area of high DMS production. Finally, summer concentrations of MSA, $\delta^{18}\text{O}$ and sodium that are comparable to average Law Dome signals are associated with weak cyclone development in the sea ice region close to Law Dome.

These results highlight the effects of circulation patterns on the Law Dome snow pit record. Deep ice core records from coastal Antarctic sites influenced mainly by the procession of cyclonic systems are likely to be sensitive to changes in circulation patterns through the palaeoclimate record. This three-period study provides some insight into potential source regions and transport mechanisms influencing summer snow pit signals at Law Dome, and demonstrates the value in using these techniques for comparing meteorological conditions with well dated snow pits and firn cores.

Chapter 8 will examine accumulation periods preserved deeper in the *Rama* and *Matilda* snow pits, as well as from high resolution co-located firn cores. Potential source regions and transport mechanisms are considered for chemical and isotopic signals observed during specific events. The comparative techniques outlined in this chapter will form the basis for identifying a database of events that will allow comparisons between chemical and isotopic signals, and meteorological conditions.

Chapter 8

Investigation of Specific Meteorological Events Preserved in High Resolution Snow Pit and Firn Core Records

8.1 Overview

Drawing on the techniques demonstrated in the pilot study (Chapter 7), this chapter aims to conduct a comprehensive investigation of events preserved in a number of snow pit and firn core records from Law Dome. The aim of the event scale investigation is to provide a more detailed examination of potential source regions and transport mechanisms influencing the seasonal signals presented in Chapter 6.

The chapter begins with an overview of current seasonal studies from Law Dome ice cores. The glaciological and meteorological tools that are used in the comparative study are also defined. The main discussion involves building up a dataset of events where the chemical and $\delta^{18}\text{O}$ signals are directly compared with observed meteorological conditions. This comparison is structured into the four Austral calendar seasons. Finally, the chapter concludes with a discussion on how results from the comparative study may be applied to interpreting deep ice cores from Law Dome.

8.2 Current Seasonal Studies from Law Dome Ice Cores

There are currently four studies from deep ice cores at Law Dome that describe the seasonality of isotopic and chemical species and provide an indication of “typical” signals preserved during each calendar season. Morgan and van Ommen (1997) describe the seasonality in late-Holocene $\delta^{18}\text{O}$ using a composite signal from stacked data covering 684 years from the deep DSS ice core. Curran and others (1998a) describe the seasonality in trace ion species from a similar composite using 28 years of data, while Palmer (2002) provides a longer term seasonality study of trace ion species using a composite from 695 years of ice core data. Finally, Curran and others (2002) provide an examination of the seasonal deposition of MSA over a 273 year epoch (AD 1727 – 2000). These long term studies allow the identification of typical seasonal signals, with unusual or extreme events not apparent in the composite signal due to their infrequent occurrence and/or coarser sampling resolution for the longer term studies.

Summer (December, January, February) signals at Law Dome tend to be characterised by maximum concentrations of $\delta^{18}\text{O}$, MSA, nitrate and non-sea salt sulphate. The seasonal composite drawn from Curran and others (1998a) shows mid-summer peaks in MSA and non-sea salt sulphate occurring simultaneously. The summer peak in $\delta^{18}\text{O}$ also tends to occur mid-summer (Morgan and van Ommen, 1997), and more recent studies have shown that the mid-summer $\delta^{18}\text{O}$ signal tends to coincide with the MSA and non-sea salt sulphate peaks (Chapter 6, this thesis; McMorrow and others, 2003). Nitrate concentrations are generally characterised by high levels during summer. Curran and others (1998a) describe a nitrate distribution characterised by a sharp peak in mid-summer, while the longer time frame studied by Palmer (2002) suggests nitrate may peak in early summer. The sea salt ions (sodium, chloride, magnesium, potassium, sulphate and calcium) are generally characterised by minimum concentrations during summer seasons.

Autumn (March, April, May) signals generally involve declining levels of $\delta^{18}\text{O}$, MSA, nitrate and non-sea salt sulphate, and increasing concentrations of sea salts. The seasonal signal in $\delta^{18}\text{O}$ shows minimum levels are reached during mid-autumn, continuing through the winter and rising again during spring (Morgan and van Ommen, 1997). This distribution imitates the coreless winter in air temperature measurements in the Antarctic, and provides evidence for a strong link between $\delta^{18}\text{O}$ and air temperatures at Law Dome. A relative maximum in sea salts

during autumn has been observed at Law Dome, and attributed to increased storm activity (Curran and others 1998a). However, a similar autumn relative maximum was not observed during the longer trace ion chemical record studied by Palmer (2002).

Sea salt concentrations tend to dominate the ionic budget during winter (June, July, August) seasons, with the broad winter peak in sea salts generally attributed to increased storminess over the Southern Ocean at this time. Winter signals are also generally characterised by minimum levels of $\delta^{18}\text{O}$, MSA, nitrate and non-sea salt sulphate.

Spring (September, October, November) signals tend to mirror the autumn trend, and are characterised by increasing levels of $\delta^{18}\text{O}$, MSA, nitrate and non-sea salt sulphate and decreasing sea salt concentrations. A spring relative maximum in nitrate is observed in both trace ion seasonality studies for Law Dome, preceding a sharp increase in concentrations to the summer maximum (Curran and others, 1998a; Palmer, 2002). The spring relative maximum in nitrate is also found to correspond with a similar feature of enhanced sea salt concentrations, with possible interpretations including either a maritime source of nitrate during storm events, or scavenging of nitrate by the sea salt aerosol (Palmer, 2002). The other summer species ($\delta^{18}\text{O}$, MSA, non-sea salt sulphate) tend to follow a gradual increase during spring and reaching maximum levels during mid-summer.

The four seasonality studies for Law Dome described above provide a useful starting point to facilitate further analysis into specific events influencing Law Dome during each calendar season. The following sections further investigate the seasonality of Law Dome chemical and $\delta^{18}\text{O}$ signals using a combination of glaciological and meteorological tools.

8.3 Glaciological and Meteorological Tools

8.3.1 Glaciological Tools

Trace chemical and $\delta^{18}\text{O}$ records are drawn from the high resolution snow pits and firn core records discussed in previous chapters of this thesis. A suite of chemical and isotopic signals are considered, including $\delta^{18}\text{O}$, MSA, non-sea salt sulphate, nitrate and sea salts (indicated by sodium). The examination of specific events are drawn from the *Matilda* and *Rama* snow pits and the *DSS0102* and *S0k* firn cores (Table 8.1). The chemical and $\delta^{18}\text{O}$ signals are determined

from Section 5.2.2 of this thesis, specifically Figures 5.4 (*Matilda*), 5.6 (*Rama*), 5.5 (*DSS0102*) and 5.7 (*S0k*).

Table 8.1: Details of the snow pits and firn cores used in the event scale examination

Snow Pit or Firn Core	Date Sampled or Drilled	Depth (m)	Sample Resolution (cm)	Approximate Record Start	Approximate Record End	Relevant Figure in Chapter 5
Matilda	24-Dec-01	2.25	2.5	Summer 01/02	Summer 00/01	5.4
Rama	1-Mar-00	2	2.5	Summer 99/00	Winter 98	5.6
DSS0102	26-Dec-01	10	2.5	Summer 01/02	Summer 94/95	5.5
S0k	24-Dec-01	10	2.5	Summer 99/00	Winter 92	5.7

Dating the Chemical and $\delta^{18}O$ Records

Event scale dating of the chemical and $\delta^{18}O$ records is drawn from Section 5.2 of this thesis, and due to increased dating uncertainties associated with depths greater than 3 m (Section 5.3), the analysis is restricted to pit and core material in the 0 – 3 m depth range. The discussion is focused around a dataset of events that are grouped into the Austral calendar seasons. Seasons are defined as summer (December, January, February), autumn (March, April, May), winter (June, July, August) and spring (September, October, November).

Events are defined by positive accumulation steps observed in the AWS accumulation records, with the steps grouped according to techniques outlined in Section 5.2.1 of this thesis. These techniques consider two factors when grouping positive accumulation steps into events. First, accumulation steps which occur close together in time (less than a week) and from a particular synoptic situation are grouped into a single event. This consideration recognises that specific events are likely to result from meteorological situations that influence Law Dome over days rather than weeks. Second, the chemical and isotopic signature for each event is examined, and events characterised by a sharp change in the signals within a short time period are separated into distinct events. This consideration recognises that sharp changes in the meteorological situation may occur over Law Dome, providing a mechanism for two distinctive air masses influencing Law Dome over adjacent days. Finally, events that result in net accumulation of less than 3 cm are excluded from the analysis to further minimise uncertainties associated with the dating technique.

Differentiation in Dating between Pilot Study and Chapter 8

It should be noted that Event 29 (discussed in Section 8.5) corresponds to Period 3 (P3) from the pilot study outlined in Chapter 7 and reported by McMorrow and others (2002). The pilot study was conducted to provide insight into potential source regions and transport mechanisms for chemical and isotopic signals, and to demonstrate the validity of the comparative techniques. The results presented in this chapter for Event 29 show a more detailed investigation of the synoptic meteorology and back trajectory analysis not available at the time of the pilot study. The dates for P3 and Event 29 differ slightly. For the pilot study P3 was dated to involve accumulation from 21 – 28 December 1999 (Table 7.1; Chapter 7). Examination of the synoptic meteorology for P3 showed the influence of two cyclonic systems during the period, yet both systems involved a similar source region and transport path (Chapter 7). However, during the dating process outlined in this thesis (Chapter 5), the parameters set for defining an accumulation event differ slightly compared to the pilot study and resulted in the classification of Event 29 to involve accumulation from 27 – 31 December 1999 (Table 8.2).

In order to ensure consistency between the pilot study discussed in Chapter 7, and the results reported in McMorrow and others (2002), the dating for P3 was not re-defined in this thesis (in Chapter 7). It should be noted that the dates for the net accumulation steps do not differ between the pilot study (Chapter 7, McMorrow and others (2002)) and Chapter 8, rather the *grouping* of net accumulation days is refined in Chapter 5 of this thesis. This refined grouping for events is reflected in the discussion on Event 29 in Chapter 8. Re-defining the dates for Event 29 did not impact on the conclusions drawn from Chapter 7 and McMorrow and others (2002) as the same cyclonic system was found to dominate the synoptic meteorology.

8.3.2 Meteorological Tools

The discussion draws on three types of meteorological data. Local meteorological conditions at Law Dome are recorded by the co-located AWS. Parameters including atmospheric pressure (station-level pressure), air temperature, wind speed and wind direction are used in the analysis. Synoptic scale meteorological conditions are determined using a combination of AVHRR infrared satellite imagery and back trajectory analysis. AVHRR satellite imagery is obtained from the Antarctic Cooperative Research Centre (Neal Young, pers. comm., 2002). The images used in the analysis are chosen to reflect the cloud cover and circulation patterns influencing Law Dome in the days leading up to the accumulation event. Back trajectories are

obtained from the Bureau of Meteorology general circulation model (GASP modelled data) and provided by the University of Melbourne (Ian Simmonds, pers. comm., 2003). They are calculated using the 500 hPa level wind speed and direction from the GASP model of atmospheric conditions from the source region (Law Dome drilling site) on the date with the largest amount of net accumulation, and back calculated for ten days. The back trajectories indicate both the transport path and the speed of transport of the air mass influencing net accumulation events. The speed of transport is determined by the space between dots on the trajectories, with larger spaces representing faster movement along the trajectory caused by stronger wind speeds. The accuracy of the back trajectory decreases as time from the source input values increase. Therefore, faster trajectories are generally more accurate further back in distance than slower trajectories. The combination of high resolution chemical and isotopic records, and contemporaneous local and synoptic scale meteorology provides a comprehensive dataset for the comparative study.

8.3.3 Comparing Chemical and $\delta^{18}\text{O}$ Signals with Meteorological Observations

Event scale investigations are conducted by comparing chemical and isotopic signals preserved in the snow pits and firn core records with contemporaneous local and synoptic scale meteorological data. Section 8.4 provides an overview of the meteorological conditions across all four seasons. Results from the event-scale investigations, including comparisons between chemical and isotopic signals, and meteorological observations, are outlined in Sections 8.5 – 8.8 of this chapter. Within each section (season), the comparative results are drawn from the chemical and $\delta^{18}\text{O}$ records (Figs. 5.4 – 5.7; Chapter 5), and the local and synoptic meteorological conditions associated with each event (Figs. 8.1 – 8.17; Appendix 8A (summer); Figs. 8.18 – 8.32; Appendix 8B (autumn); Figs. 8.33 – 8.47; Appendix 8C (winter); Figs. 8.48 – 8.63; Appendix 8D (spring)). The comparative results are summarised in tables and grouped into seasons (Tables 8.2 – 8.5).

8.4 Meteorological Conditions Across All Four Seasons

8.4.1 Local Meteorological Conditions

Summer Events

The local meteorological conditions associated with each summer event indicate similar characteristics (Table 8.2; Figs. 8.1 – 8.4). Atmospheric pressure tends to be centred around the mean summer pressure of 826 hPa (Chapter 4), with Events 20, 42 and 30 showing an exception. Event 20 is associated with higher than mean summer pressures, and Events 42 and 30 exhibit lower than mean summer pressures. Air temperatures during summer events are also similar to mean summer values (-13°C , Chapter 4), falling within one standard deviation for summer events (6°C , Chapter 4). However, it is interesting to note that all events with the exception of Event 27 are associated with temperatures higher than mean levels for at least part of the accumulation period. This trend is consistent with the potential warm bias in accumulation events preserved in ice cores discussed in Chapter 4. Wind speeds during each summer event are relatively high and all events show higher than mean summer wind speeds (6 ms^{-1} , Chapter 4) for at least part of the accumulation period. Moreover, wind speeds tend to decline during the events (Figs. 8.1 – 8.4). High and declining wind speeds during an accumulation event is consistent with the approach of a cyclonic system or cloud cell, and the drop in wind speed provides an opportunity for snowfalls to accumulate and form part of the snow pit or ice core record. Finally, wind direction during each summer event varies between 90° and 145° , with most events exhibiting more easterly component winds around 110° .

The similarity in the local meteorology associated with each summer event suggests that these parameters are not reliable indicators to explain variations in summer chemical and $\delta^{18}\text{O}$ signals.

Autumn Events

The local meteorological conditions associated with each autumn event also indicate similar characteristics (Table 8.3; Figs. 8.18 – 8.20). Atmospheric pressure tends to be centred about the mean autumn pressure of 820 hPa (Chapter 4), with the exception of Event 10 (characterised by higher than mean pressure) and Event 37 (characterised by lower than mean pressure). Most events exhibit warmer than the mean levels of -26°C determined in Chapter 4 at some stage during the precipitation event. This is consistent with the warm bias for precipitation events discussed in further detail in Chapter 4. Events 13, 14, 17, 50 and 51 show

sustained warm temperatures over a number of days, consistent with the intrusion of a maritime air mass from either a cyclonic system (Events 14 and 51) or disorganised cloud (Event 17). In contrast, Events 12 and 37 show a large range in temperatures through the precipitation event. Event 12 indicates a sharp drop in air temperatures during the precipitation event, suggesting the intrusion of a cold air mass over Law Dome. Event 37 indicates the reverse conditions, consistent with the passing of a cold front over Law Dome, characterised by a warm front at the leading edge of the system, and cold air following the front. Wind speeds for the autumn events are generally higher than the average autumn wind speeds across the four year record (6 ms^{-1} , Chapter 4). Similar to the summer events, wind speeds tend to decline during the precipitation event, allowing snowfalls to settle and form the snow pit record. Event 15, associated with a disorganising cyclone, provides an exception to higher than average wind speeds with lower than average wind speeds recorded during the two day accumulation event. Finally, wind direction during the autumn events show some variance from the mean levels of 121° (Chapter 4). Events 17, 37 and 38 are centred around the mean autumn wind direction. Event 12 is characterised by more southerly wind directions, and Events 11, 14, 16 and 51 exhibit more easterly component winds.

Wind directions during the autumn events show some variance, yet the remaining local meteorological parameters indicate similar conditions for each event. This suggests that local meteorological conditions are not reliable indicators to explain variations in autumn chemical and isotopic signals.

Winter Events

The local meteorological conditions associated with each winter event indicate some variability (Table 8.4; Figs. 8.33 – 8.36). Event 8 is characterised by low atmospheric pressure and relatively warm temperatures compared to the mean winter pressure (821 hPa) and temperature (-26°C) for the four year record (see Chapter 4). Wind speeds during Event 8 are relatively high and involve wind speeds with a significant easterly component. These conditions are consistent with the influence of a strong cyclonic system passing over Law Dome. Events 9, 36, 46, 47 and 49 record local pressure and temperature levels that are closer to the mean winter levels determined in Chapter 4. It is interesting to note that six events (Events 6, 9, 36, 46, 47 and 49) are comparable to mean winter temperatures, while the other seasons tend to show more events with warmer than average temperatures. This effect is consistent with the relatively low standard deviation for winter temperatures (3.6°C ; Chapter 4) compared to other

seasons, and reflects a reduction in temperature variability during winter. Events 7, 24 and 48 show distinctly warmer than average temperatures, while Event 5 shows colder temperatures. Atmospheric pressure shows some variability between events, with Events 7 and 24 characterised by average winter pressure levels, and Events 5, 6 and 48 characterised by lower atmospheric pressure. The high wind speeds and easterly component winds during Events 7, 36 and 46 are also consistent with the influence of a strong cyclonic system on Law Dome. It is not possible to comment on the wind speed and wind direction observations during the remaining winter events due to sensor faults limiting data availability. Figures 8.33 – 8.36 indicate lengthy episodes through the winter periods where the wind sensors were faulty. The cause of this sensor failure is uncertain, although field observations suggest that sensor failure tends to occur during periods of cold, low wind events due to a build up of hoar frost on the sensors. However, these field observations were limited to the two (summer) field seasons conducted during this research, and therefore do not provide a definitive cause for wind sensor failure.

The increased variability in local meteorological conditions during winter events may indicate that local meteorology can be used to differentiate specific chemical and isotopic signals. Local meteorology is therefore considered, where appropriate, in further discussion on possible explanations for chemical and isotopic signals during winter events.

Spring Events

The local meteorological conditions associated with spring events show some variability (Table 8.5; Figs. 8.48 – 8.51). For events that concur with expected spring signals (Events 3, 4, 32, 33, 34 and 35), local atmospheric pressure levels are consistent with mean spring levels (819 hPa, Chapter 4) except for Event 32 where lower than mean pressure is recorded. For events that differ from expected signals (Events 2, 22, 31, 43, 44 and 45) there is a large range in atmospheric pressure. Atmospheric pressure levels during these “unusual” events are centred around the mean spring pressure, although the range in pressure tends to be larger than the standard deviation calculated in Chapter 4 (9.5 hPa), with the exception of Event 22 which involves accumulation over a single day. This larger range in atmospheric pressure for spring events may indicate the presence of intense cyclonic systems, and is consistent with the general poleward shift and increase in intensity in the circumpolar trough during spring (King and Turner, 1997). Of the 12 spring events examined here, 10 are associated with warmer than mean spring temperatures (-21°C, Chapter 4), consistent with the warm bias in precipitation

events that is discussed in Chapter 4. Events 2 and 23 are exceptions, with both events associated with colder than mean spring temperatures. Wind speeds during spring events are also generally higher than mean spring wind speeds (6ms^{-1} , Chapter 4), and consistent with the intrusion of cyclonic systems onto Law Dome. Finally, wind direction indicates a wide range of variability between the events. Events 4 and 32 are associated with the mean spring wind direction of 120° (see Chapter 4), while Events 33, 34, 22 and 45 are characterised by more easterly component winds. Events 31, 43 and 44 exhibit a wide range of wind directions during the precipitation event, and the remaining events did not record wind speed or direction data.

The increased variability in local meteorological conditions during spring events may indicate that local meteorology can be used to differentiate specific chemical or isotopic signals. Local meteorology is therefore considered, where appropriate, in further discussion on possible explanations for chemical and isotopic signals during spring events.

8.4.2 Synoptic Meteorological Conditions

Figures 8.5 – 8.17, 8.21 – 8.32, 8.37 – 8.47, 8.52 – 8.63 show AVHRR satellite imagery and back trajectories for events across all seasons. These images are used to infer the synoptic situation and transport paths for the air masses influencing Law Dome during each event. Synoptic conditions are also summarised in Tables 8.2 – 8.5.

At the synoptic scale there is a mixture of well developed, strong cyclonic systems, and weak, disorganised cloud activity for events across all seasons. Further, the event trajectories indicate a mixture of transport paths that include direct (straight line) trajectories from the source region, cyclonic trajectories similar in shape to the quasi-stationary cyclonic system located at $55\text{--}60^\circ\text{S}$, $60\text{--}90^\circ\text{E}$ (Jones and Simmonds, 1993), and disorganised trajectories that involve transport over some part of the Antarctic continent or along the Antarctic coastline prior to deposition at Law Dome. All seasons are associated with a mixture of the three descriptions of synoptic situations, implying there is no bias in the type of synoptic meteorology influencing particular seasons.

8.5 Summer Events Preserved in High Resolution Snow Pits and Firn Cores

Table 8.2: Summer events preserved in Law Dome snow pits and firn cores

Event Characteristics							Local Meteorology				Synoptic Meteorology		Chemical/ $\delta^{18}\text{O}$ Signal	Possible Explanation
Seasonal Pattern	Event Num.	Date Start	Date Finish	Date(s) with Highest Net Accumulation	Net Accum. (cm)	Pit or Core	Pressure (hPa)	Temp. ($^{\circ}\text{C}$)	Wind Speed (ms^{-1})	Wind Direction ($^{\circ}$)	Synoptic Situation*	Back Trajectory		
Concur	18	18 Jan 2001	24 Jan 2001	24 Jan 2001	10	Matilda	827 - 835	-12 to -8	2 – 8	90 – 140	strong cyclone	direct trajectory, low latitude ¹ source region to northwest of Law Dome, rapid** northwesterly approach	expected summer signals (high $\delta^{18}\text{O}$, MSA, non-sea salt sulphate, nitrate, low sea salts)	$\delta^{18}\text{O}$: warm temperatures compared to other seasons, distant source region, some fractionation expected along transport route MSA/non-sea salt sulphate: low and midlatitude source regions to northwest of Law Dome where there marine productivity is expected to be high Sea salts: strong cyclonic system mechanism for production of sea salt aerosols yet slow approach encourages rain-out of heavy sea salt aerosols Nitrate: unsure
Concur	19	5 Jan 2001	9 Jan 2001	9 Jan 2001	10	Matilda	817 – 830	-11 to -9	3 – 12	110	strong cyclone	cyclonic trajectory, midlatitude ² source region to northwest of Law Dome, slow northerly approach		
Concur	20	26 Dec 2000	29 Dec 2000	28 Dec 2000	7	Matilda	840 – 845	-15 to -8	3 – 13	90 – 160	strong cyclone	cyclonic trajectory, low latitude source region to northwest of Law Dome, slow northwesterly approach		
Concur	42	7 Dec 1998	8 Dec 1998	All days	3	Rama	810	-10	4 – 8	90	strong cyclone	direct trajectory, midlatitude source region northwest of Law Dome, slow northwesterly approach		
Concur	27	3 Feb 2000	4 Feb 2000	4 Feb 2000	10	Rama	826 – 831	-17 to -15	5 – 8	145	disorganised cloud cells	disorganised trajectory, low latitude source region to north of Law Dome further back in time, slow southerly approach	expected summer signals (high $\delta^{18}\text{O}$, MSA, non-sea salt sulphate, nitrate, low sea salts)	$\delta^{18}\text{O}$: warm temperatures compared to other seasons, local source region and limited fractionation MSA/non-sea salt sulphate: high marine productivity expected over local sea ice zone Sea salts: limited sea salt aerosols expected over sea ice zone Nitrate: unsure
Concur	28	24 Jan 2000	25 Jan 2000	25 Jan 2000	9	Rama	820 – 827	-12	7 – 11	110 – 120	disorganised cloud cells	disorganised trajectory, midlatitude source region to northwest of Law Dome further back in time, slow southerly approach		
Concur	41	27 Dec 1998	29 Dec 1998	All days	4	Rama	827 - 830	-13 to -11	10 – 14	130	disorganised cloud cells	disorganised trajectory, high latitude ³ source region to northwest of Law Dome further back in time, slow northeasterly approach		
Differ	1	11 Dec 2001	23 Dec 2001	18 Dec 2001	10	Matilda	811 – 839	-17 to -8	2 – 9	110 – 270	weak cyclone	cyclonic trajectory, midlatitude source region to nothwest of Law Dome, slow northerly approach	high sea salts***	Sea salts: northerly approach and minimal transport over sea ice zone (maximum transport over open ocean) encourages increased sea salt aerosols production
Differ	25	27 Feb 2000	27 Feb 2000	27 Feb 2000	6	Rama	820	-14	10	120	disorganising cyclone	cyclonic trajectory, mid-high latitude source region to northwest of Law Dome, slow northerly approach		
Differ	21	30 Nov 2000	3 Dec 2000	All days	8	Matilda	823 – 830	-11	3 – 16	120 – 130	disorganised cloud cells	disorganised trajectory, continental source region, slow southerly approach	low MSA, mid non-sea salt sulphate, high nitrate*	MSA: continental air mass Non-sea salt sulphate/nitrate: intrusion of stratospheric air mass
Differ	29	27 Dec 1999	31 Dec 1999	28 Dec 1999	11	Rama	822 – 830	-17 to –9	6 – 15	110 – 150	strong cyclone	cyclonic trajectory, midlatitude source region to northwest of Law Dome, rapid transport and then slow approach from northwest	enhanced MSA, non-sea salt sulphate*	MSA/non-sea salt sulphate: midlatitude source region to northwest of Law Dome where marine productivity is expected to be high
Differ	26	24 Feb 2000	24 Feb 2000	24 Feb 2000	14	Rama	832	-14	10	110	strong cyclone	cyclonic trajectory, low latitude source region to north of Law Dome, slow northeasterly approach	low MSA, non-sea salt sulphate*	MSA/non-sea salt sulphate: low latitude source region to north of Law Dome where marine productivity expected to be low
Differ	30	18 Dec 1999	23 Dec 1999	23 Dec 1999	7	Rama	810 – 825	-20 to -10	3 – 14	100 - 360	strong cyclone	cyclonic trajectory, low latitude source region to northwest of Law Dome, rapid approach from northwest	mid-range MSA, non-sea salt sulphate*	MSA/non-sea salt sulphate: low latitude source region, possibly indicates low latitudes are characterised by lower marine productivity compared to midlatitudes

* The synoptic situation describes the ‘intensity’ of the cyclonic system, using AVHRR satellite imagery and comparing events across the complete dataset examined in this thesis. Strong cyclonic systems are characterised by a well defined and tight ‘comma’ shape to the cloud patterns, while weak cyclonic systems are characterised by a less defined ‘comma’ shape and lower cloud intensity.

¹ Low latitudes defined as 35 – 45 °S.

** ‘Rapid’ transport is determined using a combination of storm tracking using AVHRR satellite imagery, and comparing the speed of the back trajectory for this system with other back trajectories examined in this research (see Appendices A-D).

² Midlatitudes defined as 45 – 55 °S.

³ High latitudes defined as > 55 °S.

*** Other species characterised by expected summer signals

8.5.1 Events that Concur with Expected Summer Chemical and Isotopic Signals

Of the thirteen summer events examined in this study, seven events concur with expected summer chemical and isotopic signals, namely high levels of $\delta^{18}\text{O}$, MSA, non-sea salt sulphate and nitrate, and low concentrations of sea salts (Table 8.2). Four of these events are associated with strong cyclonic systems, while three events are associated with disorganised cloud cells.

A similar transport path is evident for the four events characterised by strong cyclonic systems (Events 18, 19, 20 and 42), and each air mass is sourced from the low latitudes to the northwest of Law Dome (Figs. 8.5 – 8.7, 8.11). The trajectories for Events 19 and 42 show a cyclonic pattern associated with the quasi-stationary cyclone located to the northwest of Law Dome with a northerly (Event 19) or northwesterly (Event 42) approach to Law Dome (Figs. 8.6, 8.11). Event 18 also falls into this pattern, although the trajectory shows a faster, more direct route from the low latitudes and approaching Law Dome from the northwest (Fig. 8.5). Event 20 shows a slightly different trajectory with the air mass projecting into lower latitudes (35°S) (Fig. 8.7). The cyclonic synoptic meteorology associated with these four summer events suggest a distant (low latitude) source region and rapid advection of air to Law Dome.

The remaining three summer events that concur with expected chemical and isotopic signals (Events 27, 28 and 41) are characterised by disorganised cloud activity (Table 8.2; Figs. 8.8 – 8.10). All three trajectories indicate the air mass travelled through the region to the northwest of Law Dome, yet the meridional extent of the trajectory is varied. Event 27 is characterised by a trajectory extending into low latitudes (42°S), while trajectories for Events 28 and 41 are limited to a higher latitude zone (55-60°S). Moreover, the transport path is less direct for these events compared to the four cyclonic summer events, and the trajectories indicate the air mass travelled over the Antarctic continent before reaching Law Dome. It is interesting to note that all three trajectories associated with disorganised cloud systems show a slow approach of the air mass over the sea ice zone before reaching the Antarctic coastline. The slow and disorganised transport mechanisms influencing these events suggest that the chemical and isotopic signals are likely to be associated with a local (high latitude) source region.

The two discrete synoptic situations and associated transport mechanisms for these similar summer events implies two distinct processes may influence Law Dome during “typical” summer periods.

$\delta^{18}\text{O}$

Rapid advection of air from low latitudes is consistent with the high $\delta^{18}\text{O}$ signals maintained in the snow pit record for the cyclonic events (Events 18, 19, 20 and 42). Long range transport of an air mass from the low latitudes will generally result in substantial fractionation of heavy isotopes (^{18}O), leading to low $\delta^{18}\text{O}$ values in polar regions. However, if rapid advection occurs, there is limited time available for fractionation during transport and the air mass will maintain a higher $\delta^{18}\text{O}$ signal. In contrast, the disorganised trajectories associated with Events 27, 28 and 41 are more likely to reflect a high latitude source region. The disorganised events are associated with shorter transport distances between the high latitude source region and Law Dome. Shorter transport distances will limit the amount of fractionation of the heavy (^{18}O) isotope prior to precipitation at Law Dome, leading to a relatively high $\delta^{18}\text{O}$ signature in the ice core.

The discussion presented above provides an indication of two potential processes that may produce a similar $\delta^{18}\text{O}$ signature in the snow pit or ice core record. Further sections of this chapter will examine other synoptic situations associated with specific $\delta^{18}\text{O}$ signals to build on these results.

Marine Biogenic Indicators: MSA and Non-Sea Salt Sulphate

High summer concentrations of the marine biogenic sulphur compounds (MSA, non-sea salt sulphate) are generally attributed to increased biological activity in the Southern Ocean during summer (eg. Legrand and Pasteur, 1998; Curran and others, 1998a). The dissolved trace ion species such as MSA and non-sea salt sulphate are more likely to be characterised by a dynamic transport process. That is, MSA and non-sea salt sulphate aerosols will be “picked up” and “rained out” continuously along the trajectory. The combination of processes such as increased wave activity (lofting more marine aerosols into the atmosphere), increased DMS production, and direct transport from biologically productive areas will influence the final marine biogenic sulphur signals associated with Antarctic precipitation. It is beyond the scope of this study to identify increased DMS production, however previous research into the spatial distribution of DMS may provide an indication of likely productive areas.

The high MSA and non-sea salt sulphate concentrations preserved during the cyclonic events (Events 18, 19, 20 and 42) are consistent with a combination of increased wave activity from the strong cyclonic system and advection of marine biogenic sulphur from a low latitude region

associated with high concentrations of marine biota. The area around Heard Island (50°S, 70°E) is a known area of marine productivity at this time of year (Curran and others, 1998b), and all four cyclonic trajectories indicate rapid transport from this region to Law Dome.

In contrast, the disorganised trajectories and high latitude source region associated with Events 27, 28 and 41 suggest the sea ice zone may provide an important source of marine biogenic sulphur for these local events. This result is more consistent with previous studies that have attributed MSA and non-sea salt sulphate enhancement during summer to the release of biota from melting sea ice during spring (Smith and Nelson, 1986; Knox, 1994; Legrand and Pasteur, 1998). The decay of marine biota at the edge of the sea ice and within cracks and leads in the sea ice zone during summer is an expected summer source of marine biogenic sulphur, yet direct transport from low latitude source regions through strong cyclonic events may also be an important process influencing summer MSA and non-sea salt sulphate signals at Law Dome.

Sea Salts

The low sea salt concentrations observed during these four events appears to be inconsistent with the strong cyclonic systems and rapid advection of marine air onto Law Dome. Previous studies have attributed low summer sea salt concentrations to the reduced intensity of cyclonic systems in the Southern Ocean during summer (Legrand and others, 1998; Curran and others, 1998a; Wagenbach and others, 1998a). Less intense cyclonic systems are characterised by lower wind speeds and produce smaller waves that, in turn, restrict the amount of sea salt particles lofted into the atmosphere. However, the results presented here for these four summer events show an important transport mechanism that is consistent with low sea salt concentrations preserved in the Law Dome snow pits. All four summer events associated with strong cyclonic systems show an air mass with a slow trajectory over the sea ice zone on approach to Law Dome. Sea salt aerosols that are lofted into the atmosphere over the open ocean are relatively large, and during transport of the air mass these large sea salt aerosols are readily “rained out” (Fitzgerald, 1991). The slow approach of the air mass towards Law Dome gives an opportunity for the large sea salt aerosols to “rain out”, leaving an air mass depleted in sea salt aerosols.

Nitrate

The Antarctic nitrate signal is complex and potential sources for nitrate preserved in Antarctic snow include dissolved organic nitrate from the ocean (Skoog and others, 2001), downward stratospheric transport of nitrogen originating in the atmosphere from lightning (Legrand and Delmas, 1986)), the oxidation of nitric acid (Legrand and others, 1989), the formation of polar stratospheric clouds comprised mainly of nitric acid (Legrand and Kirchner, 1990), and the formation of odd nitrogen species through incident solar and geomagnetic charged particles (Dreschhoff and Zeller, 1998). The mechanisms influencing the nitrate signal during with these summer events remains uncertain due mainly to the complexity of the potential sources for Antarctic nitrate.

8.5.2 Events that Differ from Expected Summer Chemical and Isotopic Signals

The six remaining summer events (Events 1, 25, 21, 29, 26, 30) differ from the expected summer chemical and isotopic signals (Table 8.2). Investigation of signals that vary from the expected summer events are useful for two reasons. First, differences in the climatic conditions observed during “typical” (events that show expected seasonal signals (see Section 8.2)) and “unusual” events (events that differ from expected seasonal signals) provides further evidence for the importance of particular climate conditions that produce “typical” summer signals. Second, identifying the potential source region and transport mechanism for an event with a particular chemical and isotopic signal can enhance our understanding of potential climate conditions influencing similar events preserved in deeper ice cores where contemporaneous meteorological observations are unavailable.

Enhanced Summer Sea Salts (Events 1 and 25)

Events 1 and 25 are associated with enhanced concentrations of sea salts, diverting from the low concentrations typically found during summer periods at Law Dome (Figs. 5.4, 5.6; Chapter 5). All other chemical and $\delta^{18}\text{O}$ signals are similar to those expected for summer levels and include high levels of MSA, non-sea salt sulphate $\delta^{18}\text{O}$. Event 1 involves accumulation from 18 – 24 December 2001 (mid-summer) and is associated with a weak cyclonic system (Fig. 8.12). The back trajectory shows a source region from the midlatitudes (50°S, 70°E) with the air mass moving quickly from the midlatitudes towards Law Dome and approaching Law Dome from the north. Event 25 involves accumulation on 27 February 2000 (late summer) and is associated with disorganising cloud cells from weak cyclonic systems that developed around 58°S, 95°E (Fig. 8.13). The back trajectory shows a source region at a higher latitude compared

to Event 1, yet the transport path is similar and indicates the air mass approaches Law Dome from the north.

High summer sea salt concentrations have previously been attributed to intense cyclonic systems intruding onto Law Dome (Curran and others, 1998a; Palmer, 2002). Events 1 and 25 indicate that high sea salt concentrations can be associated with weak cyclonic systems. These examples suggest factors other than cyclone intensity may influence the sea salt signal. Both enhanced sea salt events involve an air mass that approaches Law Dome from due north. In contrast, the low summer sea salt events described in the previous section are associated with an air mass that approaches Law Dome from the east or northeast. The approach of the air mass from due north of Law Dome is consistent with a more direct transport path from the open ocean towards Law Dome, facilitating uplift of sea salt aerosols along the trajectory. The northerly approach may explain the enhanced summer sea salt signals observed at Law Dome, and implies that atmospheric circulation variations are an important factor influencing the summer sea salt signal.

The influence of circulation changes on the Law Dome sea salt signal has implications for interpreting deep ice cores. Past climate reconstruction of the sea salt record has generally interpreted high sea salt concentrations as the result of increased storminess in the Southern Ocean (Curran and others, 1998a; Palmer, 2002). In addition, recent studies have highlighted the potential for the sea ice zone and the formation of frost flowers on the sea ice to produce high sea salt signals (Perovich and Richter-Monge, 1994; Ranikin and others, 2000; Rankin and others, 2004). However, the results presented here highlight the potential sensitivity of the Law Dome region to changes in atmospheric circulation patterns associated with changing global climate. The link between atmospheric circulation patterns and sea salt signals from other seasons will be explored further in subsequent sections of this Chapter.

Deviation Between MSA and Non-Sea Salt Sulphate (Event 21)

The sulphur compounds (MSA, non-sea salt sulphate) observed in Antarctic precipitation tend to coincide during summer and are generally attributed to a marine biogenic source (Legrand, 1997; Curran and others, 1998a; Minikin and others, 1998). However, Event 21 provides an example where the MSA and non-sea salt sulphate signals differ during summer (Fig. 5.6; Chapter 5). MSA concentrations are declining, while non-sea salt sulphate concentrations indicate a distinct peak. Further, the non-sea salt sulphate peak coincides with a similar peak in

nitrate. MSA is a unique species that is only sourced from marine biogenic activity, while non-sea salt sulphate may have multiple sources including volcanic activity, mineral dust and stratospheric input (Legrand, 1995; Legrand, 1997; Minikin and others, 1998).

Event 21 involves accumulation from 30 November – 3 December 2000 (early summer) and is associated with weak cloud cells over Law Dome (Fig. 8.14). The back trajectory shows the air mass travelled over inland Antarctica prior to reaching Law Dome (Fig. 8.14). The low concentrations of MSA and sea salts are consistent with an air mass that has travelled over the Antarctic continent and indicate that the signal is not influenced by a marine air mass. The simultaneous peaks in non-sea salt sulphate and nitrate suggest the non-sea salt sulphate signal is sourced from a location or process that is linked with nitrate rather than marine biogenic sulphur.

Downward mixing of stratospheric air provides a potential mechanism for the co-deposition of non-sea salt sulphate and nitrate. Stratospheric intrusion of nitrate and non-sea salt sulphate species is consistent with the timing of the breakdown of the polar vortex, and the formation of polar stratospheric clouds, at this time of year (Legrand and Kirchner, 1990). Event 21 is dated for early summer, and the chemical and $\delta^{18}\text{O}$ signature appears to be more consistent with expected signals during spring rather than summer (see Chapter 6). Spring events are examined in more detail in Section 8.8 of this chapter.

Enhancement of Summer Marine Biological Indicators (Event 29)

Event 29 is characterised by enhanced summer signals of the marine biogenic indicators (MSA, non-sea salt sulphate) (Fig. 5.6; Chapter 5). Concentrations of MSA and non-sea salt sulphate reach $1.6\mu\text{EqL}^{-1}$ and $2.8\mu\text{EqL}^{-1}$ respectively, considerably higher than the average concentrations of MSA ($0.10\mu\text{EqL}^{-1}$) and non-sea salt sulphate ($0.85\mu\text{EqL}^{-1}$) from longer term studies at Law Dome (Anne Palmer, pers. comm., 2005).

The synoptic meteorology observed during Event 29 involves the presence of a strong cyclonic system to the northwest of Law Dome with a well developed front passing over Law Dome on 28 December 1999 (Fig. 8.15). The frontal cloud band extends well into the low latitudes, providing the mechanism for circulating air onto Law Dome. The back trajectory supports this cyclonic circulation, with the source region located around Heard Island (50°S , 70°E) and the

air mass moving quickly towards Law Dome. The trajectory shows the air mass slowing down over the sea ice zone and approaching Law Dome from the northwest.

The enhancement of marine biological indicators (MSA, non-sea salt sulphate), as well as a pronounced peak in $\delta^{18}\text{O}$, may be explained by rapid advection of air from the low latitudes. This theory was presented above for the four cyclonic summer events that concur with expected summer signals. These events show similar transport paths from the Heard Island region. Heard Island is a known area of high concentrations of marine biota (Curran and others, 1998b), and rapid advection of the air mass from this region is consistent with enhanced marine biogenic indicators in the snow pit. Further, rapid advection of low latitude air is consistent with the pronounced peak in $\delta^{18}\text{O}$. However, these factors do not adequately explain the difference between the enhancement of marine biogenic signals for Event 29, and the lower MSA and non-sea salt sulphate concentrations comparable to average summer levels and associated with the four cyclonic events sourced from this same region. Possible explanations may include variability in the source of DMS production for this particular time period, the time the parcel of air has been in contact with the ocean surface along the trajectory, or the extent the MSA and non-sea salt sulphate aerosols have been “rained out” by precipitation along the trajectory. It is beyond the scope of this thesis to examine the potential influence of these factors, yet the analysis does indicate the likelihood that the Heard Island region is an important source region for marine biogenic sulphur compounds for Law Dome.

Low or Declining Marine Biological Indicators (Events 26 and 30)

Events 26 and 30 are associated with low or declining concentrations of the marine biogenic indicators (MSA, non-sea salt sulphate) (Fig. 5.6; Chapter 5), diverting from the high concentrations typically found in summer snow at Law Dome. $\delta^{18}\text{O}$ values and sea salt concentrations for these events are comparable to average summer concentrations at Law Dome, and are characterised by high $\delta^{18}\text{O}$ and low sea salt concentrations (Fig. 5.6; Chapter 5).

Event 26 involves accumulation on 24 February 2000 (late summer). This single day of accumulation is associated with a strong cyclonic system that began developing on 21 February in the region 55°S, 105°E (Fig. 8.16). The back trajectory shows a source region in the low latitudes just south of Australia (35°S, 120°E). The air mass moves quickly from the low latitudes to Law Dome, slowing down from 60°S and approaching Law Dome from the northeast. This trajectory differs from events that concur with expected summer signals, and

the air mass is sourced from the coastline south of Australia rather than the Heard Island region. Heard Island is a known area of marine biological activity, while the region south of Australia is generally characterised by lower concentrations of marine biota (Curran and others, 1998b). A source region just south of Australia is consistent with low concentrations of MSA and non-sea salt sulphate. The low sea salt concentrations can be explained by the slowing of the air mass over the sea ice zone on approach to Law Dome, allowing “rain out” of the heavy sea salt aerosols before reaching Law Dome.

Event 30 involves accumulation from 18 – 23 December 1999 (mid-summer) and is characterised by a strong cyclonic system that developed in the region 45°S, 70°E (Fig. 8.17). The back trajectory shows a fast moving air mass that is sourced from low latitudes (42°S), north of the Heard Island region. The air mass is sourced from a warm region where both temperature and concentrations of marine biota are expected to be high. The snow pit record shows a distinct trough in non-sea salt sulphate, $\delta^{18}\text{O}$ and MSA, although concentrations are still in the mid-high range (Fig. 5.6; Chapter 5). The rapid transport of the air mass is expected to result in high $\delta^{18}\text{O}$ values preserved in the snow pit due to rapid advection of the air from low latitudes and limited time available for fractionation of the heavy (^{18}O) isotope. The mid-concentrations of MSA and non-sea salt sulphate are consistent with a source region where marine productivity is high, but may indicate the more northerly source region has resulted in increased “rain out” of the marine biogenic sulphur compounds during transport.

Events 26 and 30 both show a source region characterised by lower latitudes when compared with the Heard Island source region observed during the cyclonic summer events that show higher MSA and non-sea salt sulphate signals. This finding highlights the potential sensitivity of marine biogenic indicators (MSA, non-sea salt sulphate) preserved in Law Dome ice cores to changes in atmospheric circulation.

8.5.3 Concluding Remarks: Summer

This section examined a number of events preserved in Law Dome snow pits during summer months. Events that concur with expected summer signals, namely high levels of MSA, $\delta^{18}\text{O}$, non-sea salt sulphate and nitrate, and low concentrations of sea salts are associated with a mixture of strong cyclonic systems and disorganised cloud cells. The strong cyclonic events are characterised by trajectories that indicate a source region to the north west of Law Dome, while the disorganised trajectories suggest a higher latitude and more localised source region.

The high $\delta^{18}\text{O}$ signals during events that concur with expected summer signals were found to be associated with two distinct processes. During the strong cyclonic events, rapid advection of air from low latitudes will restrict fractionation of heavy (^{18}O) isotopes and result in a high $\delta^{18}\text{O}$ signal. In contrast, the high $\delta^{18}\text{O}$ signals observed for the disorganised events and associated local (high latitude) source regions is likely to be the result of limited fractionation of heavy (^{18}O) isotopes due to the short transport distance between the source and Law Dome.

Summer marine biogenic sulphur compounds are expected to be sourced from the sea ice zone (Legrand and Pasteur, 1998). However, the Heard Island region (50°S, 70°E) to the northwest of Law Dome, a known area of marine productivity, may provide an important additional source region for summer MSA and non-sea salt sulphate during strong cyclonic events. Moreover, a particular event that preserved enhanced summer concentrations of MSA and non-sea salt sulphate was found to be associated with rapid advection of air from this region, providing further evidence for the potential importance of the Heard Island region for marine biological indicators at Law Dome.

The low sea salt concentrations observed during events that concur with expected summer signals are attributed to two effects. First, the weaker cyclones observed during summer result in reduced uplift of sea salt aerosols compared to the stronger winter events. Second, the slow transport of the air mass over the sea ice zone to Law Dome allows “rain out” of the heavy sea salt particles. This theory was supported by comparing the trajectories of the low sea salt events with summer events characterised by high sea salts. The low sea salt events were characterised by a north-easterly approach to Law Dome. In contrast, the high sea salt events were associated with trajectories that showed a due north approach to Law Dome. The approach of the air mass from due north of Law Dome is consistent with a more direct transport path from the open ocean towards Law Dome, facilitating uplift of sea salt aerosols

along the trajectory. The northerly approach may explain enhanced summer sea salt events, and implies that atmospheric circulation variations are an important factor influencing the summer sea salt signal.

Finally, the mechanisms influencing the nitrate signals during summer events remains uncertain due mainly to the complexity of the potential sources of Antarctic nitrate. However, the examination of a particular event characterised by high nitrate and non-sea salt sulphate, and low MSA, indicates the potential for stratospheric input of nitrate and non-sea salt sulphate. This event is dated as early summer, and may be more indicative of a spring chemical and isotopic signature.

8.6 Autumn Events Preserved in High Resolution Snow Pits and Firn Cores

Table 8.3: Autumn events preserved in Law Dome snow pits and firn cores

Event Characteristics							Local Meteorology				Synoptic Meteorology		Chemical/ $\delta^{18}\text{O}$ Signal	Possible Explanation
Seasonal Pattern	Event Num.	Date Start	Date Finish	Date(s) with Highest Net Accumulation	Net Accum. (cm)	Pit or Core	Pressure (hPa)	Temp. (°C)	Wind Speed (ms^{-1})	Wind Direction (°)	Synoptic Situation	Back Trajectory		
Concur	13	8 Apr 2001	9 Apr 2001	9 Apr 2001	24	Matilda	817 – 822	-12 to -8	7 – 14	100 – 140	weak cyclone	cyclonic trajectory, midlatitude ⁴ source region to northwest of Law Dome, slow northerly approach	expected autumn signals (declining $\delta^{18}\text{O}$, MSA, non-sea salt sulphate, nitrate, increasing sea salts)	$\delta^{18}\text{O}$: cooling temperatures, distant source region, some fractionation expected along transport route MSA/non-sea salt sulphate: reduction in biological activity as autumn progresses Sea salts: strong cyclonic system mechanism for production of sea salt aerosols yet slow approach encourages rain-out of heavy sea salt aerosols resulting in mid concentrations Nitrate: unsure
Concur	50	14 May 1998	18 May 1998	14 May 1998	20	S0k	800 – 830	-22 to -17	7 – 15	110 – 130	strong cyclone	cyclonic trajectory, midlatitude source region to northwest of Law Dome, slow northerly approach		
Differ	11	9 May 2001	12 May 2001	All days	16	Matilda	825 – 835	-22 to -15	6 – 17	80 – 120	strong cyclone	disorganised trajectory, high latitude ⁵ source region northwest of Law Dome, slow northwesterly approach	low sea salts*	Sea salts: slow approach encourages rain-out of heavy sea salt aerosols
Differ	12	28 Apr 2001	5 May 2001	28 Apr 2001	24	Matilda	810 – 827	-27 to -20	2 – 11	120 – 160	strong cyclone	disorganised trajectory, high latitude source region to northwest of Law Dome, slow northerly approach		
Differ	14	30 Mar 2001	2 Apr 2001	30 Mar 2001	11	Matilda	817 – 830	-16 to -12	0 – 15	80 – 100	strong cyclone	cyclonic trajectory, midlatitude source region to northwest of Law Dome, slow easterly approach		
Differ	51	11 May 1998	13 May 1998	12 May 1998	8	S0k	817 – 820	-20 to -17	15 – 21	110	strong cyclone	cyclonic trajectory, mid-high latitude source region to northwest of Law Dome, slow northerly approach		
Differ	10	23 May 2001	23 May 2001	23 May 2001	10	Matilda	840	-15	10	110	strong cyclone	cyclonic trajectory, low latitude ⁶ source region to north of Law Dome, rapid northerly approach	low sea salts*	Sea salts: unsure, expect high sea salts from rapid trajectory, could indicate low latitude source region
Differ	15	28 Mar 2001	29 Mar 2001	All days	6	Matilda	823	-11	1	100	disorganising cyclone	direct trajectory, low latitude source region to north of Law Dome, rapid northerly approach		
Differ	37	19 May 1999	22 May 1999	19 May 1999	4	Rama	805 – 813	-30 to -21	1 – 7	110 – 120	weak cyclone	direct trajectory, high latitude (coastline) source region to west of Law Dome, slow westerly approach	low sea salts*	Sea salts: transport path over coastline and sea ice zone, no transport over open ocean
Differ	16	23 Mar 2001	29 Mar 2001	27 Mar 2001	17	Matilda	823 – 841	-21 to -13	12 – 15	70 – 90	strong cyclone	direct trajectory, low latitude source region, rapid northerly approach	high MSA, non-sea salt sulphate, $\delta^{18}\text{O}$ (Event 16), low sea salts (Event 17)*	MSA/non-sea salt sulphate: rapid advection of air from known area of biological activity $\delta^{18}\text{O}$ (Event 16): rapid advection from low latitudes Sea salts (Event 17): slow easterly approach over sea ice zone encourages rain-out of heavy sea salt aerosols
Differ	17	28 Feb 2001	3 Mar 2001	3 Mar 2001	13	Matilda	812 – 824	-16 to -11	3 – 10	110 – 125	disorganised cloud cells	cyclonic trajectory, midlatitude source region to northwest of Law Dome, slow easterly approach		
Differ	38	13 Mar 1999	13 Mar 1999	13 Mar 1999	7	Rama	820 – 826	-21 to -15	8 – 10	120	strong cyclone	cyclonic trajectory, low latitude source region to northwest of Law Dome, rapid northeasterly approach	high non-sea salt sulphate, mid nitrate, $\epsilon\eta\alpha\nu\chi\epsilon\delta$ sea salt peak*	Non-sea salt sulphate/nitrate: unsure, could indicate intrusion of stratospheric air mass Sea salts: rapid trajectory from oceanic region

⁴ Midlatitudes defined as 45 – 55 °S.
⁵ High latitudes defined as > 55 °S.
* Other species characterised by expected autumn signals
⁶ Low latitudes defined as 35 – 45 °S.

8.6.1 Events that Concur with Expected Autumn Chemical and Isotopic Signals

Of the twelve autumn events examined in this study, only two events (Events 13 and 50) concur with expected autumn chemical and isotopic signals, namely declining levels of $\delta^{18}\text{O}$, MSA, non-sea salt sulphate, nitrate and increasing concentrations in sea salts (Table 8.3). Both these events are characterised by cyclonic systems, although the intensity of each cyclone is varied. Event 13 is characterised by a weak cyclone, determined by the absence of a well defined cyclonic signature in the cloud, yet the system itself involves thick cloud. This cyclone developed at relatively high latitudes to the west of Law Dome (65°S , 90°E) and moved due east before dissipating over Law Dome (Fig. 8.21). Conversely, Event 50 is associated with a strong cyclone with a well defined cyclonic shape in the cloud system. This cyclone also developed within the same high latitude band to the northwest of Law Dome (60°S , 105°E) (Fig. 8.22). The back trajectories show that Event 13 involves transport from the midlatitude region to the north of Heard Island despite the high latitude development of the cyclone (Fig. 8.21). However, the trajectory also indicates that the approach to Law Dome is relatively slow, and this reduces the level of confidence in the accuracy of the earlier section of the trajectory. It is more likely, given the weak cyclone development in the high latitudes, that the chemical and $\delta^{18}\text{O}$ signals are also influenced by these higher latitudes. In contrast, Event 50 is characterised by a much tighter trajectory and a source region constrained to the high latitude area to the northwest of Law Dome ($50\text{--}55^{\circ}\text{S}$) (Fig. 8.22).

The identification of only two autumn events that concur with expected autumn signals may indicate that autumn tends to be characterised by increased variability in meteorological conditions and atmospheric circulation. Increased variability in meteorological conditions is expected to result in enhanced variability in the chemical and $\delta^{18}\text{O}$ signals for autumn events. Longer term seasonality studies of the ice core that determine the seasonal cycle through a composite of a number of years are unlikely to capture this autumn variability. Previous seasonality studies for Law Dome ice cores have tended to concentrate on the well defined summer and winter variability in chemical and isotopic signals, with autumn and spring signals more difficult to determine (Morgan and van Ommen, 1997; Curran and others, 1998a, Palmer 2002, Curran and others, 2002). The high resolution, well dated snow pits presented here provide evidence that autumn chemical and isotopic signals may involve enhanced variability compared to other seasons.

Enhanced variability in autumn events may, in part, be due to the transitional nature of the autumn season. The autumn months are characterised by shifting meteorological patterns in the Southern Ocean as the circumpolar trough shifts poleward and the general intensity of the cyclones increase (King and Turner, 1997). Moreover, studies show that the circumpolar trough is characterised by a semi-annual oscillation where minimum pressures are recorded during autumn and spring. Declining levels of $\delta^{18}\text{O}$, MSA, nitrate and non-sea salt sulphate, and increasing concentrations of sea salts are consistent with shifting meteorological patterns during autumn.

$\delta^{18}\text{O}$

The mid $\delta^{18}\text{O}$ levels for the two events that concur with expected autumn signals can be explained by cooling temperatures in the Southern Ocean during autumn. In addition, the back trajectories indicate these events are sourced from the midlatitudes, and fractionation of the heavy (^{18}O) isotope is expected to occur during transport to Law Dome. The mid $\delta^{18}\text{O}$ levels is likely to be a result of both cooling temperatures and $\delta^{18}\text{O}$ fractionation during transport from the midlatitudes.

Marine Biogenic Indicators: MSA and Non-Sea Salt Sulphate

The mid-level and declining concentrations in the marine biogenic sulphur compounds (MSA, non-sea salt sulphate) are also consistent with the transitionary nature of autumn. Biological productivity in the Southern Ocean diminishes at the end of summer and as autumn progresses, resulting in markedly reduced levels of DMS production and marine biogenic sulphur lofted into the atmosphere (Curran and Jones, 2000). In addition, as the circumpolar trough shifts poleward during autumn, the uplift of marine biogenic particles into the atmosphere is likely to occur in the region of cyclogenesis, which follows the poleward migration of the circumpolar trough (King and Turner, 1997). High latitudes are not expected to be associated with biological activity at this time of year (Curran and Jones, 2000), and the more southerly source region for MSA and non-sea salt sulphate is consistent with declining marine biogenic indicators in the snow pit record.

Sea Salts

The explanation for mid-concentrations and increasing sea salts for the two events that concur with expected autumn signals is unclear. It is expected that a well developed cyclonic system that formed close to Law Dome would result in high sea salt concentrations. However, the

trajectories for both these autumn events indicate the air masses slowed down on approach to Law Dome, providing a mechanism for some of the sea salts to “rain out” over the sea ice zone before reaching Law Dome.

Nitrate

The nitrate signals preserved during both autumn events that concur with expected seasonal signals provide limited insight into the nitrate cycle influencing Law Dome during autumn. Event 13 is characterised by low nitrate concentrations with a signature determined by three small peaks coinciding with similar peaks in non-sea salt sulphate (Fig. 5.3; Chapter 5). Due to the absence of a similar signal in the MSA record, the non-sea salt sulphate features are probably not reflecting a marine biogenic signal. The nitrate and non-sea salt sulphate signals may reflect a stratospheric input during this event, however stratospheric downward mixing of air is not expected at this time of year (Legrand and Kirchner, 1990). Further studies into the link between nitrate and non-sea salt sulphate may provide a greater understanding of the autumn nitrate signal.

8.6.2 Events that Differ from Expected Autumn Chemical and Isotopic Signals

The 10 remaining autumn events (Events 10, 11, 12, 14, 15, 16, 17, 37, 38 and 51) differ from expected autumn chemical and isotopic signals (Table 8.3). Investigation of signals that vary from the expected autumn events are particularly useful due to the identification of only two events that concur with expected autumn signals. As discussed above, the transitional nature of the autumn season may result in a higher variability in autumn chemical and isotopic signals compared to other seasons.

Low Autumn Sea Salts (Events 10, 11, 12, 14, 15, 37 and 51)

Events 10, 11, 12, 14, 15, 37 and 51 are associated with low concentrations of sea salts and divert from the expected higher or increasing sea salts for autumn events (Figs. 5.4, 5.6, 5.7; Chapter 5). All other chemical and isotopic concentrations are comparable to typical autumn signals. The Southern Ocean is characterised by a marked shift in the position and strength of the circumpolar trough in the equinoctial seasons (autumn and spring), with the development of more intense cyclonic systems closer to the Antarctic continent during autumn and spring (King and Turner, 1997). It is expected that this deepening of the circumpolar trough in autumn would tend to produce ice core signals with high sea salt concentrations. Intense cyclonic systems provide a mechanism for the production of sea salt aerosols over the Southern Ocean,

and the high latitude formation of the cyclone would result in limited “rain out” of the sea salt aerosols on approach to Law Dome. However, the snow pit and firn core records for this four year study preserved seven events that are associated with low sea salt concentrations. The low sea salt signature for each of these events results from a variety of synoptic situations and source regions, and have been grouped into three possible explanations (Table 8.3).

Low Sea Salts – Slow Approach to Law Dome

Events 11, 12 and 51 are associated with a high latitude source region and cyclonic trajectory, consistent with the intensity and position of the circumpolar trough for this time of year (Figs. 8.24, 8.25, 8.32). However, these trajectories also show a marked reduction in the transport speed of the air mass on approach to Law Dome in comparison with the two events that concur with expected autumn events (mid-high sea salt concentrations) (Event 13, Fig. 8.21; Event 50, Fig. 8.22). Event 14 shows a cyclonic trajectory that is further north and consistent with the quasi-stationary cyclone located at 55 – 60°S, 60 – 90°E (Jones and Simmonds, 1993). The trajectory for Event 14 indicates transport from a midlatitude source region and a slow approach to Law Dome from the east (Fig. 8.26). The lower approach speeds associated with these low sea salt events are consistent with depleted sea salt concentrations at Law Dome resulting from “rain out” of the sea salt aerosols along the trajectory. These results also build on the possible explanation for low sea salt events associated with cyclonic systems that are observed during summer (Section 8.5).

Low Sea Salts – Low Latitude (Distant) Source Region

In contrast, the trajectories for Events 10 and 15 show rapid transport from the low latitudes to Law Dome (Figs. 8.23, 8.27). A rapid approach to Law Dome is expected to result in higher sea salt concentrations, as the air mass has not had time to “rain out” the heavy sea salt particles during transport over the sea ice zone prior to deposition at Law Dome. However, it is interesting to note that both these rapid trajectories also indicate the air mass is sourced from low latitudes compared to the events discussed in the previous paragraph. Perhaps the low latitude (distant) source region has allowed increased “rain out” of the heavy sea salt particles during transport over the open ocean to Law Dome. This hypothesis suggests that these events have “dropped off” sea salts over the ocean during transport without “picking up” additional aerosols. It is beyond the scope of this thesis to consider the vertical position of the air mass during the trajectory and discuss this hypothesis further. However, it is recommended that future research draw on three dimensional trajectories (that show the vertical position of the air

mass during transport) to provide a more robust analysis of low sea salt events associated with rapid transport from low latitudes.

Low Sea Salts – Coastline Trajectory

Finally, Event 37 shows a different synoptic situation and trajectory for the low sea salt event preserved in the snow pit (Fig. 8.30). This event is characterised by weak cyclonic activity in the midlatitudes to the northwest of Law Dome (55°S, 100°E), with a weak cloud band extending from the system onto Law Dome (Fig. 8.30a,b). However, the trajectory indicates a high latitude source region for the precipitation at Law Dome, involving an air mass with a trajectory along the Antarctic coastline and approaching Law Dome from due west (Fig. 8.30c). A high latitude source region from the Antarctic coastline is consistent with the low sea salt signature preserved in the snow pit. Transport of the air mass over the sea ice zone adjacent to the Antarctic coastline would limit the uplift of sea salt aerosols along the trajectory, and result in low sea salt concentrations in precipitation at Law Dome.

Enhanced Autumn Marine Biogenic Indicators (Events 16 and 17)

The enhancement of marine biogenic indicators outside the main mid-summer peak in MSA and non-sea salt sulphate has been identified in longer ice core records at Law Dome (Palmer, 2002; Curran and others, 2002). These spring or autumn peaks have tended to be attributed to rapid advection of an air mass sourced from low latitudes. This section draws on two autumn events (Events 16 and 17) to provide a more detailed investigation of potential source regions for autumn enhancement of marine biogenic indicators.

Events 16 and 17 show distinct peaks and high concentrations of MSA and non-sea salt sulphate (Figs. 5.4, 5.6; Chapter 5). Event 16 is characterised by a strong cyclonic system with a cloud band that extends well into the low latitudes (50°S) (Fig. 8.28a,b). The trajectory associated with Event 16 is consistent with the satellite imagery, and shows rapid advection of air from the low latitude region due north of Law Dome (38°S, 110°E) (Fig. 8.28c). Rapid advection of air from low latitudes is consistent with the high concentration of marine biogenic indicators (MSA, non-sea salt sulphate) and high levels of $\delta^{18}\text{O}$ preserved in the snow pit. Biological productivity of the high latitude Southern Ocean diminishes at the end of summer, while marine biota from low latitudes remain active (Curran and Jones, 2000). Rapid advection of air from these low latitudes provides the mechanism for transport of MSA and non-sea salt sulphate particles to Law Dome. In addition, rapid advection of air from low latitudes is

consistent with high levels of $\delta^{18}\text{O}$ in the snow pit. Rapid advection of air from the low latitudes, resulting in limited fractionation of the heavy (^{18}O) isotopes during transport, provides an explanation for the relatively high $\delta^{18}\text{O}$ values in the snow pit.

Event 17 shows a slightly different chemical and isotopic signal, and is associated with different meteorological conditions. Figure 5.5 (Chapter 5) indicates that Event 17 is characterised by high MSA and non-sea salt sulphate concentrations, and $\delta^{18}\text{O}$ and sea salt values that are more comparable to expected autumn events. The satellite imagery shows a disorganised cloud system over Law Dome during Event 17 that does not provide a connection with lower latitudes (Fig. 8.29a,b). The trajectory for Event 17 supports this result, and shows a midlatitude source region to the northwest of Law Dome (Fig. 8.29c). The trajectory indicates that the air mass passes just south of the Heard Island region, with a marked reduction in transport speed on approach to Law Dome. Transport from the midlatitudes, coupled with a slow approach to Law Dome, is a mechanism that is consistent with the mid-levels of $\delta^{18}\text{O}$ preserved in the snow pit. The large distance travelled from the midlatitudes, and the reduction in transport speed on approach to Law Dome, both facilitate fractionation of the heavier (^{18}O) isotope leading to low $\delta^{18}\text{O}$ values in the snow pit. This reduction in transport speed on approach to Law Dome is also consistent with the low sea salt concentrations, and builds on the possible explanations for other low sea salt events discussed in other sections. An explanation for the high marine biogenic indicators in the snow pit record is less certain. Mid-high latitude regions in the Southern Ocean during autumn are not expected to contain significant biological activity (Curran and Jones, 2000). However, the air mass passes just south of the Heard Island region, and the high MSA and non-sea salt sulphate signals may be reflecting the influence of this area of known biological activity.

Deviation Between MSA and Non-Sea Salt Sulphate (Event 38)

The strong link between marine biological activity and the sulphur compounds of MSA and non-sea salt sulphate tend to result in co-deposition of these ion, particularly during summer when marine biological activity in the Southern Ocean is high. However, there are times where the MSA and non-sea salt sulphate signals differ in Law Dome ice cores. Event 38 provides an example for deviations between MSA and non-sea salt sulphate, where non-sea salt sulphate concentrations are high, and MSA concentrations are mid-range and more comparable to expected autumn signals (Fig. 5.6; Chapter 5). Event 38 is associated with a strong cyclonic system and rapid advection of air from the low latitudes to Law Dome (Table 8.3; Fig. 8.31).

These conditions are expected, from events analysed in other sections of this chapter, to result in high marine biogenic indicators and high $\delta^{18}\text{O}$ values. However, MSA and $\delta^{18}\text{O}$ values remain mid-level, while non-sea salt sulphate concentrations are enhanced. In addition, the nitrate signals shows a distinct peak. A possible explanation for the chemical and isotopic signal associated with Event 38 remains uncertain, although the co-deposition of non-sea salt sulphate and nitrate may indicate stratospheric intrusion of air. It is beyond to scope of this thesis to provide analysis of downward mixing of air during events, yet Event 38 highlights the potential for autumn to be influenced by stratospheric intrusion of air.

8.6.3 Concluding Remarks: Autumn

This section examined a number of events preserved in Law Dome snow pits and firn cores during autumn months. The meteorological conditions associated with autumn in the Southern Ocean are influenced by shifting circulation patterns from the poleward migration and increase in intensity of the circumpolar trough. There were only two events that were identified as concurring with expected autumn signals, namely declining levels of $\delta^{18}\text{O}$, MSA, non-sea salt sulphate and nitrate, and increasing concentrations of sea salts. Both these events were found to be associated with the formation of strong cyclonic systems that formed in the midlatitudes.

The identification of ten events that differed from expected autumn signals may indicate that autumn is characterised by enhanced variability in meteorological conditions. The marked poleward shift in both the location and the intensity of the circumpolar trough during autumn is likely to impact on the variability of the ice core record. This variability may not be captured in seasonality studies that involve calculating seasonal signals from a composite of a number of years. However, it is important to consider the variability of autumn chemical and isotopic signals when interpreting the longer ice core record.

The cooling high latitude temperatures during autumn lead to increased fractionation of water vapour that may be sourced from the midlatitudes, and this leads to lower $\delta^{18}\text{O}$ values than typically expected. In addition, with the exception of a single event characterised by rapid transport, the autumn events are generally associated with moderate transport speeds from the potential source region to Law Dome. Moderate transport speeds are consistent with some fractionation of the heavy (^{18}O) isotope prior to deposition at Law Dome. In contrast, the single high $\delta^{18}\text{O}$ event observed during autumn was found to be associated with rapid advection of air from the low latitudes. These results build on the potential explanation for the high $\delta^{18}\text{O}$ events

observed during summer and discussed in the previous section (Section 8.5), and provide further evidence for a strong link between atmospheric circulation and the $\delta^{18}\text{O}$ signal at Law Dome in addition to links with air temperature.

Seven autumn events are characterised by low sea salt concentrations, diverting from the mid-high sea salt concentrations that are expected during autumn. The occurrence of low sea salt concentrations during autumn is counter-intuitive to the poleward shift and increase in intensity of the circumpolar trough during autumn. These low sea salt events were found to be associated with a combination of synoptic situations, and were grouped into three possible explanations. Four events were found to be associated with a marked deceleration of the trajectory on approach to Law Dome. This slow approach encourages “rain out” of heavy sea salt aerosols prior to deposition at Law Dome, and builds on the discussion of low sea salt events identified in Section 8.5. Two events were found to be associated with a low latitude (distant) source region and rapid transport to Law Dome. A possible explanation for these low latitude sea salt events remains uncertain, although the large distance travelled may have allowed “rain out” of the heavy sea salt particles during transport over the open ocean. This hypothesis relies on the assumption that sea salt particles are not “picked up” along the transport route for these specific events, and further research that involves three dimensional trajectories is recommended. Finally, a single low sea salt event was found to be associated with weak cyclonic activity and a coastline trajectory on approach to Law Dome. Transport of the air mass over the sea ice zone adjacent to the Antarctic coastline is consistent with low sea salt concentrations at Law Dome due to limited exposure to open water than therefore limited production of sea salt aerosols along the trajectory. The identification of three distinct explanations for low sea salt events, based on variations in synoptic meteorology and atmospheric circulation, highlights the impact that atmospheric circulation can have on the sea salt signal preserved at Law Dome.

An examination of enhanced autumn marine biogenic indicators revealed a combination of meteorological conditions were found to influence the MSA and non-sea salt sulphate signals. Rapid advection of marine air from low latitudes provides an explanation for autumn enhancements of marine biogenic indicators coupled with higher $\delta^{18}\text{O}$ values. In contrast, lower levels of $\delta^{18}\text{O}$ and enhanced marine biogenic indicators were found to be associated with advection of air from the Heard Island region. This latter example may provide further

evidence for the importance of this region for MSA signals preserved at Law Dome, particularly for MSA and non-sea salt peaks dated outside the summer season.

Finally, processes influencing the nitrate signal during autumn remain uncertain due to the complexity of the nitrate ion. The examination of a single event characterised by high concentrations of nitrate and non-sea salt sulphate may provide an indication of downward stratospheric mixing of air, although it is beyond the scope of this thesis to explore these mechanisms further.

8.7 Winter Events Preserved in High Resolution Snow Pits and Firn Cores

Table 8.4: Winter events preserved in Law Dome snow pits and firn cores

Event Characteristics							Local Meteorology				Synoptic Meteorology		Chemical/ $\delta^{18}\text{O}$ Signal	Possible Explanation
Seasonal Pattern	Event Num.	Date Start	Date Finish	Date(s) with Highest Net Accumulation	Net Accum. m.	Pit or Core	Pressure (hPa)	Temp. (°C)	Wind Speed (ms^{-1})	Wind Direction (°)	Synoptic Situation	Back Trajectory		
Concur	8	30 Jun 2001	30 Jun 2001	30 Jun 2001	10	Matilda	809	-17	16	100	strong cyclone	cyclonic trajectory, low latitude ⁷ source region to northwest of Law Dome, slow northeasterly approach	expected winter signals (low $\delta^{18}\text{O}$, MSA, non-sea salt sulphate, nitrate, high sea salts)	$\delta^{18}\text{O}$: cold temperatures in Southern Ocean during winter MSA/non-sea salt sulphate : low biological activity during winter Sea salts : strong cyclonic system mechanism for production of sea salt aerosols Nitrate : unsure
Concur	9	4 Jun 2001	5 Jun 2001	All days	18	Matilda	826 – 827	-22 to -21	na	na	strong cyclone	direct trajectory, midlatitude ⁸ source region to northwest of Law Dome, rapid northwesterly approach		
Concur	36	2 Jun 1999	8 Jun 1999	7, 8 Jun 1999	7	Rama	820 – 827	-22 to -18	2 – 20	70 – 130	strong cyclone	cyclonic trajectory, midlatitude source region to northwest of Law Dome, slow northerly approach		
Concur	49	29 Jun 1998	5 Jul 1998	4 Jul 1998	7	Rama	800 – 820	-35 to -24	na	na	strong cyclone	cyclonic trajectory, high latitude ⁹ source region to north of Law Dome, slow northerly approach	expected winter signals (low $\delta^{18}\text{O}$, MSA, non-sea salt sulphate, nitrate, high sea salts)	$\delta^{18}\text{O}$: cold air temperatures MSA/non-sea salt sulphate : low biological activity during winter Sea salts : unsure, expect low sea salts slow northerly approach Nitrate : unsure
Differ	5	24 Aug 2001	24 Aug 2001	24 Aug 2001	3	Matilda	809	-40	na	na	strong cyclone	disorganised trajectory, high latitude (continental) source region to south of Law Dome, slow southerly approach	high $\delta^{18}\text{O}^*$	$\delta^{18}\text{O}$: unsure, seems inconsistent, perhaps uncertainty in dating?
Differ	6	31 Jul 2001	5 Aug 2001	4 Aug 2001	10	Matilda	805 – 815	-26 to -18	na	na	strong cyclone	direct trajectory, high latitude source region to northwest of Law Dome, slow northerly approach	high $\delta^{18}\text{O}^*$	$\delta^{18}\text{O}$: rapid advection of air from low or midlatitudes
Differ	7	10 Jul 2001	12 Jul 2001	All days	4	Matilda	825 – 833	-16 to -13	10	60 – 90	strong cyclone	direct trajectory, midlatitude source region to northwest of Law Dome, rapid northerly approach		
Differ	24	19 Aug 2000	27 Aug 2000	20 Aug 2000	21	DSS0102	811 – 836	-20 to -13	na	na	strong cyclone	direct trajectory, midlatitude source region to northwest of Law Dome, slow northerly approach		
Differ	46	20 Aug 1998	20 Aug 1998	20 Aug 1998	11	Rama	825	-25	14	125	disorganising cyclone	direct trajectory, low latitude source region to northwest of Law Dome, slow northerly approach		
Differ	47	23 Jul 1998	23 Jul 1998	23 Jul 1998	9	Rama	818	-25	na	na	disorganising cyclone	cyclonic trajectory, midlatitude source region to northwest of Law Dome, slow easterly approach		
Differ	48	19 Jul 1998	20 Jul 1998	All days	11	Rama	802 – 810	-18	na	na	strong cyclone	disorganised trajectory, high latitude source region to northwest of Law Dome, slow northerly approach	high $\delta^{18}\text{O}$, low sea salts [*]	$\delta^{18}\text{O}$: unsure Sea salts : slow approach encourages rain-out of heavy sea salt aerosols

⁷ Low latitudes defined as 35 – 45 °S.
⁸ Midlatitudes defined as 34 – 55 °S
⁹ High latitudes defined as > 55 °S.
^{*} Other species characterised by expected autumn signals

8.7.1 Events that Concur with Expected Winter Chemical and Isotopic Signals

Of the eleven winter events examined in this study, four events concur with expected winter chemical and isotopic signals, namely low levels of $\delta^{18}\text{O}$, MSA, non-sea salt sulphate and nitrate, and high concentrations of sea salts (Table 8.4). All four events that concur with expected signals are associated with strong cyclonic systems.

A similar transport path is evident for Events 8, 9 and 36, with a trajectory that indicates potential source regions in the low to midlatitudes (Table 8.4; Figs. 8.37 – 8.39). Event 8 shows a tight cyclonic system, reflected by a similar tight cyclonic trajectory, that formed in the region to the northwest of Law Dome (Fig. 8.37). Event 9 shows a different cyclonic system that is associated with a thick, wide cloud band and an absence of the typical cyclonic circulation (Fig. 8.38a,b). The trajectory for Event 9 also reflects this absence of cyclonic circulation and indicates a source region further west, rapid advection from the source region, and approaching Law Dome from the northwest (Fig. 8.38c). The trajectory for Event 36 is similar to Event 8, with a tight cyclonic system that formed in the region to the northwest of Law Dome and a trajectory that shows transport from the midlatitudes and approaching Law Dome from the north (Fig. 8.39).

Although Event 49 is also characterised by a strong cyclonic system, the synoptic situation indicates a more intense system and the intrusion of a front characterised by very cold air passing over Law Dome. The cold air mass is indicated by speckled cloud in the wake of the cloud band (Fig. 8.40a,b), and is supported by the cold air temperatures recorded at the AWS (Table 8.4; Fig. 8.33). The trajectory for Event 49 indicates a high latitude source region, consistent with the development of a cold air mass influencing Law Dome.

$\delta^{18}\text{O}$

Low $\delta^{18}\text{O}$ levels associated with Events 8, 9 and 36 (Figs. 5.4, 5.6; Chapter 5) are consistent with the general reduction in air temperatures in the Southern Ocean during winter (Dansgaard, 1964). The absence of rapid advection from the low to midlatitudes for these events enables fractionation of the heavy (^{18}O) isotope to occur during transport and further reduces the $\delta^{18}\text{O}$ value. In contrast, Event 49, also associated with low $\delta^{18}\text{O}$ values (Fig. 5.6; Chapter 5), shows a back trajectory that indicates a high latitude source region (Fig. 8.40c). Event 49 is characterised by the intrusion of a cold air mass over Law Dome, indicated by the very low air temperatures recorded by the AWS (Table 8.4; Fig. 8.33), and the speckled cloud identified on

the satellite imagery (Fig. 8.40a,b). These conditions are consistent with the low $\delta^{18}\text{O}$ values recorded in the snow pit and provide further evidence for a strong link between $\delta^{18}\text{O}$ and site temperature at Law Dome.

Marine Biogenic Indicators: MSA and Non-Sea Salt Sulphate

The absence of MSA and non-sea salt sulphate features during winter events is consistent with the absence of marine biological activity in the Southern Ocean at this time of year (Curran and Jones, 2000).

Sea Salts

Three of the four events that concur with expected seasonal signals are characterised by advection of air from the low to midlatitudes (Events 8, 9 and 36), however there is some variation in the synoptic situation and the chemical signals between these events. Event 9 involves a direct trajectory from the midlatitudes (Fig. 8.38), in contrast to the cyclonic trajectories associated with Events 8 and 36 (Figs. 8.37, 8.39). The cloud system associated with Event 9 indicates a wide, thick cloud band rather than the tight cyclonic circulation for Events 8 and 36. The sea salt signals for Event 9 also differ slightly compared to Events 8 and 36. The signals are still consistent with the expected winter signature of high sea salts, yet the sodium concentrations for Event 9 are lower ($2.4\mu\text{EqL}^{-1}$) compared to Events 8 ($6\mu\text{EqL}^{-1}$) and 36 ($10.8\mu\text{EqL}^{-1}$) (Figs. 5.4, 5.6; Chapter 5). The cyclonic system associated with Event 9 is characterised by a low pressure gradient, as indicated by the relatively high and constant atmospheric pressure recorded by the AWS during the accumulation event (826 – 827 hPa, Table 8.4; Fig. 8.36). A cyclonic system with a low pressure gradient has the effect of reducing the geopotential flow within the system, leading to lower surface wind speeds. Lower surface wind speeds will lead to a reduction in the production of sea salt aerosols, thereby providing a possible explanation for the lower sea salts associated with Event 9.

These three low to midlatitude events provide evidence for a link between the intensity of a cyclonic system, driven by the atmospheric pressure gradient within the system, and sea salt concentrations preserved in the ice core at Law Dome. Previous studies on the Law Dome sea salt record have drawn this conclusion, and attributed high sea salt concentrations to enhanced storm activity over the Southern Ocean (Curran and others, 1998a; Palmer, 2002). However, other events examined in this chapter, particularly in summer and autumn (Sections 8.5, 8.6), show that the sea salt signal may also be influenced by changes in atmospheric circulation

rather than changes in the intensity of the cyclone. Events examined in summer and autumn provide evidence for enhanced sea salt activity to be related to a northward trajectory of the air mass on approach to Law Dome, rather than an intense cyclonic system. It is recommended that both cyclone intensity and atmospheric circulation variations are considered when interpreting sea salt records from deep ice cores at Law Dome.

Nitrate

Finally, a possible explanation for low concentrations of nitrate occurring during events that concur with expected winter signals remains uncertain, due mainly to the complexity of potential sources for Antarctic nitrate.

8.7.2 Events that Differ from Expected Winter Chemical and Isotopic Signals

The remaining seven winter events (Events 5, 6, 7, 24, 46, 47 and 48) differ from the expected winter chemical and isotopic signature (Table 8.4). All of these events show high $\delta^{18}\text{O}$ signals, indicating a possible deviation of $\delta^{18}\text{O}$ from expected cold winter temperatures. The other trace chemical signals exhibit winter concentrations comparable to expected winter signals (Figs. 5.4 – 5.6; Chapter 5).

High Winter $\delta^{18}\text{O}$ (Events 5, 6, 7, 24, 46, 47 and 48)

The $\delta^{18}\text{O}$ signal is generally used as a temperature indicator, with many studies reconstructing past temperatures from $\delta^{18}\text{O}$ records in deep ice cores (eg. Picciotto and others, 1960; Morgan, 1979; Bradley and Jones, 1993; Schotterer and others, 1997; Morgan and van Ommen, 1997). Section 6.3.1 (Chapter 6) of this thesis provides a direct comparison between site temperature and $\delta^{18}\text{O}$ signals preserved in the *DSS0102* firn core, and found that variations in $\delta^{18}\text{O}$ are in excellent agreement with observed variations in local temperature. This indicates that the $\delta^{18}\text{O}$ signal is an excellent proxy for temperature at Law Dome. However, other factors such as atmospheric circulation, altitude and continental effects may also influence the $\delta^{18}\text{O}$ signal preserved in ice cores (Kato, 1978; Bromwich and Weaver, 1983; Zwally and others, 1998; Araguas-Araguas, 2000). Examination of the seven high winter $\delta^{18}\text{O}$ events identified in this study allows us to gain a greater understanding of when the $\delta^{18}\text{O}$ signal may not reflect the temperature record.

The results show that these high winter $\delta^{18}\text{O}$ events are characterised by a variety of synoptic meteorological conditions (Table 8.4; Figs. 8.41 – 8.47). Event 5 indicates a synoptic situation that is not expected to produce high winter $\delta^{18}\text{O}$ values (Fig. 8.41). The back trajectory shows a source region for the air mass that involves the Antarctic continent. The local meteorological conditions provide further evidence for the intrusion of continental air due to the very cold temperatures recorded at Law Dome (Table 8.4; Fig. 8.36). The intrusion of cold continental air is expected to produce low $\delta^{18}\text{O}$ values, and is inconsistent with the high $\delta^{18}\text{O}$ signature preserved during Event 5 (Fig. 5.4; Chapter 5). Event 5 is characterised by precipitation that occurred on 1 day (24 August 2001), producing 3 cm of net accumulation (Table 8.4). The satellite imagery associated with this event indicates a strong cyclonic system with the typical cyclonic circulation and cloud band that extends into the midlatitudes. This system approaches Law Dome on 23 August 2001 (Fig. 8.41a), and travels over Law Dome on 24 August 2001 (Fig. 8.41b). The cold temperatures at Law Dome, and advection of cold air from the Antarctic continent, are consistent with the passing of the front on 24 August 2001. However, the absence of wind speed and direction observations from the AWS during this event prevents further discussion on the transport mechanisms influencing the precipitating air mass at Law Dome. In this case, the high $\delta^{18}\text{O}$ values may actually be associated with a source region and transport mechanism resulting from the maritime cyclonic system influencing Law Dome on 23 August 2001 rather than the southerly change following the front on 24 August 2001.

Events 6, 7, 24, 46 and 47 are all associated rapid advection of air from low or midlatitudes through strong cyclonic systems (Figs. 8.42 – 8.46). Rapid advection of low or midlatitude air onto Law Dome is consistent with high $\delta^{18}\text{O}$ values preserved in the snow pits and firn cores. Rapid advection of air to Law Dome limits fractionation of the heavy (^{18}O) isotope during transport, and results in a high $\delta^{18}\text{O}$ signal in the snow pit. McMorrow and others (2001, 2002) have shown other events where rapid advection of air from lower latitudes have produced high $\delta^{18}\text{O}$ values, and the results presented here provide further evidence for the influence of atmospheric circulation on the $\delta^{18}\text{O}$ record at Law Dome. The high $\delta^{18}\text{O}$ events examined in McMorrow and others (2001, 2002) were also associated with high sea salt concentrations, probably caused by the intense cyclonic system and the production of sea salt aerosols through high surface wind speeds. Events 6, 7, 24, 36 and 47 presented here are also associated with high sea salt concentrations (Figs. 5.4, 5.6; Chapter 5), providing further evidence for the influence of intense storm events on the sea salt record at Law Dome.

In contrast, Event 48 is characterised by high $\delta^{18}\text{O}$ values and a distinct drop in sea salt concentrations (Fig. 5.6; Chapter 5). The synoptic situation during Event 48 also varies compared to the other unusual winter events examined above. The satellite imagery and back trajectory for Event 48 show a tight cyclonic system that formed in the high latitudes to the northwest of Law Dome (Fig. 8.47a,b), with slow transport from the source region to Law Dome (Fig. 8.47c). These conditions are consistent with reduced sea salt concentrations, with slow transport providing a mechanism for “rain out” of the heavy sea salt aerosols. In addition, the high latitude source region, and subsequent short transport distance between source and Law Dome, is consistent with the high $\delta^{18}\text{O}$ values in the snow pit due to restricted fractionation of heavy (^{18}O) isotopes.

8.7.3 Concluding Remarks: Winter

This section examined a number of events preserved in Law Dome snow pits and firn cores during winter months. Events that concur with expected winter signals, namely low concentrations of MSA, non-sea salt sulphate, nitrate and $\delta^{18}\text{O}$, and high concentrations of sea salts, were found to be associated with well developed cyclonic systems, a midlatitude source region and relatively slow transport to Law Dome.

The low $\delta^{18}\text{O}$ values observed during events that concur with expected winter signals are probably attributed to the general reduction in air temperatures in the Southern Ocean during winter. These events were found to be associated with either a midlatitude source region and a slow transport mechanism, allowing fractionation of the heavy (^{18}O) isotope, or a high latitude source region characterised by cold air temperatures. Identification of high winter $\delta^{18}\text{O}$ events showed an important difference in the transport mechanism influencing the $\delta^{18}\text{O}$ signal. These high winter $\delta^{18}\text{O}$ events are generally associated with strong cyclonic systems and rapid advection of air from lower latitudes, in contrast to the slow transport mechanisms that influenced the low $\delta^{18}\text{O}$ winter events. These events build on the results presented in other sections of this chapter, where high $\delta^{18}\text{O}$ events are associated with rapid advection of air from lower latitudes. These events also highlight the importance of atmospheric circulation on the $\delta^{18}\text{O}$ record at Law Dome.

The high concentrations of sea salts preserved during events that concur with expected winter signals are consistent with the intrusion of well developed cyclonic systems. However, the relatively slow transport paths for these “typical” events may contribute to “rain out” of the

heavy sea salt aerosols compared to events characterised by rapid advection of air. Closer examination of the high sea salt events revealed some variability in the sea salt signal, with higher sea salts associated with more intense cyclonic systems. These results provide further evidence for the link between the intensity of the cyclonic system and the sea salt record, although events in other seasons (particularly summer and autumn) highlight the additional impact that atmospheric circulation may have on the sea salt signal.

The low concentrations of marine biogenic indicators (MSA, non-sea salt sulphate) during winter are consistent with the absence of biological activity in the Southern Ocean at this time of year.

Finally, the results presented here suggest that winter at Law Dome is relatively stable compared to other seasons. All the chemical signals, with the exception of $\delta^{18}\text{O}$, are characterised by expected winter signals. The low sensitivity of these signals during winter may reflect the stability of the synoptic meteorological conditions in the Law Dome region at this time of year. Meteorological studies report that the circumpolar trough is relatively stable during winter months (King and Turner, 1997), in sharp contrast to autumn and spring when the circumpolar trough is undergoing a significant poleward shift and increase in intensity. Seasonal variability in the meteorological conditions is expected to be reflected by similar variability in the ice core signals, and the results presented in this study provide some evidence for that link.

8.8 Spring Events Preserved in High Resolution Snow Pits and Firn Cores

Table 8.5: Spring events preserved in Law Dome snow pits and firn cores

Event Characteristics							Local Meteorology				Synoptic Meteorology		Chemical/ $\delta^{18}\text{O}$ Signal	Possible Explanation
Seasonal Pattern	Event Num.	Date Start	Date Finish	Date(s) with Highest Net Accumulation	Net Accu m.	Pit or Core	Pressure (hPa)	Temp. (°C)	Wind Speed (ms^{-1})	Wind Direction (°)	Synoptic Situation	Back Trajectory		
Concur	3	14 Sep 2001	21 Sep 2001	14 Sep 2001	13	Matilda	811 – 819	-29 to -21	na	na	weak cyclone	disorganised trajectory, midlatitude ¹⁰ source region to northwest of Law Dome, slow northerly approach	expected spring signals (increasing $\delta^{18}\text{O}$, MSA, non-sea salt sulphate, nitrate, declining sea salts)	$\delta^{18}\text{O}$: increasing air temperatures in Southern Ocean, distant source region and some fractionation of heavy (^{18}O) isotope MSA/non-sea salt sulphate: increasing biological activity as spring progresses Sea salts: strong cyclonic system mechanism for production of sea salt aerosols yet slow approach encourages rain-out of heavy sea salt aerosols resulting in mid concentrations Nitrate: unsure, possibly stratospheric intrusion of nitrate
Concur	4	1 Sep 2001	7 Sep 2001	1 Sep 2001	8	Matilda	808 – 822	-23 to -17	4 – 16	110 – 150	strong cyclone	cyclonic trajectory, high latitude ¹¹ source region to north of Law Dome, slow northerly approach		
Concur	32	22 Oct 1999	27 Oct 1999	22 Oct 1999	14	Rama	801 – 811	-18 to -16	3 – 13	110 – 150	strong cyclone	direct trajectory, midlatitude source region northwest of Law Dome, rapid northwesterly approach		
Concur	33	21 Oct 1999	21 Oct 1999	21 Oct 1999	5	Rama	818	-18	7	110	strong cyclone	direct trajectory, low latitude ¹² source region to northwest of Law Dome, slow northerly approach		
Concur	34	11 Oct 1999	17 Oct 1999	All days	7	Rama	810 – 824	-25 to -11	2 – 11	60 – 110	strong cyclone	direct trajectory, midlatitude source region to northwest of Law Dome, slow easterly approach		
Concur	35	2 Sep 1999	10 Sep 1999	All days	3	Rama	805 – 820	-31 to -18	na	na	strong cyclone	disorganised trajectory, high latitude (continental) source region, slow westerly approach	expected spring signals (increasing $\delta^{18}\text{O}$, MSA, non-sea salt sulphate, nitrate, declining sea salts)	$\delta^{18}\text{O}$: increasing air temperatures in high latitudes, limited time for fractionation of heavy (^{18}O) isotopes MSA/non-sea salt sulphate: low marine biological indicators for continental air mass Sea salts: low marine biological indicators for continental air mass Nitrate: unsure, possibly stratospheric intrusion of nitrate
Differ	2	2 Oct 2001	6 Oct 2001	All days	4	Matilda	804 – 822	-28 to -20	na	na	strong cyclone	direct trajectory, high latitude source region to west of Law Dome, slow westerly approach	low sea salts*	Sea salts: unsure, expect high sea salts from rapid trajectory, could indicate low latitude source region
Differ	22	23 Nov 2000	23 Nov 2000	23 Nov 2000	12	DSS0102	835	-17	14	110	disorganising cyclone	direct trajectory, midlatitude source region to northwest of Law Dome, rapid northwesterly approach		
Differ	31	10 Nov 1999	16 Nov 1999	11, 12 Nov 2000	6	Rama	820 – 838	-19 to -14	2 – 7	40 – 150	disorganised cloud cells	disorganised trajectory, high latitude (continental) source region, slow southerly approach	low sea salts*	Sea salts: transport path over coastline and sea ice zone, no transport over open ocean
Differ	43	23 Nov 1998	29 Nov 1998	23 Nov 1998	14	Rama	815 – 843	-10 to -9	3 – 10	90 - 180	strong cyclone	direct trajectory, low latitude source region to north of Law Dome, slow northerly approach	High MSA, non-sea salt sulphate, $\delta^{18}\text{O}$ (Event 16), low sea salts (Event 17)*	MSA/non-sea salt sulphate: $\delta^{18}\text{O}$: Sea salts:
Differ	44	16 Nov 1998	22 Nov 1998	All days	8	Rama	825 – 841	-17 to -11	3 – 12	0 – 120	weak cyclone	disorganised trajectory, high latitude source region to northwest of Law Dome, slow westerly approach		
Differ	45	16 Oct 1998	19 Oct 1998	19 Oct 1998	8	Rama	800 – 832	-18 to -16	2 – 11	90 – 120	strong cyclone	direct trajectory, low latitude source region to northwest of Law Dome, rapid northerly approach	high non-sea salt sulphate, mid nitrate, enhanced sea salt peak*	Non-sea salt sulphate/nitrate: Sea salts:

¹⁰ Midlatitudes defined as 45 – 55 °S.
¹¹ High latitudes defined as > 55 °S.
¹² Low latitudes defined as 35 – 45 °S.
* Other species characterised by expected autumn signals

8.8.1 Events that Concur with Expected Spring Chemical and Isotopic Signals

Of the twelve spring events examined in this study, six events (Events 3, 4, 32, 33, 34, 35) concur with expected spring chemical and isotopic signals, namely increasing levels of $\delta^{18}\text{O}$, MSA, non-sea salt sulphate, nitrate, and declining concentrations of sea salts (Table 8.5). Shifting chemical and isotopic signals is consistent with the changing meteorological patterns that occur during spring. Similar to autumn conditions discussed in Section 8.6, spring undergoes a semi-annual oscillation that involves a deepening and poleward migration of the circumpolar trough (King and Turner, 1997). These shifting meteorological patterns may result in increased variability in the chemical and isotopic signals during spring events.

Event 3 involves the intrusion of a weak cyclonic onto Law Dome, while the remaining events are associated with strong cyclonic systems (Table 8.5; Figs. 8.52 – 8.57). The back trajectory associated with Event 3 is consistent with the presence of a weak cyclonic system, and the transport shows an unusual loop and slow approach to Law Dome (Fig. 8.52). In this case the source region is unclear, and the slow approach to law Dome may not accurately depict the transport path.

The remaining spring events that concur with expected signals all show strong cyclonic systems, yet the trajectories for these systems vary between events. Event 4 is characterised by a tight trajectory constrained to the high latitudes and a slow transport mechanism towards Law Dome (Fig. 8.53). In contrast, Events 32, 33 and 34 are characterised by low or midlatitude source regions and rapid advection of air to Law Dome (Figs. 8.54 – 8.56). Finally, Event 35 shows a trajectory sourced from the Antarctic continent and approaching Law Dome from due west along the Antarctic coastline (Fig. 8.57).

The identification of a variety of potential source regions associated with these events that concur with expected spring signals may indicate a mixture of transport mechanisms can influence the expected spring chemical and isotopic signature.

$\delta^{18}\text{O}$

The increasing $\delta^{18}\text{O}$ values observed during spring events may be attributed to a general increase in air temperatures as spring progresses. In addition, for Events 3, 32, 33 and 34, associated with low or midlatitude source regions, fractionation of heavy (^{18}O) isotopes during transport will reduce the $\delta^{18}\text{O}$ value to be more comparable to the high latitude source region

events (Event 4). Event 35 indicates a slightly different situation, characterised by a continental air mass intruding over Law Dome. In this case the cause for the mid level $\delta^{18}\text{O}$ values remains uncertain, although the general increase in Antarctic air temperatures at this time of year may provide a simple explanation.

Marine Biogenic Indicators: MSA and Non-Sea Salt Sulphate

The increasing MSA and non-sea salt sulphate concentrations observed during these spring events are consistent with the general increase in biological activity in the oceans as spring progresses. Sea ice concentrations around the Antarctic tend to be highest during early spring, and biological activity at higher latitudes generally begins to increase during late spring and summer as the sea ice melts. Early spring biogenic indicators may be reflecting a lower latitude source since marine biological activity begins to increase earlier at these lower latitudes. The low MSA and non-sea salt sulphate signals preserved during Event 4 are consistent with the absence of marine biological activity in the Southern Ocean during early spring. Event 4 involves accumulation from 1 – 7 September 2001, before the release of marine biota from melting sea ice is expected to occur. Event 35, also associated with an early spring event (2 – 10 September 1999) also shows low concentrations of MSA and non-sea salt sulphate. However, Event 35 is associated with a continental air mass which is consistent with low marine biogenic indicators in accumulation at Law Dome. The higher concentrations of MSA and non-sea salt sulphate observed in the later spring events (Events 3, 32, 33, 34) are consistent with increasing marine biological activity as spring progresses.

Sea Salts

Most of the events that concur with the expected spring signals of declining sea salt concentrations are associated with strong cyclonic systems. It is expected that strong cyclonic systems would produce enhanced sea salt concentrations in accumulation at Law Dome. However, these events are also characterised by a marked reduction in speed of the trajectory on approach to Law Dome. As discussed in previous sections of this chapter, a reduction in the speed of the trajectory on approach to Law Dome may facilitate “rain out” of the heavy sea salt particles, resulting in a reduced sea salt concentration preserved at Law Dome. The exception to these “slow approach” trajectories is Event 32, which is characterised by a rapid northwesterly approach to Law Dome. The sea salt concentrations for Event 32 are higher than the other events, providing further evidence for the argument that trajectory approach speed is an important factor influencing the sea salt signal at Law Dome. Event 35 shows a different

mechanism influencing the sea salt record. In this case, the low sea salt concentrations are associated with a continental air mass, and depleted sea salt aerosols are expected.

Nitrate

The synoptic meteorological conditions associated with mid level nitrate signals preserved during spring events provide limited insight into the nitrate cycle influencing Law Dome during spring. Previous studies have attributed downward mixing of stratospheric air as a major potential source for spring nitrate in Antarctica (Legrand and Kirchner, 1990). The synoptic meteorology and back trajectories for the spring events examined in this study neither support or disagree with these previous studies.

8.8.2 Events that Differ from Expected Spring Chemical and Isotopic Signals

The six remaining spring events (Events 2, 22, 31, 43, 44, 45) differ from the expected spring chemical and isotopic signals (Table 8.5).

Low Sea Salts and $\delta^{18}\text{O}$ (Event 2)

Event 2 is characterised by a strong cyclonic system that formed in the high latitudes to the west of Law Dome (Fig. 8.58). Both the local and synoptic meteorology indicate a cold air mass, with local temperatures below mean levels (Table 8.5; Fig.8.51) and AVHRR imagery showing speckled cloud in the wake of the cloud band (Fig. 8.58). Moreover, the back trajectory indicates a transport path that passes along the Antarctic coastline and approaches Law Dome from due west. These conditions are consistent with an air mass passing over Law Dome that is depleted in $\delta^{18}\text{O}$ and sea salt concentrations. In addition, the coastline transport path is consistent with low sea salt concentrations due to reduced sea salt aerosol production over the sea ice zone. This event highlights the sensitivity of $\delta^{18}\text{O}$ and sea salt indicators to event-scale circulation changes in addition to seasonal changes. In this case the strong cyclonic system influencing Law Dome is characterised by a slightly different source region and transport mechanism than the expected quasi-stationary cyclone located to the northwest of Law Dome (Jones and Simmonds, 1993), and this unusual circulation pattern provides the mechanism for an unusual chemical and isotopic signal.

Enhanced Spring Nitrate (Events 22, 44 and 45)

Nitrate typically shows an erratic seasonal cycle preserved in Antarctic ice cores, with maximum concentrations occurring during late spring or early summer (Curran and others, 1998; Wagenbach and others, 1998b; Kreutz and others, 1999). The results presented in Chapter 6 of this thesis, and in McMorrow and others (2004), indicate that the Law Dome nitrate maxima occurs during spring and precedes the main mid-summer $\delta^{18}\text{O}$ and MSA peaks. Spring enhancement of nitrate is consistent with the transport of nitrogen species from the stratosphere to the troposphere through the weakening of the polar vortex at this time of year. However, long range tropospheric transport of anthropogenic nitrate can not be ruled out. Examination of the synoptic meteorological conditions associated with the enhanced spring nitrate signals preserved in this study may provide further insight into the likely source region for spring nitrate.

Events 22, 44 and 45 all show an enhanced nitrate signature, with concentrations reaching $1.2 - 1.6\mu\text{EqL}^{-1}$ (Figs. 5.5 – 5.6; Chapter 5), higher than mean spring nitrate concentrations determined from longer term records at Law Dome ($0.30\mu\text{EqL}^{-1}$; Anne Palmer, pers. comm., 2005). The enhanced nitrate events are associated with strong cyclonic systems and varying source regions (Figs. 8.59, 8.62 – 8.63). Event 22 involves a disorganising cyclone and a trajectory characterised by rapid advection of air from the midlatitudes (Fig. 8.59). Event 44 shows a tighter cyclonic trajectory and a high latitude source region (Fig. 8.62). Finally, Event 45 is characterised by a strong cyclonic system and rapid advection of air from the midlatitudes (Fig. 8.63). Events 22 and 45 are consistent with nitrate sourced from long range tropospheric transport, while Event 44 provides evidence for a local source region. Therefore, the mechanisms influencing these nitrate events remain unclear.

In all three events, the enhanced nitrate peak coincides with a peak in non-sea salt sulphate and the absence of a similar peak in MSA (Figs. 5.5 – 5.6; Chapter 5). Non-sea salt sulphate concentrations in Antarctic ice cores result from a number of sources including the oxidation of dimethylsulphide (DMS) from marine biota, volcanic eruptions, stratospheric input, continental dust and anthropogenic activities (Legrand, 1995). Previous studies from Law Dome ice cores have determined that marine biogenic sulphate provides the largest contribution to the non-sea salt sulphate signal, with volcanic eruptions providing a significant source during periods of volcanic activity (Curran and others, 1998; Palmer, 2002; Palmer and others, 2001). The contribution of localised continental dust and anthropogenic activities to the non-sea salt

sulphate signal preserved in Law Dome ice cores is expected to be minimal due to the isolation of the Antarctic continent from potential source regions, while contributions of stratospheric non-sea salt sulphate is unknown. In contrast, the oxidation of DMS from marine biota is the only source of MSA in Antarctic ice cores (Curran and others, 1998). The absence of a coinciding peak in MSA during these enhanced nitrate and non-sea salt sulphate events suggests that marine biogenic nitrate is not a major contributor to the non-sea salt sulphate signature during these events.

In the Antarctic region the transport of nitrogen species from the stratosphere to the troposphere occurs through the weakening of the polar vortex and subsequent downward mixing of air during spring and summer (Whitlow and others, 1992; König-Langlo and others, 1998). Polar stratospheric clouds (PSCs), comprised of nitric acid trihydrate, generally form during the weakening of the polar vortex (Legrand and Kirchner, 1990). The combination of these two effects provides an explanation for the co-deposition of stratospheric nitrate and non-sea salt sulphate during spring. Events 22, 44 and 45 provide examples of events where enhanced spring nitrate is likely to be sourced from the stratosphere or long range tropospheric, rather than local or regional sources.

Enhanced Spring Marine Biogenic Indicators (Events 31 and 43)

The enhancement of marine biogenic indicators outside the main mid-summer peak in MSA and non-sea salt sulphate has been identified in longer ice core records at Law Dome (Palmer, 2002; Curran and others, 2002). Enhanced autumn MSA and non-sea salt sulphate events from the records presented here are discussed in Section 8.6 of this thesis. Section 8.6 identifies two autumn events that show enhanced marine biogenic signals, with one event attributed to rapid advection of air from the midlatitudes, and the other event showing a mid-high latitude source region just south of Heard Island. Similarly, the enhanced spring marine biogenic indicators show a combination of synoptic situations. Event 31 is associated with a high latitude source region and a transport path that approaches Law Dome from the west along the Antarctic coastline (Fig. 8.60). In contrast, Event 43 shows a northerly trajectory that extends well into the low latitudes (Fig. 8.61).

Previous studies have attributed spring enhancement of marine biogenic indicators to the rapid advection of air from lower latitudes (McMorrow and others, 2002; Curran and others, 2002). Event 43 provides further evidence for the production of non-summer enhancements in MSA

and non-sea salt sulphate through a midlatitude or low latitude source region and rapid advection transport mechanism. It is interesting to note that Event 43 is associated with a weak cyclonic system, indicated by the relatively narrow cloud band, the absence of a well defined “comma” at the base of the front (Fig. 8.61), and the relatively high atmospheric pressure recorded at Law Dome (Table 8.5; Fig. 8.48). The presence of a weak cyclonic system is also consistent with the relatively low sea salt concentrations preserved in the snow pit, and reduced production of sea salt aerosols (Fig. 5.6; Chapter 5). However, AVHRR satellite imagery indicates a long “tail” of cloud extending north from the base of the system, indicating a connection with lower latitudes (Fig. 8.61a,b). Rapid advection of air from low latitudes during Event 43 is consistent with the high concentration of marine biogenic indicators (MSA, non-sea salt sulphate) preserved in the snow pit. The biological productivity of the high latitude Southern Ocean remains low during spring, while marine biota from low latitudes is more productive (Curran and Jones, 2000). The rapid advection of air from these low latitudes provides the mechanism for transport of MSA and non-sea salt sulphate particles to Law Dome.

Event 31 indicates a high latitude source region and transport mechanism for the enhanced spring MSA and non-sea salt sulphate peaks, with a continental source region and transport along the Antarctic coastline (Fig. 8.60). These conditions are not expected to produce enhanced spring marine biogenic indicators due to the absence of biological activity in the continental region. The chemical and isotopic signature associated with Event 31 is particularly unexpected from the synoptic situation, and includes high and distinct peaks in MSA, non-sea salt sulphate, $\delta^{18}\text{O}$, sea salts and nitrate (Fig. 5.6; Chapter 5). Similar chemical and isotopic events examined in this thesis have found to be associated with strong cyclonic systems and rapid advection of air from lower latitudes during other seasons (eg. autumn (Events 16, 39), summer (Event 1)). The strong cyclonic system provides the mechanism for enhanced sea salt concentrations, while the connection with lower latitudes allows long range transport of marine biogenic signals and possible anthropogenic nitrate signals. Finally, rapid advection of low latitude air and associated restricted fractionation of heavy (^{18}O) isotopes provides an explanation for high $\delta^{18}\text{O}$ signals. In contrast, Event 31 provides an example where the chemical and isotopic signature may not reflect the expected synoptic situation, and similar signals preserved in deep ice cores should be interpreted with caution.

8.8.3 Concluding Remarks: Spring

This section examined a number of events preserved in Law Dome snow pits and firn cores during spring months. Typical spring events, characterised by increasing levels of $\delta^{18}\text{O}$, MSA, non-sea salt sulphate and nitrate, and declining concentrations in sea salts, were found to be associated with well defined cyclonic systems although the intensity of each system varied. The increasing levels in $\delta^{18}\text{O}$, MSA, non-sea salt sulphate and nitrate, and declining concentrations in sea salts, are consistent with the shifting meteorological patterns that occur during spring. Spring is characterised by the intensification and poleward migration of the circumpolar trough during early spring, and events that occurred during early spring were found to reflect a chemical signature similar to winter events. In contrast, during late spring as the circumpolar trough is reducing in intensity and migrating to the north, spring events were found to reflect a chemical and isotopic signature similar to summer events.

The examination of unusual spring events at Law Dome allows a greater understanding of the atmospheric conditions influencing the chemical and isotopic signals. Examination of a low sea salt and $\delta^{18}\text{O}$ event was found to be associated with a local cyclonic system and cold air mass passing over Law Dome. This event highlights the sensitivity of these species to atmospheric circulation changes, providing implications for interpreting the longer ice core record. Enhanced spring nitrate events were also identified in the four year record, and attributed to the intrusion of stratospheric air through the breakdown of the polar vortex. Finally, enhanced spring marine biogenic indicators were found to be associated with a combination of rapid advection from lower latitudes and a high latitude source region, indicating similar events from longer ice core records should be interpreted with caution.

8.9 Concluding Remarks

This chapter provided a detailed analysis of event-scale comparisons between chemical and isotopic signals, and meteorological conditions with the aim of enhancing our understanding of the link between ice cores and climate. The analysis aimed to provide further evidence for the discussion presented in Chapter 6 on the seasonality of chemical and isotopic species at Law Dome. In addition, the event-scale investigation highlighted potential implications for interpreting longer ice core records from Law Dome.

8.9.1 Seasonal Considerations

Summer

Events that concur with expected summer chemical and isotopic signals, namely high levels of MSA, $\delta^{18}\text{O}$, non-sea salt sulphate, and nitrate, and low concentrations of sea salts, were found to be associated with a mixture of strong cyclonic systems and disorganised cloud cells. Source regions for these expected summer events were consistently found to include the region to the northwest of Law Dome, and the Heard Island (50°S, 70°E) region was common to all events. This region is a known area of marine biota and is consistent with the high concentrations of MSA and non-sea salt sulphate generally preserved during summer.

High summer $\delta^{18}\text{O}$ values in Antarctica are usually attributed to higher temperatures during summer. The results presented in this thesis found evidence for two distinct processes influencing high summer $\delta^{18}\text{O}$ signals. Events characterised by strong cyclonic systems are probably caused by a combination of high summer air temperatures and rapid advection of air from lower latitudes. In contrast, events characterised by disorganised trajectories and high latitude source regions are probably caused by a combination of relatively low air temperatures in the polar region compared to lower latitudes, and shorter transport distance of the air mass preventing fractionation of the heavy (^{18}O) isotope.

The low sea salt concentrations observed during “typical” summer events are attributed to a combination of two effects. First, the weaker cyclones observed during summer result in less uplift of sea salt aerosols compared to winter events. Second, the slow transport of the air mass over the sea ice zone to Law Dome allows “rain out” of the heavy sea salt particles. Finally, examination of the nitrate signal during expected summer events did not reveal any obvious source region or transport mechanisms influencing summer nitrate signals.

Examination of events that differ from expected summer signals enable a greater understanding of the sensitivity of the Law Dome region to changes in atmospheric circulation. High summer sea salt events were found to be attributed to weak cyclonic systems with a trajectory that approaches Law Dome from due north. This differs from the northeast trajectories associated with the expected low summer sea salt events, and highlights the sensitivity of the sea salt signal to changes in atmospheric circulation in addition to variability in cyclone intensity. Enhanced summer concentrations of marine biological indicators were found to be associated with rapid advection of air from the biologically productive Heard Island region. Conversely, summer events associated with low or declining concentrations of marine biogenic indicators were found to be associated with advection of air sourced from lower latitudes (35 – 42°S) where marine productivity is lower, and where the distant source region may have contributed to “rain out” of the marine biogenic aerosols. However, the latter consideration is based on an assumption that marine biogenic aerosols are not “picked up” along the transport route for these events.

Autumn

Events that concur with expected autumn signals, namely declining levels of $\delta^{18}\text{O}$, MSA, non-sea salt sulphate and nitrate, and increasing concentrations of sea salts, were found to be associated with the formation of strong cyclonic systems that formed in the high latitudes. Only two events that concur with expected autumn signals were identified in the four year record, compared to ten events that differ from expected signals. The high number of these “unusual” autumn events may be a reflection of the variability in meteorological conditions during autumn, caused by the poleward migration of the location and increase in intensity of the circumpolar trough at this time of year. This variability is expected to impact on the chemical and isotopic record, yet is unlikely to be captured in ice core seasonality studies that involve calculating seasonal cycles from a composite of a number of years.

The majority of events that differ from expected autumn signals were characterised by low sea salt concentrations, diverting from the mid-high sea salt concentrations generally observed during autumn events. The occurrence of low sea salt concentrations during autumn is counter-intuitive to the poleward shift and increase in intensity of the circumpolar trough during autumn. These “unusual” low sea salt events were found to be associated with a combination of cyclonic systems that formed in both the high latitudes and midlatitudes. However, all events

showed a marked deceleration of the trajectory on approach to Law Dome, allowing a mechanism for “raining out” the heavy sea salt aerosols and producing a low sea salt signature in the snow pit. This was in contrast to the “typical” mid-high sea salt events where the trajectory indicated rapid advection of air from the high latitude source region to Law Dome. The comparison between low and mid-high sea salt events occurring during autumn highlights the influence of both atmospheric circulation and intensity of the cyclonic system on the sea salt signal for Law Dome ice cores. Finally, an examination of enhanced autumn marine biogenic indicators revealed a combination of meteorological conditions were found to influence the MSA and non-sea salt sulphate signals. Rapid advection of marine air from low latitudes provided an explanation for the autumn enhancements of marine biogenic indicators coupled with high levels of $\delta^{18}\text{O}$. In contrast, lower levels of $\delta^{18}\text{O}$ and enhanced marine biogenic indicators were found to be associated with the advection of air from the Heard Island region, providing further evidence for the importance of this region for marine biogenic signals preserved at Law Dome.

Winter

Events that concur with expected winter signals, namely low concentrations of MSA, non-sea salt sulphate, nitrate and $\delta^{18}\text{O}$, and high concentrations of sea salts, were found to be associated with well developed cyclonic systems, midlatitude source regions and relatively slow transport paths towards Law Dome. The high concentrations of sea salts preserved during typical winter events are consistent with the intrusion of well developed cyclonic systems. However, the relatively slow transport paths for the typical events may contribute to “rain out” of the heavy sea salt aerosols compared to events characterised by rapid advection of air. Comparisons between these high winter sea salt events revealed some variability in the sea salt signal, with higher sea salt concentrations associated with more intense cyclonic systems. These results provide evidence for the link between the intensity of the cyclonic system and the sea salt record, although events in other seasons (particularly summer and autumn) highlight the additional impact that atmospheric circulation may have on the sea salt signal.

The low concentrations of marine biogenic indicators (MSA, non-sea salt sulphate) during winter events are consistent with low biological activity in the Southern Ocean during winter. Low concentrations of nitrate during winter events are also consistent with the absence of marine biological activity in the Southern Ocean as well as limited downward mixing of stratospheric air during winter prior to the breakdown of the polar vortex in spring. Finally, the

low values of $\delta^{18}\text{O}$ preserved during typical winter events were found to be associated with either a midlatitude source region and a slow transport mechanism, allowing fractionation of the heavy (^{18}O) isotope, or a high latitude source region characterised by cold air temperatures.

Identification of events that differ from expected winter signals in the four year record was restricted to high winter $\delta^{18}\text{O}$ events. These high winter $\delta^{18}\text{O}$ events were associated with strong cyclonic systems and rapid advection of air from lower latitudes, in contrast to the slow transport mechanisms that influenced the low $\delta^{18}\text{O}$ winter events. Rapid advection of air from lower latitudes provides a mechanism for limited fractionation of the heavy isotope (^{18}O) during transport, maintaining relatively high $\delta^{18}\text{O}$ levels in the ice core. These events provide further evidence for the results presented in McMorrow and others (2001, 2002), and highlight the importance of atmospheric circulation on the $\delta^{18}\text{O}$ record at Law Dome.

Finally, examination of winter events suggest that winter conditions at Law Dome are relatively stable compared to other seasons. All the chemical signals, with the exception of $\delta^{18}\text{O}$, are associated with typical winter signals and limited variability. The low sensitivity of these chemical signals during winter may reflect the stability of the synoptic meteorological conditions in the Law Dome region at this time of year.

Spring

Events that concur with expected spring signals, namely increasing levels of $\delta^{18}\text{O}$, MSA, non-sea salt sulphate and nitrate, and declining concentrations in sea salts, were found to be associated with well defined cyclonic systems, although the intensity of the systems varied. Spring exhibits similar meteorological conditions to autumn, and is characterised by the intensification and poleward migration of the circumpolar trough during early spring. Events that occurred during early spring were found to reflect a chemical and isotopic signature similar to winter events, while events that occurred during late spring were found to reflect a signature similar to summer events.

The examination of events that differ from expected spring signals allowed a greater understanding of the atmospheric conditions influencing the chemical and isotopic signals. Examination of an event characterised by low sea salt concentrations and low $\delta^{18}\text{O}$ values was found to be associated with a local cyclonic system and cold air mass passing over Law Dome. This event highlights the sensitivity of these species to atmospheric circulation changes,

providing implications for interpreting the longer ice core record. Enhanced spring nitrate events were also identified in the four year record, with the most likely explanation attributed to the intrusion of stratospheric air through the breakdown of the polar vortex. Finally, enhanced spring marine biogenic indicators were found to be associated with two distinct transport mechanisms. One event was characterised by rapid advection of air from lower latitudes, while the other associated with a high latitude source region. These results imply that similar non-summer peaks in marine biogenic indicators from longer ice core records should be interpreted with caution.

8.9.2 Implications for Interpreting Longer Law Dome Ice Core Records

The event-scale discussion presented in this chapter provides a detailed analysis of potential source regions and transport mechanisms influencing the Law Dome ice core record. These results enhance our understanding of the meteorological conditions that produce chemical and isotopic signals in the ice core, allowing a better understanding of the link between the ice core record and climate. Specific results highlight the importance of understanding this link when interpreting longer ice core records from Law Dome.

Marine Biogenic Indicators: MSA and Non-Sea Salt Sulphate

The marine biogenic indicators are usually interpreted from Law Dome ice cores to reflect marine biogenic activity. That is, higher MSA and non-sea salt sulphate concentrations are generally interpreted as indicating increased biological activity in the Southern Ocean (Curran and others, 1998a; Palmer, 2002; Curran and others, 2002). In addition, these studies also generally attribute the sea ice zone as a source for the marine biogenic indicators, with peaks occurring in summer when biological productivity in the sea ice zone is at a maximum. However, the results presented in this thesis indicate that lower latitudes, and the Heard Island region in particular, may provide an important additional source region for MSA and non-sea salt sulphate signals preserved in Law Dome ice cores.

Enhanced summer marine biogenic indicators were found to be associated with rapid advection of air from the Heard Island region, providing evidence for the potential for variations in atmospheric circulation to impact on MSA and non-sea salt sulphate records in addition to simple variations in marine biogenic activity. Non-summer (autumn, spring) peaks in MSA and non-sea salt sulphate were also associated with rapid advection from the Heard Island region, providing further evidence for the potential for this region to be an important source region for

marine biogenic indicators outside the summer season. This transport mechanism also highlights the potential for variations in atmospheric circulation to impact on the MSA and non-sea salt sulphate records. Interpreting the longer MSA and non-sea salt sulphate records from Law Dome should consider the potential for increases in the frequency of large storm events with connections to lower latitudes (and the Heard Island region) to cause increased MSA and non-sea salt sulphate in the ice core, rather than simply increases in biological activity in the Southern Ocean. It is recommended that these atmospheric circulation effects are considered when interpreting longer ice core records from Law Dome.

Sea Salts

Sea salt concentrations from Law Dome ice cores are usually interpreted as reflecting variations in storm intensity in the Southern Ocean, with high sea salt events indicating large storm events (Curran and others, 1998a; Palmer, 2002; Curran and others, 2002). The results presented in this thesis provides further evidence for a link between the intensity of the storm event and sea salt concentrations. High sea salt events were found to be associated with stronger cyclonic systems.

However, this thesis also presented results that provide evidence for the potential for atmospheric circulation variations to influence the sea salt signal. In particular, high sea salt events were associated with trajectories that indicate a northerly approach to Law Dome, while lower sea salt events were characterised by a north-easterly approach. A northerly approach provides maximum transport along open water before reaching Law Dome, facilitating uplift of sea salt aerosols along most of the trajectory. In addition, the event-scale investigation showed the potential for the approach speed of the air mass to influence the Law Dome sea salt signal. Events that were associated with a marked deceleration in trajectory speed on approach to Law Dome also tended to be associated with lower sea salt concentrations, with the slow approach facilitating “rain out” of the heavy sea salt aerosols. It is recommended that both cyclone intensity and atmospheric circulation variations, including speed and direction of the trajectory, are considered when interpreting sea salt records from deep ice cores at Law Dome.

Finally, limited results also indicated the potential for low sea salt events to be associated with strong cyclonic systems and a low latitude source region. The distant source region provides a possible explanation, as the heavy sea salt aerosols may have “rained out” during transport. However, this hypothesis relies on the assumption that sea salt particles, at least during these

events, are not “picked up” along the transport route. Further research using three dimensional trajectories is recommended.

$\delta^{18}\text{O}$

The Law Dome $\delta^{18}\text{O}$ signal is generally used as an indicator for air temperature (Morgan and van Ommen, 1997). The results presented in this thesis provide further evidence for a strong link between the Law Dome $\delta^{18}\text{O}$ signal and site air temperatures, yet atmospheric circulation variations were also shown to influence the $\delta^{18}\text{O}$ signal. A number of high winter $\delta^{18}\text{O}$ events were examined to determine when the $\delta^{18}\text{O}$ signal may divert from temperature signals.

Results indicate that high winter $\delta^{18}\text{O}$ events were generally associated with rapid advection of air from lower latitudes. Rapid advection of air from lower latitudes prevents fractionation of the heavy (^{18}O) isotopes during transport, resulting in a relatively high $\delta^{18}\text{O}$ signal preserved in the ice core. This result highlights the potential for atmospheric circulation changes to impact on $\delta^{18}\text{O}$ signals preserved in deeper ice core records at Law Dome. For example, reductions in the deeper Law Dome $\delta^{18}\text{O}$ records may be the result of a combination of a reduction in air temperature and/or a reduction in storm activity, breaking down the mechanism for a link between Law Dome and lower latitudes. It is recommended that both air temperature variations and atmospheric circulation variations are considered when interpreting longer $\delta^{18}\text{O}$ records from Law Dome.

Nitrate

The Antarctic nitrate signal is complex and is influenced by multiple potential sources and transport mechanisms. The results presented in this thesis show a definite spring enhancement of nitrate that tends to coincide with enhanced non-sea salt sulphate, without a corresponding enhancement of MSA. Spring enhancement of nitrate and non-sea salt sulphate is consistent with the transport of nitrogen species from the stratosphere to the troposphere through the spring weakening of the polar vortex. The absence of coinciding peaks in MSA during these high nitrate and non-sea salt sulphate events suggests that marine biogenic sulphate is not a major contributor to the non-sea salt sulphate records, and further implies the influence of either a stratospheric or long range tropospheric source influencing these spring events rather than local or regional sources. While the results presented in this thesis do not provide concrete evidence for this hypothesis, the analysis does suggest the importance of downward mixing of stratospheric air during spring. It is recommended that the interpretation of longer nitrate and

non-sea salt sulphate records from Law Dome consider potential effects of downward mixing of stratospheric air during spring.

Seasonal Variability in Meteorology

Seasonal variability in meteorology has the potential to impact on the interpretation of deeper ice core records. Interpretation of the deeper ice core record, particularly for sites that resolve sub-annual cycles, often relies on the assumption of uniform accumulation throughout the year. Indeed, sub-annual analysis on the deep record at Law Dome has often adopted this assumption (van Ommen and Morgan, 1996; Morgan and van Ommen, 1997b; Curran and others, 1998). The results presented in Chapter 4 of this thesis highlight the potential for snow accumulation to vary significantly through the year, and between years. This will not significantly affect long term studies which determine seasonality in the ice core record by averaging annual cycles of many years, but may affect studies which examine seasonality using high resolution short term records. Variability in accumulation within and between years will also affect studies which examine a particular year or epoch in detail. In these cases the accumulation variability may bias the analysis unless independent accumulation records are available and considered in the ice core interpretation.

In addition, the results presented in this chapter indicate the potential for variability in synoptic scale meteorology to impact on the chemical and isotopic signals. The results show the potential for autumn, and to a lesser extent spring, to exhibit higher variability in chemical and isotopic signals, diverting from expected seasonal signals. In contrast, summer, and in particular winter, appear to reflect more stable chemical and isotopic signals, consistent with the more stable meteorological conditions during these seasons. Higher variability during autumn and spring events is consistent with the shifting meteorological conditions that occurs in the equinoctial seasons. This higher variability may not be captured in seasonal ice core studies, where the seasonal signals are determined through averaging records over a number of years and creating a “composite” seasonal signal. However, it is useful to consider the potential enhanced variability during equinoctial seasons when interpreting longer ice cores.

Atmospheric Circulation Variability

The events examined in this thesis show the particular influence of atmospheric circulation variations on chemical and isotopic signals from Law Dome. The coastal location of Law Dome ensures the ice core records are dominated by cyclonic precipitation, with the quasi-

stationary cyclone located in the midlatitudes to the northwest of Law Dome providing a particularly strong influence. In addition, variations in these cyclonic systems provide a range of meridional source regions (low, mid or high latitude) and transport mechanisms for the chemical and isotopic signals. Variations in atmospheric circulation patterns over time are therefore expected to more strongly influence Law Dome ice core records compared to inland ice core records covering the same epoch. When interpreting deeper Law Dome ice core records, it is recommended that variations in atmospheric circulation patterns through time are considered as a potential explanation for particular chemical and isotopic signals. In addition, due to the enhanced influence of atmospheric circulation for Law Dome compared to inland ice core sites in Antarctica, atmospheric circulation variations may provide an explanation for deviations between Law Dome and inland ice core records covering a particular epoch.

Finally, the strong dependence of Law Dome on atmospheric circulation variability provides the opportunity for Law Dome ice cores to consider a wide range of palaeoclimate variations. Law Dome ice cores have the potential to comment not only on changes in meteorological observations (eg. lower temperatures in the early Holocene), but also through considering how the dominant atmospheric circulation patterns may have changed through time (eg. reduction in storm activity reflected by decreased sea salt concentrations, cyclonic systems constrained to higher latitudes resulting in reduced advection of air from lower latitudes and reflected by reduced $\delta^{18}\text{O}$ values and marine biogenic indicators). The dataset of event-scale investigations presented in this thesis provides a starting point for further research into considering how variations in chemical and isotopic signals in longer ice cores may signify atmospheric circulation variability over time.

Chapter 9

Conclusions and Recommendations for Further Research

9.1 Conclusions

The work presented in this thesis involved a detailed investigation of the link between chemical and isotopic signals preserved in Antarctic snow and meteorological observations. High resolution records of $\delta^{18}\text{O}$, sea salt ions (sodium, chloride, magnesium), marine biogenic compounds (MSA, non-sea salt sulphate) and nitrate were obtained from a series of snow pits and firn cores from the high accumulation site near Law Dome summit, East Antarctica. The snow pit and firn core records were sampled at 2.5 cm resolution, equating to approximately 50 samples per year, and allowing an ultra high resolution study of the top 10 m of the snowpack.

This study presented a detailed investigation of the spatial reproducibility of chemical and isotopic signals preserved in Law Dome ice cores. Snow pit and firn core records were compared at various scales across Law Dome to identify regional accumulation events preserved in the snowpack. Despite the effects of accumulation differences between drilling sites, surface snow redistribution by wind and surface irregularity, the results show excellent agreement in multiple high resolution chemical and $\delta^{18}\text{O}$ records up to 7.7 km apart at Law Dome. Major chemical and isotopic signals were preserved in all snow pits and firn cores at the sub-seasonal scale, and regional accumulation events were identified for further analysis and comparison with meteorological conditions.

This study also developed an accurate technique for dating high resolution snow pit and firn core records. Individual snowfall events preserved in the snow pits and firn cores were identified using an automated weather station (AWS) equipped with a snow accumulation sensor. This technique provided a high resolution dating scale for the chemical and isotopic signals that was independent of the ice core signals under investigation. The high resolution dating scale highlighted the inter-annual variability and episodic nature of snow accumulation at Law Dome, with implications for interpreting deeper ice core records.

This study presented a detailed investigation of the seasonality of chemical and isotopic signals preserved at Law Dome over four annual cycles. The unique dating technique allowed, for the first time, the examination of exact timings in the seasonality of each species. The traditional summer-maximum species of $\delta^{18}\text{O}$ and MSA showed consistent relative phasing during mid-summer over the four annual cycles. Nitrate showed an erratic seasonal cycle with a general trend characterised by narrow peaks during spring and early summer, preceding the mid-summer peaks in $\delta^{18}\text{O}$ and MSA. Non-sea salt sulphate cycles indicated similar characteristics to MSA signals during summer, but were found to be more comparable to nitrate signals during spring, autumn and winter. Finally, the sea salt species indicated a noisy seasonal cycle characterised by maximum concentrations during spring, autumn and winter.

The seasonality discussion was refined by presenting a detailed analysis of event-scale comparisons between chemical and isotopic signals, and meteorological conditions. Results from the event-scale investigation provided potential explanations for the chemical and isotopic signals in Law Dome ice cores, allowing a better understanding of the link between the ice core record and climate.

Potential source regions and transport mechanisms were examined for the marine biogenic indicators (MSA, non-sea salt sulphate). Results indicated that the seasonal variation in marine biogenic activity is reflected in the Law Dome records, and the sea ice zone provides an important source region. However, results also indicated that lower latitudes, and the Heard Island region (50°S, 70°E) in particular, may provide

an important additional source region for MSA and non-sea salt sulphate outside the summer season.

Examination of potential source regions and transport mechanisms for sea salt signals provided further evidence for a link between the intensity of the storm event and sea salt concentrations. High sea salt events were found to be associated with stronger cyclonic systems. However, results also indicated the potential for atmospheric circulation variations, including speed and direction of the trajectory, to influence the sea salt signal. Rapid advection of air from marine source regions, and a northerly approach to Law Dome, generally resulted in high sea salt concentrations.

The Law Dome $\delta^{18}\text{O}$ signal is traditionally used as an indicator for air temperature, and the results presented in this thesis provided further evidence for a strong link between the Law Dome $\delta^{18}\text{O}$ signal and site air temperatures. However, atmospheric circulation variations were also shown to influence the $\delta^{18}\text{O}$ signal, with enhanced $\delta^{18}\text{O}$ events generally associated with rapid advection of air from lower latitudes.

Examination of the nitrate signal indicated a definite spring enhancement of nitrate that coincided with enhanced non-sea salt sulphate, and without a corresponding enhancement of MSA. Spring enhancement of nitrate and non-sea salt sulphate is consistent with the transport of nitrogen species from the stratosphere to the troposphere through the spring weakening of the polar vortex. The absence of coinciding peaks in MSA during these enhanced nitrate and non-sea salt sulphate events suggests that marine biogenic sulphate is not a major contributor to the non-sea salt sulphate records, and further implies the influence of a stratospheric source influencing these spring events. While the results presented in this thesis do not provide concrete evidence for this hypothesis, the analysis does suggest the importance of downward mixing of stratospheric air during spring.

The events examined in this thesis showed the particular influence of atmospheric circulation variations on chemical and isotopic signals at Law Dome. The coastal location of Law Dome ensures the ice core records are dominated by cyclonic precipitation, with the quasi-stationary cyclone located in the midlatitudes to the

northwest of Law Dome providing a particularly strong influence. In addition, variations in these cyclonic systems provide a range of meridional source regions (low, mid or high latitude) and transport mechanisms for the chemical and isotopic signals. Variations in atmospheric circulation patterns over time are therefore expected to more strongly influence Law Dome ice core records compared to inland Antarctic ice core records covering the same epoch. When interpreting deeper Law Dome ice core records, it is recommended that variations in atmospheric circulation patterns through time are considered as a potential explanation for particular chemical and isotopic signals. In addition, due to the enhanced influence of atmospheric circulation for Law Dome compared to inland ice core sites in Antarctica, atmospheric circulation variations may provide an explanation for deviations between Law Dome and inland ice core records covering a particular epoch.

Finally, the strong dependence of Law Dome on atmospheric circulation variability provides the opportunity for Law Dome ice cores to consider a wide range of palaeoclimate variations. Law Dome ice cores have the potential to comment not only on changes in meteorological observations (eg. lower temperatures in the early Holocene), but also through considering how the dominant atmospheric circulation patterns may have changed through time (eg. reduction in storm activity reflected by decreased sea salt concentrations, cyclonic systems constrained to higher latitudes resulting in reduced advection of air from lower latitudes reflected by reduced $\delta^{18}\text{O}$ values and marine biogenic indicators). The dataset of event-scale investigations presented in this thesis provides a starting point for further research into considering how variations in chemical and isotopic signals in longer ice cores may signify atmospheric circulation variability over time.

9.2 Areas for Further Research

The results presented in this thesis highlight a number of areas for further research.

The extension of ultra high resolution records at Law Dome is recommended. This study was restricted to four annual cycles and the examination of 48 accumulation events preserved in the snow pits and firn cores. Extending the ultra high resolution

records would allow more detailed analysis of the local and synoptic meteorological conditions that are associated with the accumulation events.

The expansion of tools for analysing potential source regions and transport mechanisms is also recommended. Satellite imagery that allows the identification of marine biological activity could be compared with MSA and non-sea salt sulphate signals preserved in the snow pits and firn cores. A more detailed investigation of the sea ice extent around Law Dome throughout the year may provide more insight into source regions and transport mechanisms that influence the sea salt signal. A more detailed analysis of the downward mixing of stratospheric air through upper-atmospheric meteorological studies may provide more insight into the role of the stratosphere in the nitrate signature at Law Dome. Three dimensional trajectories that track the vertical position of the air mass as well as the horizontal transport will provide more information on how an air mass may “pick up” and “drop off” chemical and isotopic species during transport.

Finally, examining the deep DSS ice core record for chemical and isotopic signals that are similar to the unusual events detailed in this thesis is recommended. The results presented in this thesis enhance our understanding of the link between the chemical and isotopic signals during specific meteorological events. Applying this knowledge to the interpretation of deeper ice core records from Law Dome will enhance our understanding of the link between ice core signals and past climate conditions.

Reference List

Allan, B. J., N. Carslaw, H. Coe, R. A. Burgess and J. M. C. Plane, Observations of the nitrate radical in the marine boundary layer, *J. Atmos. Chem.*, 33, 129-154, 1999.

Anderson, T. L., G. V. Wolfe and S. G. Warren, Biological sulphur, clouds and climate, in *Ice Core Studies of Biogeochemical Cycles, NATO ASI Series I: Global Environmental Change*, edited by R. J. Delmas, Springer-Verlag, Berlin, pp 139-173, 1995.

Ayers, G. P., J. P. Ivey and R. W. Gillett, Coherence between seasonal cycles of dimethyl sulphide, methansulphonate and sulphate in marine air, *Nature*, 349, 404-406, 1991.

Araguas-Araguas, L., K. Fröhlich, and K. Rozanski, Deuterium and oxygen-18 isotope composition of precipitation and atmospheric moisture, *Hydrol. Process.*, 14, 1341-1355, 2000.

Bergin, M. H., J.-L. Jaffrezo, C. I. Davidson, J. E. Dibb, S. N. Pandis, R. Hillamo, W. Maenhaut, H. D. Kuhns and T. Makela, The contributions of aerosol chemical species based on snow core chemistry at Summit, Greenland, *Geophys. Res. Lett.*, 100, 16275-16288, 1995.

Bradley R. S. and P. D. Jones, 'Little Ice Age' summer temperature variations: their nature and relevance to recent global warming trends, *The Holocene*, 3, 367-376, 1993.

Bradley, R. S., Palaeoclimatology: Reconstructing climates of the Quaternary, in *International geophysics series, vol. 64*, Edited by R. Dmowska and J. R. Holton, Harcourt/Academic Press, San Diego, US, 1999.

Bromwich, D. H, and C. J. Weaver, Latitudinal displacement from main moisture source control $\delta^{18}\text{O}$ of snow in coastal Antarctica, *Nature*, 301, 145-147, 1983.

Burgermeister, S. and H.-W. Georgii, Distribution of methansulphonate, nss sulphate and dimethylsulfide over the Atlantic and North Sea, *Atmos. Envir.*, 25A, 587-595, 1991.

Charlson, R. J., J. E. Lovelock, M. O. Andreae and S. G. Warren, Oceanic phytoplankton, atmospheric sulphur, cloud albedo and climate, *Nature*, 326, 655-661, 1987.

Clausen, H. B. and C. C. Langway, The ionic deposits in polar ice cores, in *The Environmental Record in Glaciers and Ice Sheets, Dahlem Konferenzen*, edited by H. Oeschger and C. C. Langway, pp 225-248, John Wiley, New York, 1989.

Craig, H, Isotopic variation in meteoric waters. *Science*, 133, 1702-1703, 1961.

Curran, M. A. J., van Ommen, T. D., Morgan, V. I., Phillips, K. L. and A. S. Palmer, Ice core evidence for Antarctic sea ice decline since the 1950s, *Science*, 302, 1203-1206, 2003.

Curran, M. A. J., Palmer, A. S., van Ommen, T. D., Morgan, V. I., Phillips, K. L., McMorrow, A. J. and P. A. Mayewski, Post-depositional movement of methansulphonic acid at Law Dome, Antarctic, and the influence of accumulation rate, *Ann. Glaciol.*, 35, 333-339, 2002.

Curran, M. A. J. and G. B. Jones, Dimethyl sulfide in the Southern Ocean: Seasonality and flux, *J. Geophys. Res.*, 105(D16), 20541-20459, 2000.

Curran, M. A. J., T. D. van Ommen and V. Morgan, Seasonal characteristics of the major ions in the high accumulation Dome Summit South ice core, Law Dome, Antarctica, *Ann. Glaciol.*, 27, 385-390, 1998a.

Curran, M. A. J., G. B. Jones and H. Burton, Spatial distribution of DMS and DMSP in the Australasian sector of the Southern Ocean, *J. Geophys. Res.*, 103(D13), 16677-16689, 1998b.

Dansgaard, W., Stable isotopes in precipitation, *Tellus*, 16, 436-468, 1964.

Davidson, C. I., Mechanisms of wet and dry deposition of atmosphere contaminants to snow surfaces, in *Dahlem Konferenzen: The Environmental Record in Glaciers and Ice Sheets*, edited by H. Oeschger and C. C. Langway Jr, John Wiley, New York, pp 29-51, 1989.

Davidson, C. I., M. H. Bergin, H. D. Kuhns, The deposition of particles and gases to ice sheets, in *Chemical Exchange Between the Atmosphere and Polar Snow*, *NATO ASI Ser. I, vol. 43*, edited by E. W. Wolff and R. C. Bales, Springer-Verlag, New York, pp 275-306, 1996.

Delmas, R., Ice-core records of global climatic change and environmental changes, *P.Indian As-Math Sci.*, 4,307-319, 1998.

Dibb, J. E., and S. I. Whitlow, Recent climate anomalies and their impact on snow chemistry at South Pole, 1987-1994, *Geophys. Res. Lett.*, 23(10), 1115-1118, 1996.

Dreschhoff, G. A. M. and E. J. Zeller, Ultra-high resolution nitrate in polar ice as indicator of past solar activity, *Sol. Phys.*, 1997, 365-374, 1998.

Faure, G., The principles of mass spectrometer, in *Principles of Isotope Geology*, edited by G. Faure, John Wiley and Sons, New York, pp 56-65, 1986.

Fitzgerald, J. W., Marine aerosols: A review, *Atmos. Envir.*, 25A, 533-545, 1991.

Fuhrer, K., M. Hutterli and J. R. McConnell, Overview of recent field experiments for the study of the air-snow transfer of H₂O₂ and HCHO, in *Chemical Exchange Between the Atmosphere and Polar Snow*, *NATO ASI Ser. I, vol. 43*, edited by E. w. Wolff and R. C. Bales, Springer-Verlag, New York, pp 307-338, 1996.

Gibson, J. A. E., R. C. Garrick, H. R. Burton and A. R. Taggart, Dimethylsulfide and the alga *Phaeocystis pouchetii* in Antarctic coastal waters, *Mar. Biol.*, 104, 339-346, 1990.

Gloersen, P., W. J. Campbell, D. J. Cavalieri, J. C. Comiso, C. L. Parkinson and J. H. Zwally, *Arctic and Antarctic Sea Ice, 1978-1987, satellite passive-microwave observations and analysis, NASA Scientific and Technical Information Program*, Library of Congress, Washington D. C., 1992.

Gong, S. L., L. A. Barrie, J. M. Prospero, D. L. Savoie, G. P. Ayers, J. P. Blanchet and L. Spacek, Modeling sea-salt aerosols in the atmosphere 2. Atmospheric concentrations and fluxes, *J. Geophys. Res.*, 102, 3819-3830, 1997.

Goodwin, I. D., van Ommen, T. D., Curran, M. A. J., and P. A. Mayewski, Mid latitude winter climate variability in the South Indian and southwest Pacific regions since 1300 AD, *Climate Dynamics*, 22(8), 783-794, 2004.

Hall, J. S. and E. W. Wolff, Causes of seasonal and daily variations in aerosol sea-salt concentrations at a coastal Antarctica station, *Atmos. Envir.*, 32, 3669-3677, 1998.

Harder, S. L., S. G. Warren, R. J. Charlson and D. S. Covert, Filtering of air through snow as a mechanism for aerosol deposition to the Antarctic ice sheet, *J. Geophys. Res.*, 101, 18729-18743, 1996.

Harder, S. L., S. G. Warren and R. J. Charlson, Sulphate in air and snow at the South Pole: implications for transport and deposition at sites with low accumulation, *J. Geophys. Res.*, 105, 22825-22832, 2000.

Hardy, D. R., M. Vuille, C. Braun, F. Keimig and R. S. Bradley, Annual and daily meteorological cycles at high altitude on a tropical mountain, *Bull. Amer. Meteorol. Soc.*, 79(9), 1899-1913, 1998.

- Horita, J. and D. Wesolowski, Liquid-vapour fractionation of oxygen and hydrogen isotopes of water from the freezing to the critical temperature, *Geochemica Cosmochimica Acta*, 58, 3424-3437, 1994.
- Hu, S. and W. O. Smith, Jr, The effects of irradiance on nitrate uptake and dissolved organic nitrogen release by phytoplankton in the Ross Sea, *Cont. Shelf Res.*, 18, 971-990, 1998.
- Isaksson, E., Karlén, W., Magewski, P., Twickler, M. and S. Whitlow, A high-altitude snow chemistry record from Amundsenisen, Dronning Maud Land, Antarctica, *J. Glaciol.*, 47(158), 489-496, 2001.
- Kaleschke, A., Richter, A., Burrows, J., Afe, O., Heygster, G., Notholt, J., Rankin, A. M., Roscoe, H. K., Hollwedel, J., Wagner, T. and H.-W. Jacobi, Frost flowers on sea ice as a source of sea salt and their influence on tropospheric halogen chemistry, *Geophys. Res. Lett.*, 31, L16114, doi:10.1029/2004GL020655, 2004.
- Kato, K., Factors controlling oxygen isotope composition of fallen snow in Antarctica, *Nature*, 272, 46-48, 1978.
- King, J. C., P. S. Anderson, M. C. Smith and S. D. Mobbs, The surface energy and mass balance at Halley, Antarctica during winter, *J. Geophys. Res.*, 101, 19119-19128, 1996.
- King, J. C. and J. Turner, *Antarctic meteorology and climatology*, Cambridge University Press, Cambridge, 1997.
- Knox, G. A., Ice edge processes, in *The Biology of the Southern Ocean*, edited by G. A. Knox, Cambridge University Press, Cambridge, pp 245-263, 1994.
- König-Langlo, G., J. C. King and P. Pettré, Climatology of the three coastal Antarctic stations Dumont d'Urville, Neumayer, and Halley, *J. Geophys. Res.*, 103(D9), 10935-10946, 1998.

Kreutz, K. J., P. A. Magewski, S. I. Whitlow and M. S. Twickler, Limited migration of soluble ionic species in a Siple Dome, Antarctica, ice core, *Ann. Glaciol.*, 27, 371-377, 1998.

Kreutz, K. J., P. A. Mayewski, M. S. Twickler, S. I. Whitlow, J. W. C. White, C. A. Shuman, C. F. Raymond, H. Conway and J. R. McConnell, Seasonal variations of glaciochemical, isotopic and stratigraphic properties in Siple Dome (Antarctica) surface snow, *Ann. Glaciol.*, 29, 38-44, 1999.

Latham, J. and M. H. Smith, Effect on global warming of wind-dependent aerosol generation at the ocean surface, *Nature*, 347, 372-373, 1990.

Legrand, M., Chemistry of Antarctic snow and ice, *J. Phys.*, 48, 77-86, 1987.

Legrand, M., Sulphur-derived species in polar ice: A review, in: *Ice Core Studies of Biogeochemical Cycles. NATO ASI Series. 1: Global Environmental Change*, edited by R. J. Delmas, Springer-Verlag, Berlin, pp 91-119, 1995.

Legrand, M., Ice-core records of atmospheric sulphur, *Phil. Trans. R. Soc. Lond. B.*, 35, 241-250, 1997.

Legrand M. R. and R. J. Delmas, The ionic balance of Antarctic snow: a 10-year detailed record, *Atmos. Envir.*, 18, 1867-1874, 1984.

Legrand, M. R. and R. J. Delmas, Relative contributions of tropospheric and stratospheric sources to nitrate in Antarctic snow, *Tellus*, 38B, 236-249, 1986.

Legrand, M. and R. J. Delmas, Soluble impurities in four Antarctic ice cores over the last 30,000 years, *Ann. Glaciol.*, 10, 116-120, 1988.

Legrand, M., C. Feinet-Saigne, E. S. Saltzman, C. Germain, N. I. Barkov and V. N. Petrov, Ice-core record of oceanic emissions of dimethylsulphide during the last climate cycle, *Nature*, 350, 144-147, 1991.

- Legrand, M. R. and S. Kirchner, Origins and variations of nitrate in south polar precipitation, *J. Geophys. Res.*, 95, 3493-3507, 1990.
- Legrand, M. and P. Mayewski, Glaciochemistry of polar ice cores: A review, *Rev. Geophys.*, 35, 219-243, 1997.
- Legrand, M. and E. C. Pasteur, Methane sulfonic acid to non-sea-salt sulfate ratio in coastal Antarctic aerosol and surface snow, *J. Geophys. Res.*, 103(D9), 10991-11006, 1998.
- Legrand, M. R., F. Stordal, I. S. A. Isaksen and B. Rogenrud, A model study of the stratospheric budget of odd nitrogen, including effects of solar cycle variations, *Tellus*, 41B, 413-426, 1989.
- Levy, H., II, W. J. Moxim, A. A. Klonecki, and P. S. Kasibhatla, Simulated tropospheric NO_x: its evaluation, global distribution and individual source contributions, *J. Geophys. Res.*, 104, 27279-26306, 1999.
- Mann, M. E. and P. D. Jones, Global surface temperatures over the past two millennia, *Geophys. Res. Lett.*, 30(15), 1820, doi:10.1029/2003GL017814, 2003.
- Masson-Delmotte, V., Stenni, B. and J. Jouzel, Common millennial-scale variability of Antarctic and Southern Ocean temperatures during the past 5000 years reconstructed from the EPICA Dome C ice core, *The Holocene*, 14(2), 145-151, 2004.
- Masson-Delmotte, V., Delmotte, M., Morgan, V., Etheridge, D., van Ommen, T., Tartarin, S. and G. Hoffmann, Recent southern Indian Ocean climate variability inferred from a Law Dome ice core: new insights for the interpretation of coastal Antarctic isotopic records, *Climate Dynamics*, 21(2), 153-166, 2003.
- Mayewski, P. A., Kirk, K. A., White, J. W. C., Steig, E. J., Meyerson, E., Goodwin, I., Morgan, V. I., van Ommen, T. and M. A. J. Curran, A 700 year record of Southern Hemisphere extratropical climate variability, *Ann. Glaciol.*, 39(1), 127-132, 2004.

Mayewski, P. A. and M. R. Legrand, Recent increase in nitrate concentration of Antarctic snow, *Nature*, 346, 258-260, 1990.

McConnell, J. R., R. C. Bales, J. R. Winterle, H. Kuhns and C. R. Stearns, A lumped parameter model for the atmosphere-to-snow function for hydrogen peroxide, *J. Geophys. Res.*, 102(D18), 26089-26818, 1997a.

McConnell, J. R., R. C. Bales and D. R. Davis, Recent intra-annual snow accumulation at South Pole: implications for ice core research, *J. Geophys. Res.*, 102(D18), 21947-21954, 1997b.

McCracken, K. G., G. A. M. Dreschhoff, E. J. Zeller, D. F. Smart and M. A. Shea, Solar cosmic ray events for the period 1561-1994, 2, The Gleissberg periodicity, *J. Geophys. Res.*, 106, 21599-21609, 2001.

McInnes, L. M., D. S. Covert, P. K. Quinn and M. S. Germani, Measurements of chloride depletion and sulfur enrichment in individual sea-salt particles collected from remote marine boundary layer, *J. Geophys. Res.*, 90(D4), 8257-8268, 1994.

McMorrow, A. J., M. A. J. Curran, T. D. van Ommen, V. Morgan, I. Allison and M. J. Pook, Intercomparison of firn core and meteorological data, *Ant. Sci.*, 13(3), 329-337, 2001.

McMorrow, A. J., M. A. J. Curran, T. D. van Ommen, V. Morgan and I. Allison, Features of meteorological events preserved in a high resolution Law Dome snow pit, *Ann. Glaciol.*, 35, 463-470. 2002.

McMorrow, A. J., van Ommen, T.D., Morgan, V. and M. A. J Curran, Ultra high resolution seasonality of trace ion species and oxygen isotope ratios over 4 annual cycles. *Annals of Glaciology.*, 39, 34-40, 2003.

Minikin, A., D. Wagenbach, W. Graf and J. Kipfstuhl, Spatial and seasonal variations of the snow chemistry at the Filchner-Ronne Ice Shelf, Antarctica, *Ann. Glaciol.*, 20, 283-290, 1994.

Minikin, A., M. Legrand, J. Hall, D. Wagenbach, C. Kleefeld, E. Wolff, E. C. Pasteur and R. Ducroz, Sulfur-containing species (sulfate and methansulfonate) in coastal Antarctic aerosol and precipitation, *J. Geophys. Res.*, 103(D9), 10975-10990, 1998.

Möller, D., Cloud processes in the troposphere, in *Ice Core Studies of Global Biogeochemical Cycles, NATA ASI Ser. I, vol. 30*, edited by R. Delmas, Springer-Verlag, New York, pp 39-64, 1995.

Morgan, V., Oxygen isotope analysis of Antarctic snow and ice, Masters of Science thesis, Meteorology Department, University of Melbourne, 1979.

Morgan, V., and T. van Ommen, Seasonality in late-Holocene climate from ice core records, *The Holocene*, 7(3), 351-354, 1997.

Mosley-Thompson, E., J. Dai, L. G. Thompson, P. M. Grootes, J. K. Arbogast and J. F. Paskievitch, Glaciological studies at Siple Station (Antarctica): potential ice-core paleoclimatic record, *J. Glaciol.*, 37, 11-22, 1991.

Mulvaney, R., E. C. Pasteur and D. A. Peel, The ratio of MSA to non-sea-salt sulphate in Antarctic Peninsula ice cores, *Tellus*, 44B, 295-303, 1992.

Mulvaney, R. and E. W. Wolff, Evidence for winter/spring denitrification of the stratosphere in the nitrate record of Antarctic firn cores, *J. Geophys. Res.*, 98(D3), 5213-5220, 1993.

Mulvaney, R., D. Wagenbach and E. W. Wolff, Postdepositional change in snowpack nitrate from observation of year-round near-surface snow in coastal Antarctica, *J. Geophys. Res.*, 103(D9), 11021-11031, 1998.

- Naftz, D. L., Susong, D. D., Schuster, P. F., DeWayne Cecil, L., Dettinger, M. D., Michel, R. L., and C. Kendall, Ice core evidence of rapid air temperature increases since 1960 in alpine areas of the Wind River Range, Wyoming, United States, *J. Geophys. Res.*, 107(D13), 4171, doi:10.1029/2001FD000621, 2002.
- O'Dowd, C. D., M. H. Smith, I. E. Consterdine and J. A. Lowe, Marine aerosol, sea-salt, and the marine sulphur cycle: a short review, *Atmos. Envir.*, 31, 73-80, 1997.
- O'Dowd, C. D., J. A. Lowe and M. H. Smith, Coupling sea-salt and sulphate interactions and its impact on cloud droplet concentration predictions, *Geophys. Res. Lett.*, 26, 1311-1314, 1999.
- Palmer, A. S., T. D. van Ommen, M. A. J. Curran and V. Morgan, Ice-core evidence for a small solar-source of atmospheric nitrate, *Geophys. Res. Lett.*, 28, 1953-1956, 2001.
- Pasteur, E. C. and R. Mulvaney, Migration of methane sulphonate in Antarctic firn and ice, *J. Geophys. Res.*, 105(D9), 11525-11534, 2000.
- Pearce, F., Lightning sparks pollution rethink, *New Sci.*, 2066, 15, 1997.
- Peel, D. A. and R. Mulvaney, Time-trends in the pattern of ocean-atmospheric exchange in an ice core from the Weddell Sea sector of Antarctica, *Tellus*, 44B, 430-442, 1992.
- Perovich, D. K. and J. A. Richter-Monge, Surface characteristics of lead ice, *J. Geophys. Res.*, 99, 16341-16350, 1994.
- Petit, J. R., M. Briat and A. Roger, Ice age aerosol content from east Antarctic ice core samples and past wind strength, *Nature*, 293, 391-394, 1981.
- Picciotto, E., X. de Maere and I. Friedman, Isotopic composition and temperature of formation of Antarctic snow, *Nature*, 187, 857-859, 1960.

Pomeroy, J. W. and H. G. Jones., Wind-blown snow: sublimation, transport and changes to polar snow, in *Chemical Exchange Between the Atmosphere and Polar Snow*, NATO ASI Ser. I, vol. 43, edited by E. W. Wolff and R. C. Bales, Springer-Verlag, New York, pp 453-489, 1996.

Pourchet, M., F. Pinglot, and C. Lorius, Some meteorological applications of radioactive fallout measurements in Antarctic snows, *J. Geophys. Res.*, 88, 6013-6020, 1983.

Rankin, A. M., V. Auld and E. W. Wolff, Frost flowers as a source of fractionated sea salt aerosol in the polar regions, *Geophys. Res. Lett.*, 27, 3469-3473, 2000.

Rankin A. M., Wolff, E. W. and S. Martin, Frost flowers: Implications for tropospheric chemistry and ice core interpretation, *J. Geophys. Res.*, 107(D23), 4683, doi:10.1029/2002JD002492, 2002.

Rankin, A. M., Wolff, E. W. and R. Mulvaney, A reinterpretation of sea-salt records in Greenland and Antarctic ice cores?, *Ann. Glaciol.*, 39, 276-282, 2004.

Schneider, D. P., Steig, E. J. and T. van Ommen, High resolution ice-core stable-isotopic records from Antarctica: towards interannual climate reconstruction, *Ann. Glaciol.*, 41, 63-70, 2005.

Schotterer, U., K. Fröhlich, H. W. Gäggeler, S. Sandjordi and W. Stichler, Isotope records from Mongolian and Alpine ice cores as climate indicators, *Climatic Change*, 36, 287-298, 1997.

Shaw, G. E., Antarctic aerosols: a review, *Rev. Geophys.*, 26, 890112, 1988.

Siegenthaler, U., and H. Oeschger, Correlation of O-18 in precipitation with temperature and altitude, *Nature*, 285, 314-317, 1980.

Sigg, A. and A. Neftel, Evidence for a 50% increase in H₂O₂ over the past 200 years from a Greenland ice core, *Nature*, 351, 557-559, 1991.

Skoog, A., R. Lara and G. Kattner, Spring-summer cycling of DOC, DON and inorganic N in a highly seasonal system encompassing the Northeast Water Polynya, 1993, *Deep-Sea Res. Pt. 1-Oceanog. Res.*, 48, 2613-2619, 2001.

Smith, W. O. and D. M. Nelson, Importance of ice edge phytoplankton in the Southern Ocean, *Bioscience*, 36(4), 251-257, 1991.

Smith, B. T., van Ommen, T. D., and M. A. J. Curran, Methane sulphonic acid movements in solid ice cores, *Ann. Glaciol.*, 39, 540-544, 2004.

Tie, X., R. Zhang, G. Brasseur, L. Emmons and W. Lei, Effects of lightning on reactive lightning and nitrogen reservoir species in the troposphere, *J. Geophys. Res.*, 106, 3167-3178, 2001.

van Ommen, T. D., and V. Morgan, Calibrating the ice core palaeothermometer using seasonality, *J. Geophys. Res.*, 102, 9351-9357, 1997.

van Ommen, T. D., Morgan, V. I., Jacka, T. H., Woon, S. and Al. Elcheikh, Near-surface temperatures in the Dome Summit South (Law Dome) borehole, *Ann. Glaciol.*, 29, 141-144, 1999.

Vitt, F. M. and C. H. Jackman, A comparison of odd nitrogen production from 1974 through 1993 in the Earth's middle atmosphere as calculated using a two dimensional model, *J. Geophys. Res.*, 101, 6729-6739, 1996.

Wagenbach, D. F., F. Ducroz, R. Mulvaney, L. Keck, A. Minikin, M. Legrand, J. S. Hall and E. W. Wolff, Sea-salt aerosol at coastal Antarctic regions, *J. Geophys. Res.*, 103(D9), 10961-10974, 1998a.

Wagenbach, D. F., M. Legrand, H. Fischer, F. Pichlmayer and E. W. Wolff, Atmospheric near-surface nitrate at coastal Antarctic sites, *J. Geophys. Res.*, 103(D9), 11007-11020, 1998b.

Wagnon, R., R. J. Delmas and M. Legrand, Loss of volatile acid species from upper firn layers at Vostok, Antarctica, *J. Geophys. Res.*, 104, 3423-3431, 1999.

Wang, N., L. G. Thompson and J. Cole-Dai, The nature of solar activity during the Maunder Minimum revealed by the Guliya ice core record, *Chinese Sci. Bull.*, 45, 2118-2125, 2000.

Warneck, P., *Chemistry of the natural atmosphere*, International geophysical series, Academic Press, San Diego, 1988.

Welch, K. A., P. A. Mayewski and S. I. Whitlow, Methansulphonic acid in coastal Antarctic snow related to sea-ice extent, *Geophys. Res. Lett.*, 20(6), 443-446, 1993.

Whillans, I. M. and P. M. Grootes, Isotopic diffusion in cold snow and firn, *J. Geophys. Res.*, 90, 3910-3918, 1985.

Whitlow, S., P. A. Mayewski and J. E. Dibb, A comparison of major chemical species seasonal concentration and accumulation at the South Pole and Summit, Greenland, *Atmos. Envir.*, 26A, 2045-2054, 1992.

Wilson, T. R. S., Salinity and the major elements of sea water, in *Chemical Oceanography*, edited by J. P. Riley and G. Skirrow, vol. 1, pp 365-413, Academic Press, Sand Diego, California, 1975.

Wolff, E. W., J. C. Moore, H. B. Clausen, C. U. Hammer, J. Kipfstuhl and K. Fuhrer, Long-term changes in the acid and salt concentrations of the GRIP Greenland ice core from electrical stratigraphy, *J. Geophys. Res.*, 100, 16249-16264, 1995.

Wolff, E. W., Location, movement and reactions of impurities in solid ice, in *Ice Core Studies of Biogeochemical Cycles, NATO AIS Ser. I: Global Environmental Change*, edited by R. J. Delmas, Springer-Verlag, Berlin, pp 541-560, 1996.

Wolff, E. W., J. S. Hall, R. Mulvaney, E. C. Pasteur, D. Wagenbach and M. Legrand, Relationship between chemistry of air, fresh snow and firn cores for aerosol species in coastal Antarctica, *J. Geophys. Res.*, 103(D9), 11057-11070, 1998.

Worby, A. P., R. A. Massom, I. Allison, V. I. Lytle and P. Heil, East Antarctic sea ice: A review of its structure, properties and drift, in *Antarctic Sea Ice: Physical processes, interactions and variability*, *Antarctic Research Series*, edited by M. O. Jefferies, American Geophysical Union, Washington D.C., pp 41-67, 1998.

Zeller, E. J. and G. A. M. Dreschhoff, Anomalous nitrate concentrations in polar ice cores – do they result from solar particle injections into the polar atmosphere?, *Geophys. Res. Lett.*, 22, 2521-2524, 1995.

Zwally, H. J., M. Giovinetto, M. Craven, V. Morgan and I. Goodwin, Areal distribution of oxygen-isotope ratio in Antarctica: comparison of results based on field and remotely sensed data, *Ann. Glaciol.*, 27, 583-590, 1998.

Appendix A

Local and Synoptic Meteorological Conditions for Summer Events

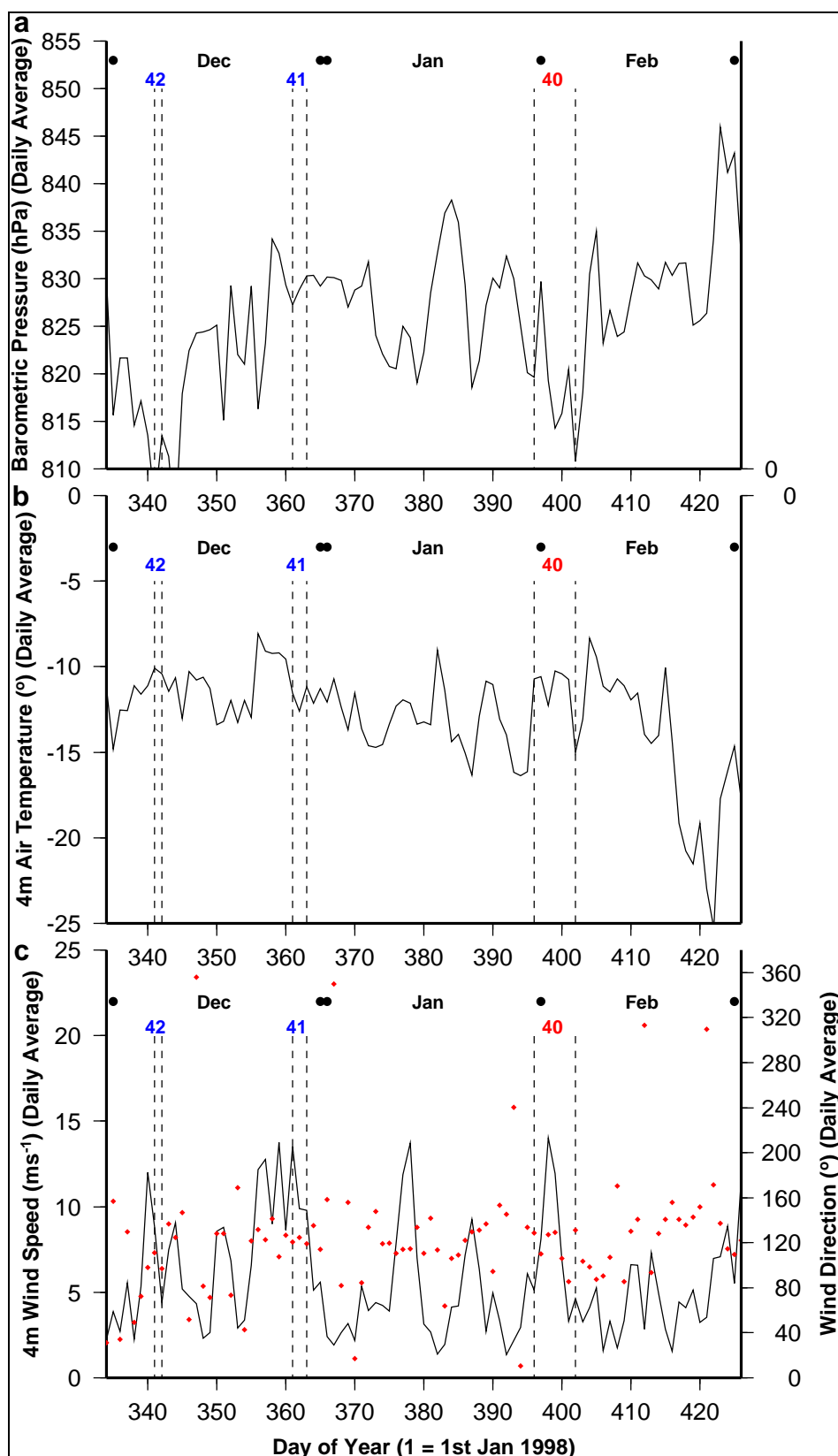


Fig 8.1: Local meteorological conditions recorded by the AWS from 1 December 1998 (Julian day 335) to 28 February 1999 (Julian day 424). (a) Station-level (SL) pressure, (b) air temperature, (c) wind speed. Events that concur (blue) and differ (red) from expected summer glaciochemical signals are illustrated.

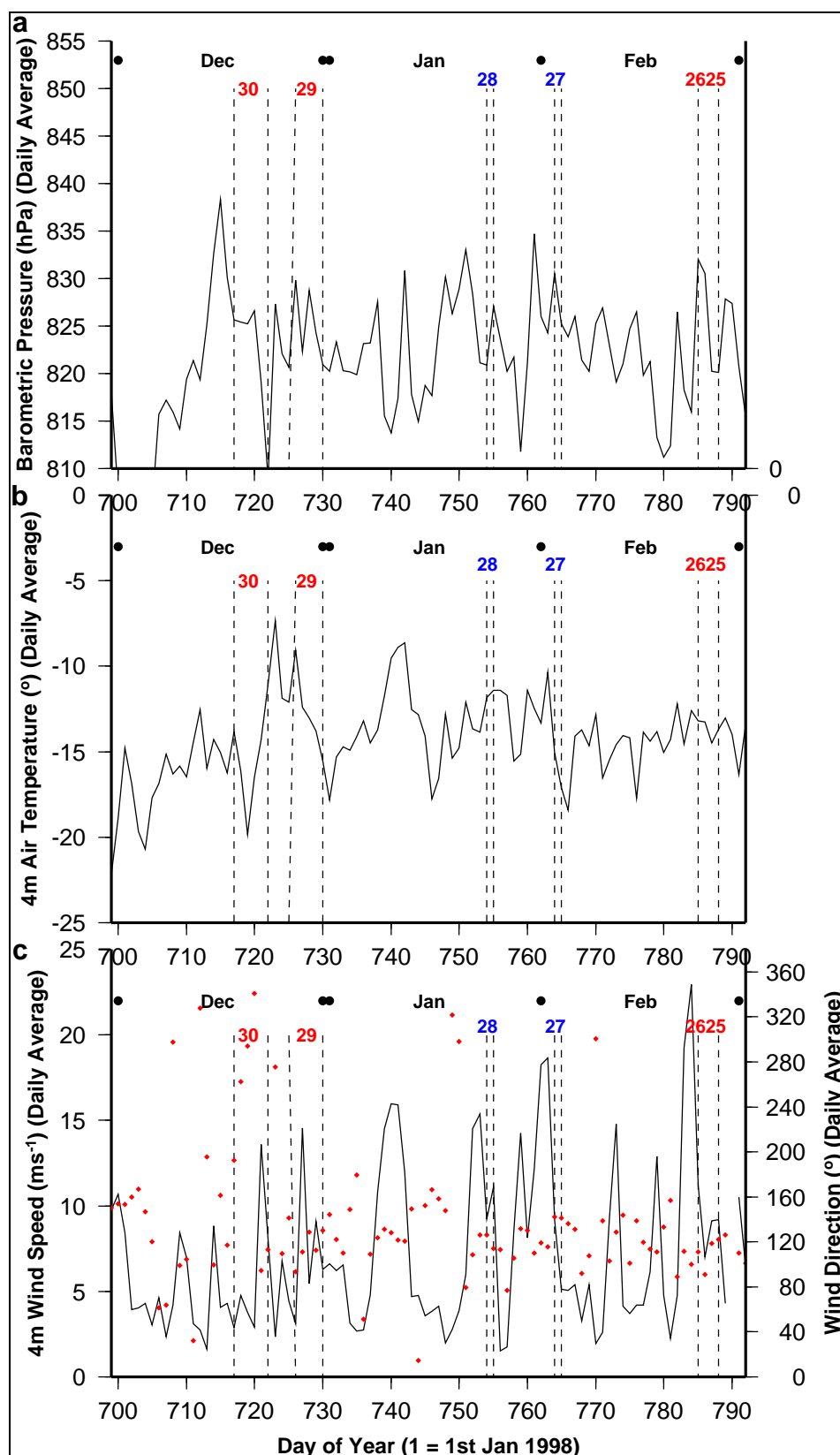


Fig 8.2: Local meteorological conditions recorded by the AWS from 1 December 1999 (Julian day 700) to 29 February 1999 (Julian day 790). (a) Station-level (SL) pressure, (b) air temperature, (c) wind speed. Events that concur (blue) and differ (red) from expected summer glaciochemical signals are illustrated.

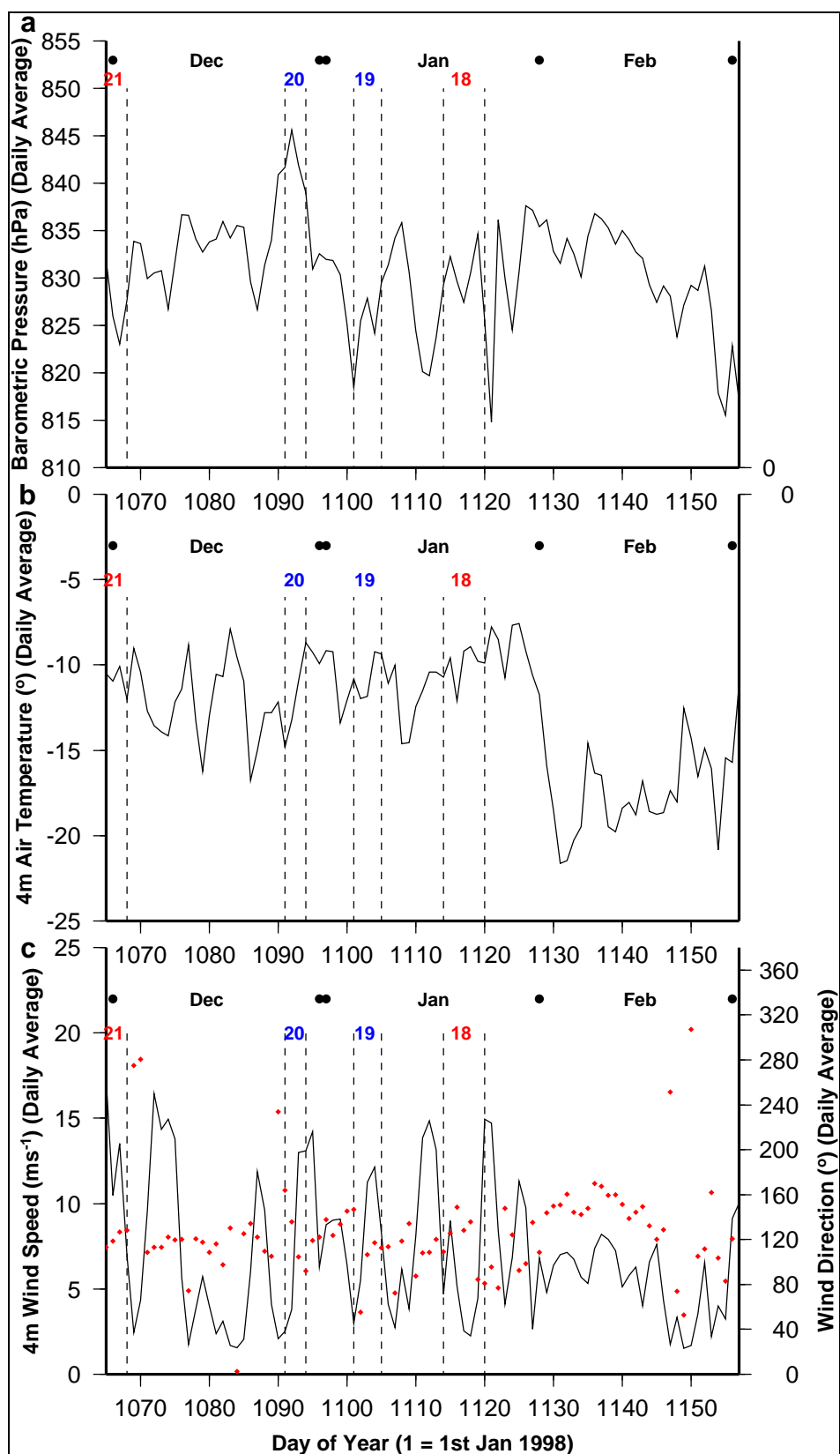


Fig 8.3: Local meteorological conditions recorded by the AWS from 1 December 2000 (Julian day 1066) to 28 February 2001 (Julian day 1155). (a) Station-level (SL) pressure, (b) air temperature, (c) wind speed. Events that concur (blue) and differ (red) from expected summer glaciochemical signals are illustrated.

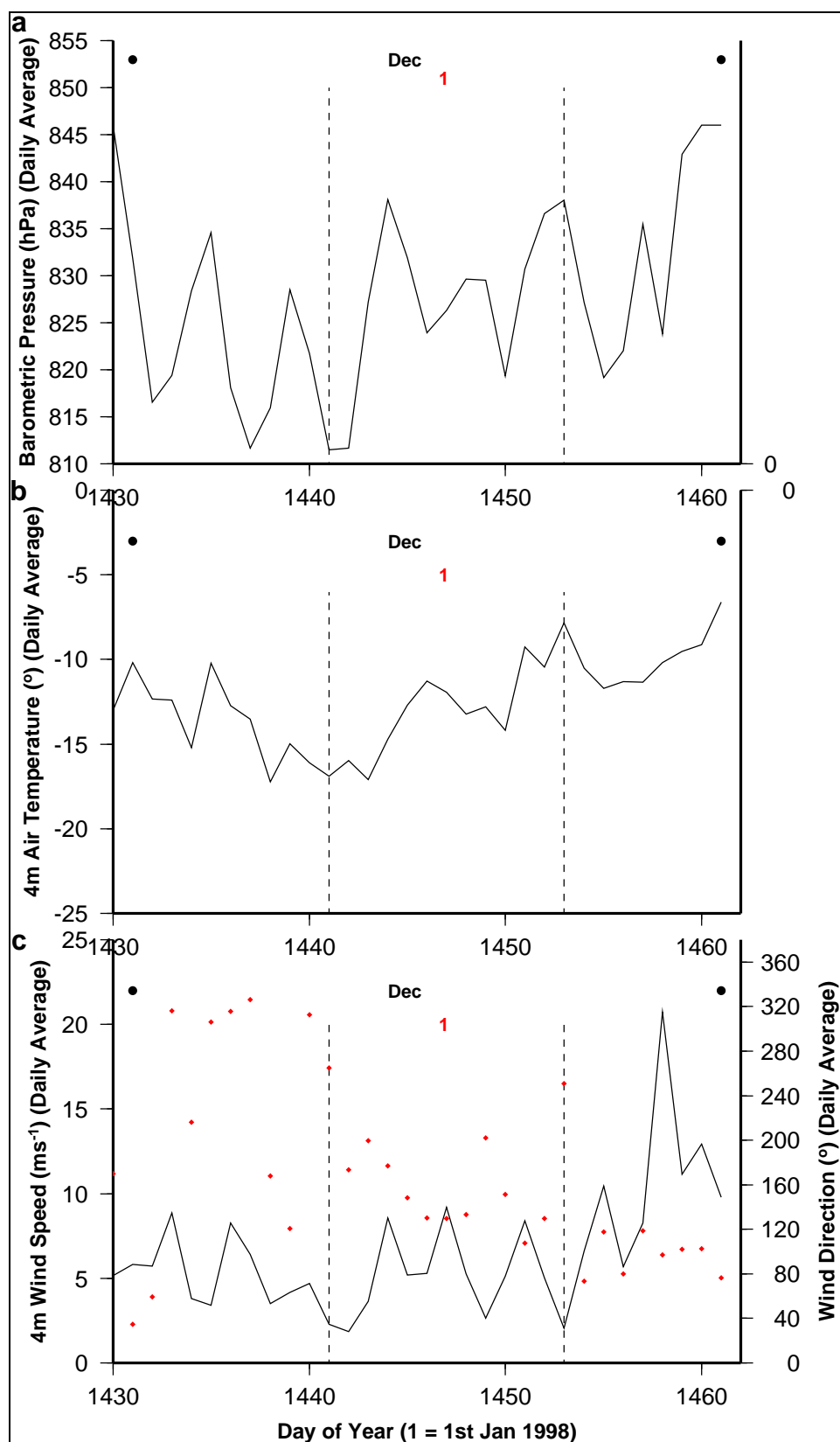


Fig 8.4: Local meteorological conditions recorded by the AWS from 1 December 2001 (Julian day 1431) to 31 December 2001 (Julian day 1461). (a) Station-level (SL) pressure, (b) air temperature, (c) wind speed. Events that concur (blue) and differ (red) from expected summer glaciochemical signals are illustrated.

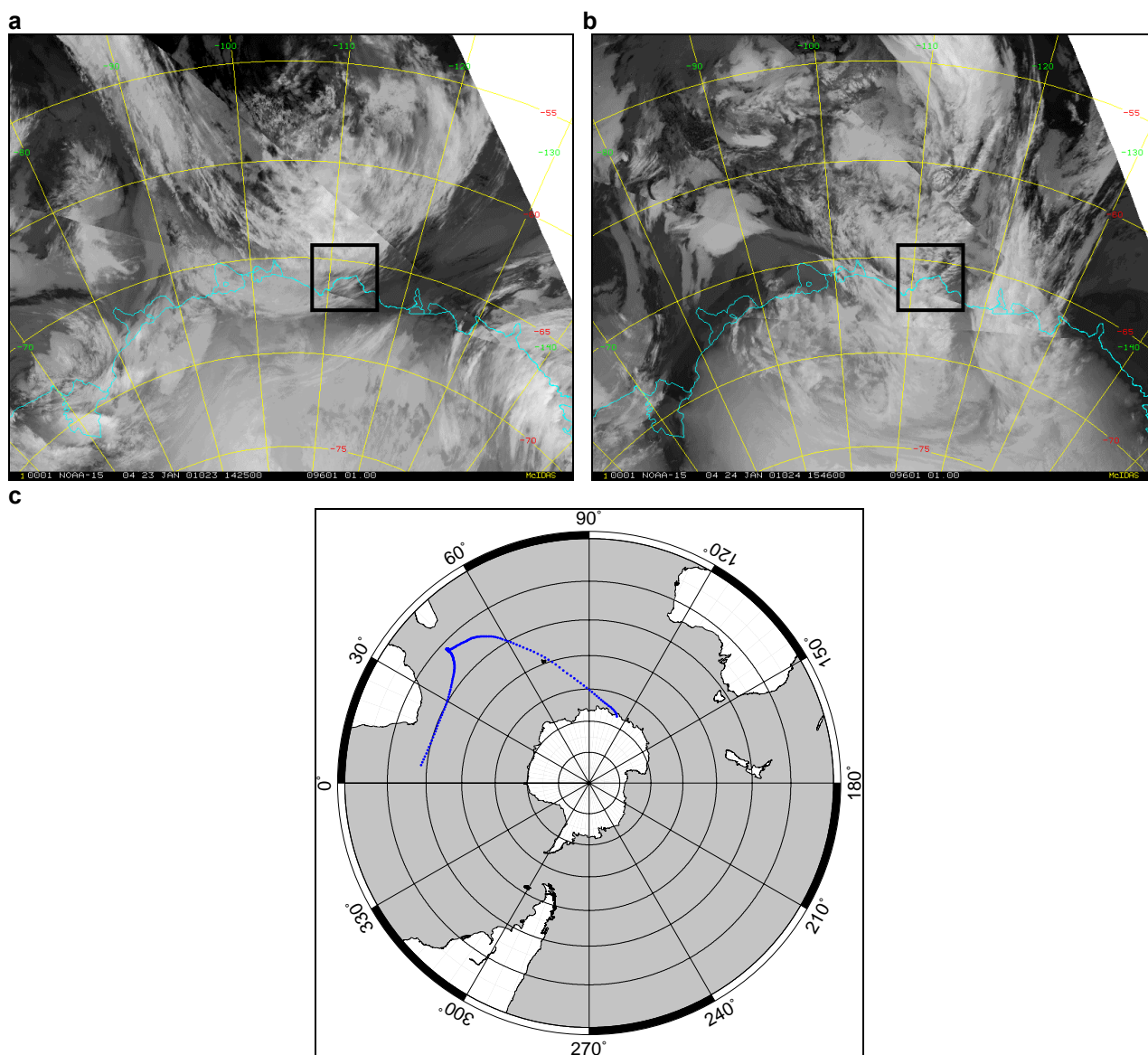


Fig 8.5: AVHRR satellite imagery (a, b) and back trajectory analysis (c) for Event 18, 18 – 24 January 2001 (Julian days 1114 – 1120): (a) 1425 UTC 23 January 2001; (b) 1546 UTC 24 January 2001; (c) 500 hPa back trajectory from 0000 UTC 24 January 2001. Law Dome is indicated in the AVHRR satellite imagery by the black box.

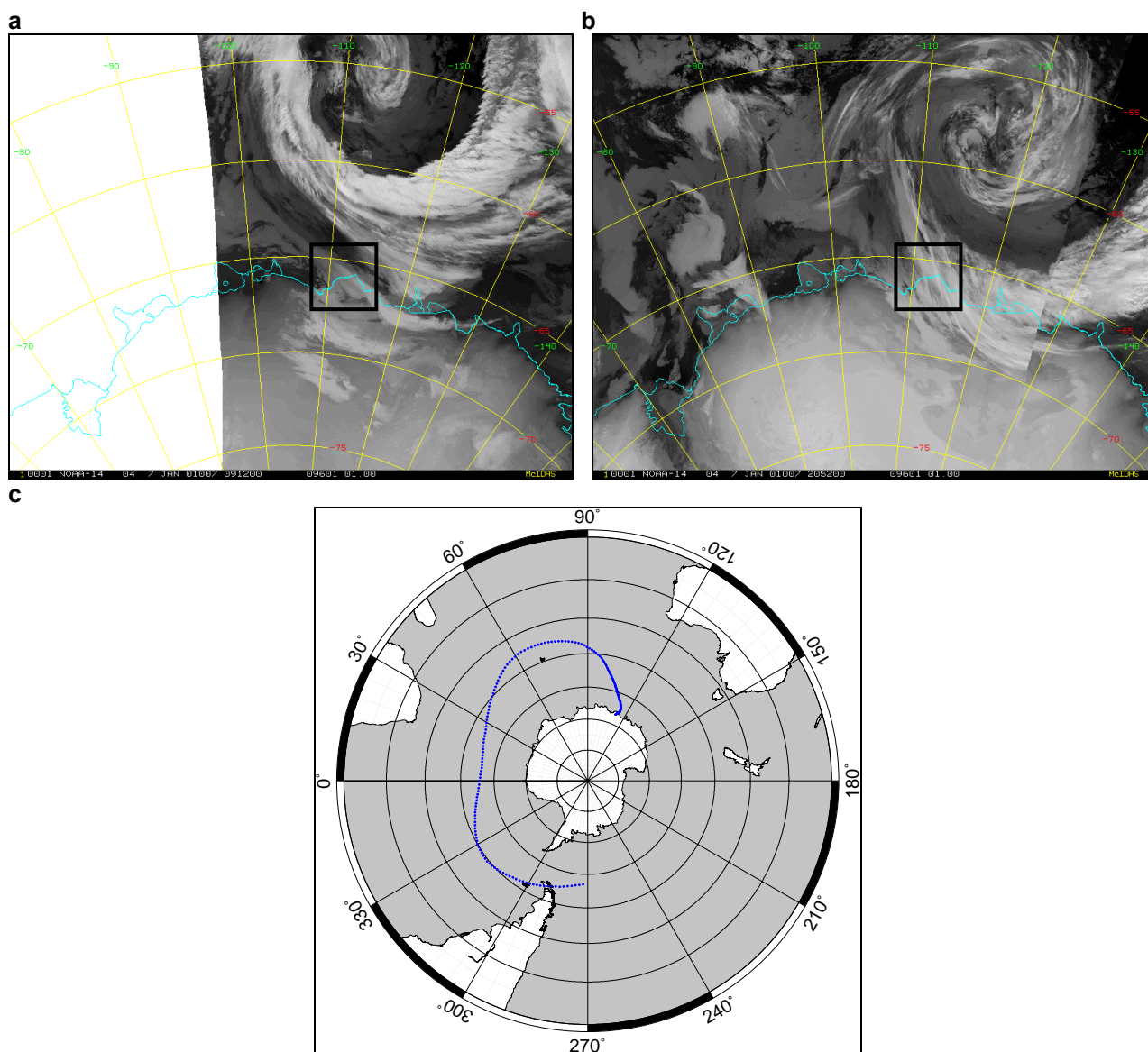


Fig 8.6: AVHRR satellite imagery (a, b) and back trajectory analysis (c) for Event 19, 5 – 9 January 2001 (Julian days 1101 – 1105): (a) 0912 UTC 7 January 2001; (b) 2052 UTC 7 January 2001; (c) 500 hPa back trajectory from 0000 UTC 8 January 2001. Law Dome is indicated in the AVHRR satellite imagery by the black box.

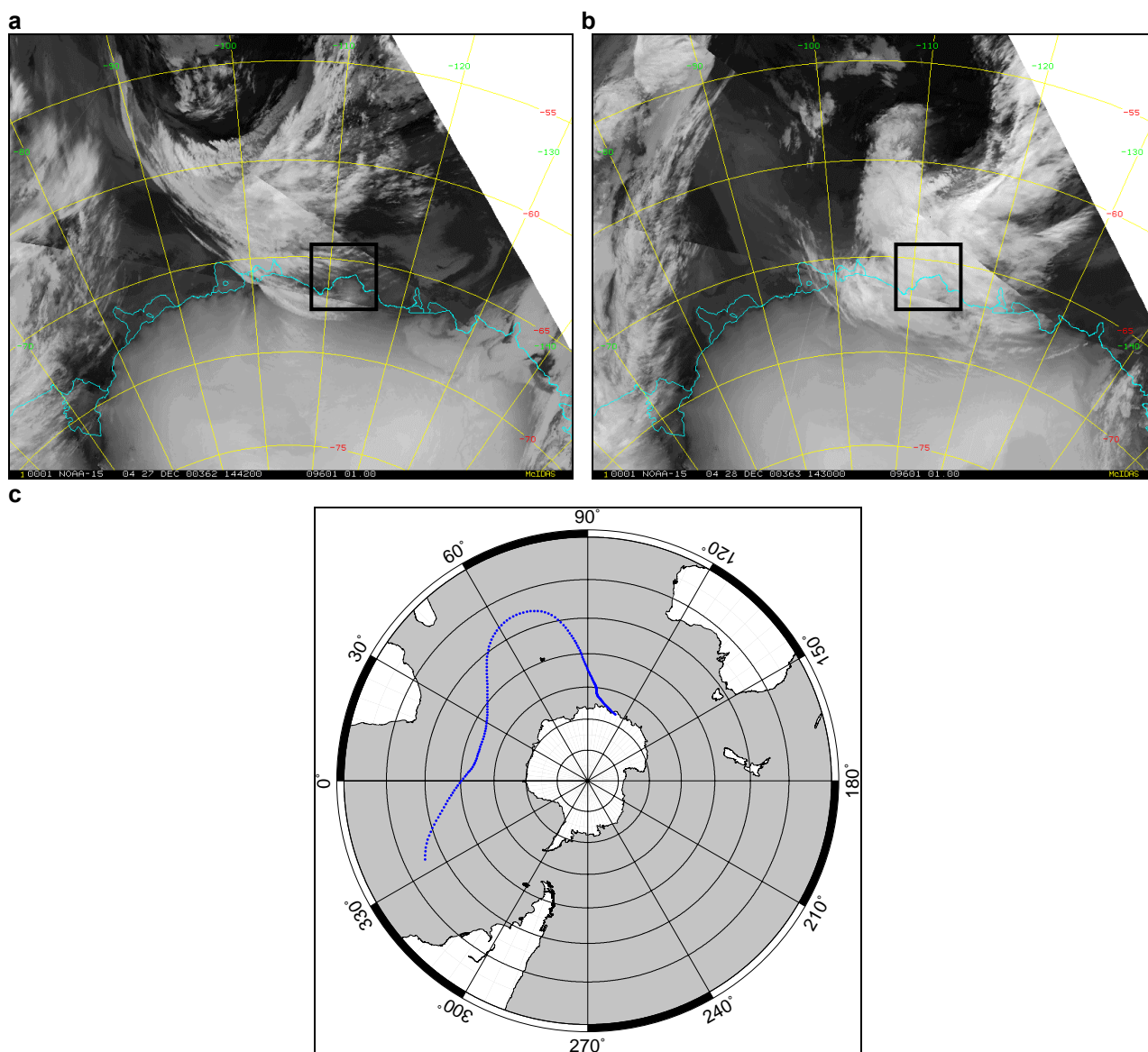


Fig 8.7: AVHRR satellite imagery (a, b) and back trajectory analysis (c) for Event 20, 26 – 29 December 2000 (Julian days 1091 – 1094): (a) 1442 UTC 27 December 2000; (b) 1430 UTC 28 December 2000; (c) 500 hPa back trajectory from 0000 UTC 28 December 2000. Law Dome is indicated in the AVHRR satellite imagery by the black box.

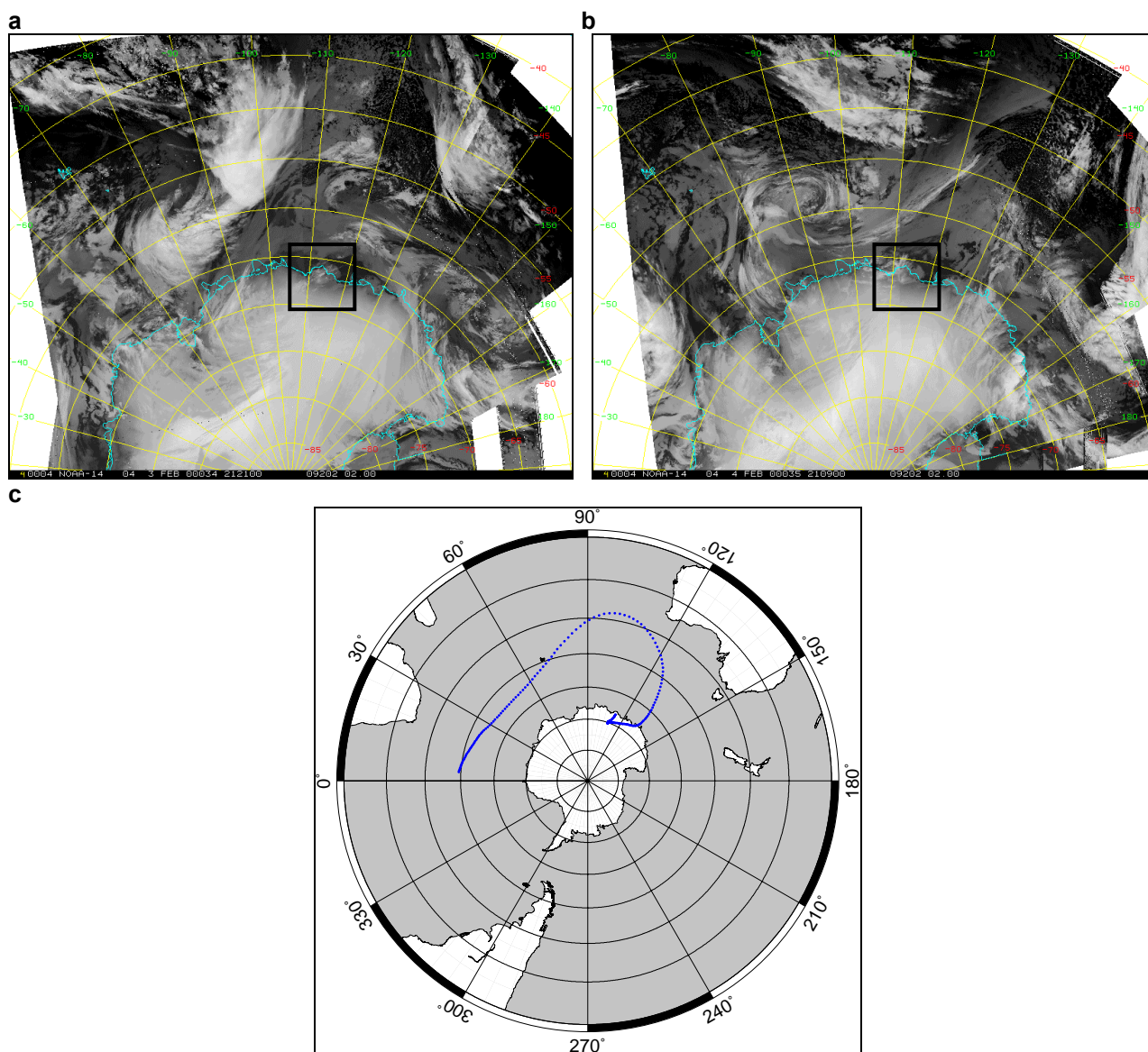


Fig 8.8: AVHRR satellite imagery (a, b) and back trajectory analysis (c) for Event 27, 3 – 4 February 2000 (Julian days 764 – 765): (a) 2121 UTC 3 February 2000; (b) 2109 UTC 4 February 2000; (c) 500 hPa back trajectory from 0000 UTC 4 February 2000. Law Dome is indicated in the AVHRR satellite imagery by the black box.

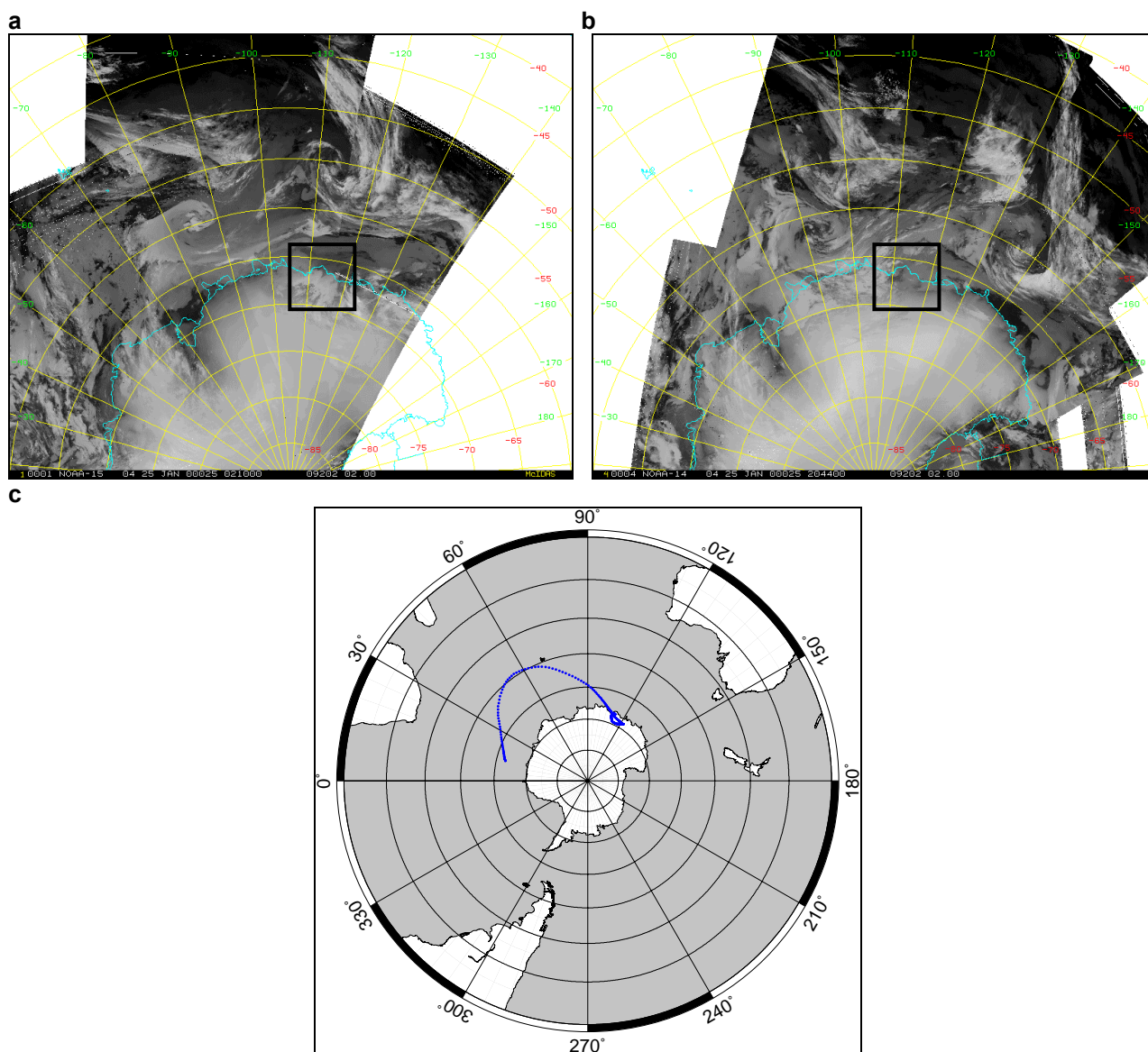


Fig 8.9: AVHRR satellite imagery (a, b) and back trajectory analysis (c) for Event 28, 24 – 25 January 2000 (Julian days 754 – 755): (a) 0210 UTC January 2000; (b) 2044 UTC January 2000; (c) 500 hPa back trajectory from 0000 UTC 25 January 2000. Law Dome is indicated in the AVHRR satellite imagery by the black box.

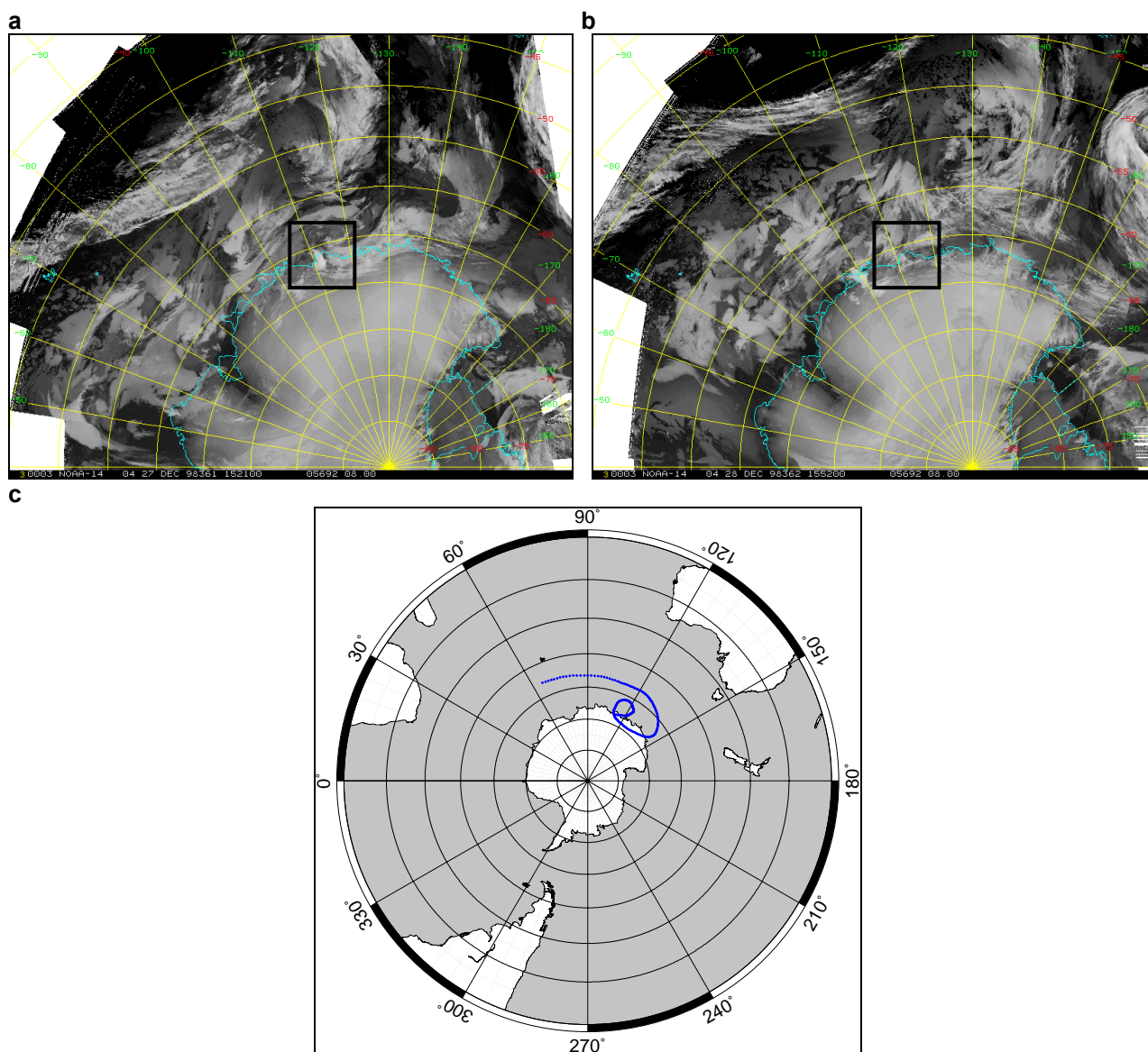


Fig 8.10: AVHRR satellite imagery (a, b) and back trajectory analysis (c) for Event 41, 27 – 29 December 1998 (Julian days 361 – 363): (a) 1521 UTC 27 December 1998; (b) 1552 UTC December 1998; (c) 500 hPa back trajectory from 0000 UTC 27 December 1998. Law Dome is indicated in the AVHRR satellite imagery by the black box.

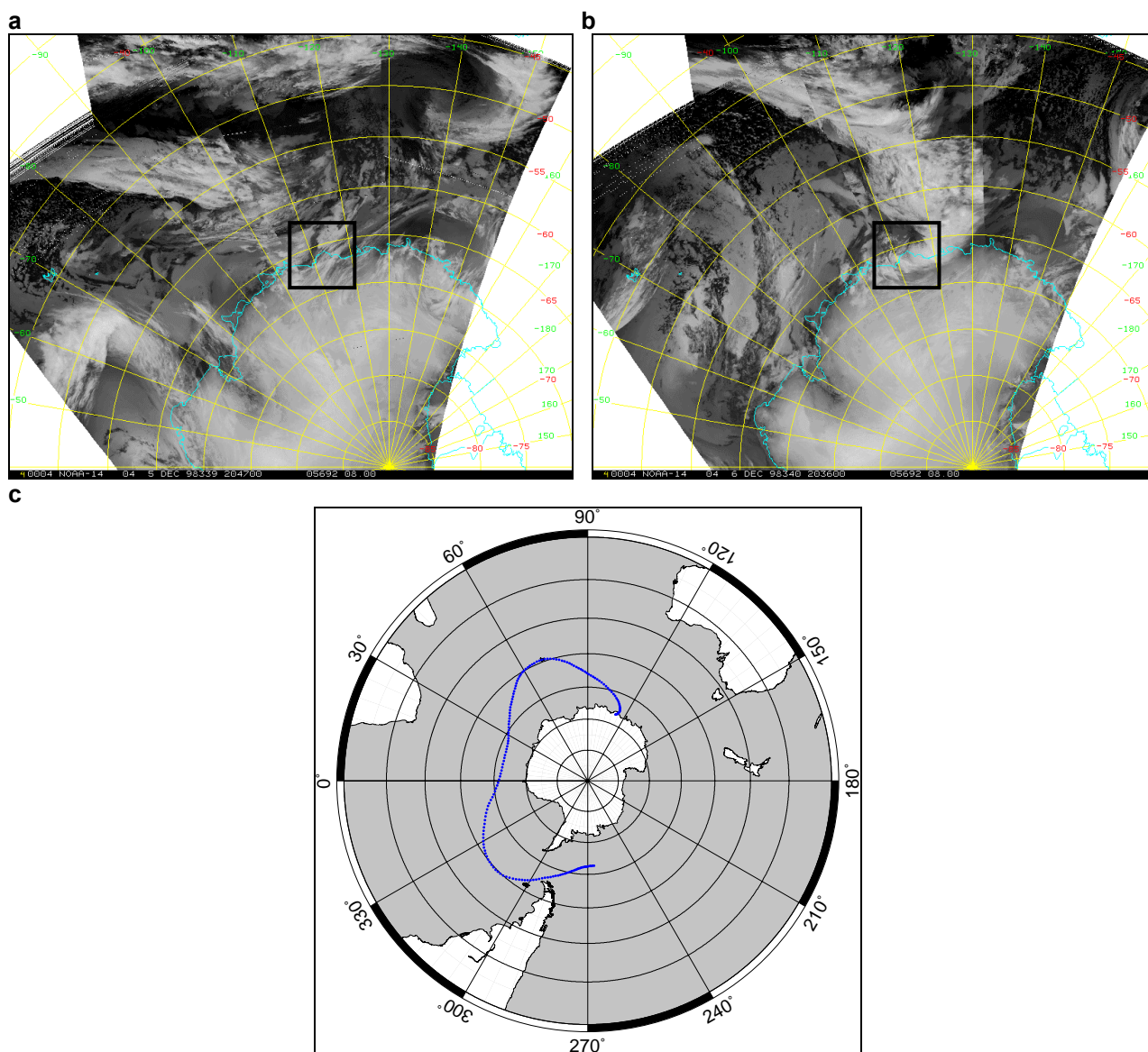


Fig 8.11: AVHRR satellite imagery (a, b) and back trajectory analysis (c) for Event 42, 7 – 8 December 1998 (Julian days 341 – 342): (a) 2047 UTC 5 December 1998; (b) 2036 UTC 6 December 1998; (c) 500 hPa back trajectory from 0000 UTC 7 December 1998. Law Dome is indicated in the AVHRR satellite imagery by the black box.

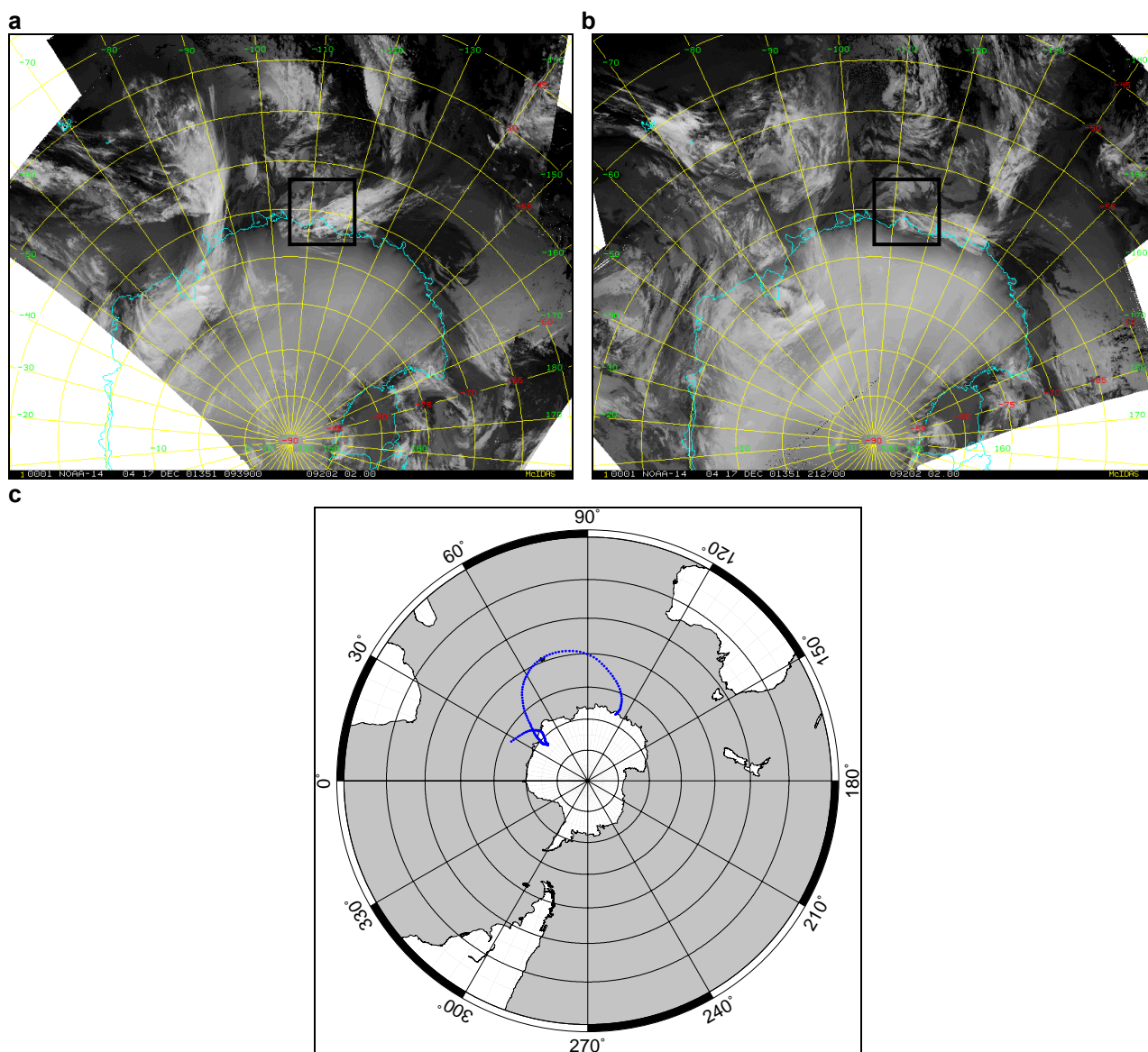


Fig 8.12: AVHRR satellite imagery (a, b) and back trajectory analysis (c) for Event 1, 11 – 23 December 2001 (Julian days 1441 – 1453): (a) 0939 UTC 17 December 2001; (b) 2127 UTC 17 December 2001; (c) 500 hPa back trajectory from 0000 UTC 17 December 2001. Law Dome is indicated in the AVHRR satellite imagery by the black box.

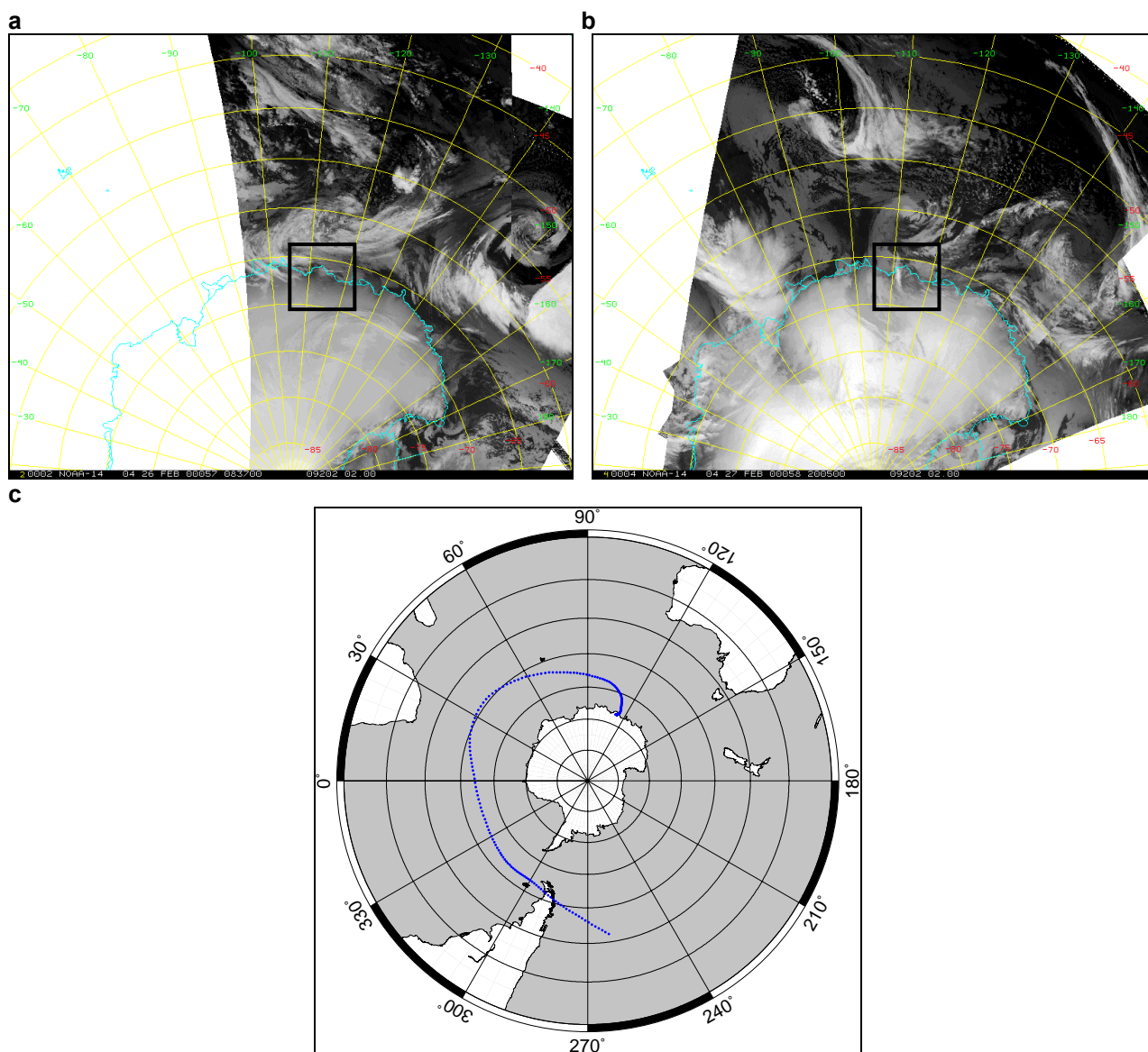


Fig 8.13: AVHRR satellite imagery (a, b) and back trajectory analysis (c) for Event 25, 27 February 2000 (Julian day 788): (a) 0837 UTC 26 February 2000; (b) 2005 UTC 27 February 2000; (c) 500 hPa back trajectory from 0000 UTC 27 February 2000. Law Dome is indicated in the AVHRR satellite imagery by the black box.

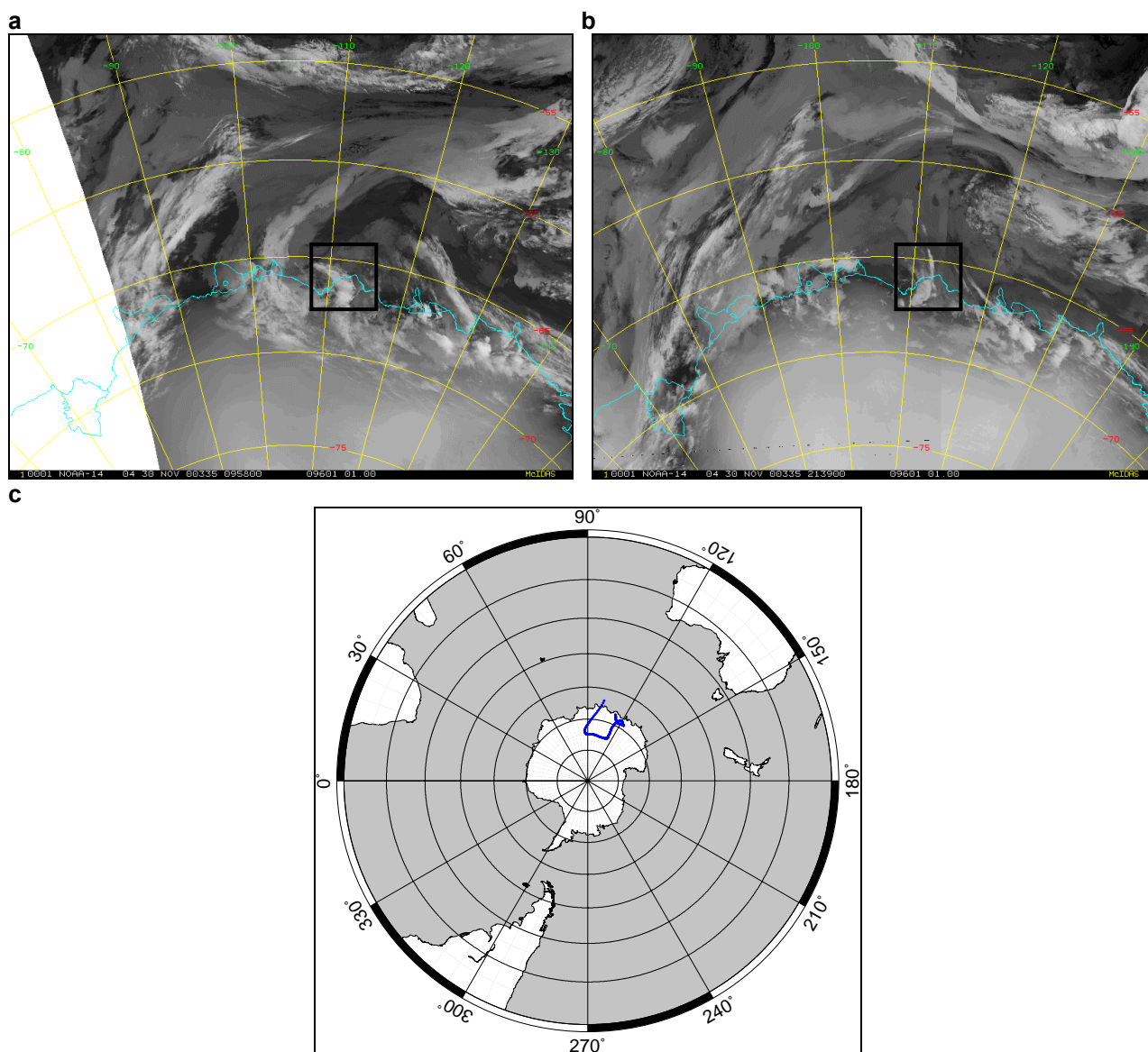


Fig 8.14: AVHRR satellite imagery (a, b) and back trajectory analysis (c) for Event 21, 30 November – 3 December 2000 (Julian days 1065 – 1068): (a) 0958 UTC 30 November 2000; (b) 2139 UTC 30 November 2000; (c) 500 hPa back trajectory from 0000 UTC 30 November 2000. Law Dome is indicated in the AVHRR satellite imagery by the black box.

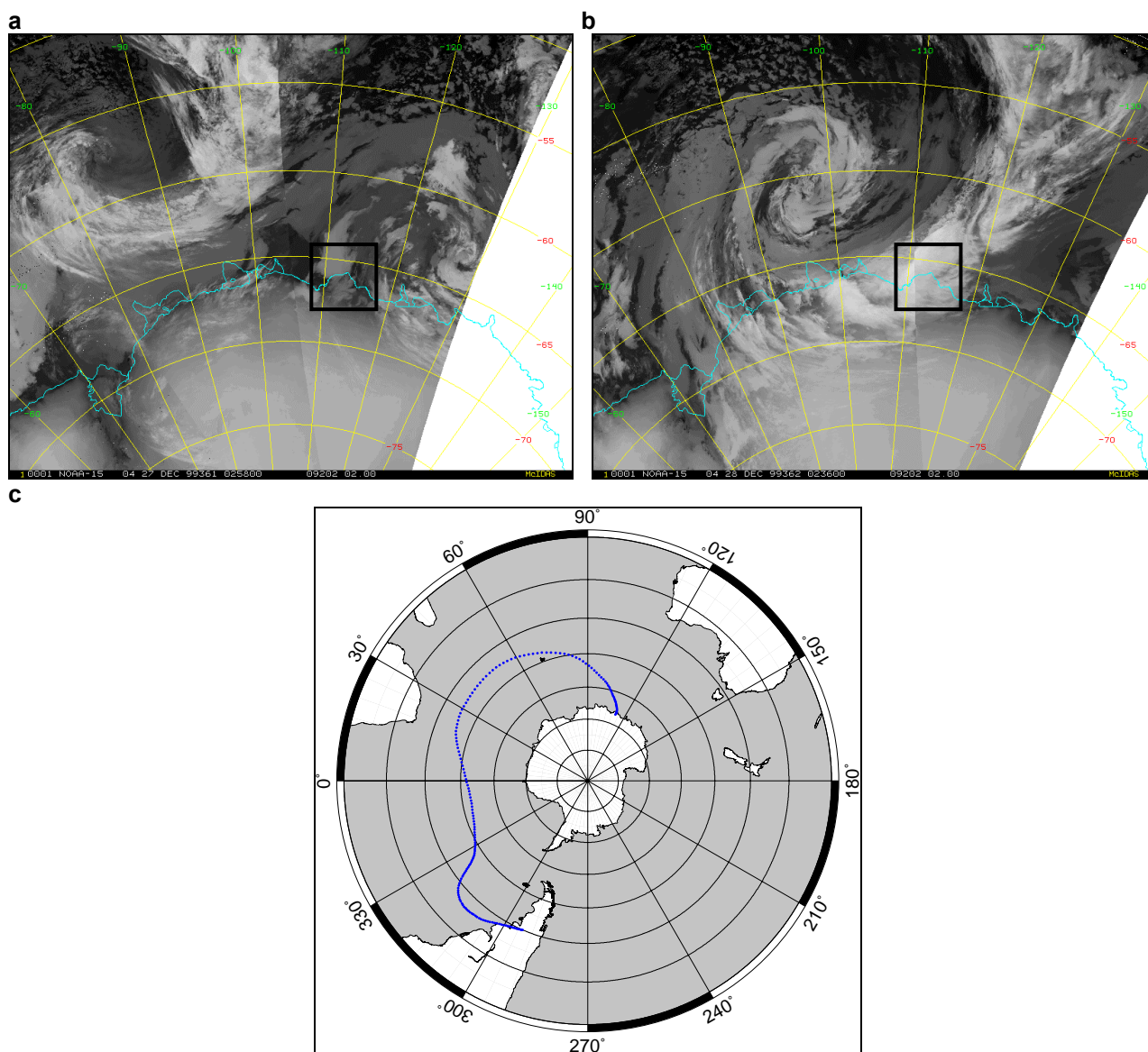


Fig 8.15: AVHRR satellite imagery (a, b) and back trajectory analysis (c) for Event 29, 27 – 31 December 1999 (Julian days 726 – 730): (a) 0258 UTC 27 December 1999; (b) 0236 UTC 28 December 1999; (c) 500 hPa back trajectory from 0000 UTC 28 December 1999. Law Dome is indicated in the AVHRR satellite imagery by the black box.

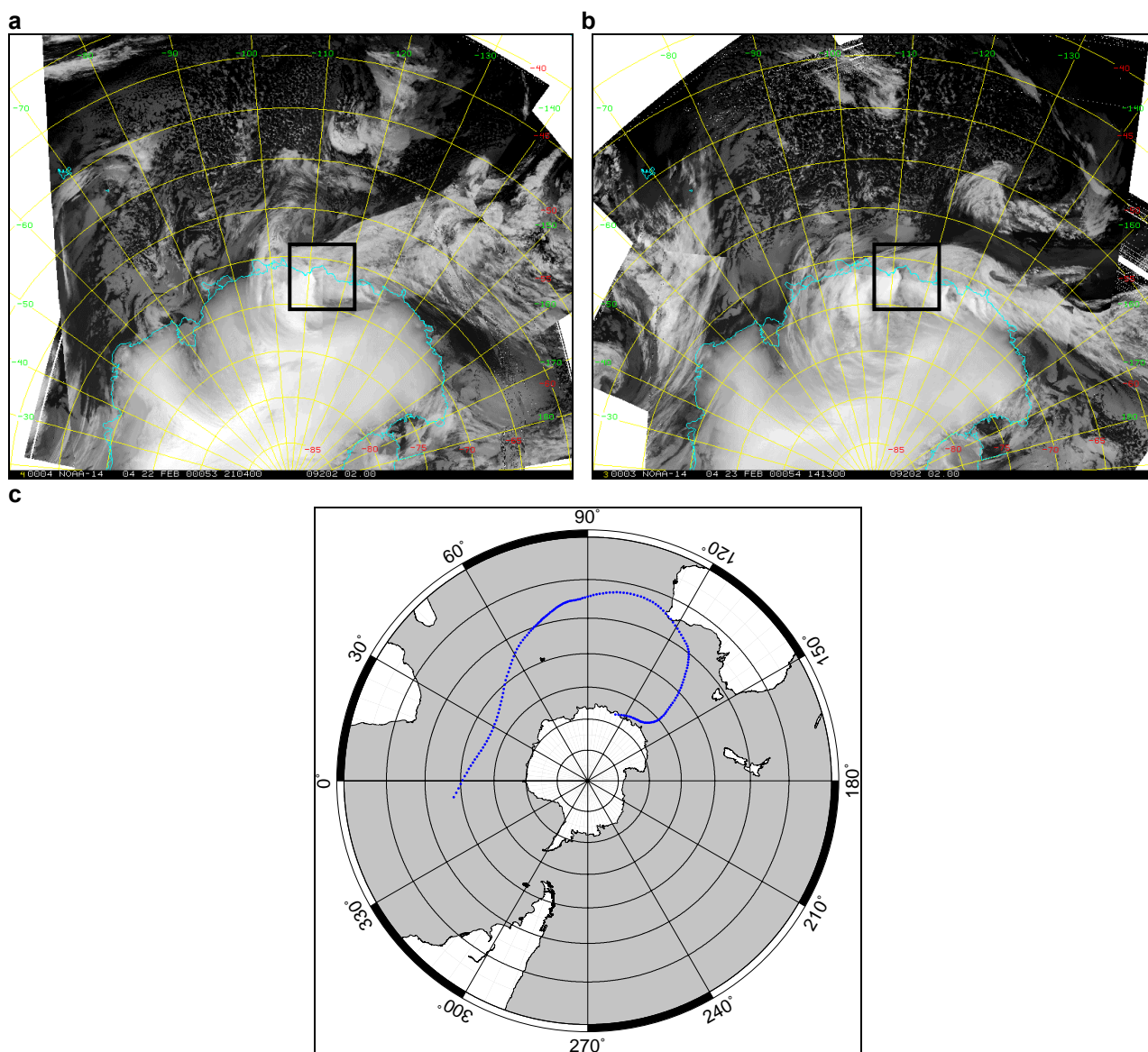


Fig 8.16: AVHRR satellite imagery (a, b) and back trajectory analysis (c) for Event 26, 24 February 2000 (Julian day 785): (a) 2104 UTC 22 February 2000; (b) 1413 UTC 23 February 2000; (c) 500 hPa back trajectory from 0000 UTC 24 February 2000. Law Dome is indicated in the AVHRR satellite imagery by the black box.

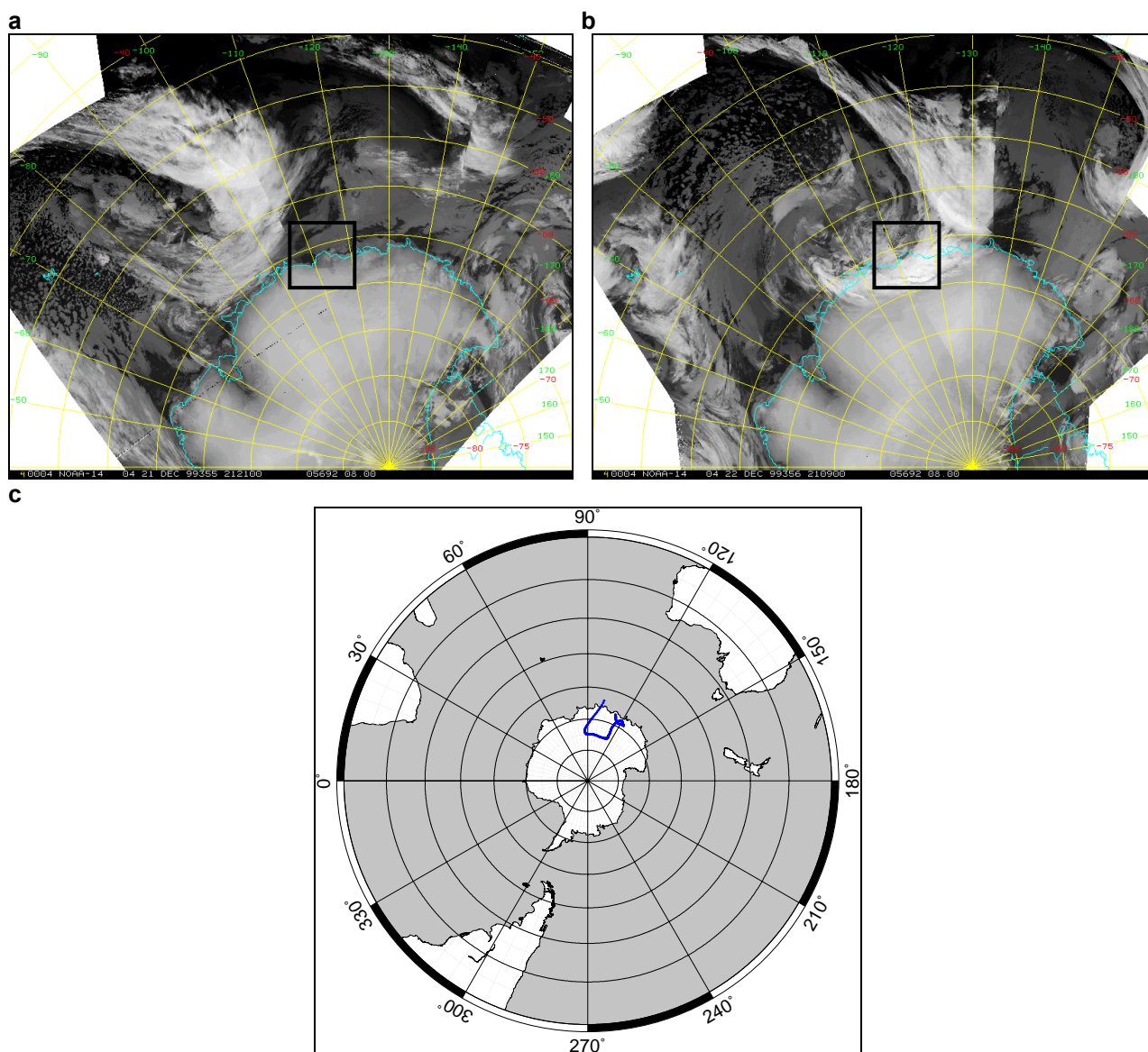


Fig 8.17: AVHRR satellite imagery (a, b) and back trajectory analysis (c) for Event 30, 18 – 23 December 1999 (Julian days 717 – 722): (a) 2121 UTC 12 December 1999; (b) 2109 UTC 22 December 1999; (c) 500 hPa back trajectory from 0000 UTC 23 December 1999. Law Dome is indicated in the AVHRR satellite imagery by the black box.

Appendix B

Local and Synoptic Meteorological Conditions for Autumn Events

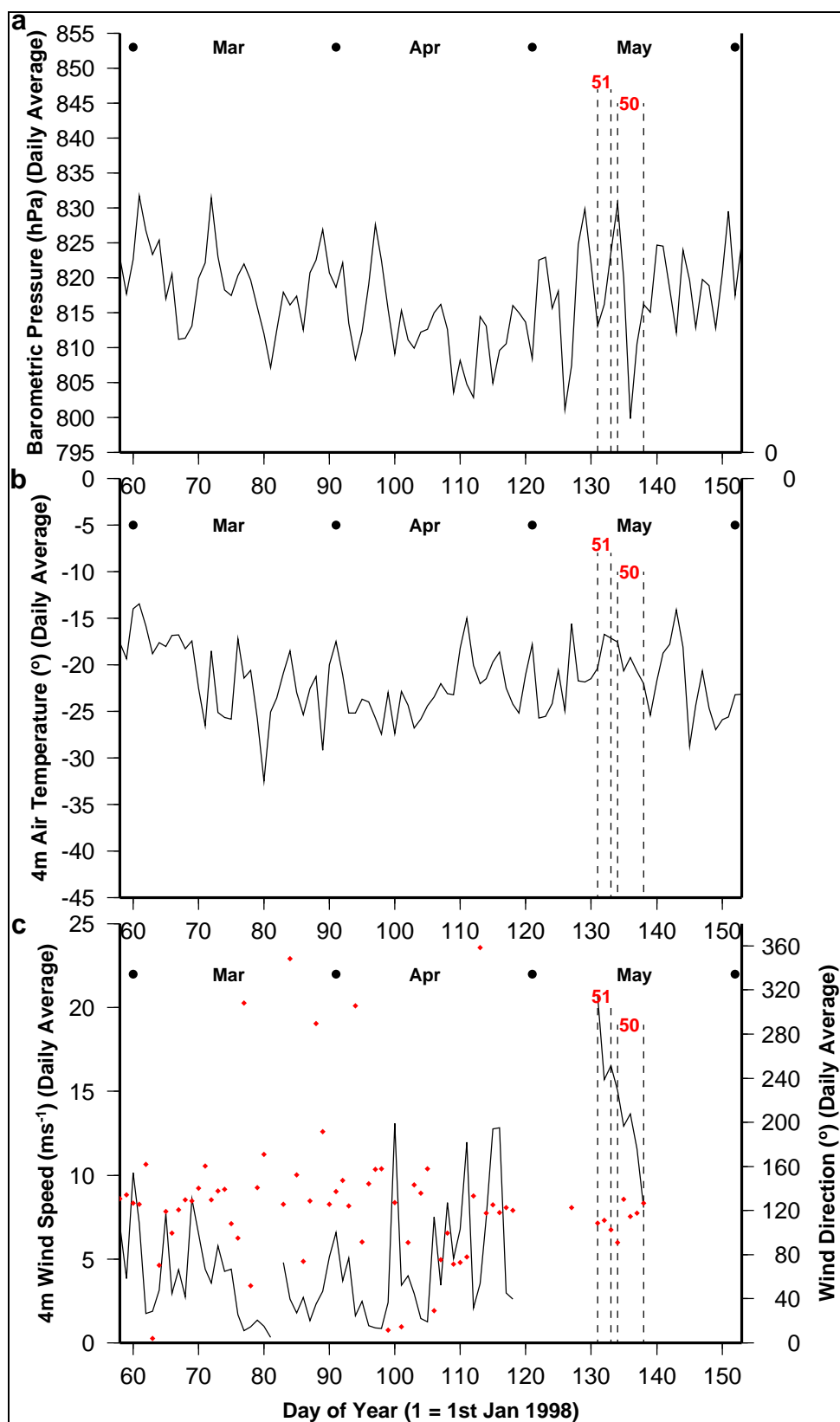


Fig 8.18: Local meteorological conditions recorded by the AWS from 1 March 1998 (Julian day 60) to 31 May 1998 (Julian day 151). (a) Station-level (SL) pressure, (b) air temperature, (c) wind speed. Events that concur (blue) and differ (red) from expected autumn glaciochemical signals are illustrated.

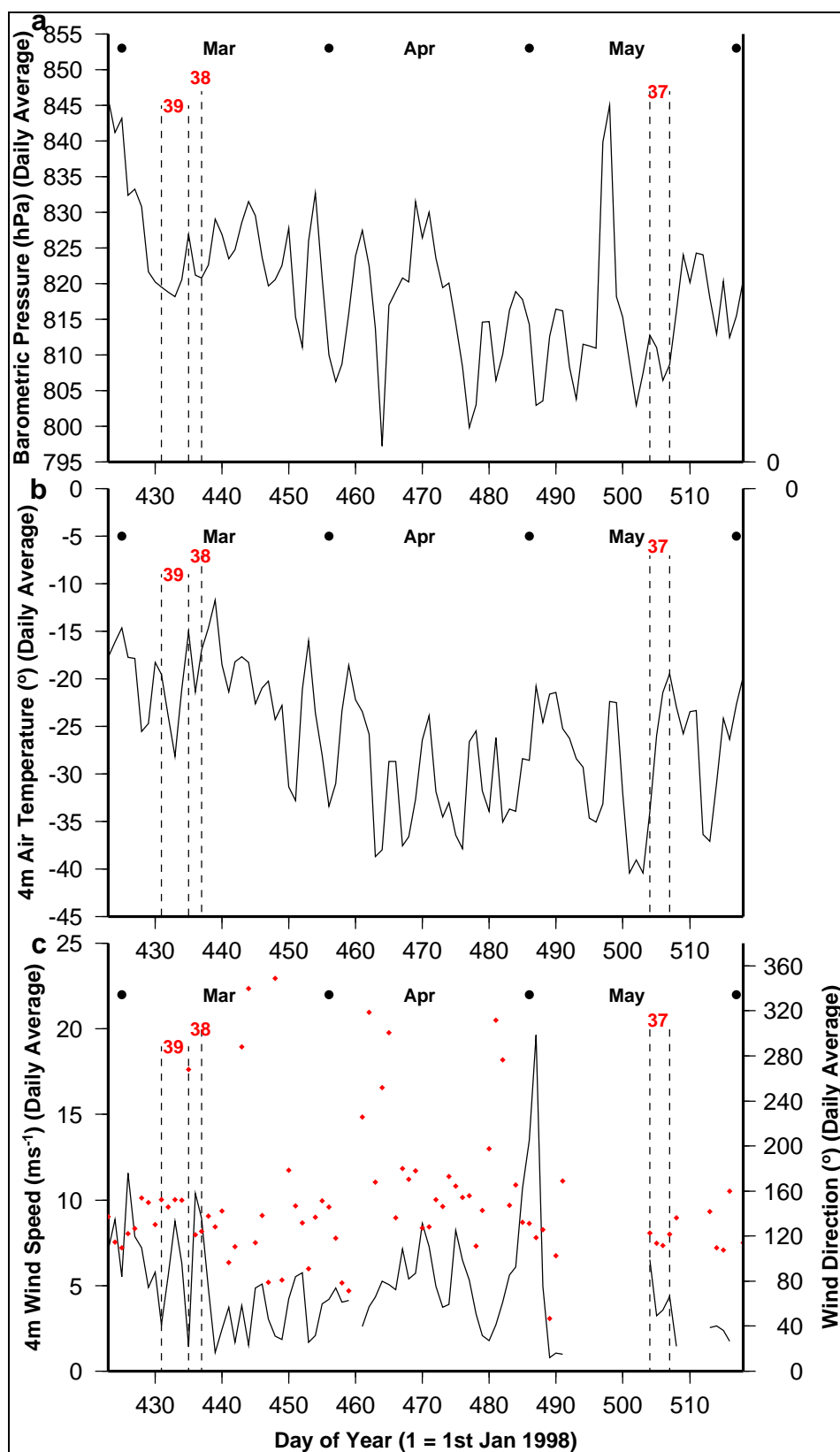


Fig 8.19: Local meteorological conditions recorded by the AWS from 1 March 1999 (Julian day 425) to 31 May 1999 (Julian day 516). (a) Station-level (SL) pressure, (b) air temperature, (c) wind speed. Events that concur (blue) and differ (red) from expected autumn glaciochemical signals are illustrated.

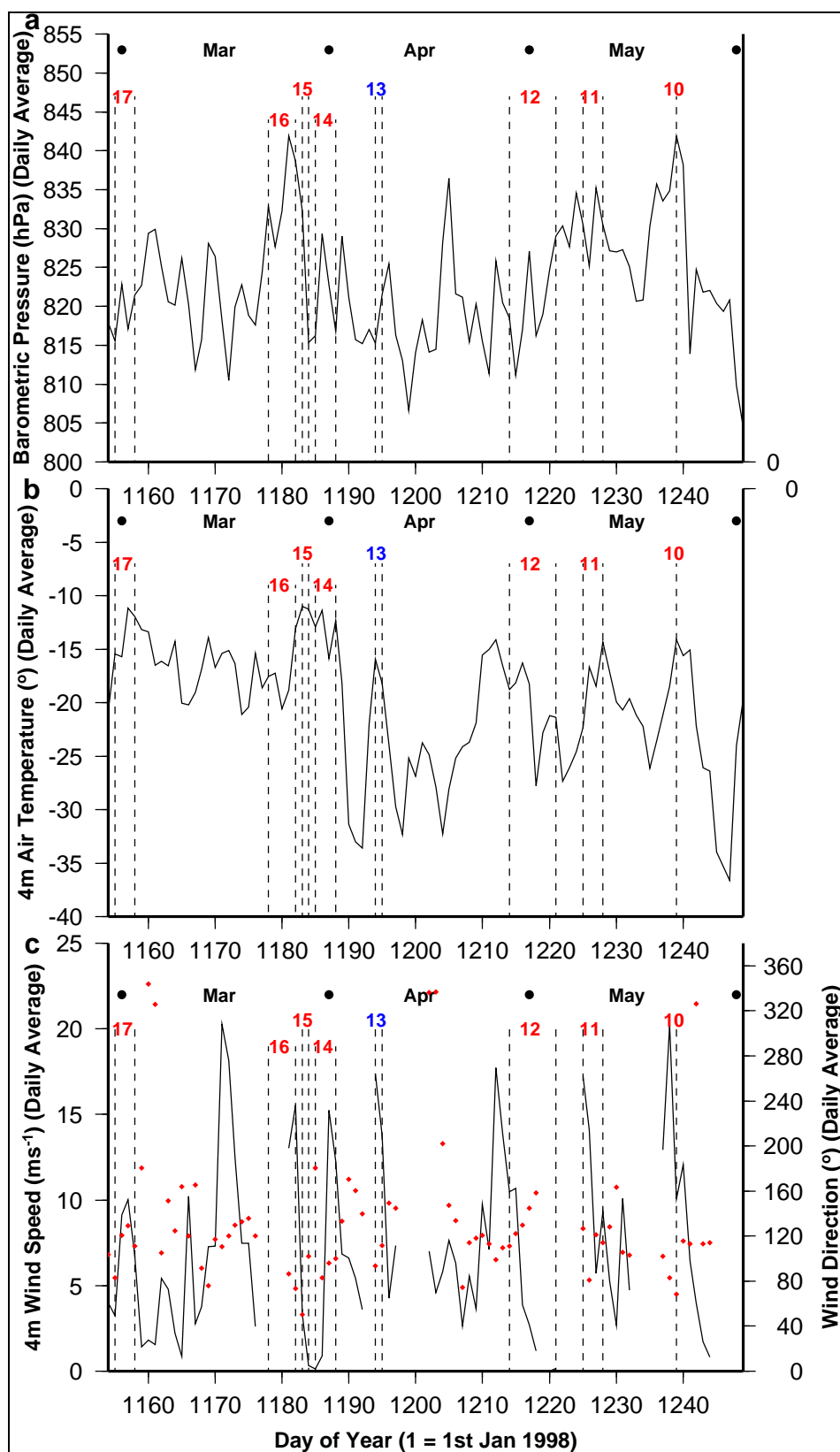


Fig 8.20: Local meteorological conditions recorded by the AWS from 1 March 2001 (Julian day 1156) to 31 May 2001 (Julian day 1247). (a) Station-level (SL) pressure, (b) air temperature, (c) wind speed. Events that concur (blue) and differ (red) from expected autumn glaciochemical signals are illustrated.

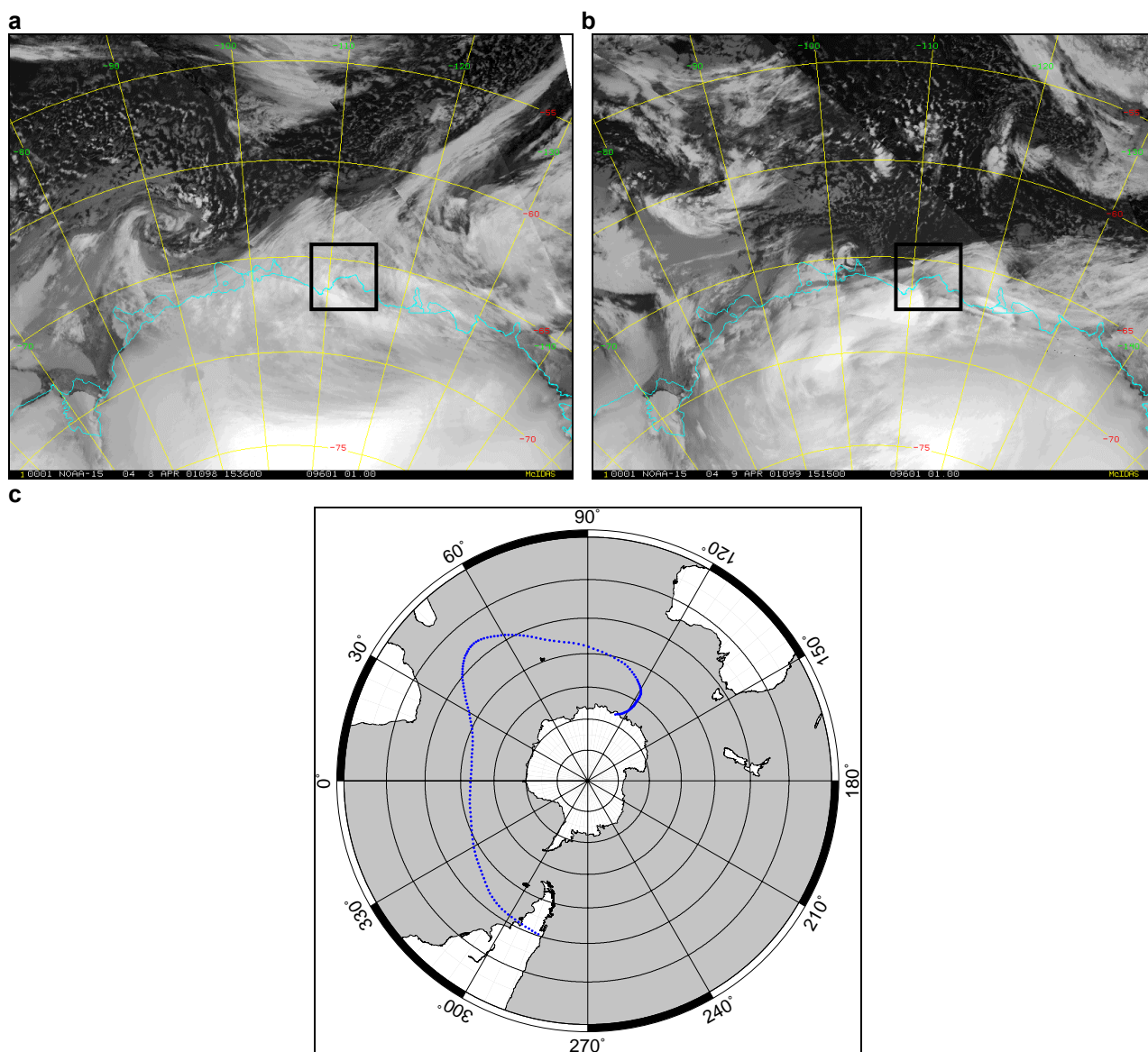


Fig 8.21: AVHRR satellite imagery (a, b) and back trajectory analysis (c) for Event 13, 8 – 9 April 2001 (Julian days 1194 – 1195): (a) 1536 UTC 8 April 2001; (b) 1515 UTC 9 April 2001; (c) 500 hPa back trajectory from 0000 UTC 9 April 2001. Law Dome is indicated in the AVHRR satellite imagery by the black box.

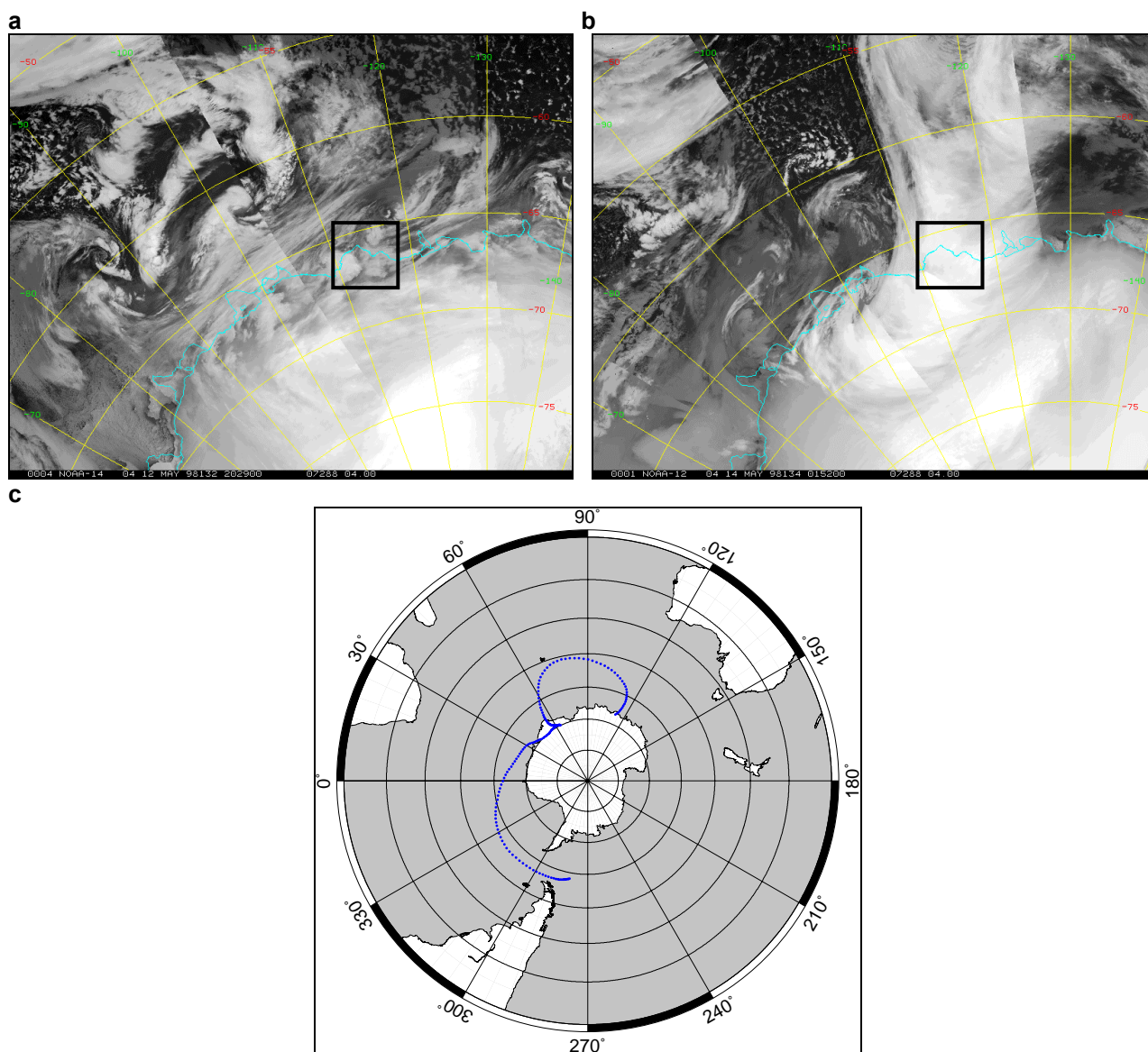


Fig 8.22: AVHRR satellite imagery (a, b) and back trajectory analysis (c) for Event 50, 14 – 18 May 1998 (Julian days 134 – 138): (a) 2029 UTC 12 May 1998; (b) 0152 UTC 14 May 1998; (c) 500 hPa back trajectory from 0000 UTC 14 May 1998. Law Dome is indicated in the AVHRR satellite imagery by the black box.

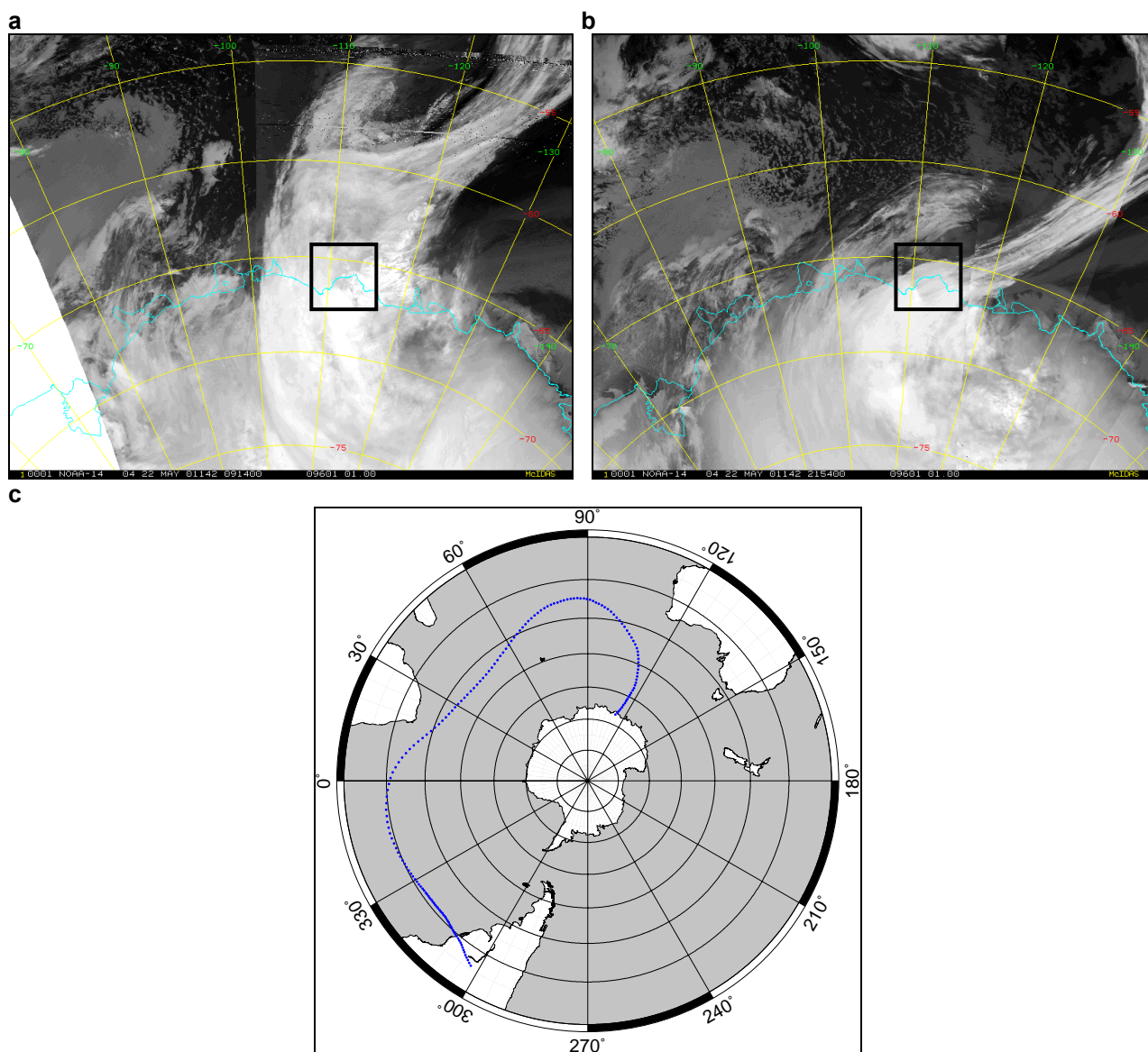


Fig 8.23: AVHRR satellite imagery (a, b) and back trajectory analysis (c) for Event 10, 23 May 2001 (Julian day 1239): (a) 0914 UTC 22 May 2001; (b) 2154 UTC 22 May 2001; (c) 500 hPa back trajectory from 0000 UTC 23 May 2001. Law Dome is indicated in the AVHRR satellite imagery by the black box.

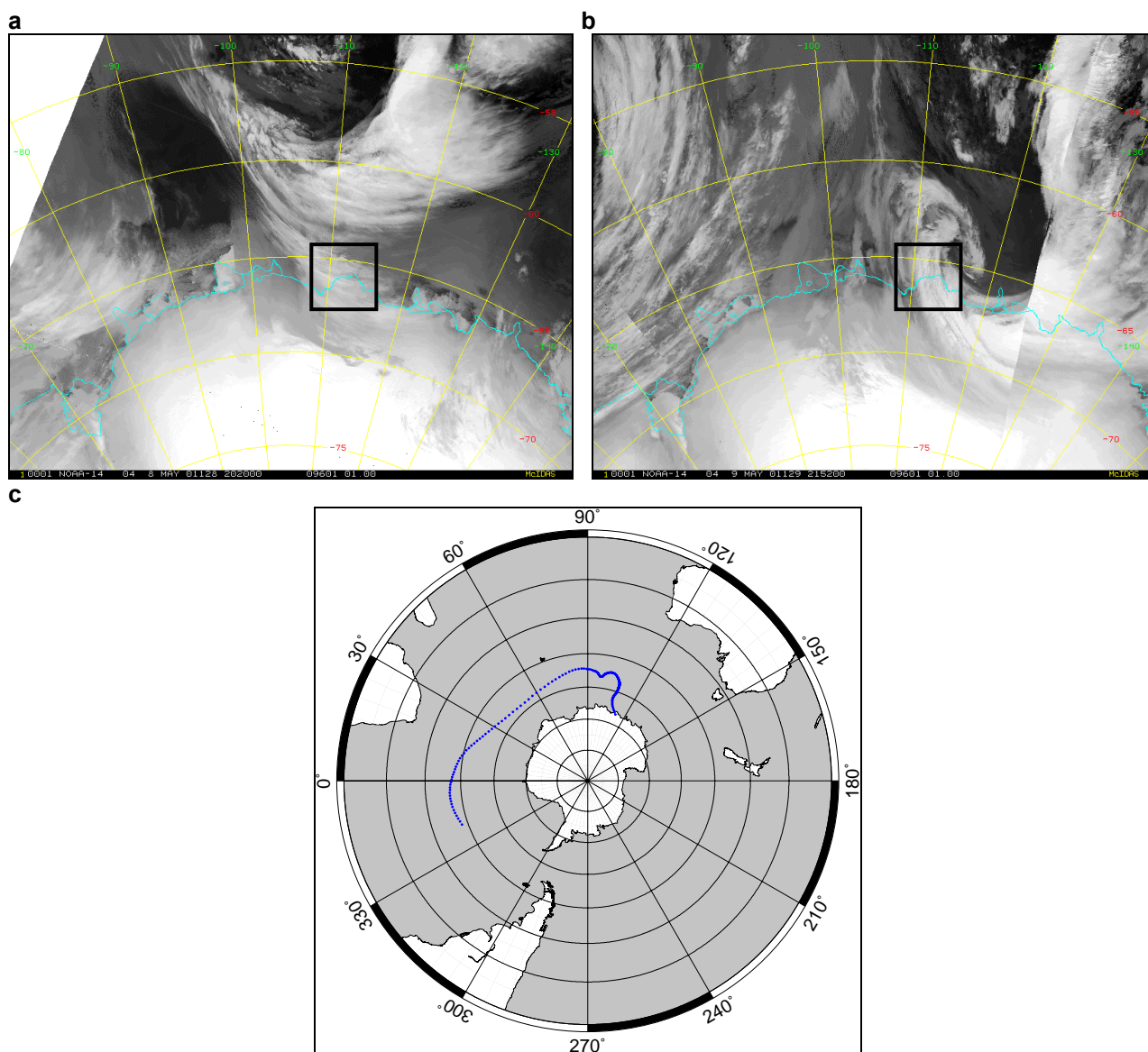


Fig 8.24: AVHRR satellite imagery (a, b) and back trajectory analysis (c) for Event 11, 9 – 12 May 2001 (Julian days 1225 - 1228): (a) 2020 UTC 8 May 2001; (b) 2152 UTC 9 May 2001; (c) 500 hPa back trajectory from 0000 UTC 9 May 2001. Law Dome is indicated in the AVHRR satellite imagery by the black box.

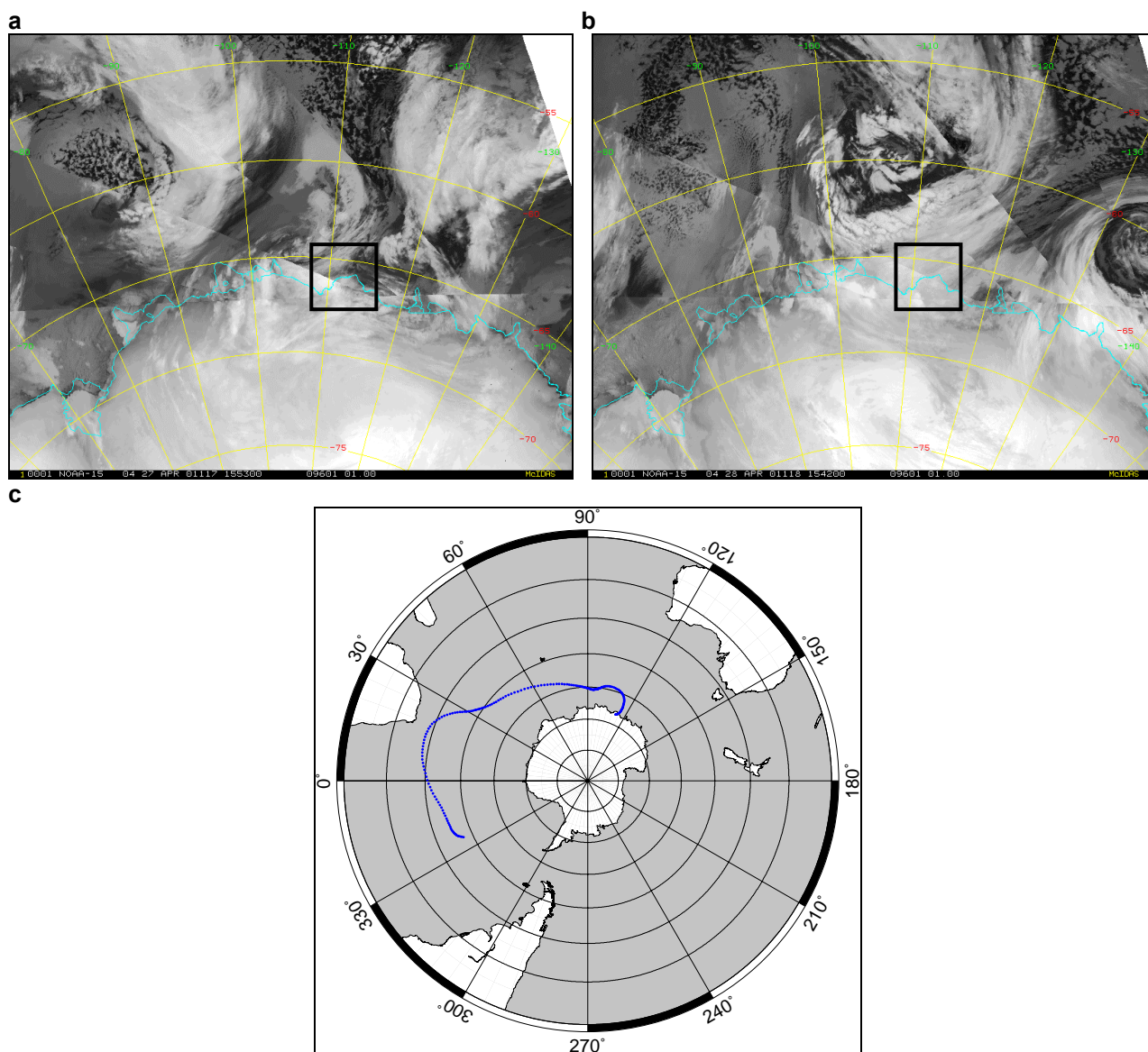


Fig 8.25: AVHRR satellite imagery (a, b) and back trajectory analysis (c) for Event 12, 28 April – 5 May 2001 (Julian days 1214 – 1221): (a) 1553 UTC 27 April 2001; (b) 1542 UTC 28 April 2001; (c) 500 hPa back trajectory from 0000 UTC 28 April 2001. Law Dome is indicated in the AVHRR satellite imagery by the black box.

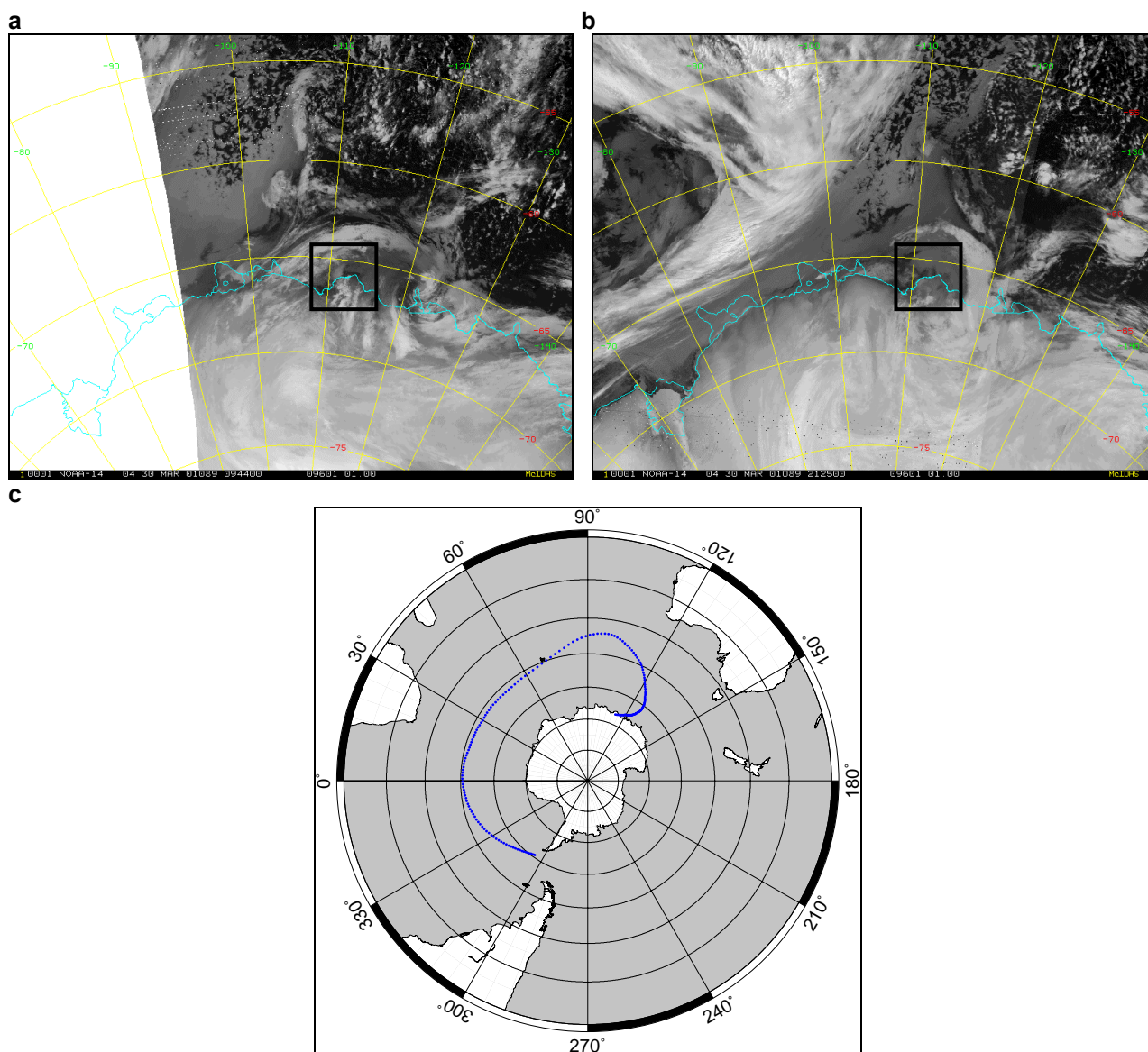


Fig 8.26: AVHRR satellite imagery (a, b) and back trajectory analysis (c) for Event 14, 30 March – 2 April 2001 (Julian days 1185 – 1188): (a) 0944 UTC 30 March 2001; (b) 2125 UTC 30 March 2001; (c) 500 hPa back trajectory from 0000 UTC 30 March 2001. Law Dome is indicated in the AVHRR satellite imagery by the black box.

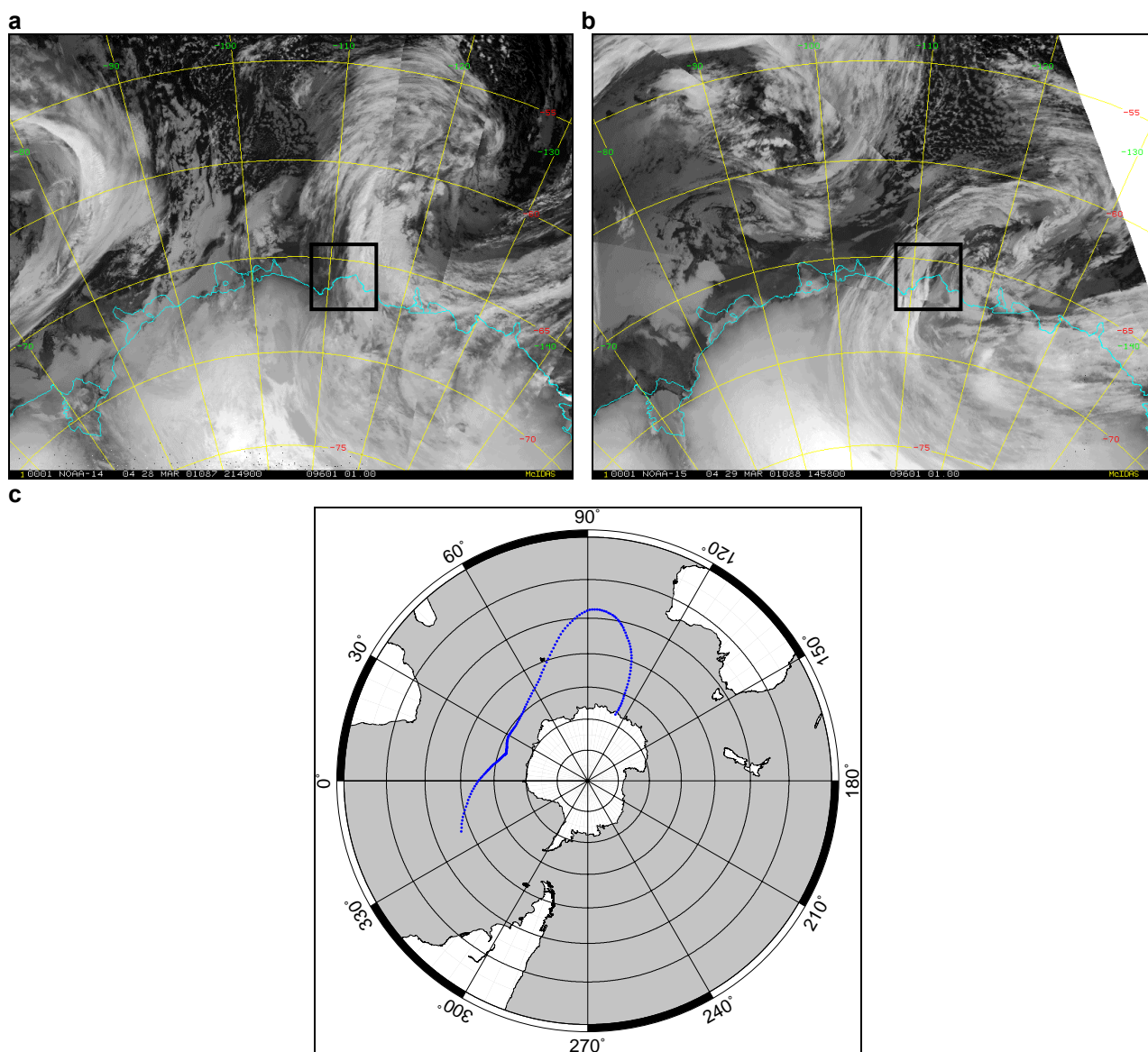


Fig 8.27: AVHRR satellite imagery (a, b) and back trajectory analysis (c) for Event 15, 28 – 29 March 2001 (Julian days 1183 - 1184): (a) 2149 UTC 28 March 2001; (b) 1458 UTC 29 March 2001; (c) 500 hPa back trajectory from 0000 UTC 28 March 2001. Law Dome is indicated in the AVHRR satellite imagery by the black box.

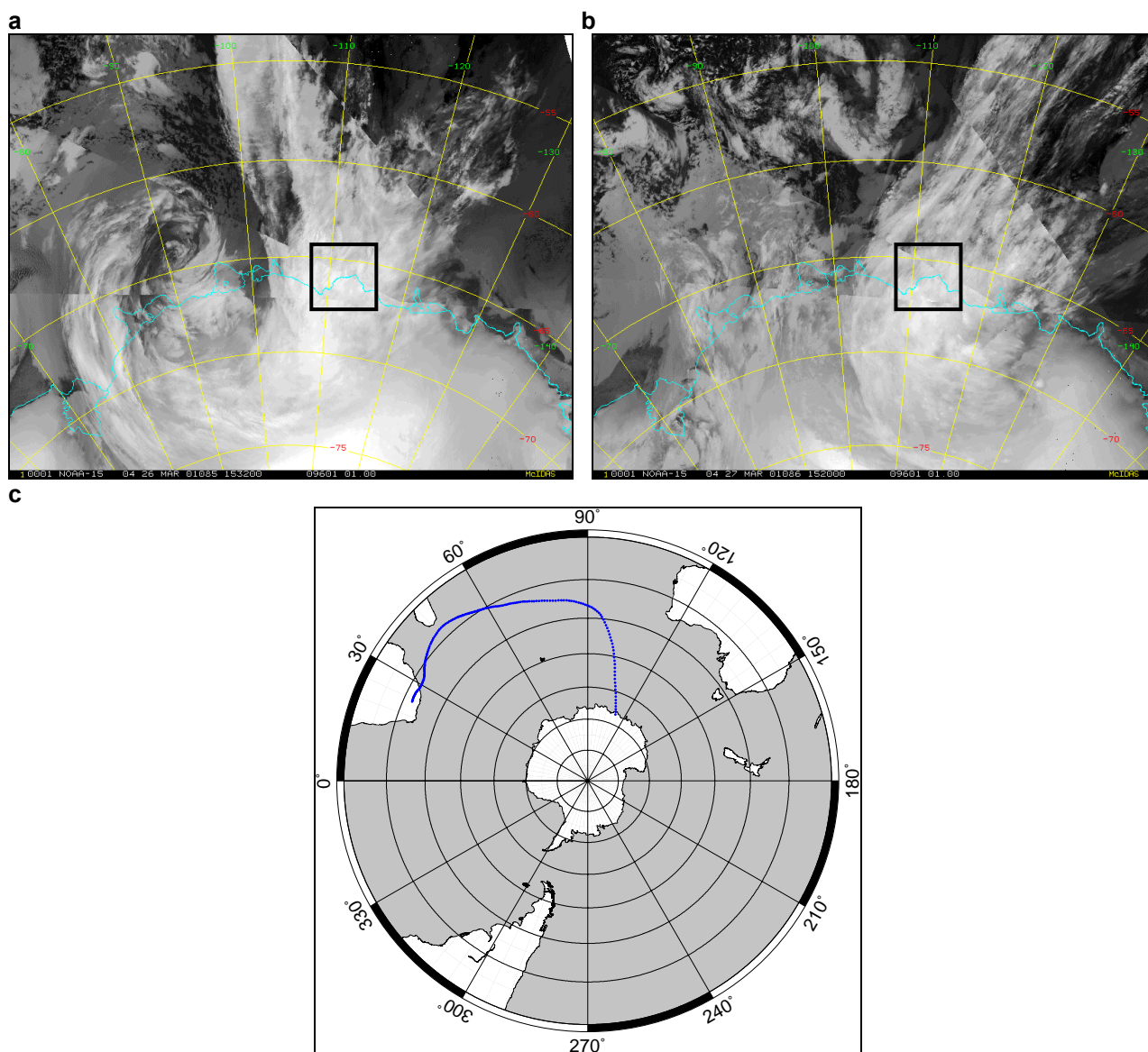


Fig 8.28: AVHRR satellite imagery (a, b) and back trajectory analysis (c) for Event 16, 23 – 27 March 2001 (Julian days 1178 – 1182): (a) 1532 UTC 16 March 2001; (b) 1520 UTC 27 March 2001; (c) 500 hPa back trajectory from 0000 UTC 27 March 2001. Law Dome is indicated in the AVHRR satellite imagery by the black box.

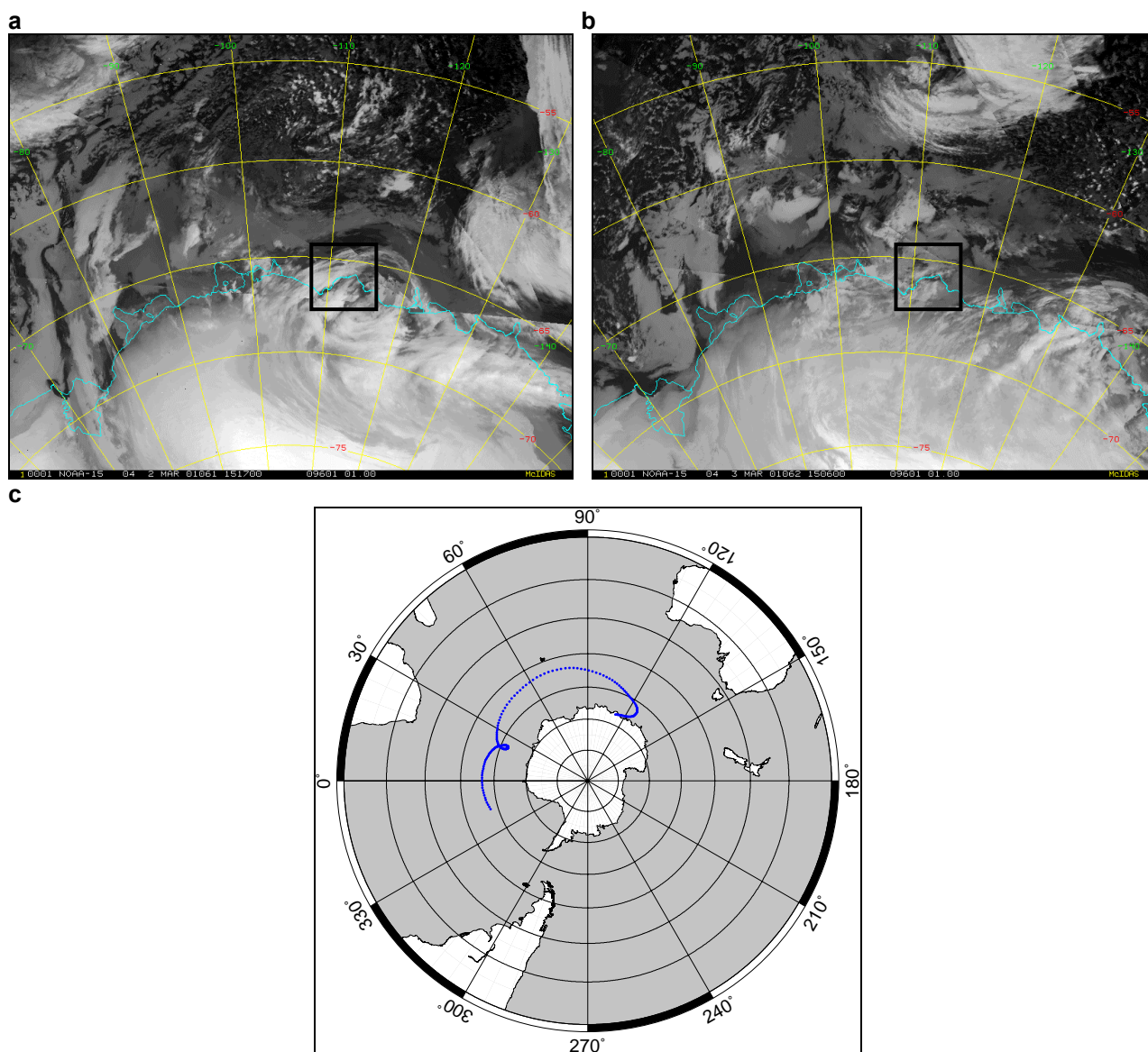


Fig 8.29: AVHRR satellite imagery (a, b) and back trajectory analysis (c) for Event 17, 28 Feb – 3 March 2001 (Julian days 1155 – 1158): (a) 1517 UTC 2 March 2001; (b) 1506 UTC 3 March 2001; (c) 500 hPa back trajectory from 0000 UTC 3 March 2001. Law Dome is indicated in the AVHRR satellite imagery by the black box.

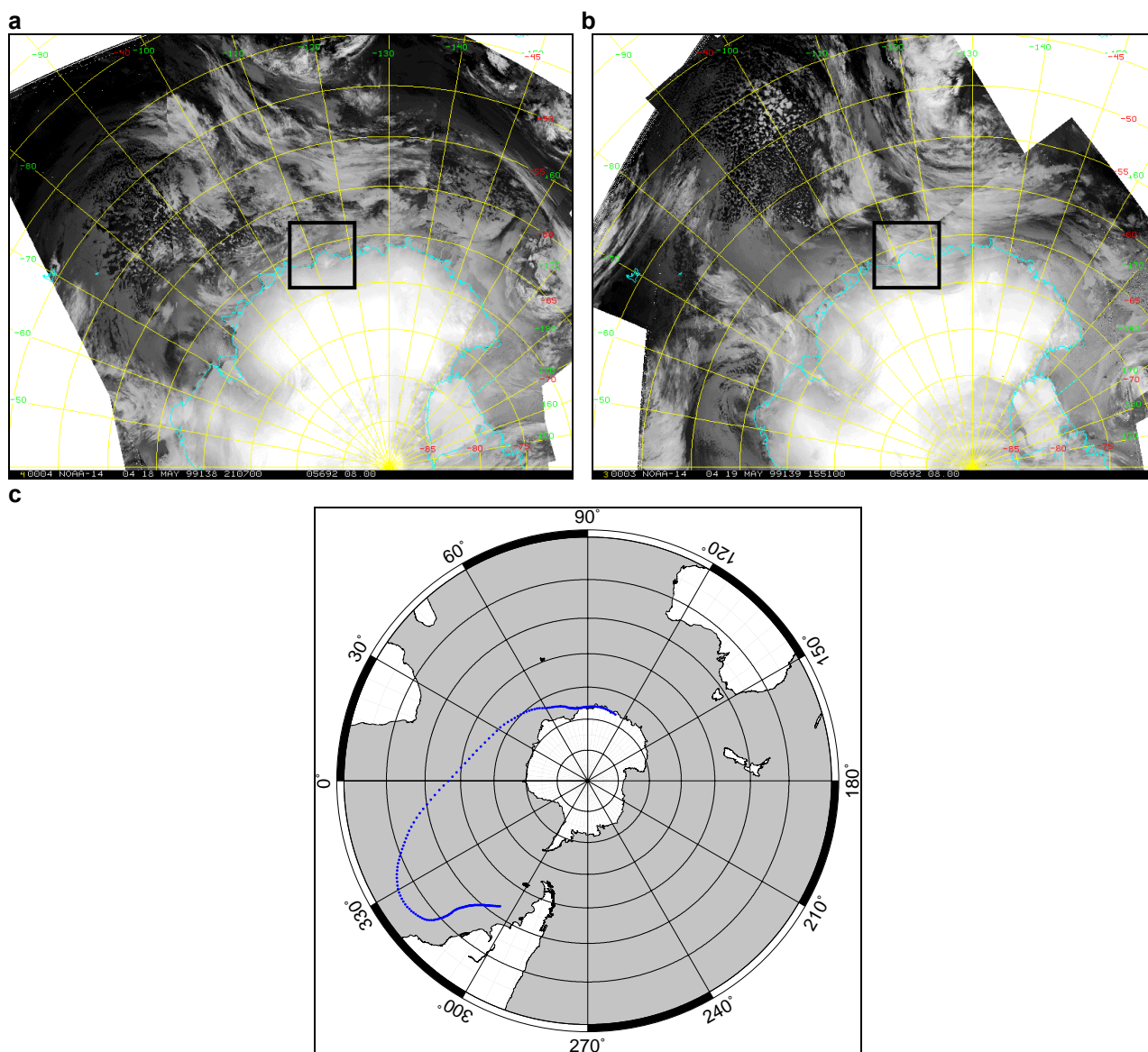


Fig 8.30: AVHRR satellite imagery (a, b) and back trajectory analysis (c) for Event 37, 19 – 22 May 1999 (Julian days 504 – 507): (a) 2107 UTC 18 May 1999; (b) 1551 UTC 19 May 1999; (c) 500 hPa back trajectory from 0000 UTC 19 May 1999. Law Dome is indicated in the AVHRR satellite imagery by the black box.

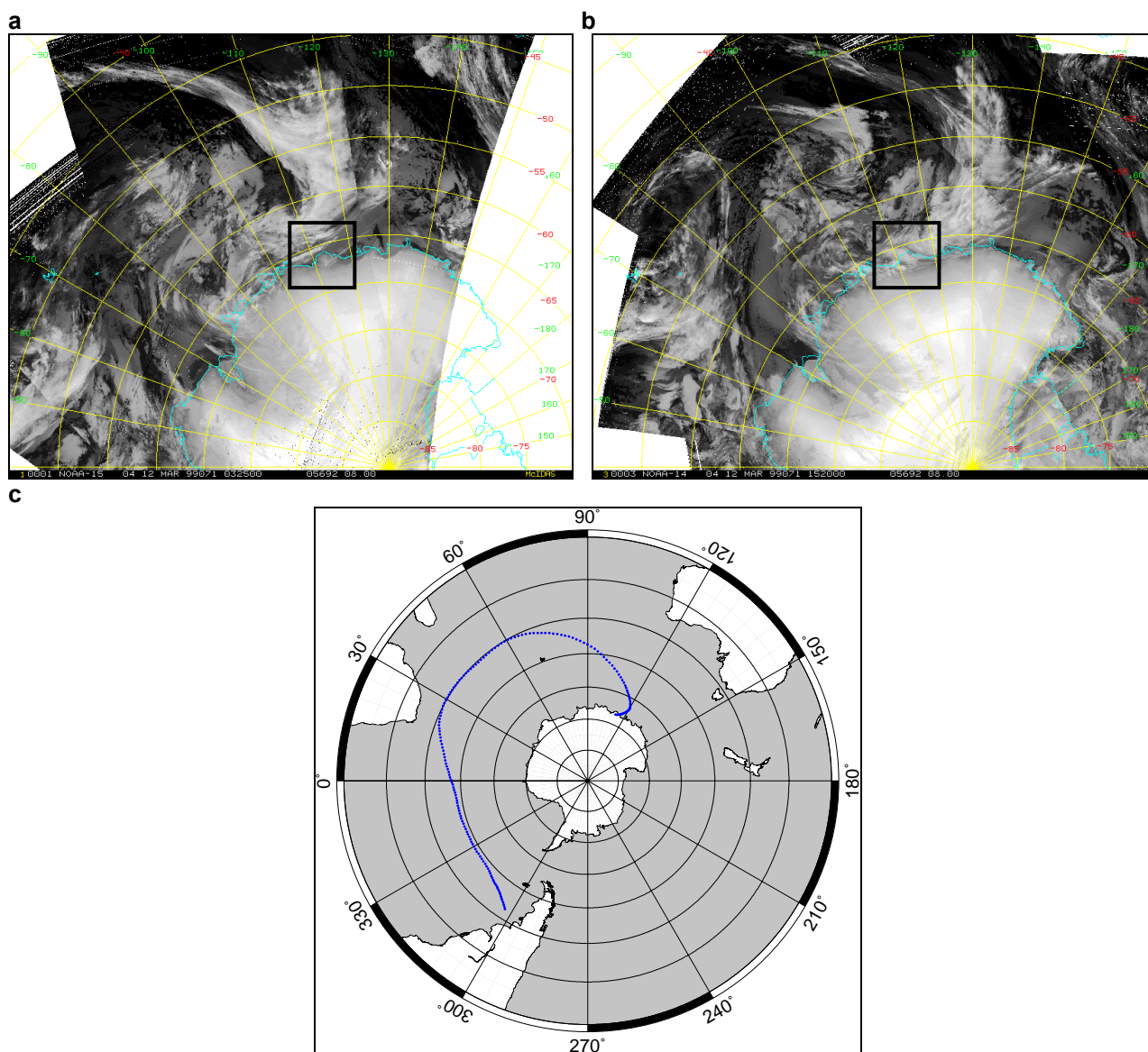


Fig 8.31: AVHRR satellite imagery (a, b) and back trajectory analysis (c) for Event 38, 13 March 1999 (Julian day 437): (a) 0325 UTC 12 March 1999; (b) 1520 UTC 12 March 1999; (c) 500 hPa back trajectory from 0000 UTC 13 March 1999. Law Dome is indicated in the AVHRR satellite imagery by the black box.

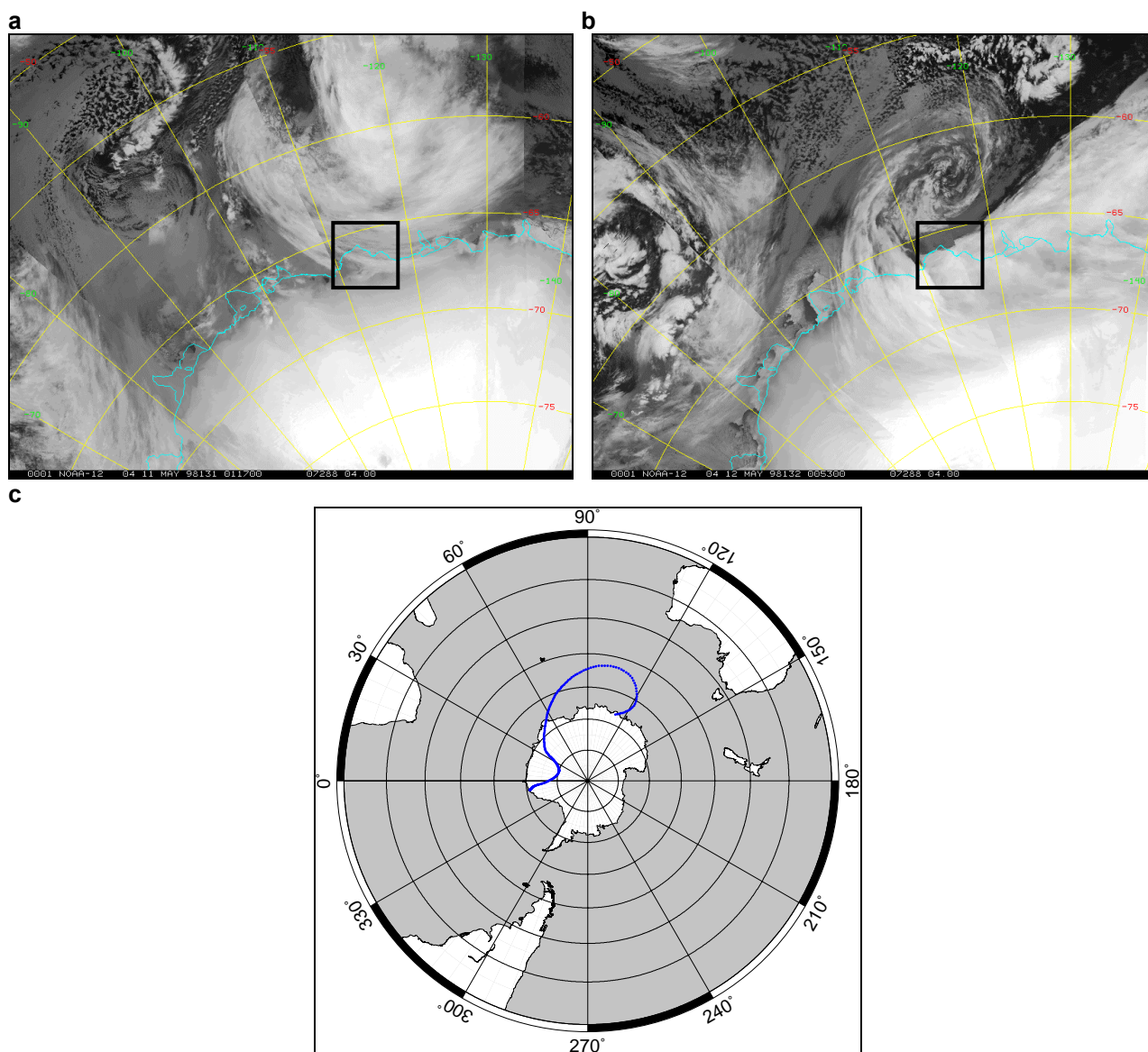


Fig 8.32: AVHRR satellite imagery (a, b) and back trajectory analysis (c) for Event 51, 11 – 13 May 1998 (Julian days 131 – 133): (a) 0117 UTC 11 May 1998; (b) 0053 UTC 12 May 1998; (c) 500 hPa back trajectory from 0000 UTC 12 May 1998. Law Dome is indicated in the AVHRR satellite imagery by the black box.

Appendix C

Local and Synoptic Meteorological Conditions for Winter Events

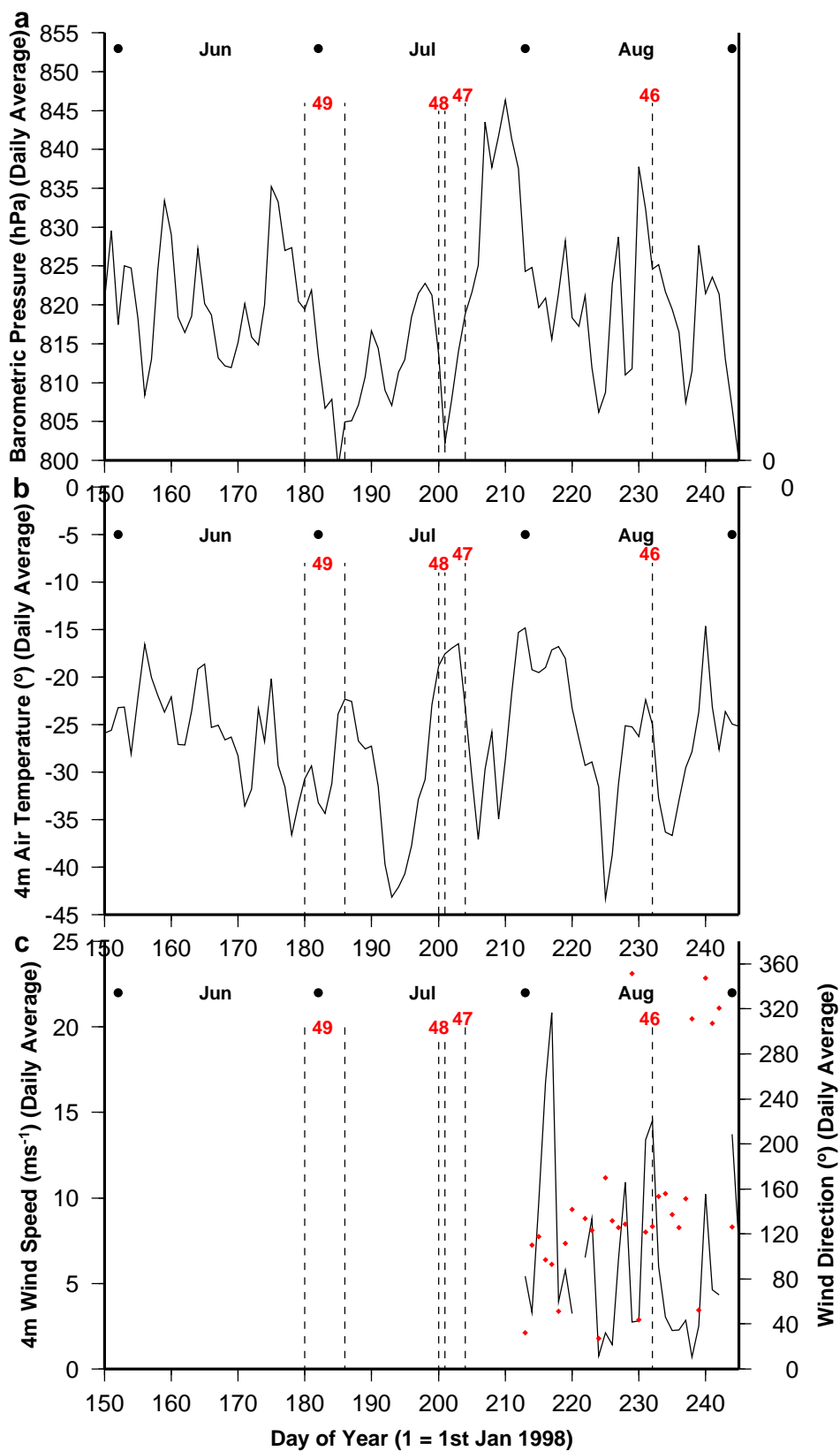


Fig 8.33: Local meteorological conditions recorded by the AWS from 1 June 1998 (Julian day 152) to 31 August 1998 (Julian day 243). (a) Station-level (SL) pressure, (b) air temperature, (c) wind speed. Events that concur (blue) and differ (red) from expected autumn glaciochemical signals are illustrated.

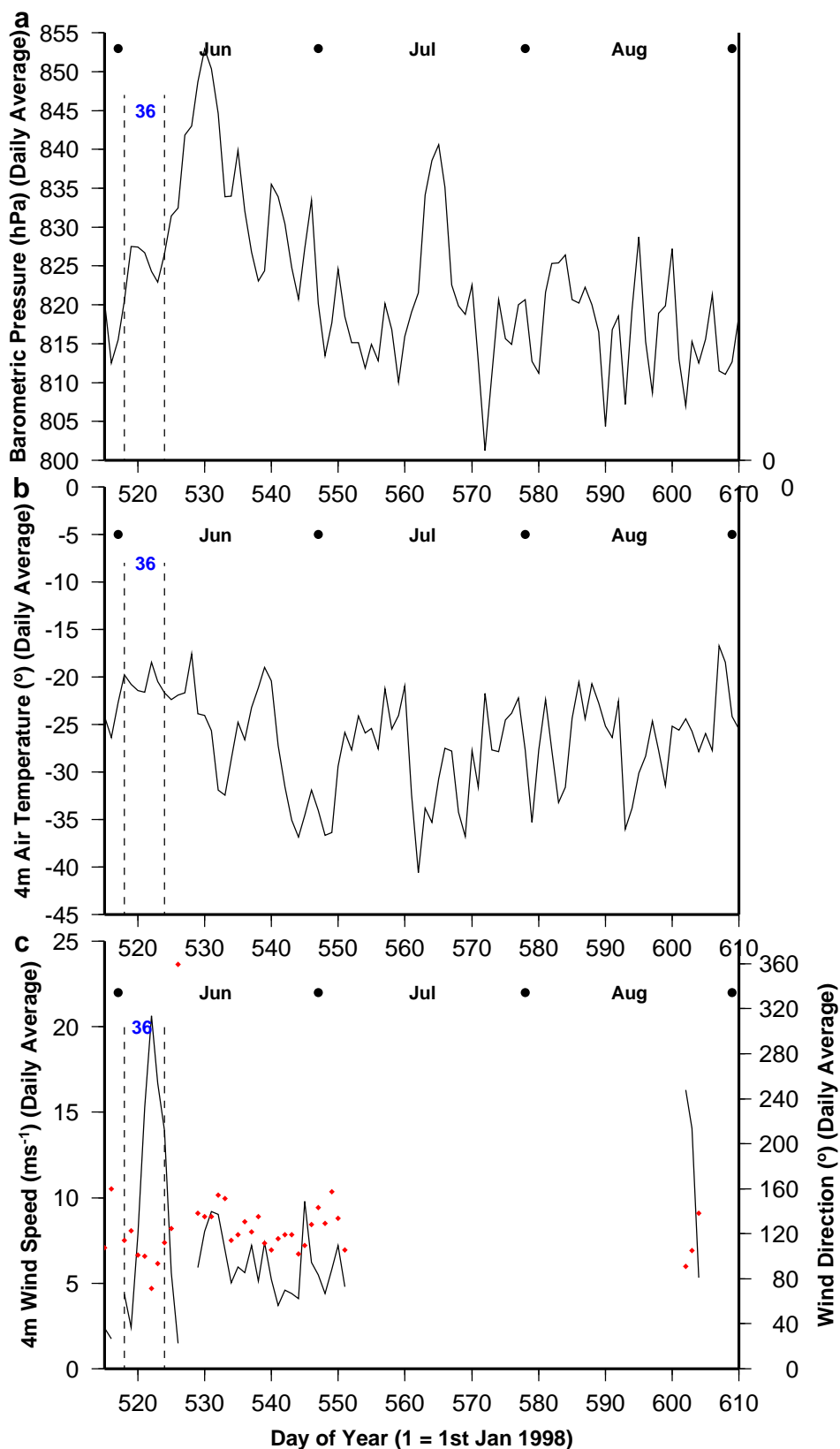


Fig 8.34: Local meteorological conditions recorded by the AWS from 1 June 1999 (Julian day 517) to 31 August 1999 (Julian day 608). (a) Station-level (SL) pressure, (b) air temperature, (c) wind speed. Events that concur (blue) and differ (red) from expected autumn glaciochemical signals are illustrated.

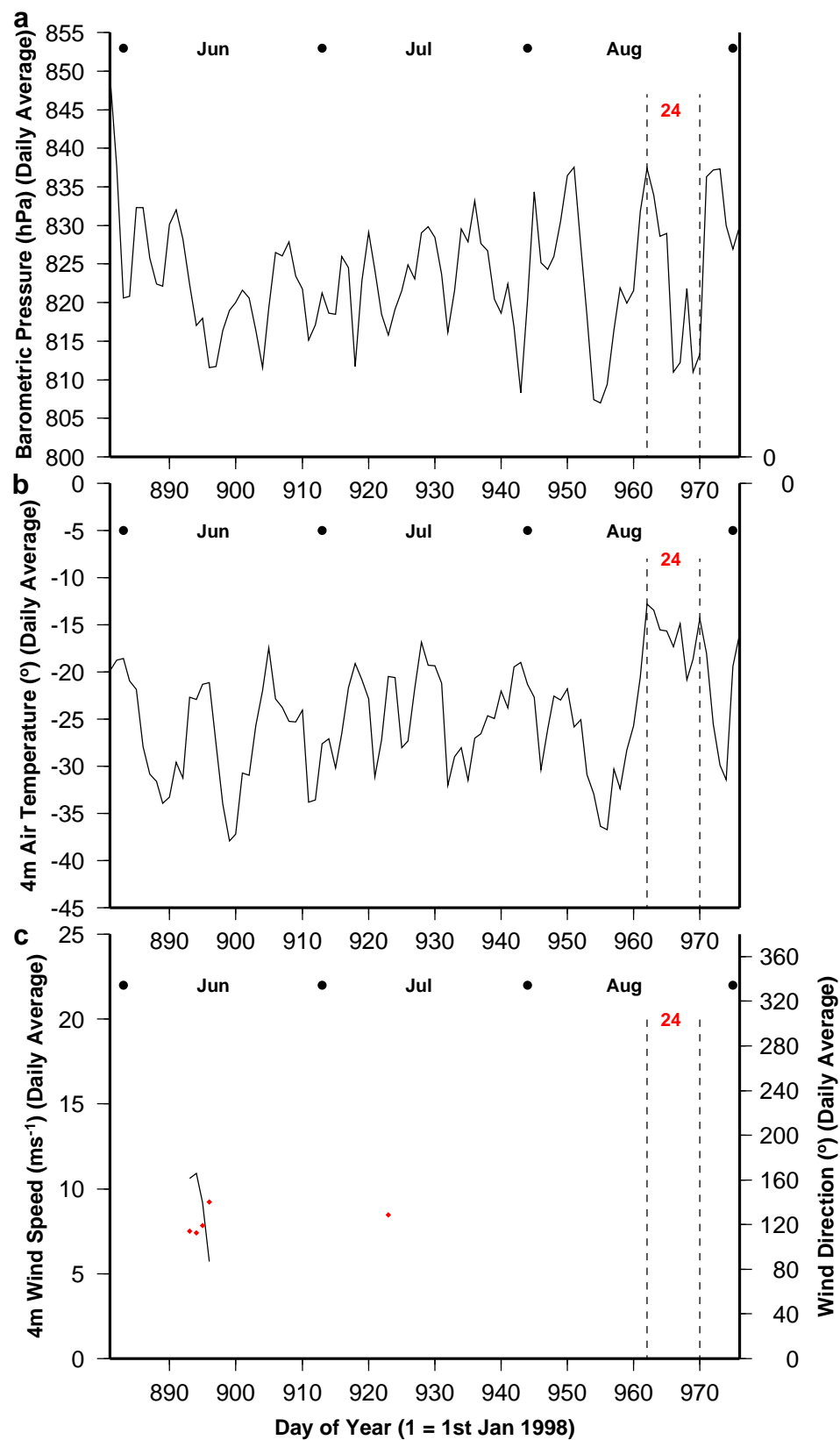


Fig 8.35: Local meteorological conditions recorded by the AWS from 1 June 2000 (Julian day 883) to 31 August 2000 (Julian day 974). (a) Station-level (SL) pressure, (b) air temperature, (c) wind speed. Events that concur (blue) and differ (red) from expected autumn glaciochemical signals are illustrated.

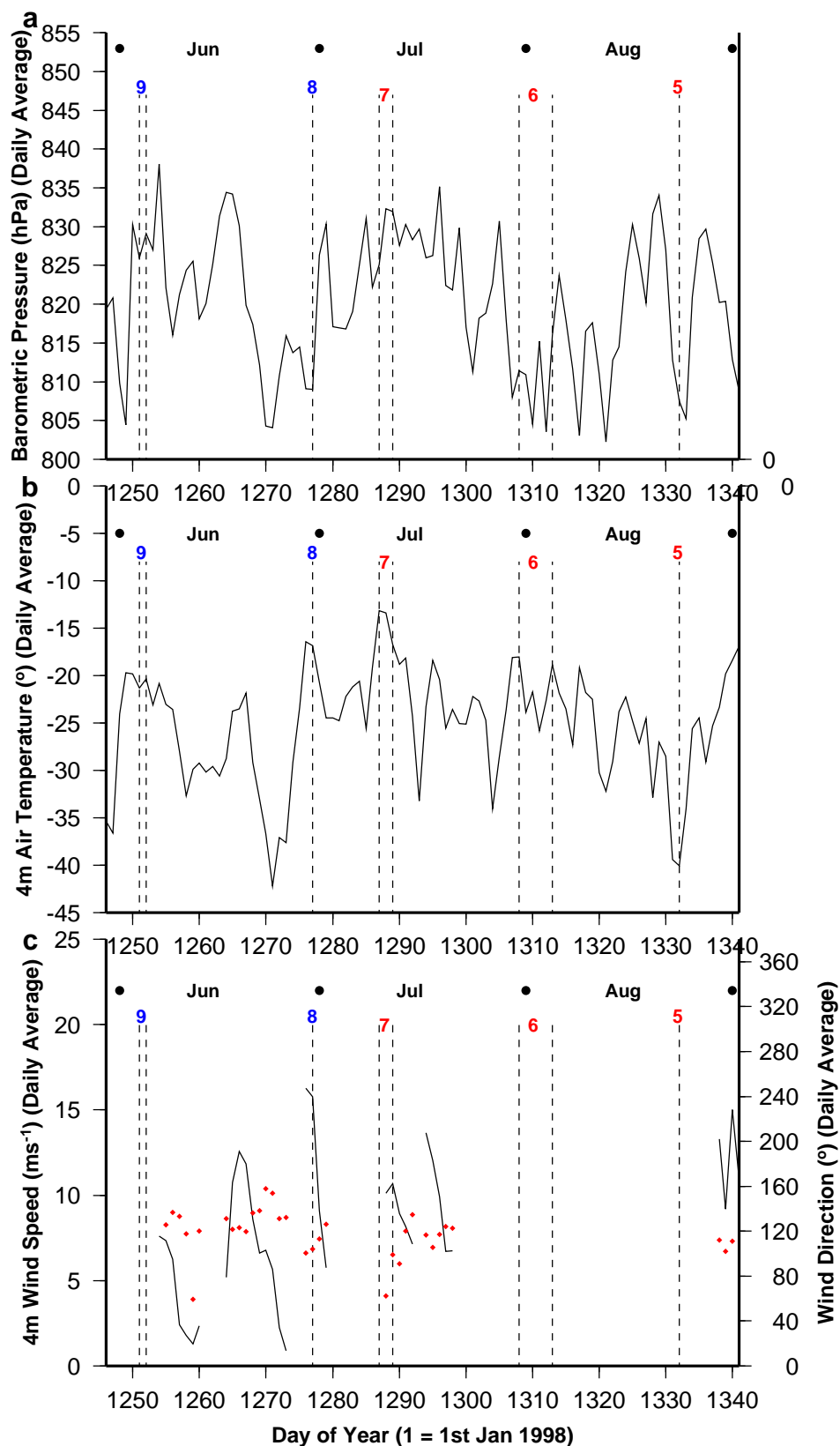


Fig 8.36: Local meteorological conditions recorded by the AWS from 1 June 2001 (Julian day 1248) to 31 August 2001 (Julian day 1339). (a) Station-level (SL) pressure, (b) air temperature, (c) wind speed. Events that concur (blue) and differ (red) from expected autumn glaciochemical signals are illustrated.

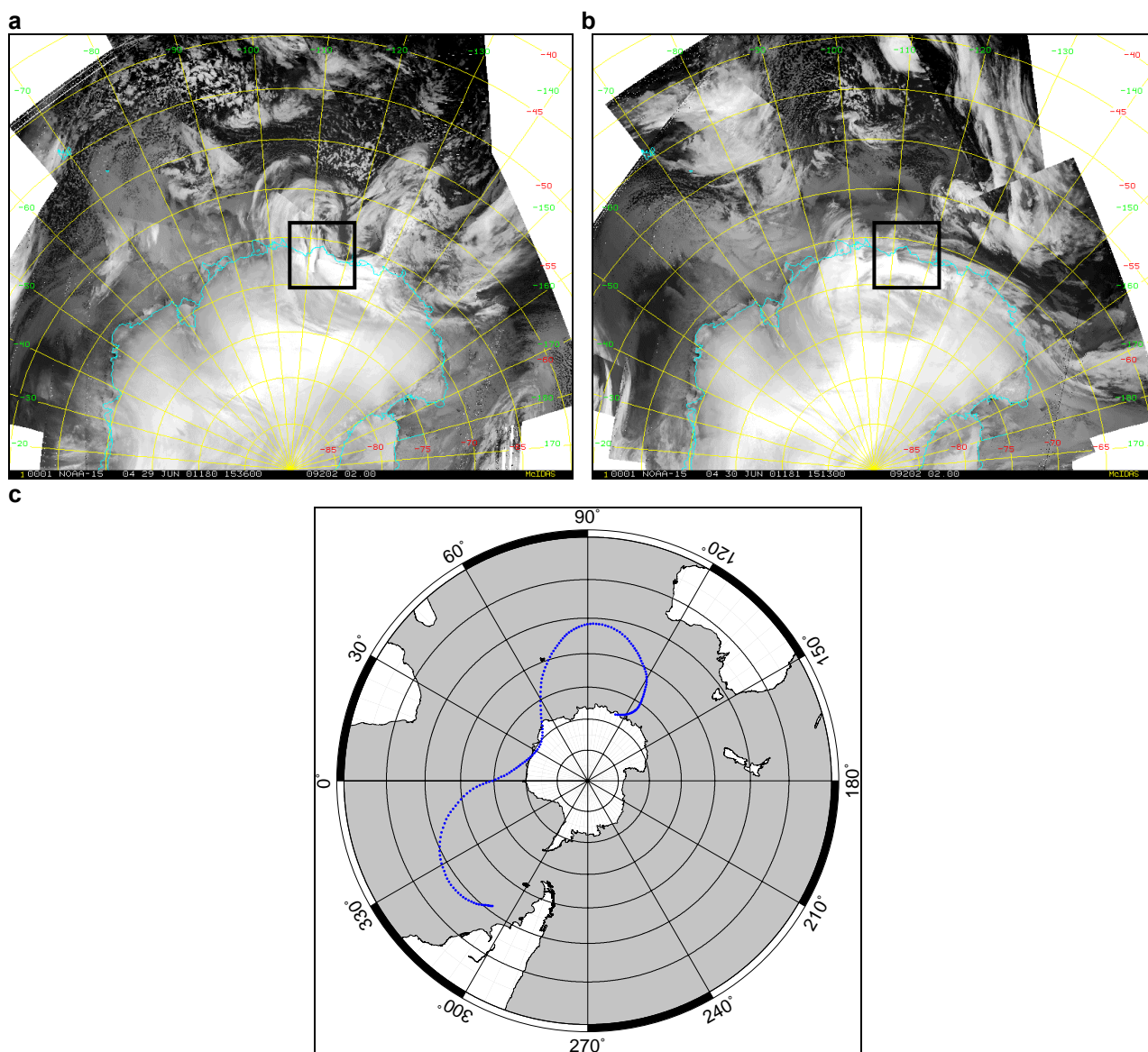


Fig 8.37: AVHRR satellite imagery (a, b) and back trajectory analysis (c) for Event 8, 30 June 2001 (Julian day 1277): (a) 1536 UTC 29 June 2001; (b) 1513 UTC 30 June 2001; (c) 500 hPa back trajectory from 0000 UTC 30 June 2001. Law Dome is indicated in the AVHRR satellite imagery by the black box.

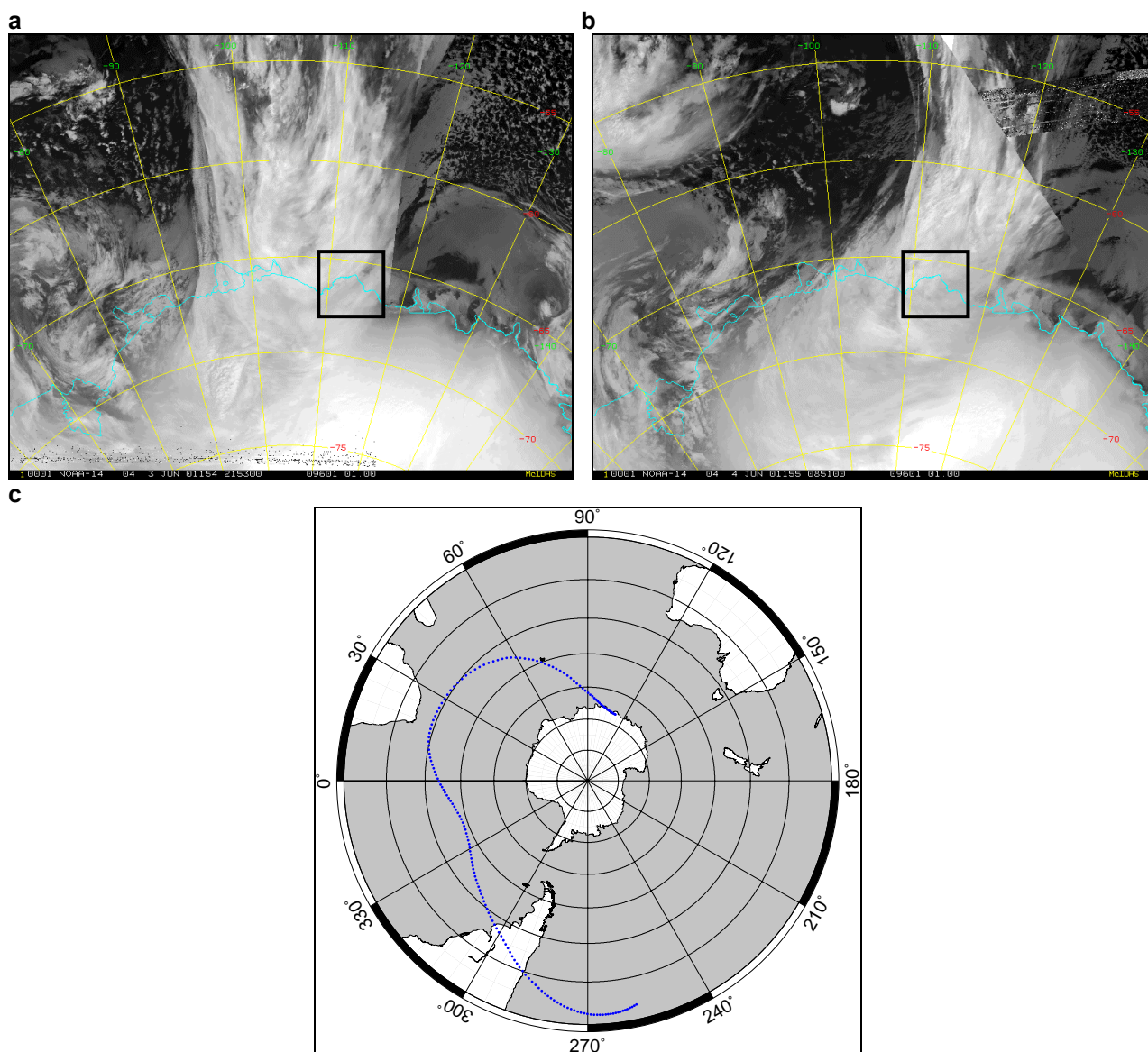


Fig 8.38: AVHRR satellite imagery (a, b) and back trajectory analysis (c) for Event 9, 4 – 5 June 2001 (Julian days 1251 – 1252): (a) 2153 UTC 3 June 2001; (b) 0851 UTC 4 June 2001; (c) 500 hPa back trajectory from 0000 UTC 4 June 2001. Law Dome is indicated in the AVHRR satellite imagery by the black box.

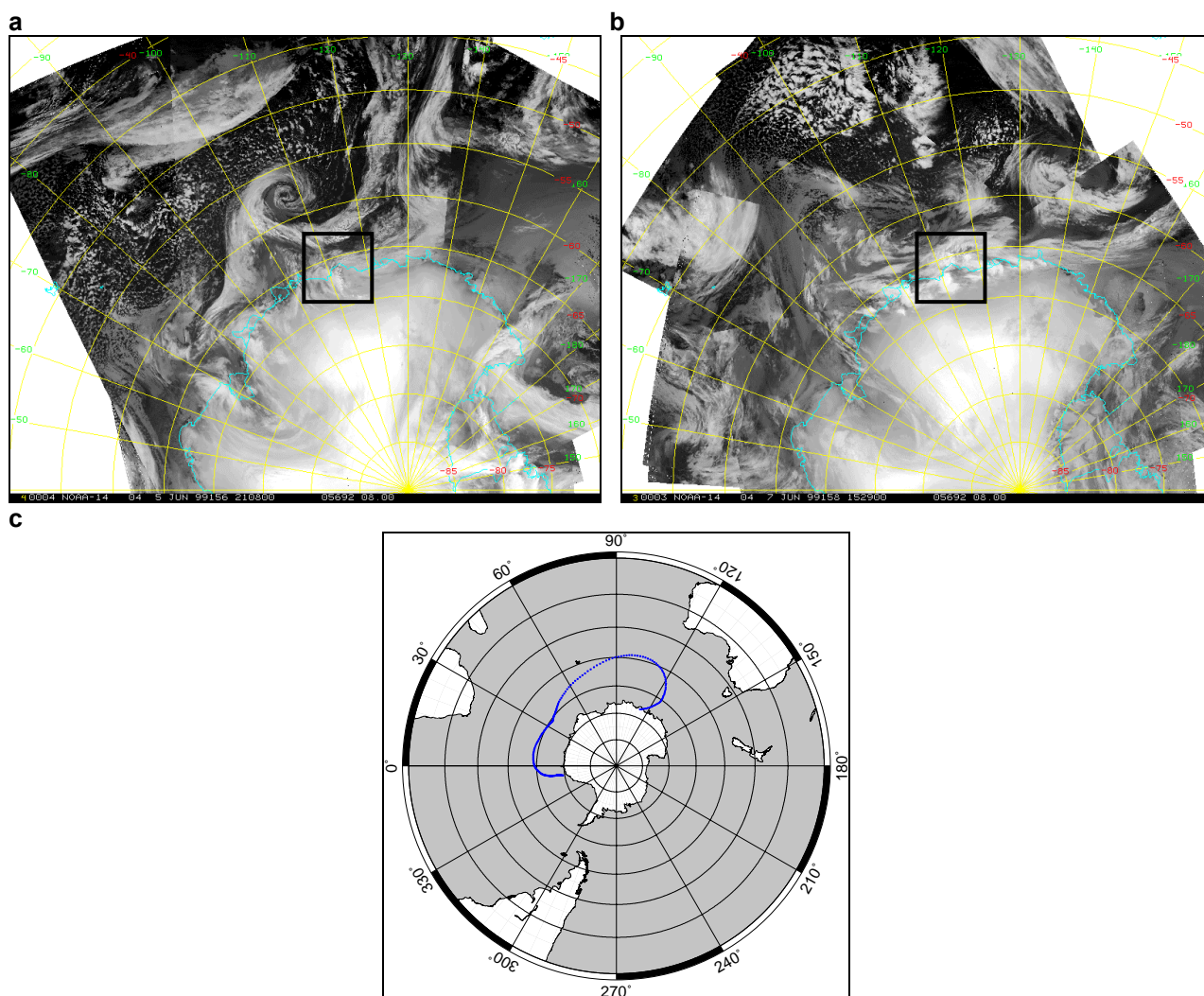


Fig 8.39: AVHRR satellite imagery (a, b) and back trajectory analysis (c) for Event 36, 2 – 8 June 1999 (Julian days 518 – 524): (a) 2108 UTC 5 June 1999; (b) 1529 UTC 7 June 1999; (c) 500 hPa back trajectory from 0000 UTC 7 June 1999. Law Dome is indicated in the AVHRR satellite imagery by the black box.

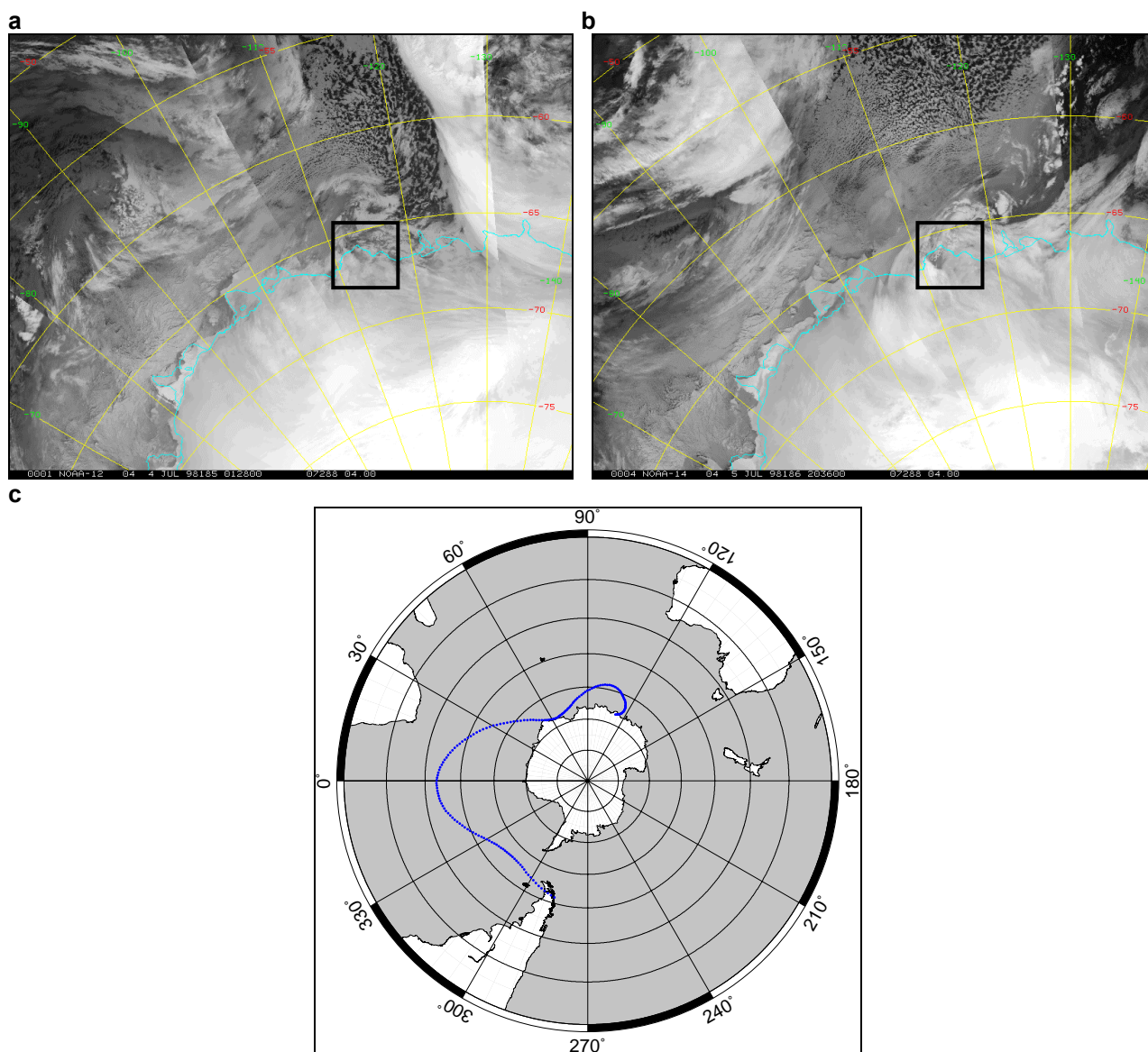


Fig 8.40: AVHRR satellite imagery (a, b) and back trajectory analysis (c) for Event 49, 29 June – 5 July 1998 (Julian days 180 – 186): (a) 0128 UTC 4 July 1998; (b) 2036 UTC 5 July 1998; (c) 500 hPa back trajectory from 0000 UTC 4 July 1998. Law Dome is indicated in the AVHRR satellite imagery by the black box.

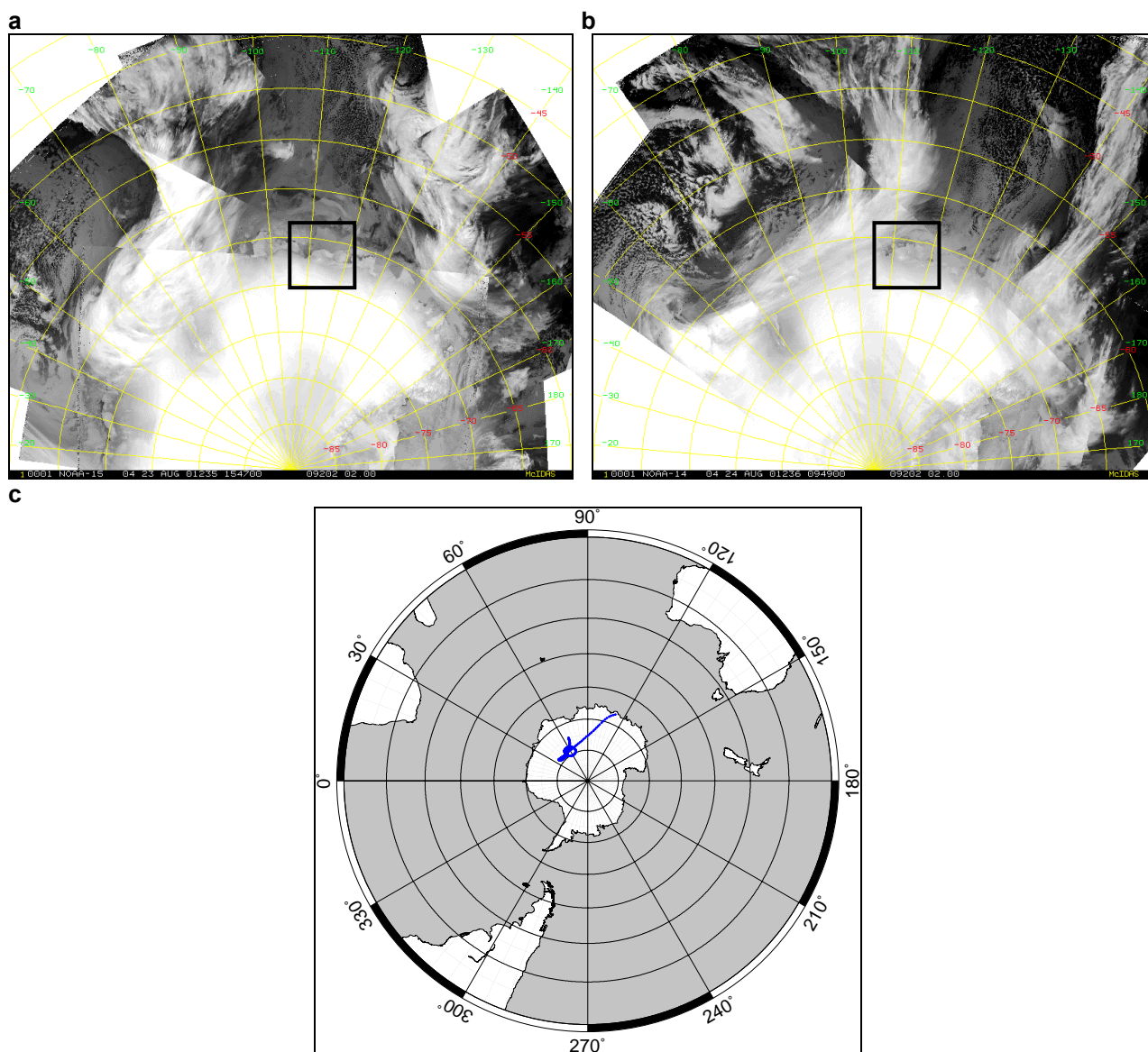


Fig 8.41: AVHRR satellite imagery (a, b) and back trajectory analysis (c) for Event 5, 24 August 2001 (Julian day 1332): (a) 1547 UTC 23 August 2001; (b) 0949 UTC 24 August 2001; (c) 500 hPa back trajectory from 0000 UTC 24 August 2001. Law Dome is indicated in the AVHRR satellite imagery by the black box.

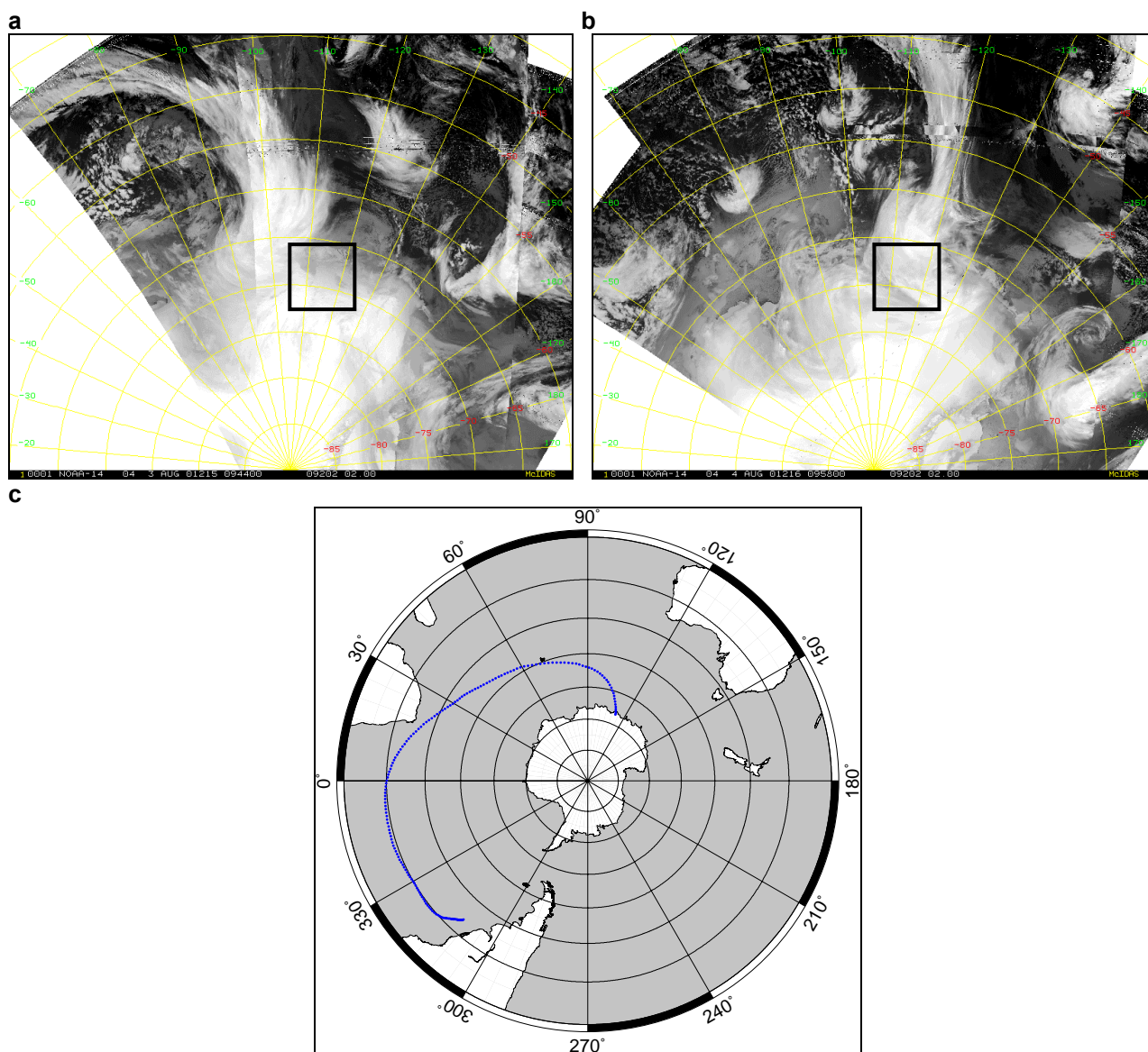


Fig 8.42: AVHRR satellite imagery (a, b) and back trajectory analysis (c) for Event 6, 31 July – 5 August 2001 (Julian days 1308 – 1313): (a) 0944 UTC 3 August 2001; (b) 0958 UTC 4 August 2001; (c) 500 hPa back trajectory from 0000 UTC 4 August 2001. Law Dome is indicated in the AVHRR satellite imagery by the black box.

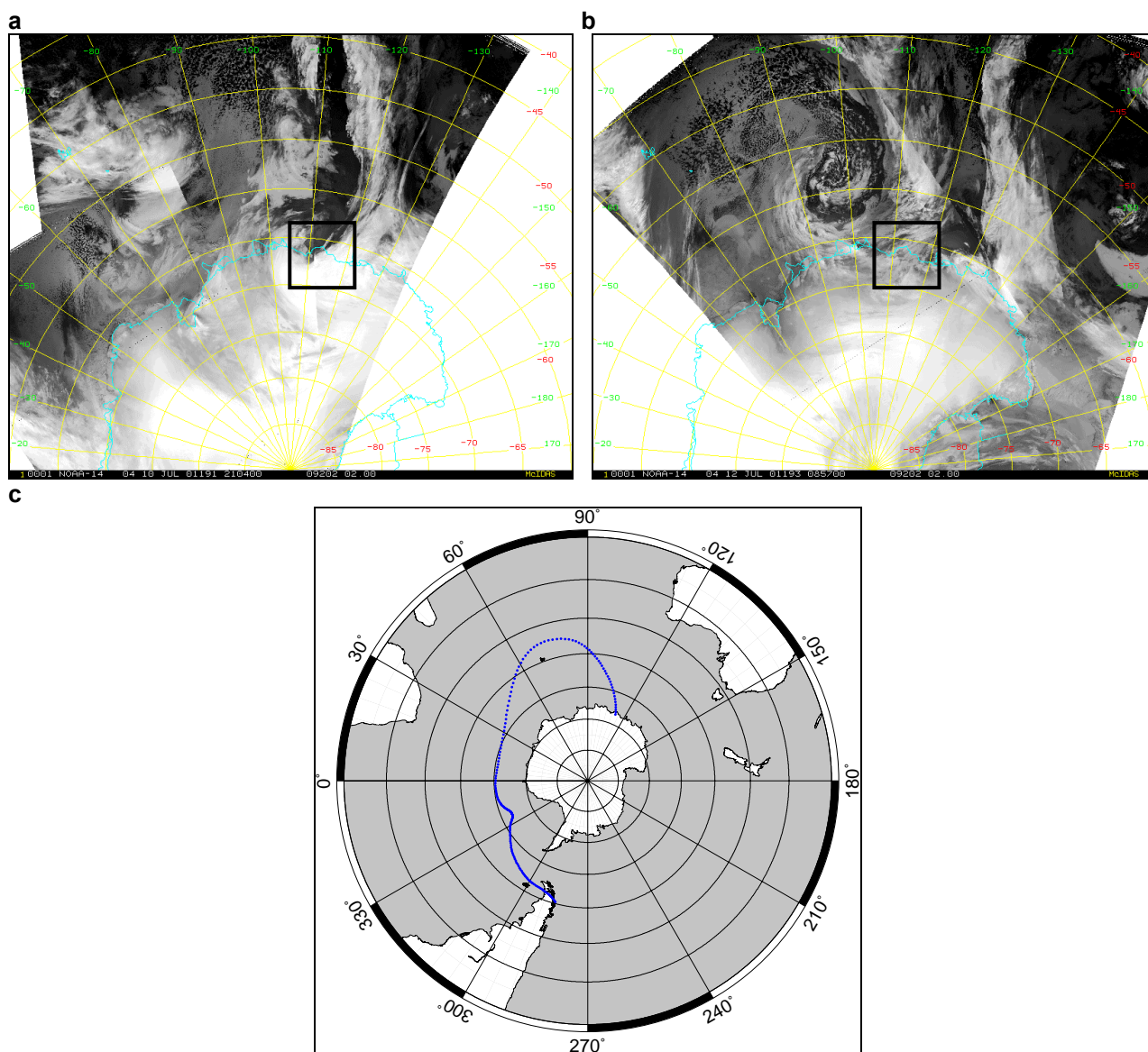


Fig 8.43: AVHRR satellite imagery (a, b) and back trajectory analysis (c) for Event 7, 10 – 12 July 2001 (Julian days 1287 – 1289): (a) 2104 UTC 10 July 2001; (b) 0857 UTC 12 July 2001; (c) 500 hPa back trajectory from 0000 UTC 10 July 2001. Law Dome is indicated in the AVHRR satellite imagery by the black box.

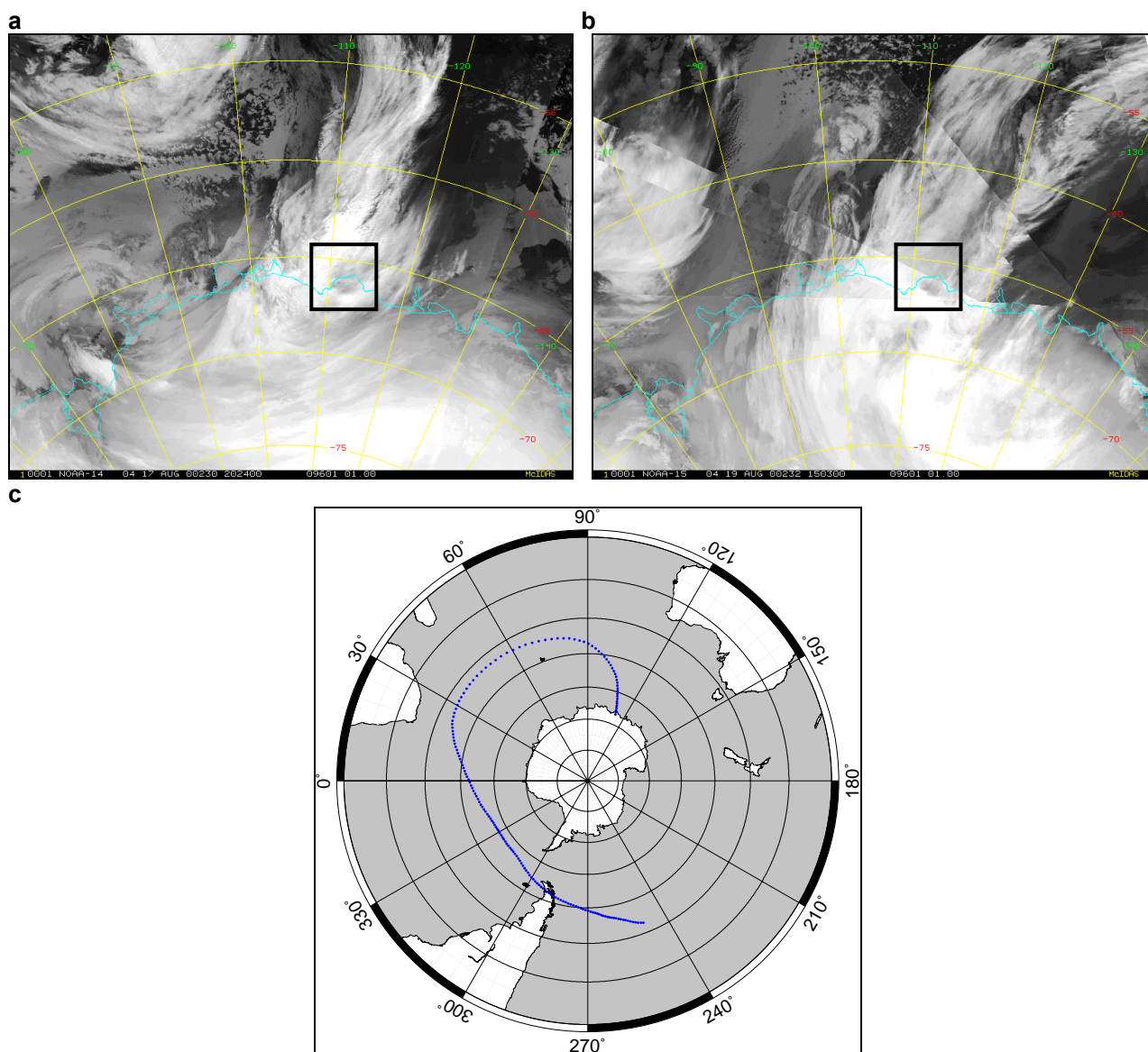


Fig 8.44: AVHRR satellite imagery (a, b) and back trajectory analysis (c) for Event 24, 19 – 27 August 2000 (Julian days 962 - 970): (a) 2024 UTC 17 August 2000; (b) 1503 UTC 19 August 2000; (c) 500 hPa back trajectory from 0000 UTC 19 August 2000. Law Dome is indicated in the AVHRR satellite imagery by the black box.

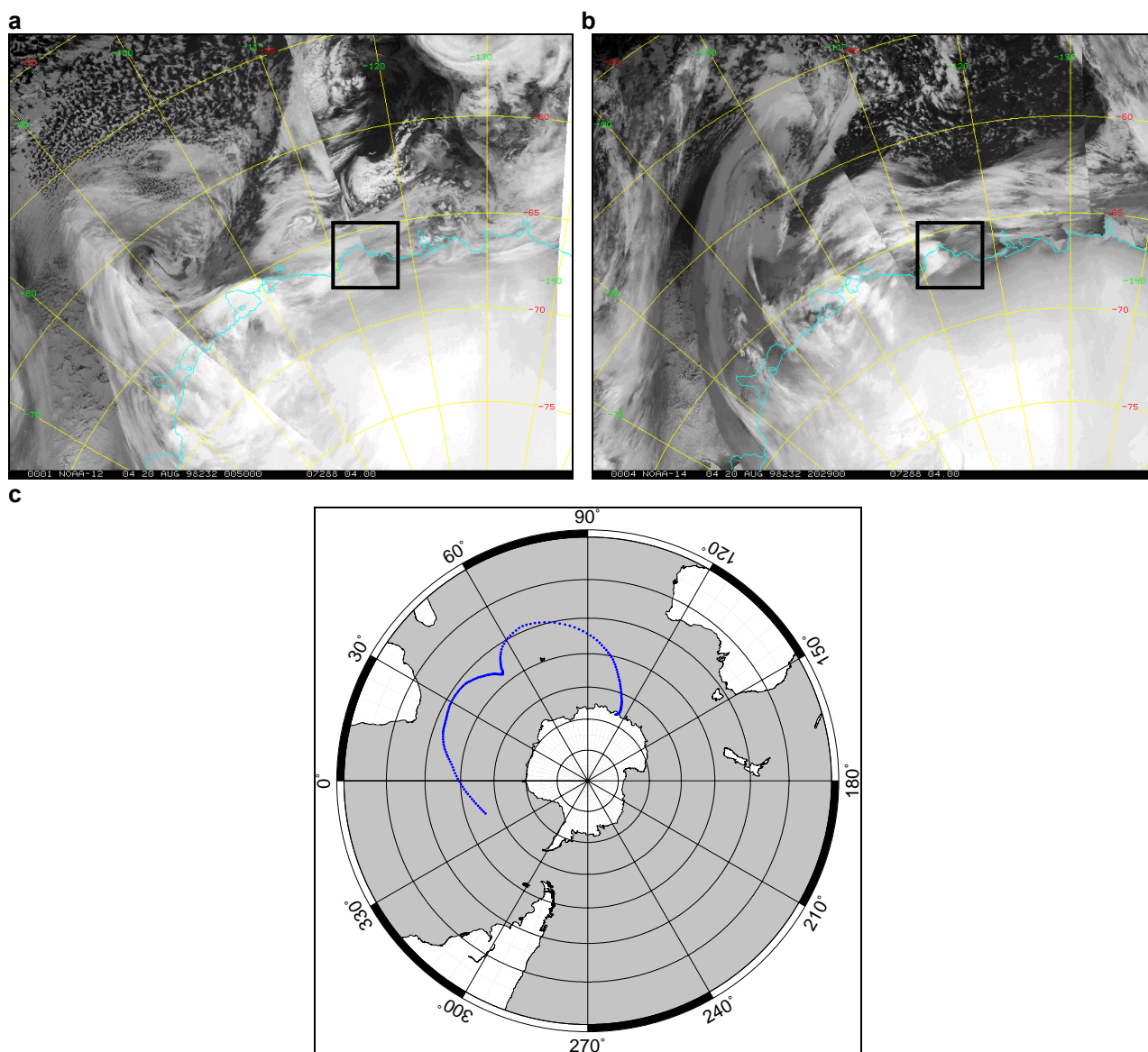


Fig 8.45: AVHRR satellite imagery (a, b) and back trajectory analysis (c) for Event 46, 20 August 1998 (Julian day 232): (a) 0050 UTC 20 August 1998; (b) 2029 UTC 20 August 1998; (c) 500 hPa back trajectory from 0000 UTC 20 August 1998. Law Dome is indicated in the AVHRR satellite imagery by the black box.

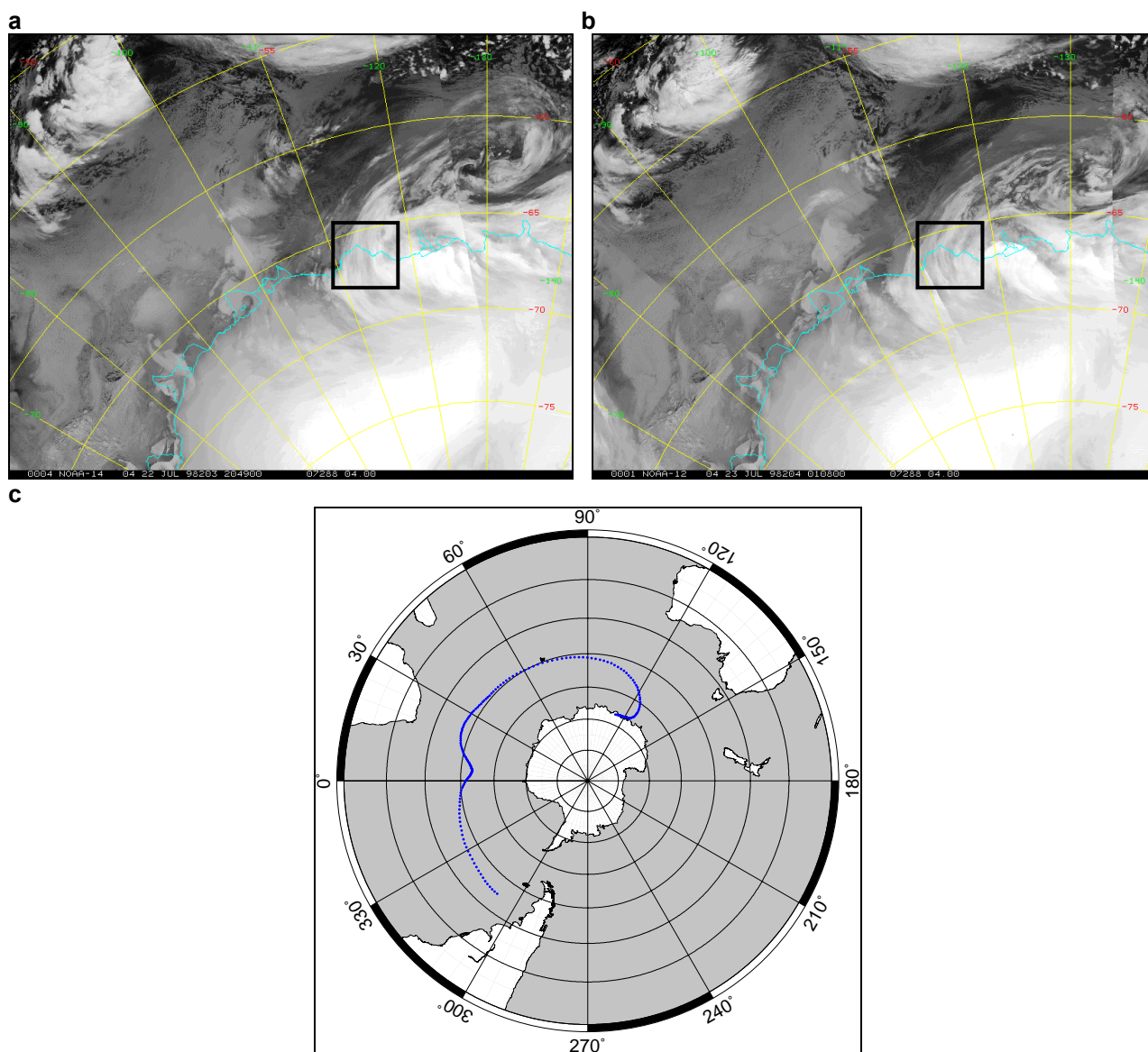


Fig 8.46: AVHRR satellite imagery (a, b) and back trajectory analysis (c) for Event 47, 23 July 1998 (Julian day 204): (a) 2049 UTC 22 July 1998; (b) 0108 UTC 23 July 1998; (c) 500 hPa back trajectory from 0000 UTC 23 July 1998. Law Dome is indicated in the AVHRR satellite imagery by the black box.

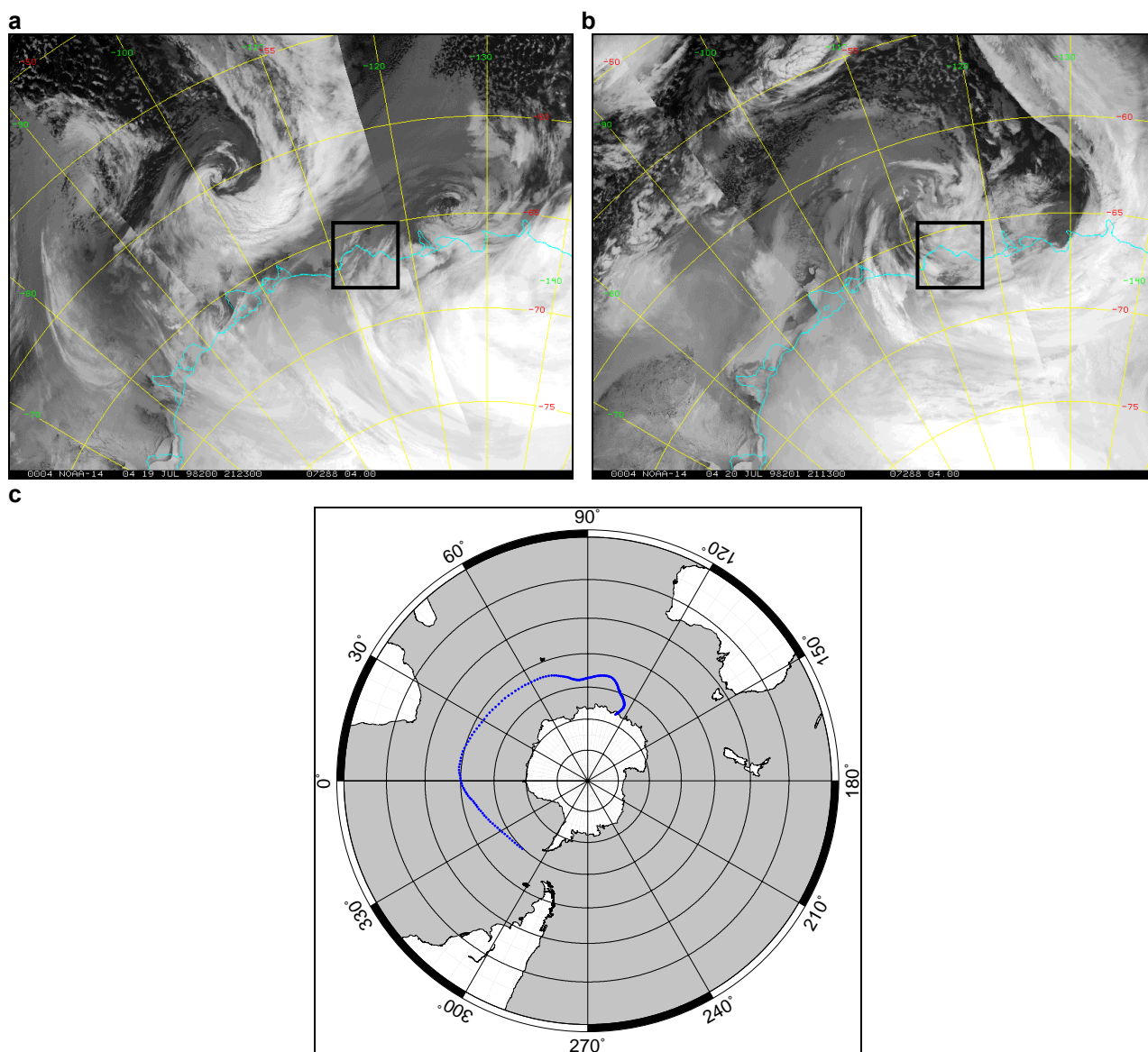


Fig 8.47: AVHRR satellite imagery (a, b) and back trajectory analysis (c) for Event 48, 19 – 20 July 1998 (Julian days 200 – 201): (a) 2123 UTC 19 July 1998; (b) 2113 UTC 20 July 1998; (c) 500 hPa back trajectory from 0000 UTC 19 July 1998. Law Dome is indicated in the AVHRR satellite imagery by the black box.

Appendix D

Local and Synoptic Meteorological Conditions for Spring Events

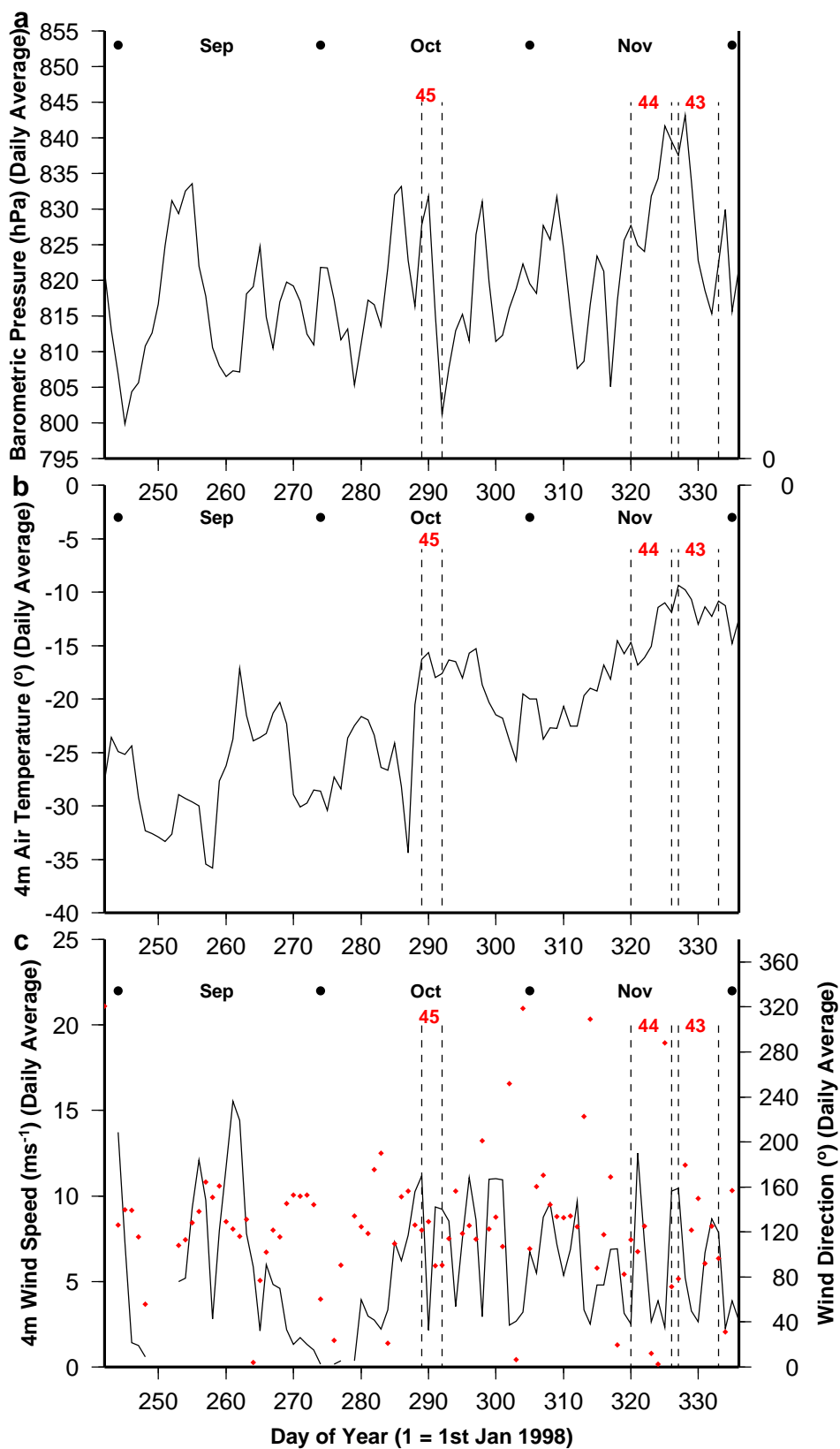


Fig 8.48: Local meteorological conditions recorded by the AWS from 1 September 1998 (Julian day 244) to 30 November 1998 (Julian day 334). (a) Station-level (SL) pressure, (b) air temperature, (c) wind speed. Events that concur (blue) and differ (red) from expected autumn glaciochemical signals are illustrated.

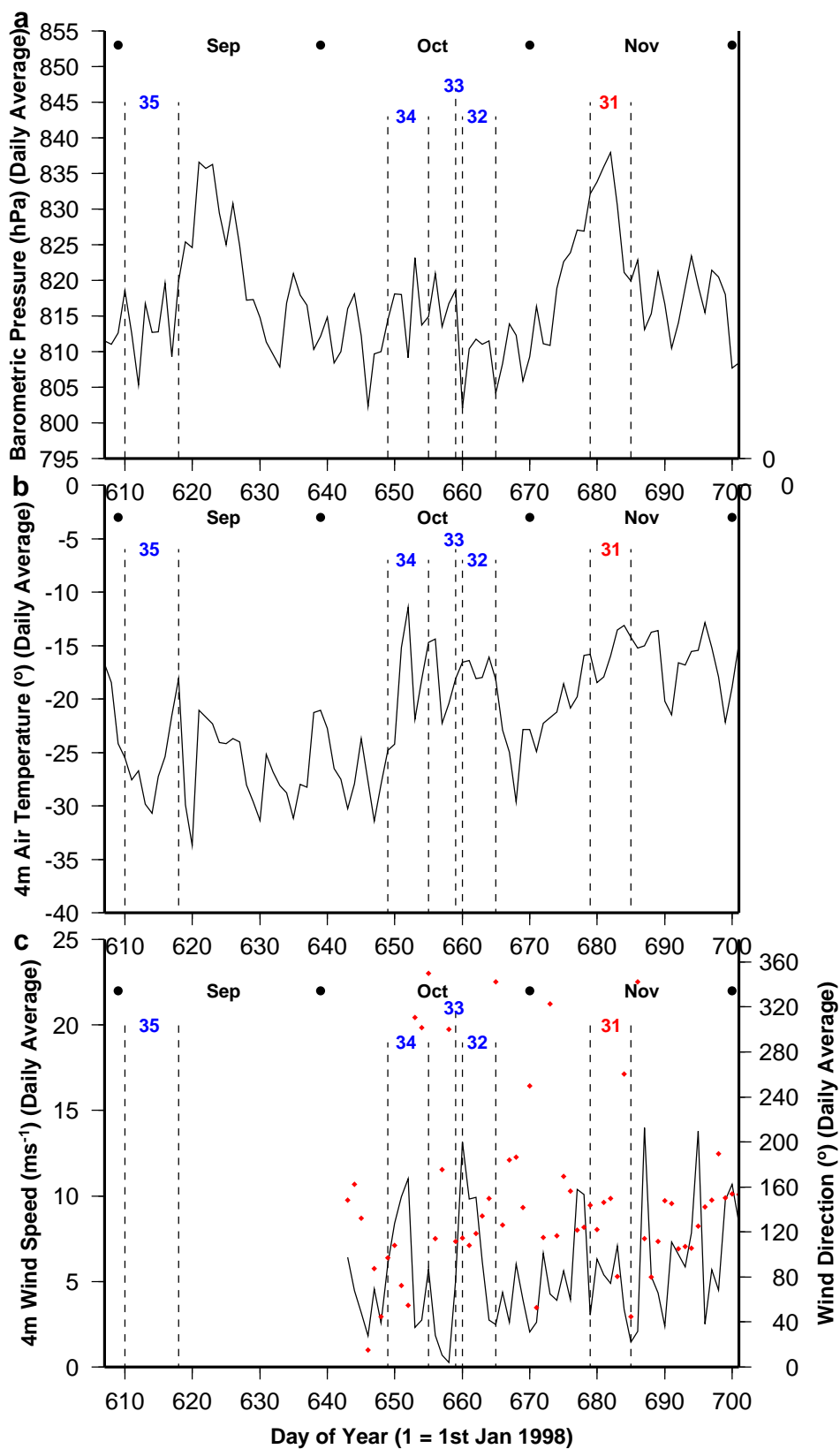


Fig 8.49: Local meteorological conditions recorded by the AWS from 1 September 1999 (Julian day 609) to 30 November 1999 (Julian day 699). (a) Station-level (SL) pressure, (b) air temperature, (c) wind speed. Events that concur (blue) and differ (red) from expected autumn glaciochemical signals are illustrated.

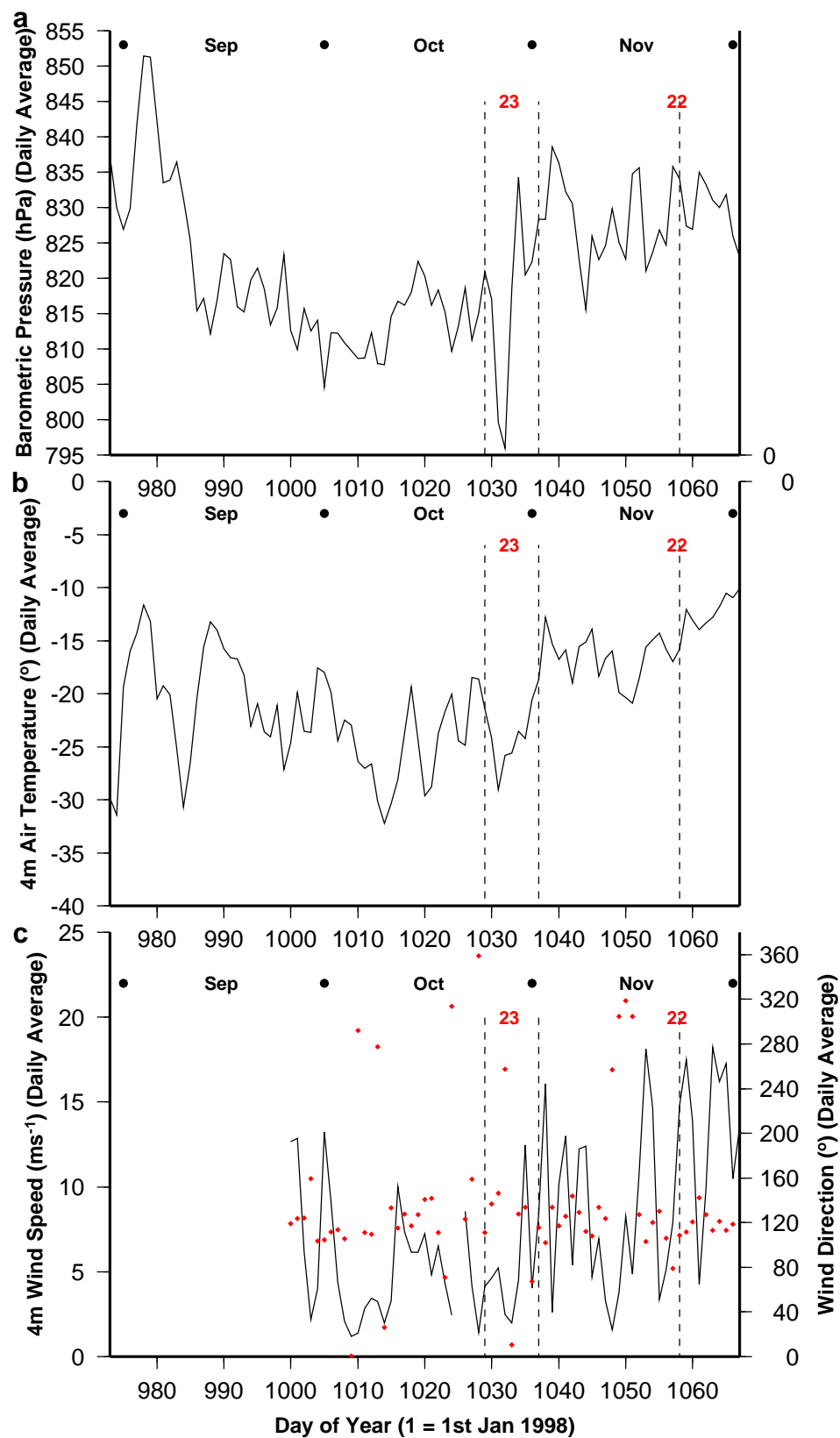


Fig 8.50: Local meteorological conditions recorded by the AWS from 1 September 2000 (Julian day 975) to 30 November 2000 (Julian day 1065). (a) Station-level (SL) pressure, (b) air temperature, (c) wind speed. Events that concur (blue) and differ (red) from expected autumn glaciochemical signals are illustrated.

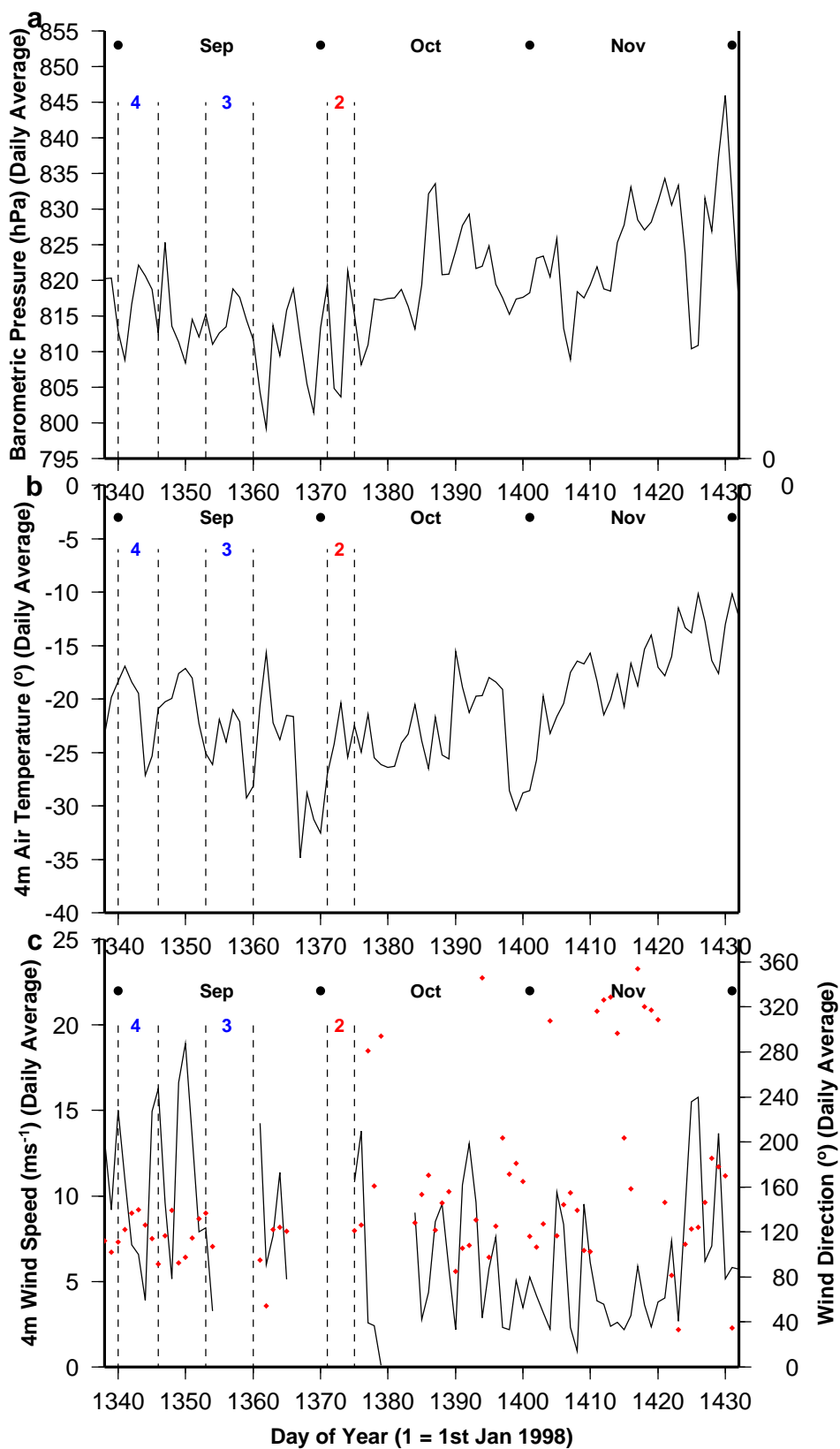


Fig 8.51: Local meteorological conditions recorded by the AWS from 1 September 2001 (Julian day 1340) to 30 November 2001 (Julian day 1430). (a) Station-level (SL) pressure, (b) air temperature, (c) wind speed. Events that concur (blue) and differ (red) from expected autumn glaciochemical signals are illustrated.

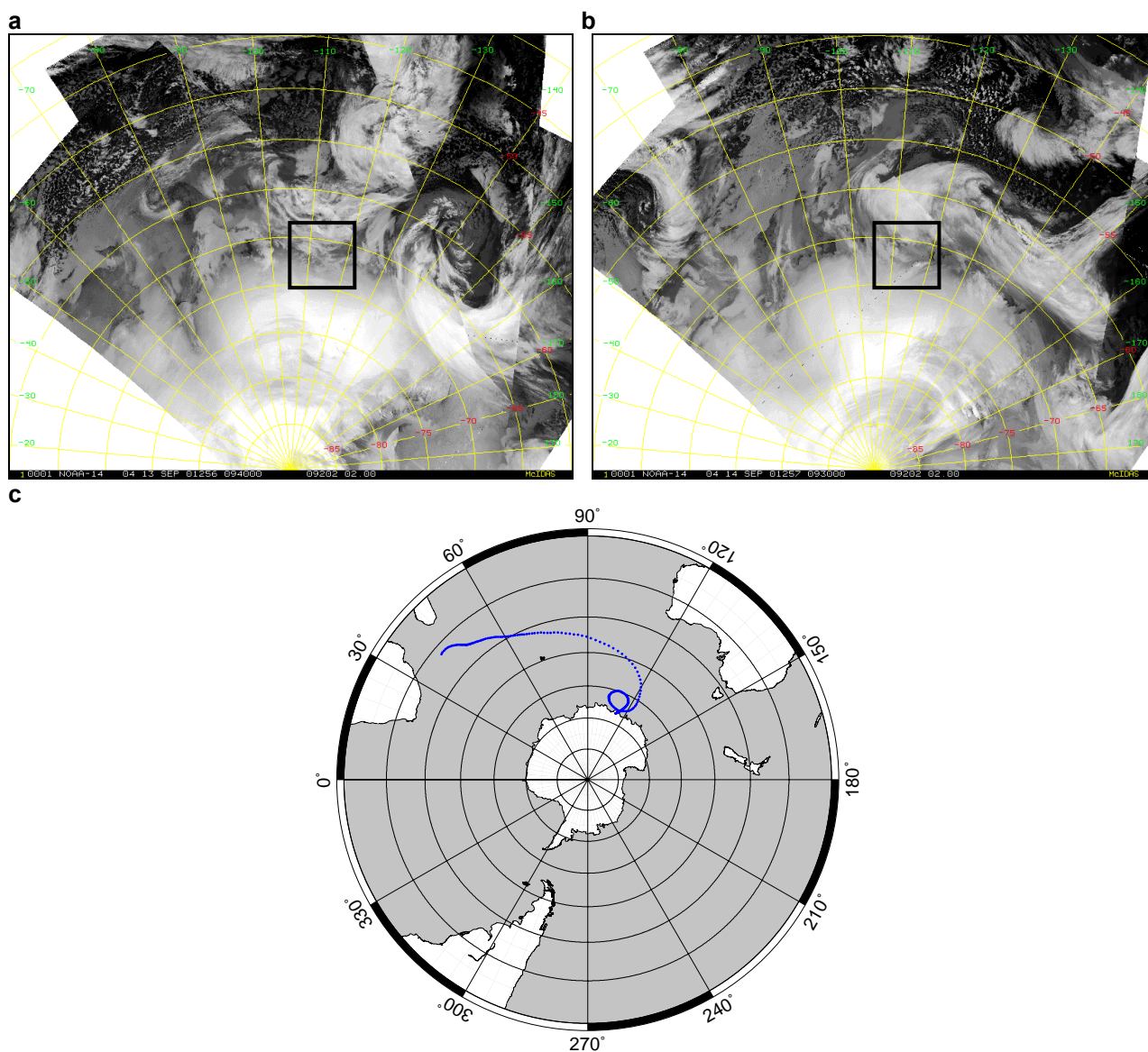


Fig 8.52: AVHRR satellite imagery (a, b) and back trajectory analysis (c) for Event 3, 14 – 21 September 2001 (Julian days 1353 – 1360): (a) 0940 UTC 13 September 2001; (b) 0930 UTC 14 September 2001; (c) 500 hPa back trajectory from 0000 UTC 14 September 2001. Law Dome is indicated in the AVHRR satellite imagery by the black box.

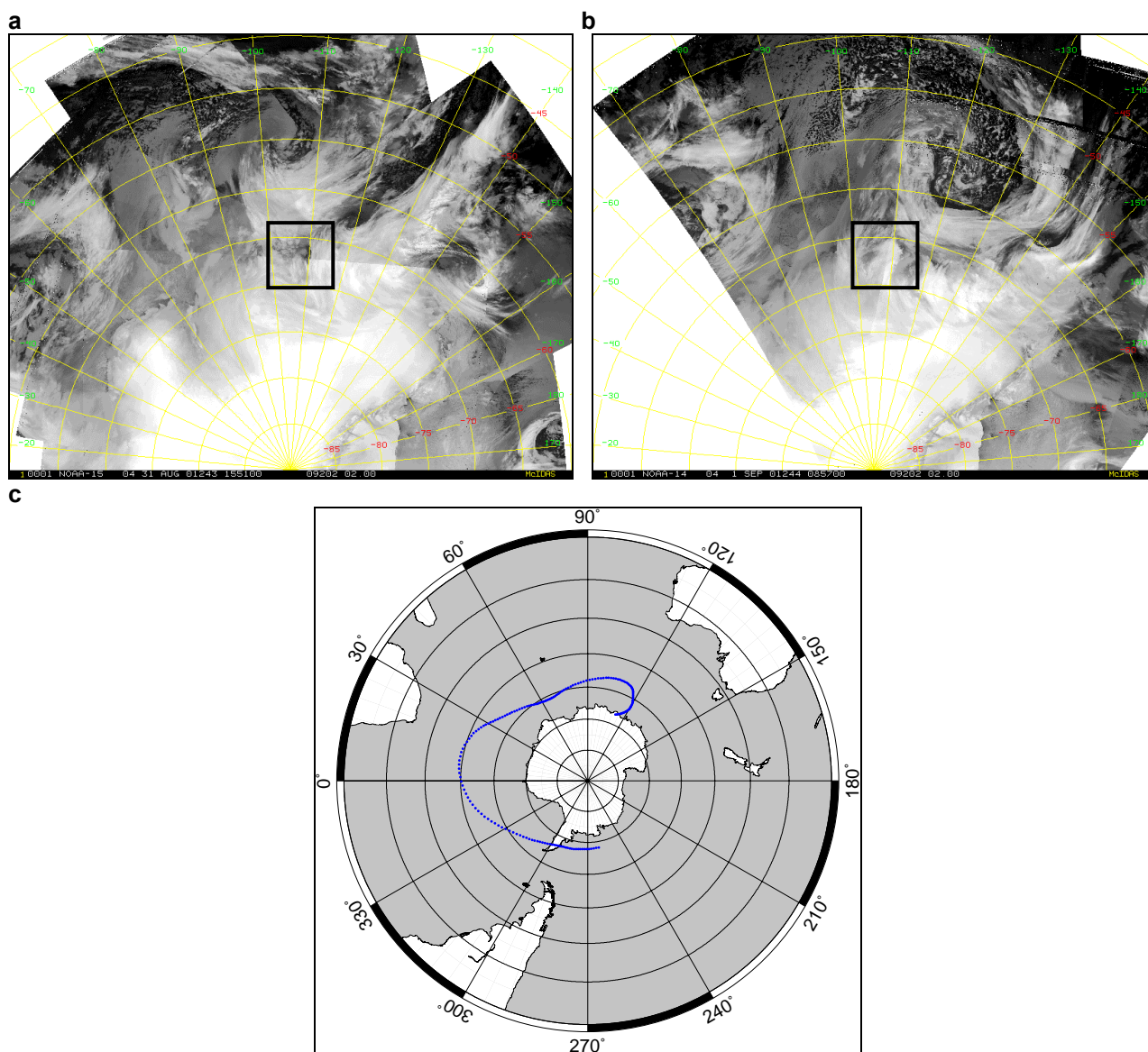


Fig 8.53: AVHRR satellite imagery (a, b) and back trajectory analysis (c) for Event 4, 1 – 7 September 2001 (Julian days 1340 - 1346): (a) 1551 UTC 31 August 2001; (b) 0857 UTC September 2001; (c) 500 hPa back trajectory from 0000 UTC 1 September 2001. Law Dome is indicated in the AVHRR satellite imagery by the black box.

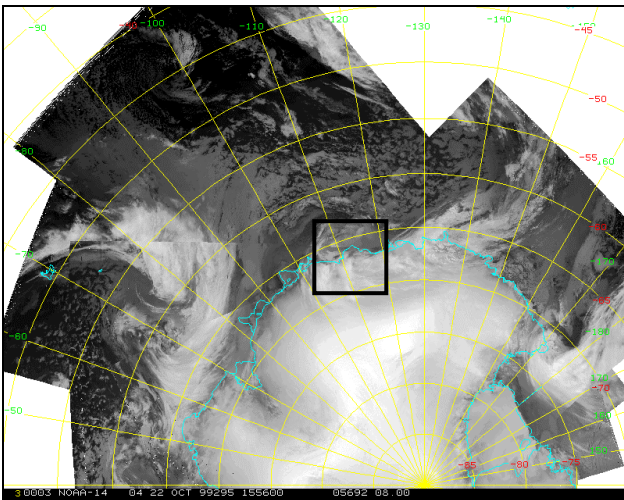
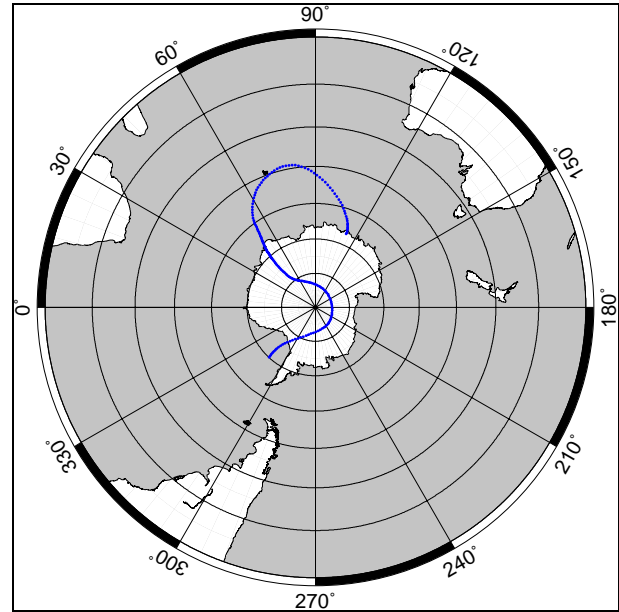
a**b**

Fig 8.54: AVHRR satellite imagery (a) and back trajectory analysis (b) for Event 32, 22 – 27 October 1999 (Julian days 660 – 665): (a) 0555 UTC 22 October 1999; (b) 500 hPa back trajectory from 0000 UTC 22 October 1999. Law Dome is indicated in the AVHRR satellite imagery by the black box. *Note: AVHRR images preceding and following 22 October 1999 were unavailable.*

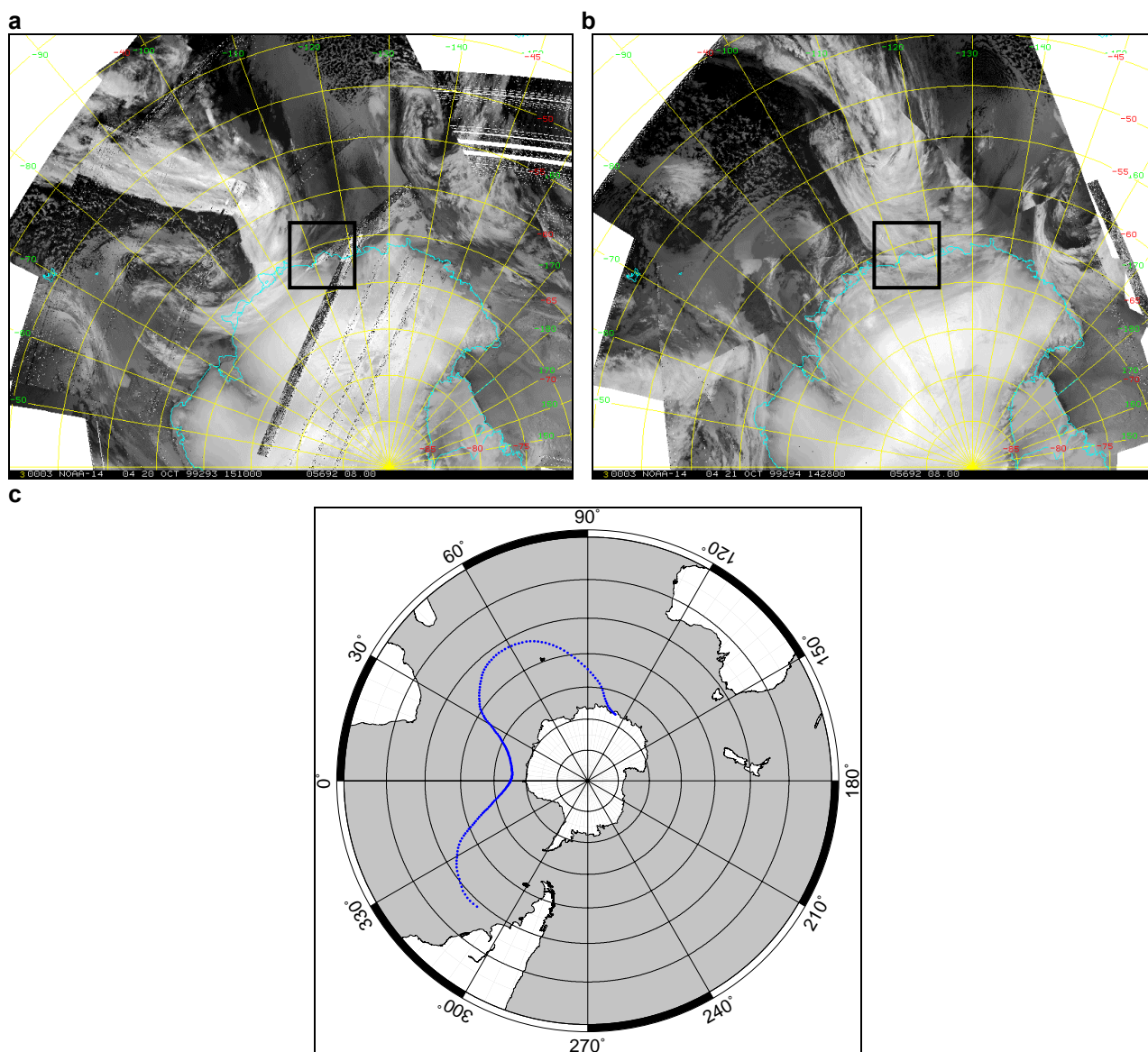


Fig 8.55: AVHRR satellite imagery (a, b) and back trajectory analysis (c) for Event 33, 21 October 1999 (Julian day 659): (a) 1510 UTC 20 October 1999; (b) 1428 UTC 21 October 1999; (c) 500 hPa back trajectory from 0000 UTC 21 October 1999. Law Dome is indicated in the AVHRR satellite imagery by the black box.

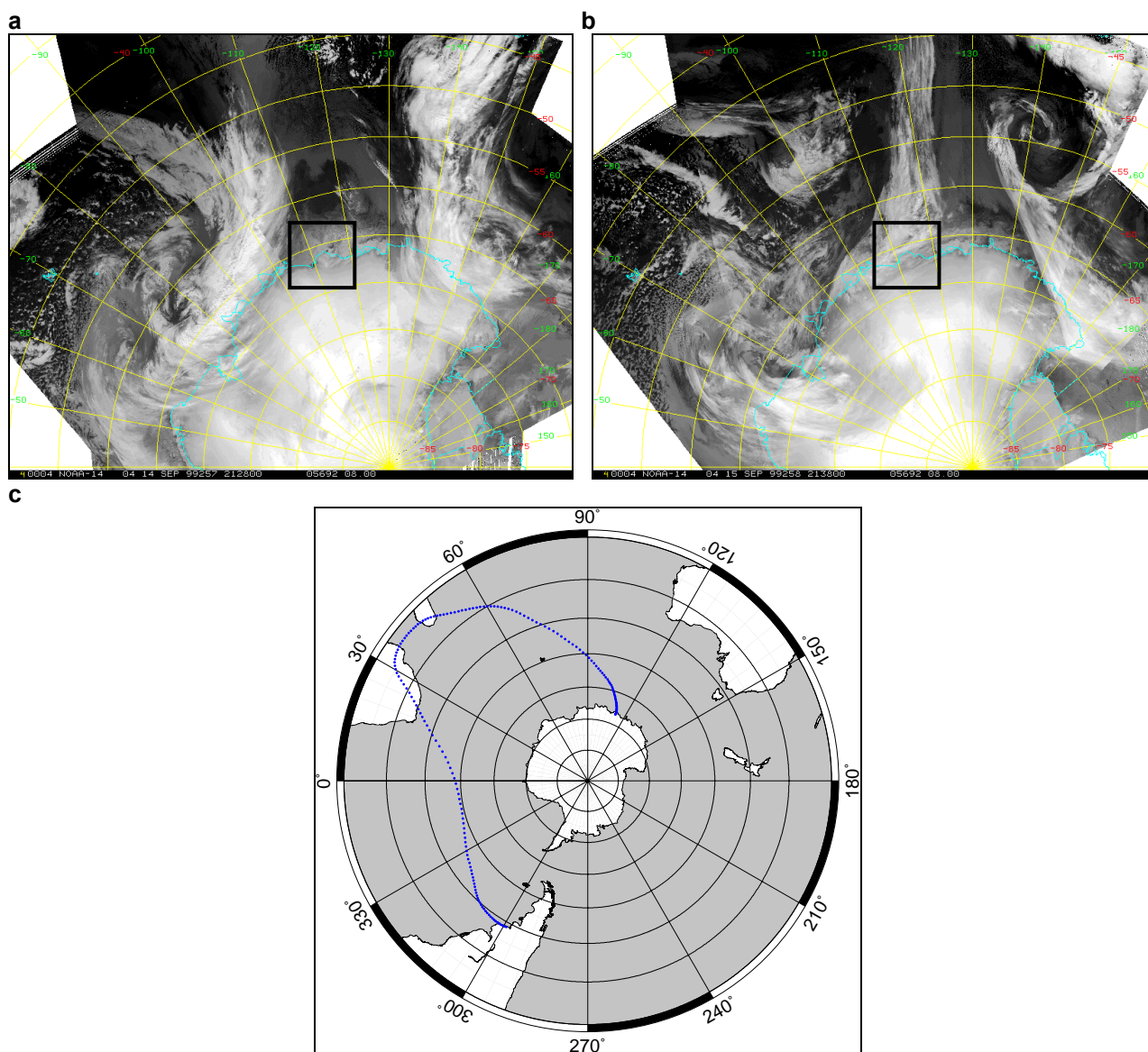


Fig 8.56: AVHRR satellite imagery (a, b) and back trajectory analysis (c) for Event 34, 11 – 17 October 1999 (Julian days 649 – 655): (a) 2128 UTC 14 October 1999; (b) 2138 UTC 15 October 1999; (c) 500 hPa back trajectory from 0000 UTC 16 October 1999. Law Dome is indicated in the AVHRR satellite imagery by the black box.

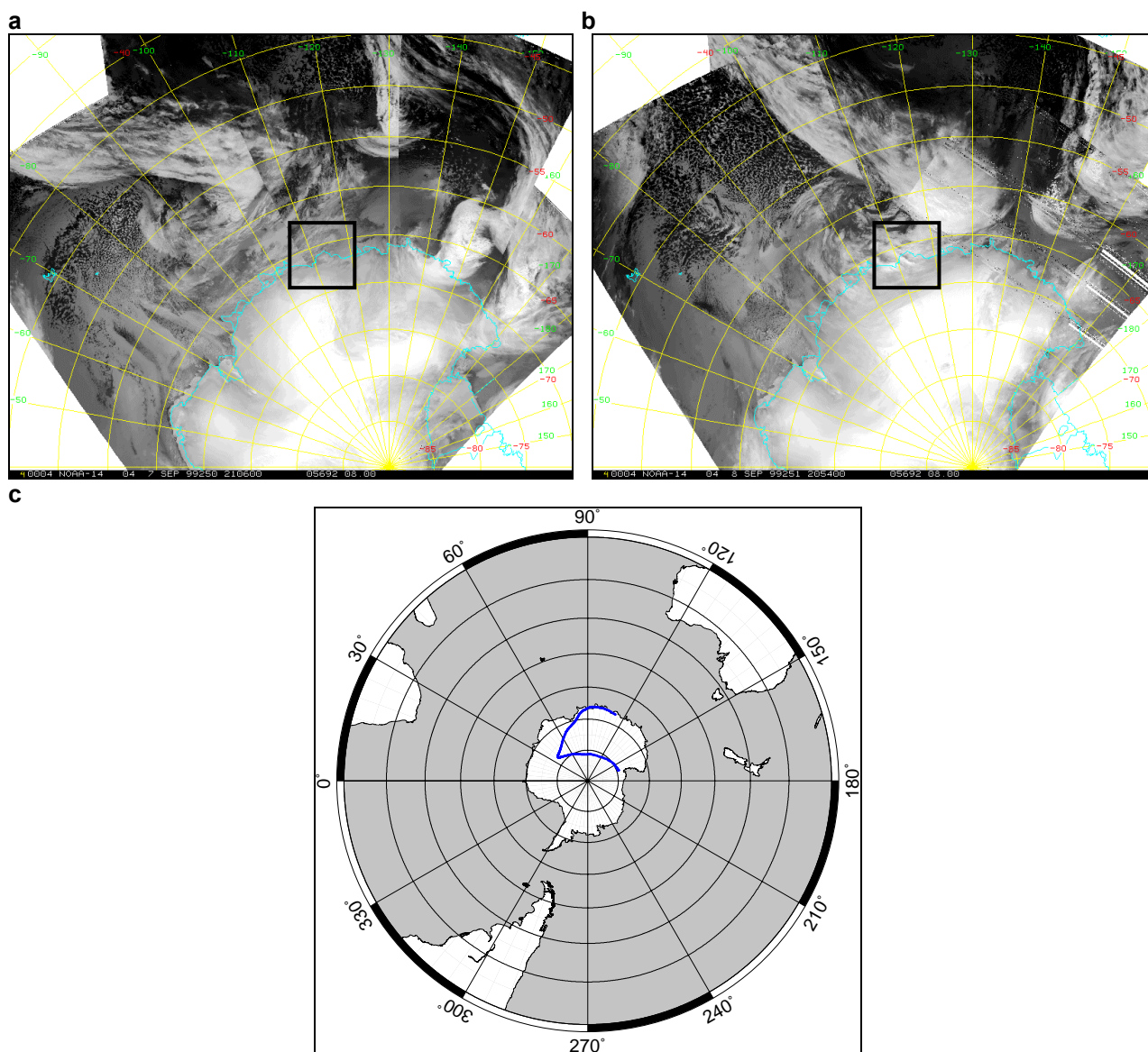


Fig 8.57: AVHRR satellite imagery (a, b) and back trajectory analysis (c) for Event 35, 2 – 10 September 1999 (Julian days 610 – 618): (a) 2106 UTC 7 September 1999; (b) 2054 UTC 8 September 1999; (c) 500 hPa back trajectory from 0000 UTC 8 September 1999. Law Dome is indicated in the AVHRR satellite imagery by the black box.

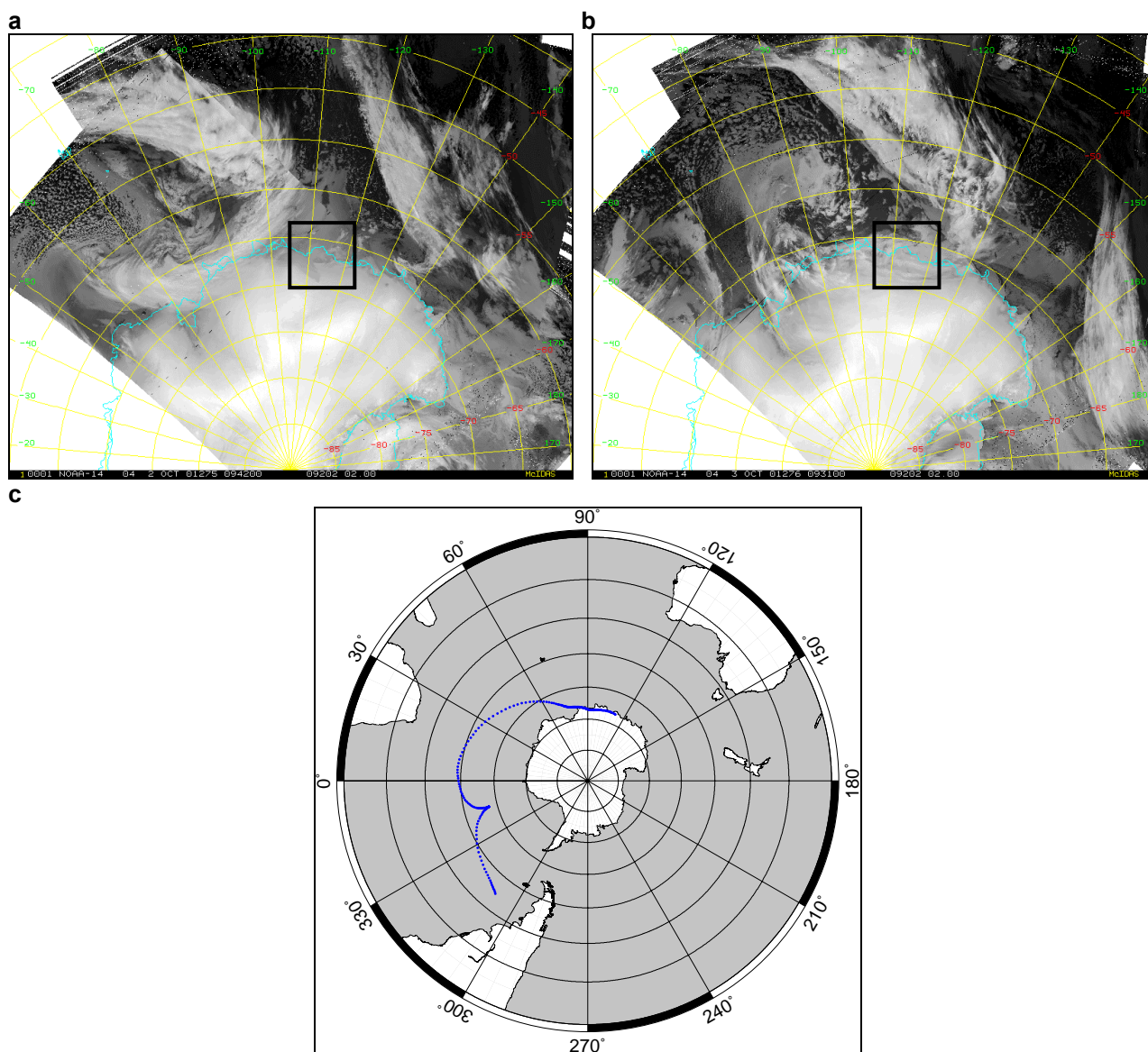


Fig 8.58: AVHRR satellite imagery (a, b) and back trajectory analysis (c) for Event 2, 2 – 6 October 2001 (Julian days 1371 – 1375): (a) 0942 UTC 2 October 2001; (b) 0931 UTC 3 October 2001; (c) 500 hPa back trajectory from 0000 UTC 2 October 2001. Law Dome is indicated in the AVHRR satellite imagery by the black box.

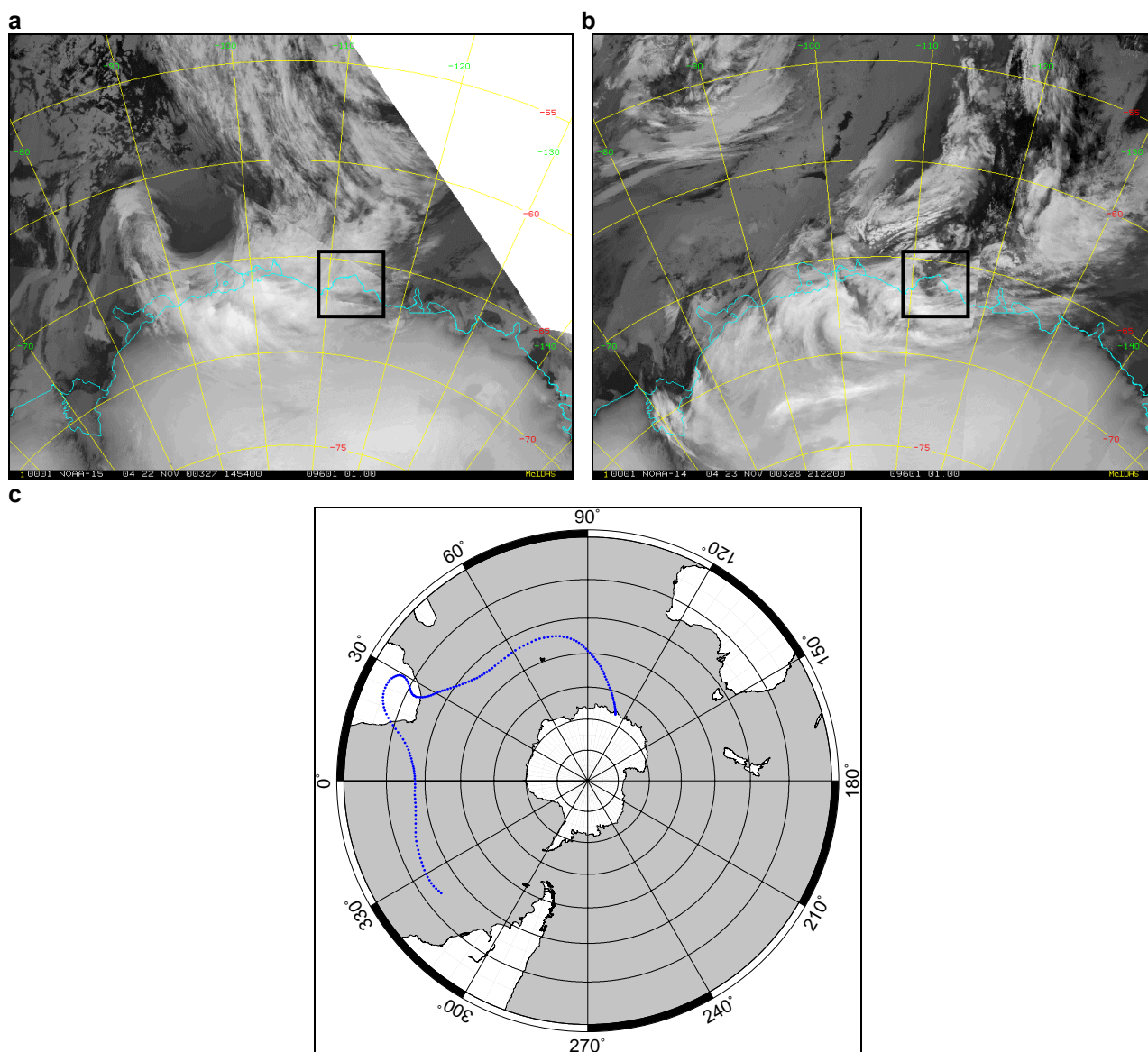


Fig 8.59: AVHRR satellite imagery (a, b) and back trajectory analysis (c) for Event 22, 23 November 2000 (Julian day 1058): (a) 1454 UTC 22 November 2000; (b) 2122 UTC 23 November 2000; (c) 500 hPa back trajectory from 0000 UTC 23 November 2000. Law Dome is indicated in the AVHRR satellite imagery by the black box.

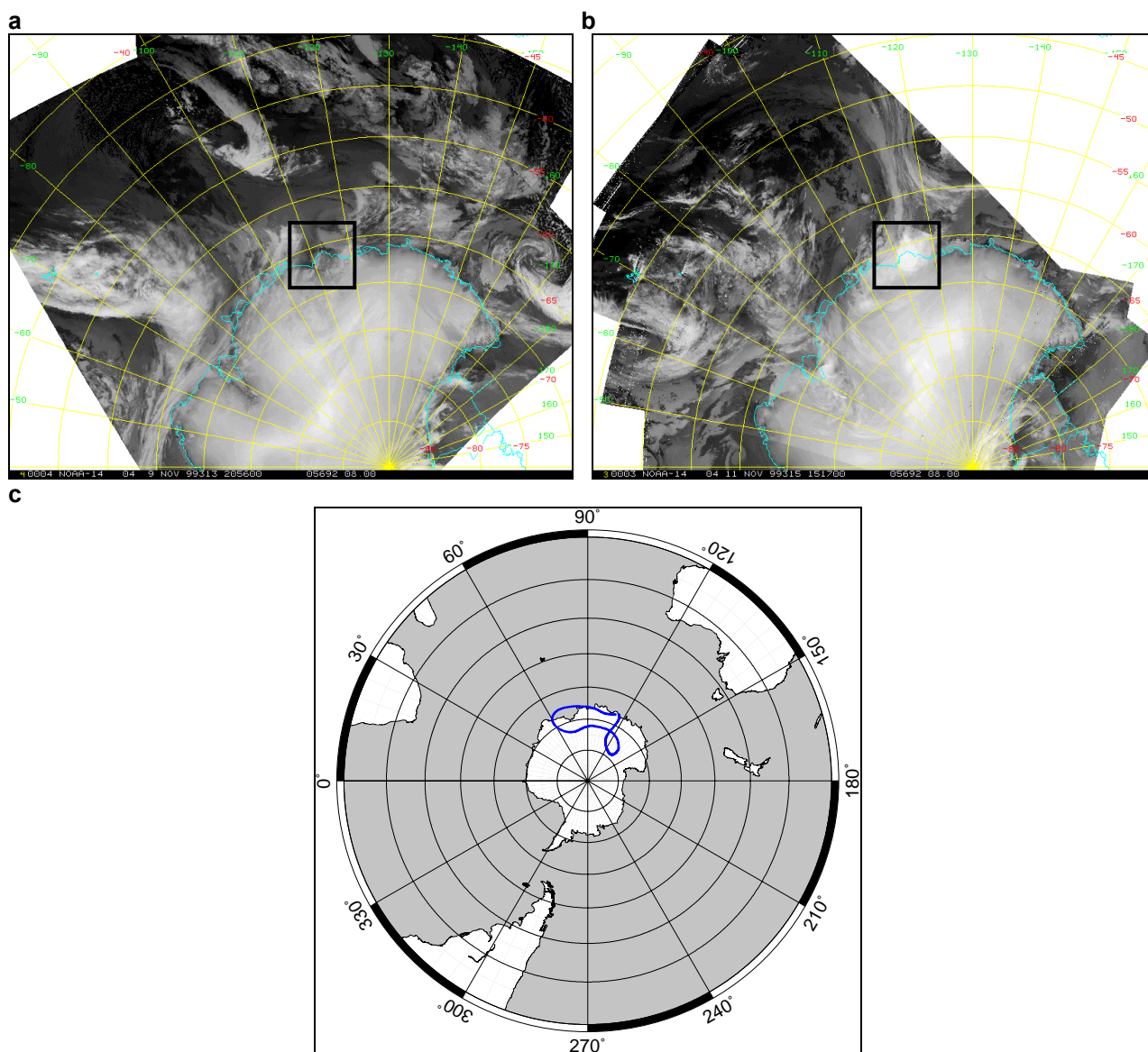


Fig 8.60: AVHRR satellite imagery (a, b) and back trajectory analysis (c) for Event 31, 10 – 16 November 1999 (Julian days 679 – 685): (a) 2056 UTC 9 November 1999; (b) 1517 UTC 11 November 1999; (c) 500 hPa back trajectory from 0000 UTC 11 November 1999. Law Dome is indicated in the AVHRR satellite imagery by the black box.

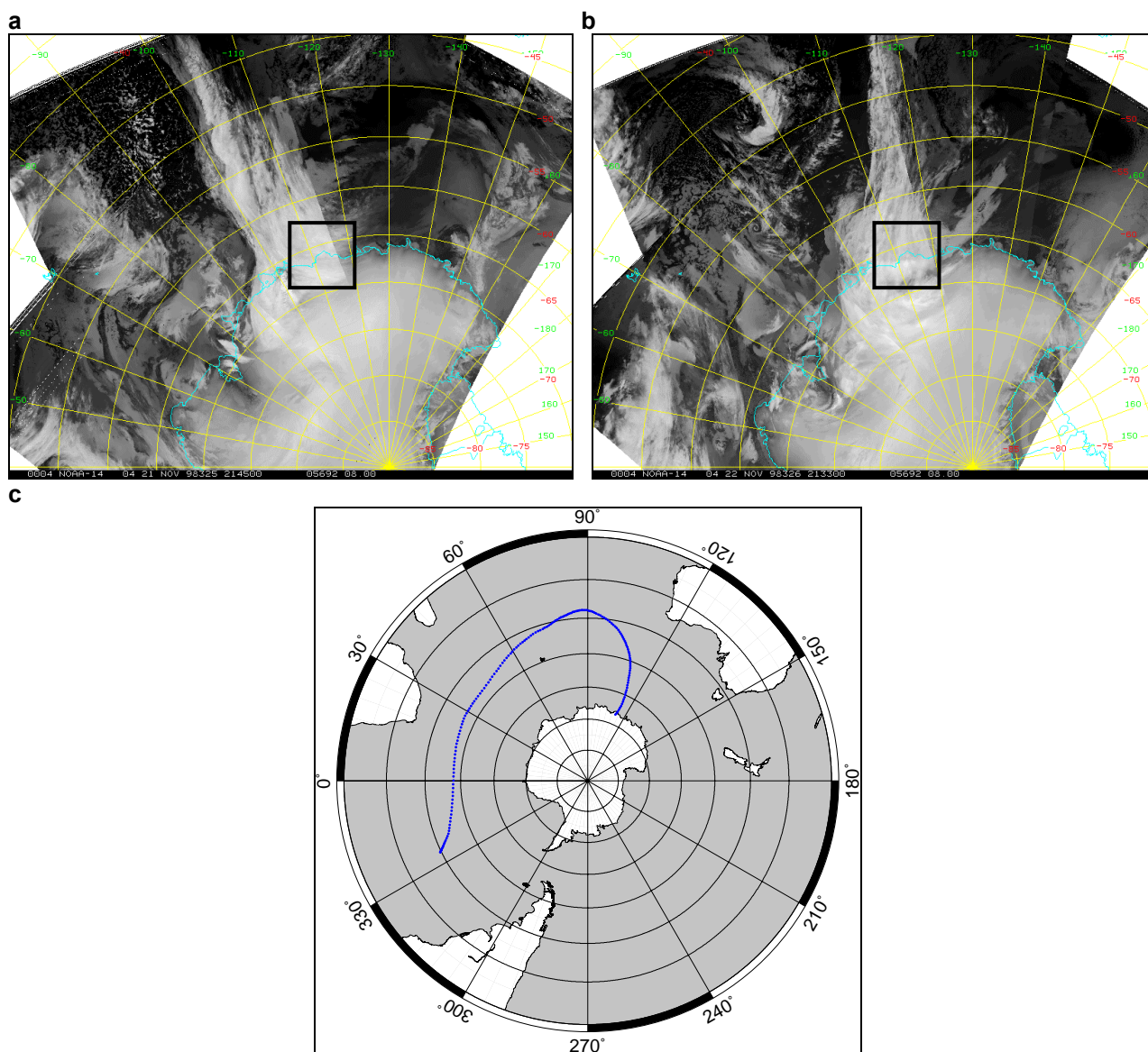


Fig 8.61: AVHRR satellite imagery (a, b) and back trajectory analysis (c) for Event 43, 23 – 29 November 1998 (Julian days 327 – 333): (a) 2145 UTC 21 November 1998; (b) 2133 UTC 22 November 1998; (c) 500 hPa back trajectory from 0000 UTC 23 November 1998. Law Dome is indicated in the AVHRR satellite imagery by the black box.

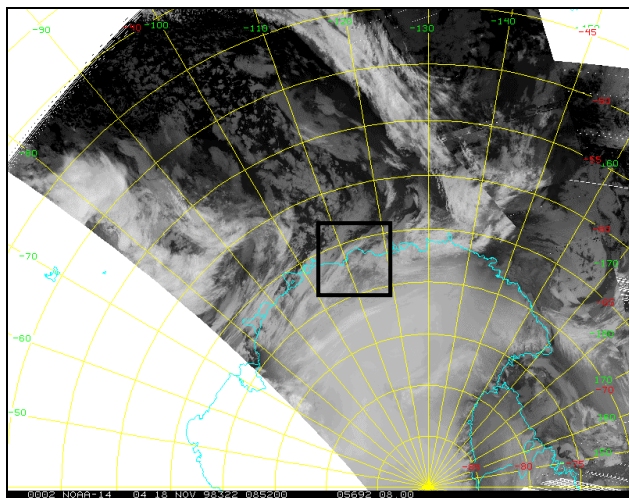
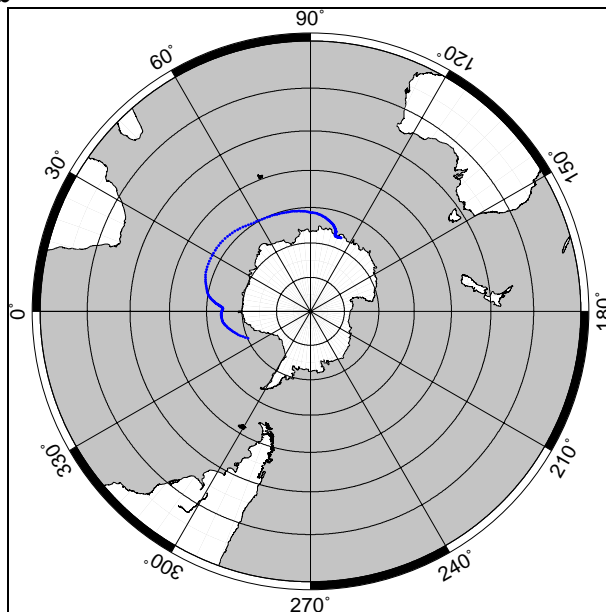
a**b**

Fig 8.62: AVHRR satellite imagery (a) and back trajectory analysis (b) for Event 44, 16 – 22 November 1998 (Julian days 320 – 326): (a) 0852 UTC 18 November 1998; (b) 500 hPa back trajectory from 0000 UTC 16 November 1998. Law Dome is indicated in the AVHRR satellite imagery by the black box. *Note: AVHRR images preceding and following 18 November 1998 were unavailable.*

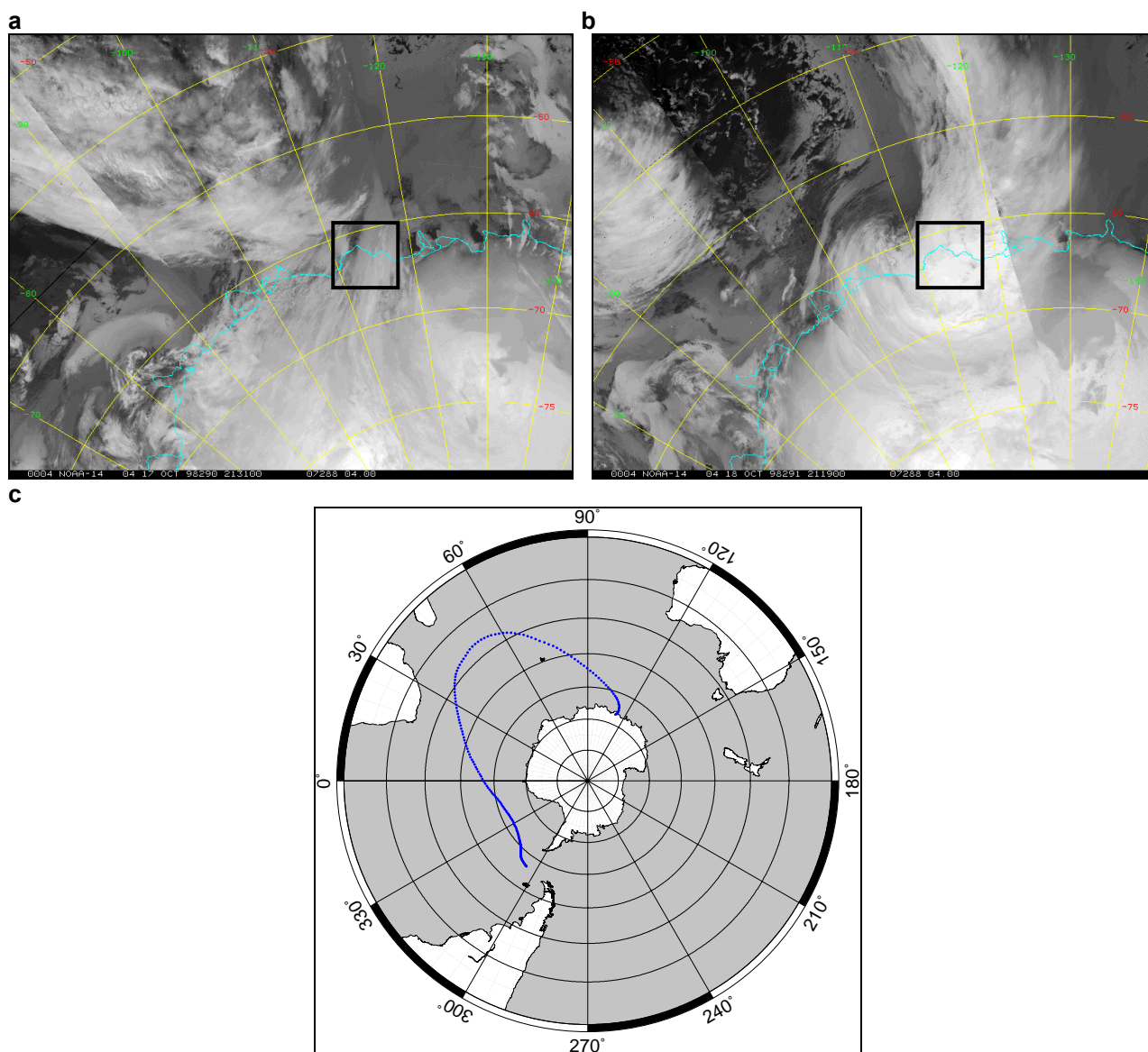


Fig 8.63: AVHRR satellite imagery (a, b) and back trajectory analysis (c) for Event 45, 16 – 19 October 1998 (Julian days 289 – 292): (a) 2131 UTC 17 October 1998; (b) 2119 UTC 18 October 1998; (c) 500 hPa back trajectory from 0000 UTC 19 October 1998. Law Dome is indicated in the AVHRR satellite imagery by the black box.